

DESIGN AND SYNTHESIS OF SHAPE-PERSISTENT ARYLENE-
ETHYNYLENE COVALENT ORGANIC POLYHEDRONS
THROUGH ALKYNE METATHESIS
AND THEIR FULLERENE-BINDING STUDY

by

Qi Wang

B.S., Peking University, Beijing, China, 2009

A thesis submitted to the

Faculty of the Graduate School of the

University of Colorado in partial fulfillment

of the requirement for the degree of

Doctor of Philosophy

Department of Chemistry & Biochemistry

2014

This thesis entitled:

“Design and Synthesis of Shape-Persistent Arylene-Ethyneylene Covalent Organic Polyhedrons

Through Alkyne Metathesis and Their Fullerene-Binding Study.”

written by Qi Wang

has been approved for the Department of Chemistry & Biochemistry

Wei Zhang, Ph. D.

David Walba, Ph. D

Date _____

The final copy of this thesis has been examined by the signatories, and we
Find that both the content and the form meet acceptable presentation standards
Of scholarly work in the above mentioned discipline.

Thesis Abstract

Wang, Qi

(Ph.D., Department of Chemistry & Biochemistry)

Design and Synthesis of Shape-Persistent Arylene-Ethyneylene Covalent Organic Polyhedrons through Alkyne Metathesis and Their Fullerene-Binding Study

Thesis directed by Prof. Wei Zhang

Shape persistent 2-D macrocycles constructed via alkyne metathesis have been well explored in the past decade. However, 3-D Covalent Organic Polyhedrons (COPs) synthesized through alkyne metathesis have been rarely studied. The objective of the work described in this thesis is to explore the efficient assembly of 3-D shape-persistent covalent organic polyhedrons through dynamic alkyne metathesis and study the relationship of the COP structures and the geometry of their building blocks. The applications COPs in host-guest chemistry, specifically the interactions with fullerenes will be discussed.

In Chapter 1, an overview of the current advances in alkyne metathesis reactions and their application in organic materials development, including design and synthesis of novel polymers, shape-persistent 2-D macrocycles, 3-D molecular cages and porous frameworks.

In Chapter 2, the design and synthesis of a tetrmeric COP with an unexpected D_{2h} symmetry through one-step alkyne metathesis from a C_3 symmetrical monomer is discussed. The

COP structure was confirmed by the signal crystal X-ray diffraction. This COP exhibits high binding affinity with C₇₀ over C₆₀ ($K_{C70}/K_{C60} > 1000$).

In Chapter 3, the synthesis of a dumbbell-shape tetrameric COP through alkyne metathesis is discussed. The formation of the tetrameric structure instead of entropically-favored dimeric one is investigated through computer modelling study. The cage also serves as a host for fullerenes.

In Chapter 4, the relationship between cage structures and the geometry of monomers in the dynamic assembly process is discussed. A dimeric cage and its interlocked cages were obtained in one-pot alkyne metathesis starting from an extend C_3 symmetry monomer.

In Chapter 5, the design and synthesis of a series of pyrene based COPs are described. These COPs exhibit strong fluorescence and significant binding affinity with fullerenes. They can be transferred into cells, which have potential applications in diagnosis. A water soluble pyrene cage was also synthesized and its biological property study is undergoing.

DEDICATION

To My Family

Acknowledgement

There are a number of people without whom this thesis might not have been written and to whom I am greatly indebted.

To my adviser, Professor Wei Zhang, who is always ready to give his guidance and support to his students. It is my great pleasure to have my doctoral program in Department of Chemistry and Biochemistry in University of Colorado at Boulder, with Professor Wei Zhang. I am grateful for having an adviser with plentiful of passion and creativities for chemistry. His expertise in organic materials area broadened my view, improved my skill set and prepared me for future explorations in science.

I thank my doctoral dissertation committee members—David Walba, Cortlandt Pierpont, Xuedong Liu and Hai Long—for their suggestions and comments during my study. I also thank my collaborators for all their contributions during my whole PhD period. I would like to thank Dr. Hai Long from National Renewable Energy Laboratory for his tremendous amount of computational modeling to help understand intra/intermolecular interactions. I would also like to thank Professor Xuedong Liu and the graduate student Eric Bunker in his group for their contribution on drug delivery and cell imaging study. I would also thank Professor Cortlandt Pierpont for helping with single crystal growing and data resolvation.

I wish to express my sincere thanks to my dear past and current group members—Yinghua Jin, Haishen Yang, Ya Du, Aibo Zhang, Jyothish Kuthanapillil, Chenxi Zhang, Ryan Denman, Athena Jin, Ryan McCaffrey, Kenji Okochi, Youlong Zhu, Chao Yu, Philip Taynton, Guolong Lu, Setareh Azarnoush, and Chris Pai. In the past five years, they gave me great ideas,

helped me solving chemistry puzzles. It is my great pleasure to spend my joyful lab time with them.

It is also dedicated to my family. To my father and mother, Jianyi Wang and Yajun Shang, who have actively supported me for all my important determinations throughout my life. Their never-end love surrounds me everywhere even though they are far away in China. I would also like to give special thanks to my husband, Chenxi Zhang, who is the one I can always trust. He is always patient with me, my random questions and thoughts, giving me tremendous support on both work and life. His love has made life much joyful.

Finally, I would like to thank financial support provided by National Science Foundation and University of Colorado at Boulder.

CONTENTS

CHAPTER 1	- 1 -
1.1. Introduction.....	- 1 -
1.2. Applications of alkyne metathesis in organic materials synthesis.	- 4 -
1.2.1. Applications of alkyne metathesis in polymer synthesis	- 4 -
1.2.2. Applications of alkyne metathesis in synthesis of macrocycles, molecular cages and frameworks	- 8 -
1.3. Conclusion and Perspectives.....	- 21 -
1.4. References.....	- 21 -
CHAPTER 2	- 25 -
2.1. Abstract.....	- 25 -
2.2. Introduction.....	- 26 -
2.3. Results and discussion	- 27 -
2.4. Experimental Section	- 36 -
2.4.1. Materials and general synthetic methods	- 36 -
2.4.2. Synthetic procedures	- 37 -
2.4.3. Attempted synthesis of 42D_{2h} through cross-coupling reactions	- 48 -
2.4.4. Scrambling experiment	- 50 -
2.4.5. Characterization of 4D_{2h}-A4	- 51 -
2.4.6. GPC data of the kinetic study	- 53 -
2.4.7. The binding study of cage 42D_{2h}-A4 with fullerene	- 54 -
2.4.8. Crystal structure report.....	- 56 -
CHAPTER 3	- 67 -
3.1. Abstract.....	- 67 -
3.2. Introduction.....	- 67 -
3.3. Results and discussion	- 69 -
3.4. Conclusion	- 79 -
3.5. Experimental Section	- 79 -
3.5.1. Materials and general synthetic methods	- 79 -
3.5.2. Synthetic procedures	- 81 -

3.5.3.	Host guest study of Cage 54D-a with Fullerenes in toluene- <i>d</i> ₈ and CS ₂	- 86 -
3.5.4.	NMR characterization of cage 54D-a	- 88 -
3.5.5.	GPC characterization	- 92 -
3.5.6.	Synthetic procedures of 53b , 54D-c , 54D-d , 53h , 53g , 53i , 54D-j	- 93 -
3.6.	References.....	- 104 -
CHAPTER 4.....		106 -
4.1.	Introduction.....	- 106 -
4.2.	Results and Discussion	- 108 -
4.3.	Conclusion	- 120 -
4.4.	Experimental Section.....	- 120 -
4.4.1.	Materials and general synthetic methods	- 120 -
4.4.2.	Compounds Preparation.....	- 122 -
4.4.3.	Kinetic study of cage formation.....	- 132 -
4.4.4.	DOSY experiment.....	- 133 -
4.4.5.	Determination of ¹³ C NMR of cage 59A-j	- 137 -
4.5.	References.....	- 140 -
CHAPTER 5.....		142 -
5.1.	Introduction.....	- 142 -
5.2.	Preliminary results and discussion	- 143 -
5.3.	Perspectives and recommendations for future	- 150 -
5.3.1.	Cage and Gd-metallocarbon fullerene complexation study for MRI contrast agent.....	- 150 -
5.3.2.	Application of pyrene-labeled COP in the mechanism study of cellular uptake of COPs.....	- 151 -
5.4.	Experimental Section.....	- 151 -
5.4.1.	Materials, general synthetic methods and biological study condition	- 151 -
5.4.2.	Synthetic procedures	- 153 -
5.4.3.	Binding study of cage 63f and 63h with fullerenes	- 158 -
5.4.4.	NMR spectrum of important compounds.....	- 162 -
5.5.	References.....	- 165 -
Bibliography		- 168 -

CHAPTER 1

Recent Applications of Alkyne Metathesis in the Synthesis of Organic Materials

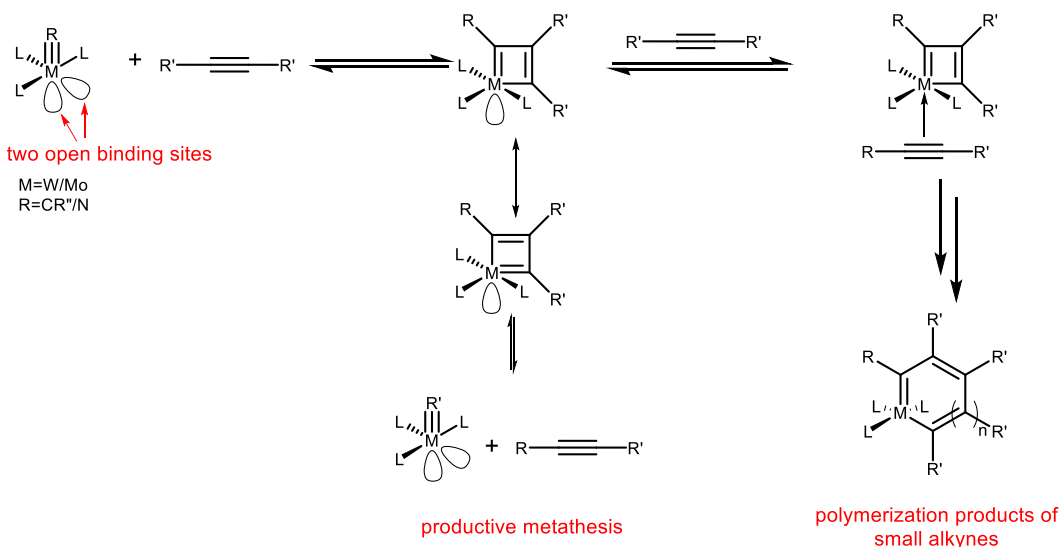
1.1. Introduction

Alkyne metathesis was first discovered in 1968 while 2-pentyne was scrambled into 2-butyne and 3-hexyne by WO_3 immobilized on silica (6.8% w/w) at 350°C.¹ Unlike the olefin metathesis, however, the impact of alkyne metathesis on organic synthesis is not very remarkable, mainly due to relatively low reactivity and limited functional group tolerance of alkyne metathesis catalysts.

After the discovery of alkyne metathesis, a few mechanisms were proposed, and the one proposed by Katz and McGinnis (Scheme 1.1) was later experimentally verified by Schrock.²⁻⁴ The metal-carbon triple bond (carbyne) reacts with an alkyne first to form a [2+2] cycloaddition intermediate, which is followed by a cycloreversion to generate a new carbon-carbon triple bond.

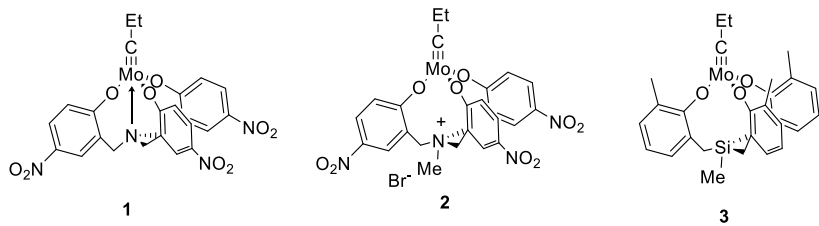
Schrock, as one of the key pioneers in the alkyne metathesis catalyst development, initiated the Schrock-type alkylidyne complexes ($\text{RC}\equiv\text{MX}_3$) containing tungsten or molybdenum

and carbon triple bond.⁵ This type of catalysts exhibit high activity and allow metathesis reactions to occur at lower temperature (25 °C). However, the small alkyne polymerization (Scheme 1.1) as a main side reaction remained as a key problem limiting the wide and scaled-up applications of alkyne metathesis which is due to two open binding sites in this type of catalysts. The mechanism of the polymerization is that small alkyne can repeatedly insert into the metal–carbon bond and form polymers through ring expansion mechanism.^{2,6} Thus the generated molybdenum(VI) vinyl alkylidene species would be unavailable for further alkyne metathesis.



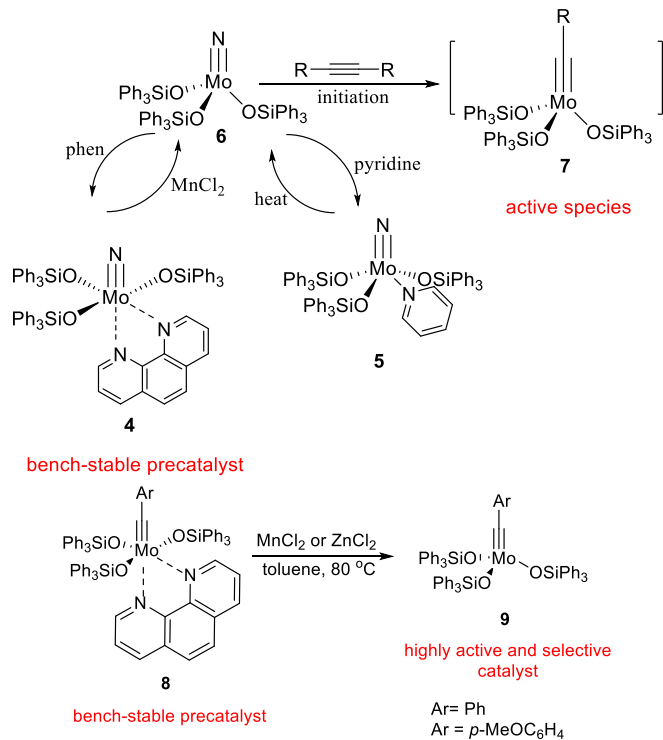
Scheme 1.1. General mechanism for desired alkyne metathesis and undesired polymerization of small alkyne substrates.

Recent studies by the Zhang group showed that blocking one alkyne binding site, either chemically through coordination or physically through spatial blocking, can efficiently prevent the small alkyne polymerization. Moreover, these amine, ammonium and silane based multidentate catalysts (**1–3**) exhibit high activity, great functional group tolerance, high stability as well as long life time. These catalysts can catalyze nitro and formyl substituted phenylpropynes which are considered tough substrates for alkyne metathesis.^{7–9}



Scheme 1.2. Multidentate alkyne metathesis catalysts developed by the Zhang group.

A significant amount of efforts was also devoted to design and synthesis of user-friendly catalysts.¹⁰⁻¹¹ The Fürstner group designed and synthesized a series of bench-stable precatalysts, which can be further activated by adding MnCl_2 or ZnCl_2 . The nitride precatalyst **4** are stable under air for 2 years and the generated activate species showed good activities for most of substrates except aldehydes and acid chlorides. Later, the alkylidyne precatalyst **8**, which can also be activated by MnCl_2 or ZnCl_2 to generate active species **9** with improved activity and stability, was synthesized.



Scheme 1.3. Bench-stable precatalysts and their activation.

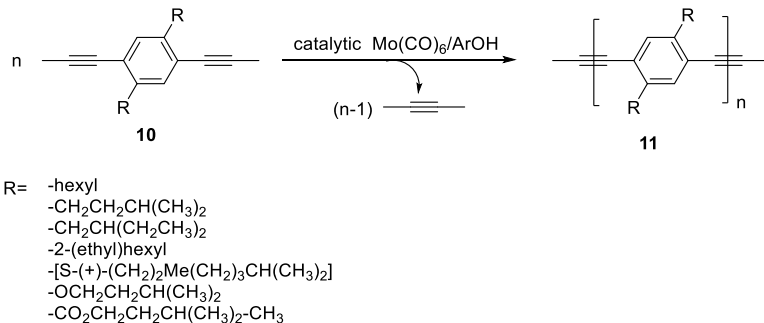
1.2. Applications of alkyne metathesis in organic materials synthesis.

Alkyne metathesis has been intensively utilized in total synthesis of natural products from its discovery¹², which will not be covered in this chapter. This introduction will focus on the important role of alkyne metathesis in the synthesis of organic materials, including polymers, 2-D and 3-D well defined, shape-persistent organic molecules and frameworks.

1.2.1. Applications of alkyne metathesis in polymer synthesis

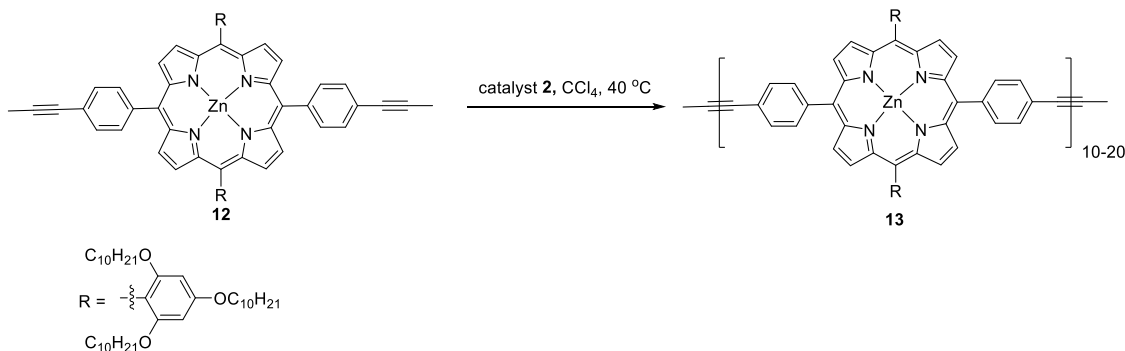
Poly(phenylenethynylene)s (PPEs) have attracted tremendous attention in the past two decades because of their great applications in light-emitting diodes, organic photovoltaics, field effect transistors, *et al.*¹³⁻¹⁵ Conventionally, the classic Heck-Cassar-Sonagashia-Hagihara reactions are used to synthesize PPEs. However, the potential drawback of the coupling reactions is that they often generate diyne defects, which will add uncertain factors to the electron property of the materials.¹⁶ In contrast, with alkyne metathesis, there will be no diyne defects generated based on the metathesis mechanism. Moreover, only one type of monomer synthesis is needed instead of the requirement for both terminal acetylenes and aryl halides in the coupling approach.

In 1997, Weiss, Bunz and Müllen used alkyne metathesis for the first time to synthesize PPEs with comparable molecular weight as the polymers obtained through Pd-catalyzed coupling reactions, thus opening the door to PPE synthesis through a totally new approach - acyclic diyne metathesis polymerization (ADIMET).¹⁷ Later, the Bunz group modified the reaction condition by using Mo(CO)₆/phenol system, which led to high yields of PPEs with different substitutes and competitive degree of polymerization.¹⁸



Scheme 1.4. PPE synthesis through ADIMET.

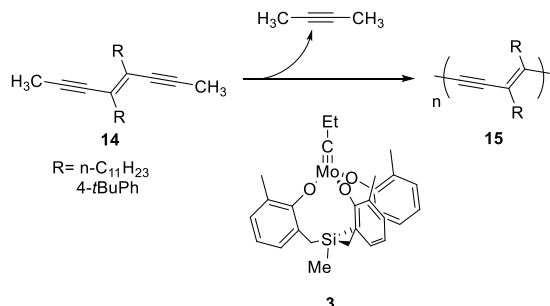
Recently, Zhang and coworkers used the triphenol ammonium coordinated catalyst **2** successfully synthesized porphyrin-based arylene ethynylene polymers.⁸ Only one ethynylene carbon signal was observed in ¹³C NMR spectrum, thus indicating defect-free conjugated porphyrin-based polymers formed.



Scheme 1.5. Synthesis of porphyrin-based arylene ethynylene polymers using alkyne metathesis.

Later the Qin group and Zhang group using the triphenolsilane coordinated catalyst **3** successfully synthesized the polydiacetylenes (PDAs) through Acyclic Enediyne Metathesis Polymerization (AEDMET).¹⁹ PDAs are well studied as conjugated polymers because of their applications in chemo and bio-sensing under stimulations.²⁰⁻²¹ However, conventionally PDAs can only be obtained through solid state polymerization which requires strict periodic packing in crystals. This represents the first time that solution-processable PDAs are synthesized through solution polymerization using AEDMET. The device fabricated from the PDAs exhibited over 100-fold cell performance than previously reported PDAs synthesized via solid state

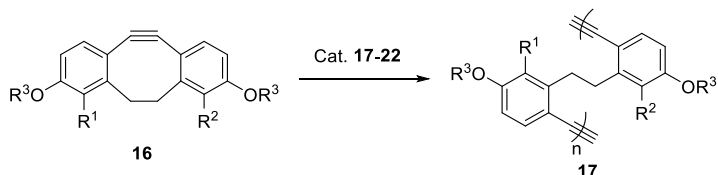
polymerization. It is worth pointing out that these PDAs could not be obtained using either Schrock catalyst or Mortreux–Mori–Bunz catalyst, thus indicating the great advantage of such multidentate alkyne metathesis catalysts in PDA synthesis.



Scheme 1.6. Synthesis of PDAs using alkyne metathesis.

The ring-opening alkyne metathesis polymerization (ROAMP) has also been explored. The first reported ROAMP was conducted by Schrock and coworkers in 1987.²²⁻²³ They found that strained cyclooctyne can undergo ring-opening polymerization catalyzed by $[(t\text{BuO})_3\text{-Mo}\equiv\text{CPr}]$, giving high molecular weight polymers but also with high polydispersity (PDI > 4). This finding suggested that this polymerization was not living and the catalyst could not distinguish between the strained alkyne bonds in cyclic monomers and those internal alkyne bonds in polymers. In order to achieve living ROAMP, the catalyst should have mild activity which can only react with strained alkynes without touching the polymer backbones so that no “back-biting” would occur. Nuckolls and Fisher recently screened a series of catalysts for ROAMP. Interestingly, when catalyst **18** was used to catalyze the ROAMP, at the initiating stage, the polymer product showed low PDI and high molecular weight ($t < 15$ s). However, when all monomers were consumed, the cross metathesis (back-biting) was observed, showing broad product distributions. Among all different ligands for molybdenum based catalysts, catalyst **19-21** gave narrow PDI and high molecular weight for polymer **17c**. Later, the Nuckolls group developed a new type of phenoxide-based catalyst **23** showing fast initiation and slow chain

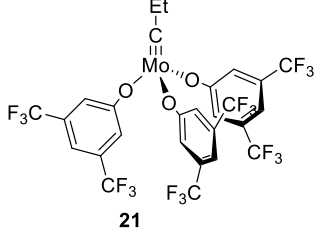
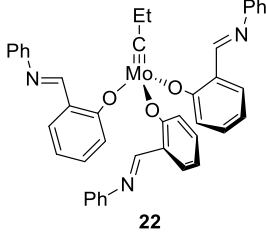
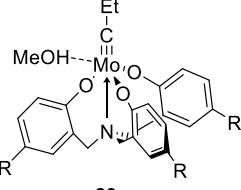
propagation. This metathesis reaction showed low PDI (PDA=1.2) as well as predicted molecular weight with monomer **16d**.²⁴ Most recently, starting with the triphenolamine coordinated Mo(VI) carbyne complex (**1**, without nitro) developed by the Zhang group, Nuckolls and coworkers activated it by MeOH in situ. The MeOH dissociation from the molybdenum catalyst **23f** with mild activity enabled the slow chain propagation. This catalyst does not require aprotic environment and catalyzes **16d** efficiently within 2 h.²⁵



Scheme 1.7. Synthesis of polymer **17** using alkyne metathesis.

Table 1.1 Polymerization results of different monomer **16** using different catalysts.

catalysts	16a: R ¹ =R ² =H R ³ =H ₁₂ H ₂₅	16b: R ¹ =H R ² =Br R ³ =C ₁₂ H ₂₅	16c: R ¹ =R ² =Br R ³ =C ₁₂ H ₂₅	16d: R ¹ =R ² =H R ³ =TIPS	16e: R ¹ =R ² =R ³ =H
	17a: Mn=54,000 PDI=2.0	17b: Mn=54,000 PDI=2.6	17c: Mn=32,000 PDI=1.8	NA	NA
18					
	NA	NA	17c: Mn=19,300 PDI=1.1	NA	NA
19					
	NA	NA	17c: Mn=248,000 PDI=1.3	NA	NA
20					

catalysts	16a: $R^1=R^2=H$ $R^3=H_{12}H_{25}$	16b: $R^1=H$ $R^2=Br$ $R^3=C_{12}H_{25}$	16c: $R^1=R^2=Br$ $R^3=C_{12}H_{25}$	16d: $R^1=R^2=H$ $R^3=TIPS$	16e: $R^1=R^2=R^3=H$
	NA	NA	17c: $Mn=170,000$ $PDI=1.3$	NA	NA
	NA	NA	NA	17d: $Mn=3,900$ $PDI=1.2$	NA
	NA	NA	NA	17d: f: $Mn=3,200$ PDI=1.2 g: $Mn=6,300$ PDI=2.4	17e: f: $Mn=6,300^*$ PDI=1.3*

f: $R=H$
g: $R=NO_2$

* After two steps: alkyne metathesis followed by $(iPr)_3SiCl$, Et_3N , 72%.

1.2.2. Applications of alkyne metathesis in synthesis of macrocycles, molecular cages and frameworks

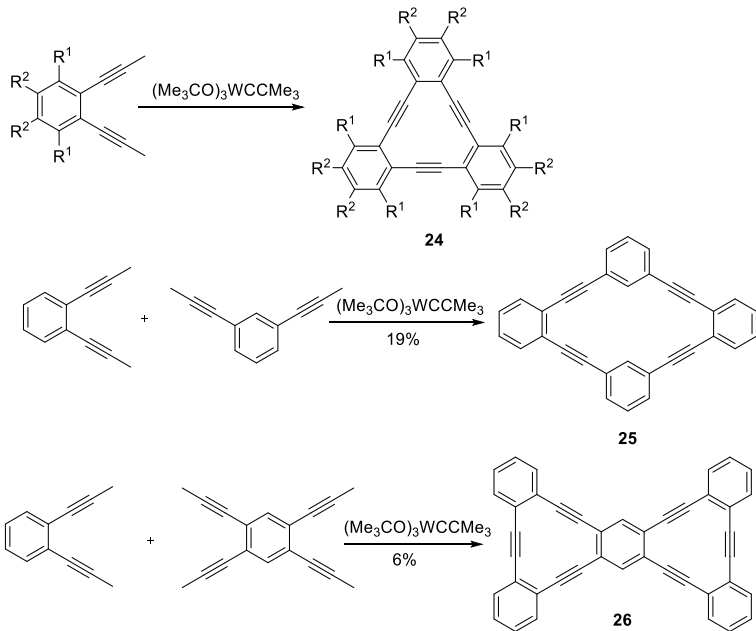
The synthesis of well-defined macrocycles and molecular cages represents a challenging task when traditional step-by-step coupling reactions are utilized. On the other hand, dynamic covalent chemistry (DCvC), as a powerful synthetic approach for thermodynamically favored products through fully reversible covalent reactions, has been utilized to synthesize well-defined molecular architectures. Alkyne metathesis, as one type of DCvC, has been utilized to synthesize shape-persistent macrocycles, molecular cages and frameworks. Under alkyne metathesis conditions, the carbon-carbon triple bonds can exchange with one another and the systems can

undergo “self-correction” procedures to generate the most stable products after reaching equilibrium. Also because of the linear and rigid nature of alkyne groups, the ethynylene-linked products will be robust and shape-persistent.

1.2.2.1. Alkyne metathesis applications in the synthesis of 2-D shape-persistent macrocycles

There have been great interests in shape-persistent arylene ethynylene macrocycles (AEMs) as building blocks for supramolecular materials due to their novel properties. The first reported AEM was synthesized by the Staab group back in 1974 with only 4.6% yield.²⁶ The method used was six-fold Stephens-Castro coupling. Later, Sonogashira coupling was widely used to synthesize this type of macrocycles. Such cross-coupling based synthetic approach is generally efficient and has wide functional group tolerance. However, its big disadvantage is that the product distribution is kinetically controlled, thus stringent reaction conditions, such as concentration and temperature, are needed.

In the past one decade or so, people have explored the synthesis of arylene ethynylene macrocycles via alkyne metathesis. The first reported AEMs were synthesized by the Bunz group in 2000.²⁷ Even though the final product was a mixture of polymers (major) and macrocycles (minor), presumably due to low activity of the catalyst, it showed the possibility of synthesizing AEMs via alkyne metathesis. Three years later, the Whitener and Vollhardt groups synthesized triangle macrocycles **24** and rhombus-shaped macrocycles **25** via alkyne metathesis in good yields. More impressively, ortho-dehydrobenzannulenes **26** was also obtained.²⁸



Scheme 1.8. Synthesis of triangle macrocycle **24**, rhombus macrocycle **25** and ortho-dehydrobenzannulenes **26**.

Later, Moore and coworkers systematically studied the dynamic feature of AEM formation via alkyne metathesis.²⁹⁻³² In order to drive the reaction to most favored macrocycle products more efficiently, precipitation-driven method was developed. Given the development of phenol-based alkyne metathesis catalysts and precipitation driven method, the yields of the desired hexameric phenylene ethynylene macrocycles **27** starting from meta-disubstituted benzenes were significantly improved to 80%, and the tetrameric carbazole based macrocycles **27** were obtained in 84% yield. Moore and coworkers also confirmed the dynamic nature in the macrocycles **26** formation by monitoring the reaction progress by gel permeation chromatography (GPC), which showed long oligomers (> 6 repeating units) are formed at the early stage of the reaction and then slowly converted back to more stable hexameric macrocycles.³¹ These observations illustrated that oligomers formed quickly by losing end groups, however under reversible conditions, macrocycles have lower free energy than oligomers (entropy drivien), thus lower energy species enriched at the equilibrium and large oligomers

transformed into macrocycles. Interestingly, besides hexamers, pentamers and heptamers were also observed as minor species. Comparing hexameric macrocycles with oligomers, the enthalpy was very similar because they both have minimum angle strain. But the entropy of macrocycles was much higher because a larger number of molecules are formed than the oligomer/polymer case. Pentameric macrocycles was less favored because its higher angle strain increased the enthalpy; heptameric or even octameric macrocycles decreased the number of molecules resulting in less entropy contribution, therefore these macrocycles did not exist as major species. Scrambling experiment between two hexameric AEMs with different side chains was conducted and fully scrambled products were observed on MALDI-MS. This experiment revealed the full reversibility of carbon-carbon triple bonds formation of these phenylene ethynylene macrocycles under alkyne metathesis condition, further supporting that these macrocycles are the most thermodynamically favored products.

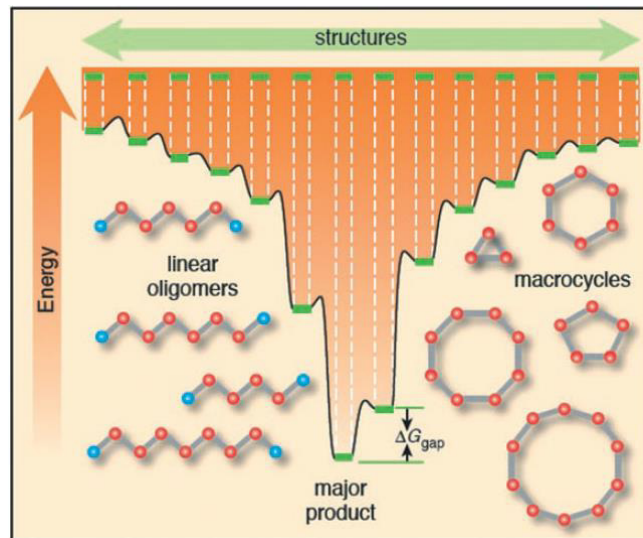
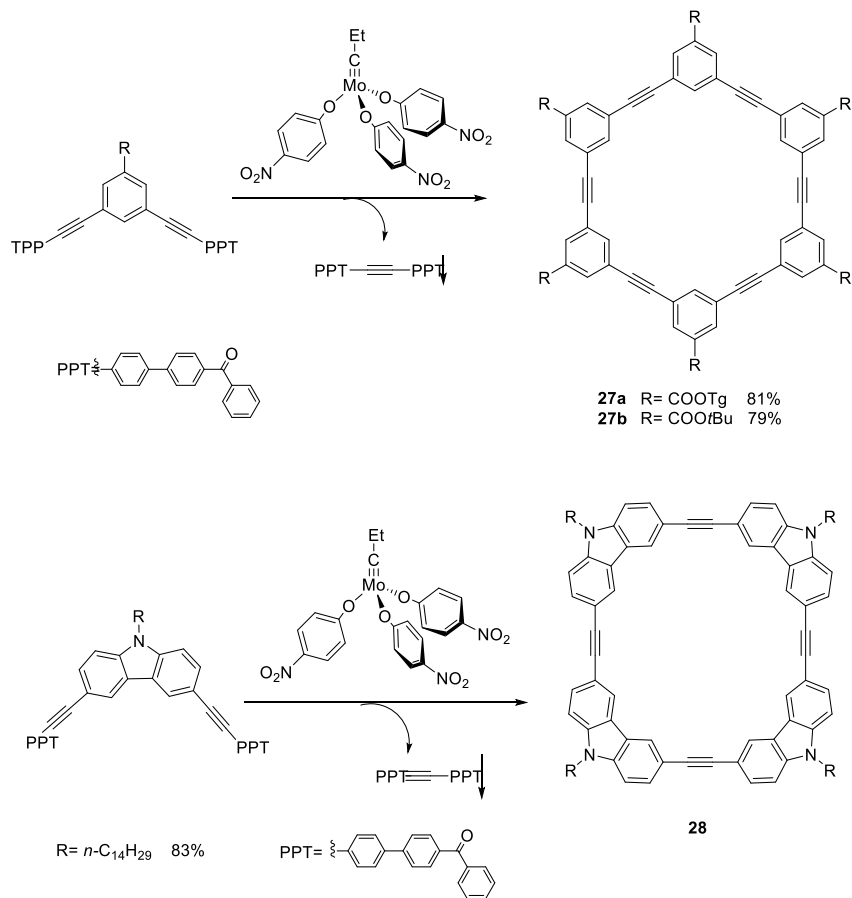


Figure 1.1. The cyclooligomerization energy landscape. As the degree of conversion increases, the end groups are removed, driving the reaction to oligomers and macrocycles. The energy gap (ΔG_{gap}) is the energy difference between the most stable product and the second stable product. The energy landscape determines the final products distribution under reversible conditions.



Scheme 1.9. Synthesis of macrocycles **27** and **28**.

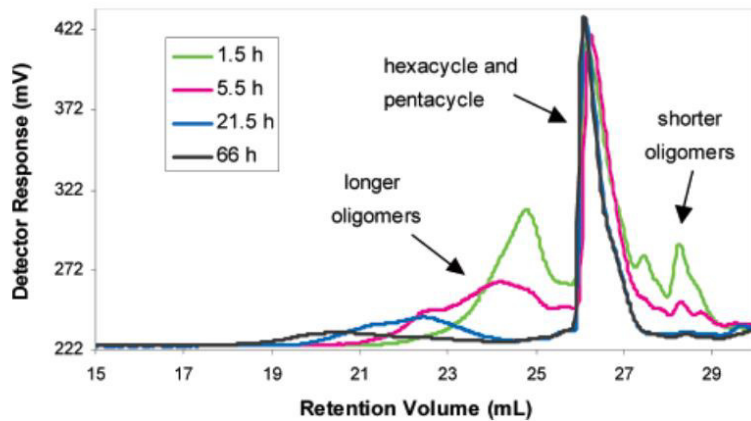
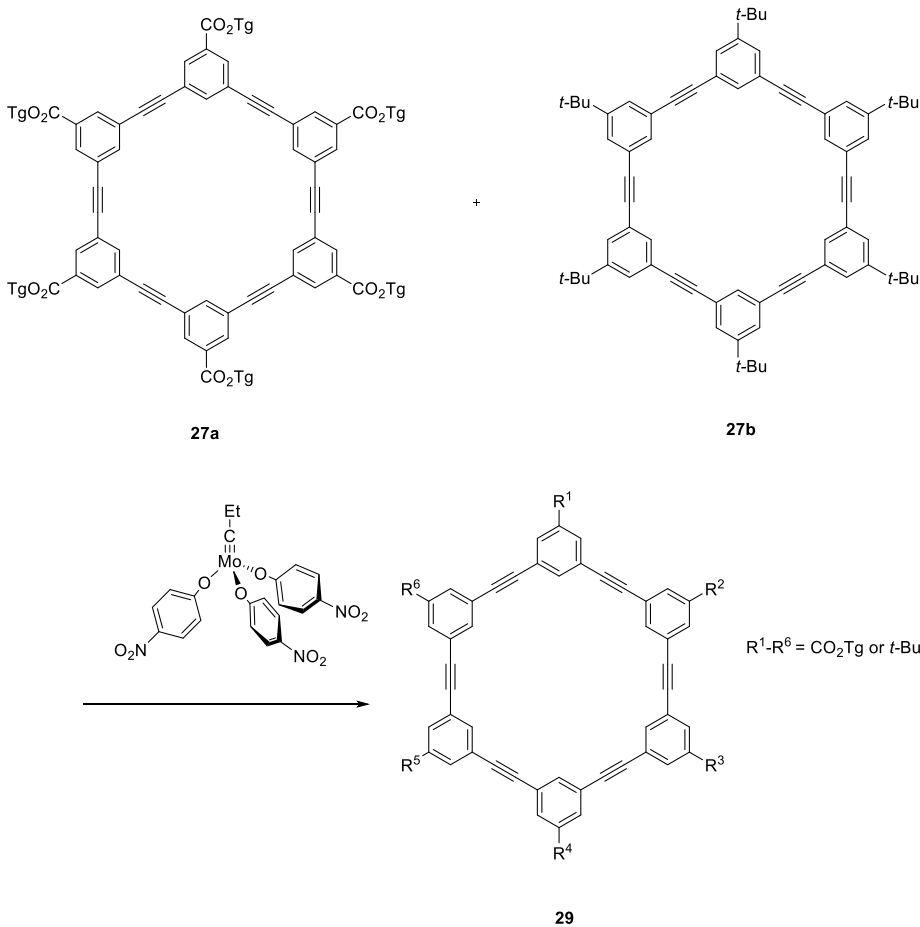


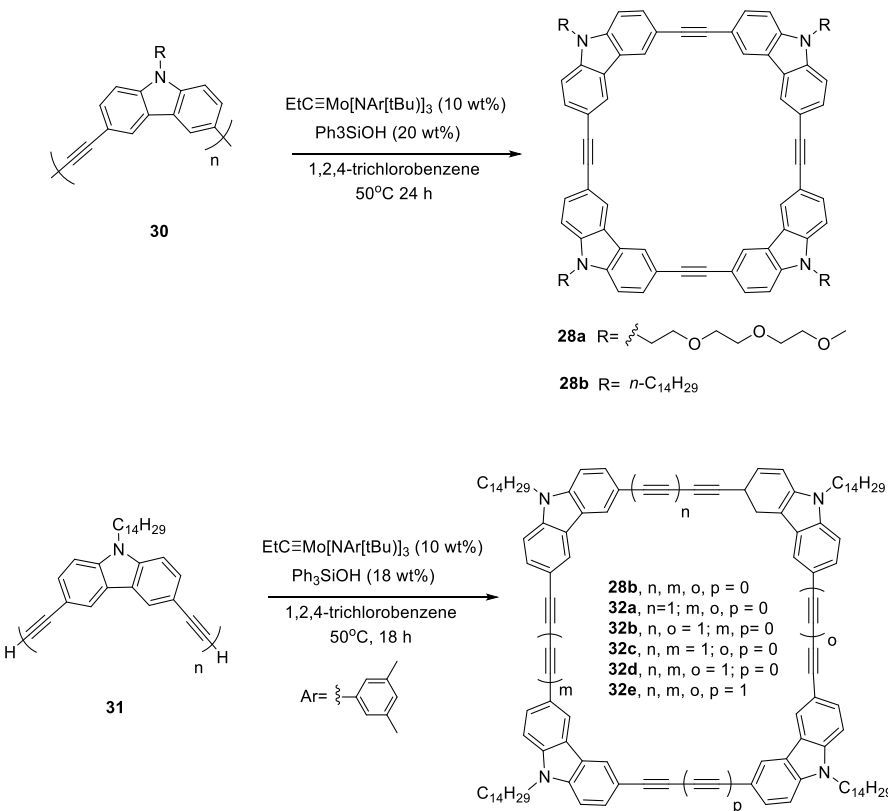
Figure 1.2. Time course of macrocycle formation of **27a** through alkyne metathesis monitored by GPC data.



Scheme 1.10. Scrambling experiment of **27a** and **27b**.

Very recently, Moore and coworkers developed so-called depolymerization-macrocyclization method to synthesize AEMs from polymers through alkyne metathesis.³³⁻³⁶ The advantage of depolymerization-macrocyclization is to avoid using not very atom-economic precipitation driven method to drive the alkyne metathesis to completion. They studied the depolymerization from both carbazolylethynylene polymers and carbazolylbutadiyne polymers. Unsurprisingly both cases showed low molecular weight species formed in high yields. From the carbazolylethynylene polymers as starting polymers, single species AEM **28** was formed, which is the same product as starting from diaryle carbazole monomers. Interestingly, the metathesis products starting from carbazolylbutadiyne polymers were mixtures of macrocycles **28** and **32**.

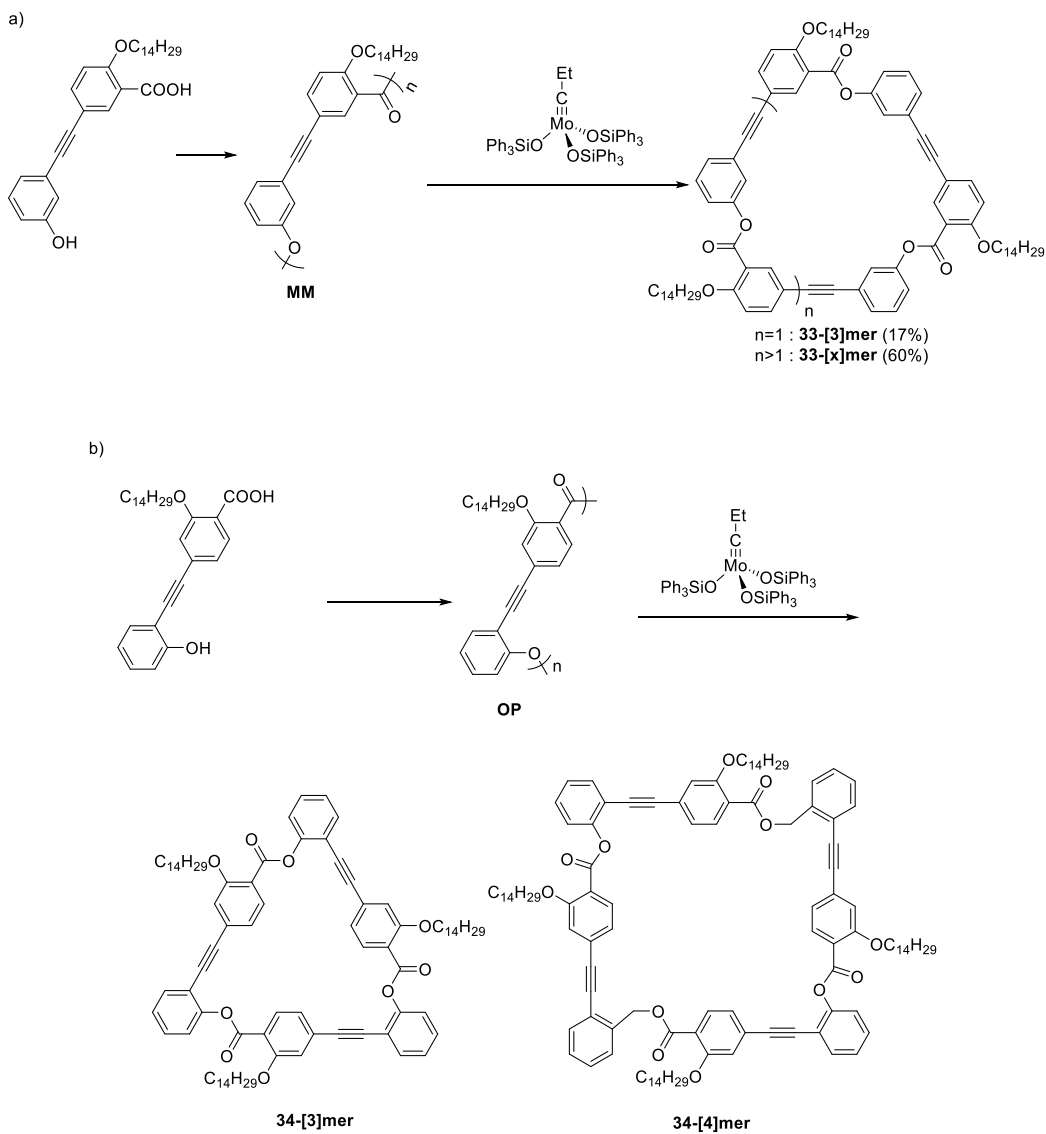
with different numbers of diyne incorporated which was observed on MALDI-MS. This observation can be easily rationalized by little free energy differences between these macrocycles.



Scheme 1.12. Synthesis of **28** and **32** using depolymerization-macrocyclization of carbazolylethyne and carbazolylbutadiyne polymers.

Later the Moore group conducted another interesting study showing that, by using more flexible, directional-defining ester linker polymers **MM** and **OP**, the nondirectional alkyne macrocycles distributions via alkyne metathesis are highly related to the relative position of alkyne bond and ester group. The products from polymer **MM** after metathesis showed a wide product distribution, macrocycles **33-[x]mer** with the number of building blocks from 3-8. In great contrast, from polymers **OP**, the product distribution was much narrower, showing only 3 and 4 building blocks in one macrocycle **34-[x]mer**. Among all the AEMs, the esters' direction varies in the **33-[x]mer**, because *meta*-substitution alkynes on both sides of ester group gave no

energy difference on all possible AEMs. For comparation, the *ortho*- and *para*- substituted alkynes on two sides of one ester group show dramatic energy difference on different macrocycles, thus only resulting in two possible macrocycles.³⁵ This study provided some insight into how the geometries, shapes, and degrees of freedom affect the product distributions through dynamic covalent chemistry, and could guide future rational design of 2-D macrocycles.



Scheme 1.13. Synthesis of **33** and **34** from polymer **MM** and **OP** using depolymerization-macrocyclization method.

1.2.2.2. Alkyne metathesis applications in the synthesis of 3-D shape-persistent molecular cages

In recent years, discrete 3-D organic cage molecules have attracted great attention due to their unique properties and wide applications.³⁷ With their intrinsic porosity, shape-persistent cage compounds have been studied in gas adsorption, gas separation (e.g., CO₂/N₂ or CO₂/CH₄ separation)³⁸⁻⁴⁰, guest recognition⁴¹⁻⁴⁴, as well as molecular “flasks”⁴⁵. Moreover, their great potential in newly explored applications such as catalysis and drug delivery is highly attractive.

However, nowadays, most commonly used dynamic metathesis reactions for organic cage molecules are imine condensation/metathesis^{38-41,46} and boronic acid and diol condensation^{43,47}. Alkyne metathesis, which has been successfully utilized in synthesis of 2-D shape-persistent macrocycles, has not been fully explored in synthesizing 3-D molecular cages. Only until very recently, the Zhang group further expanded the application of alkyne metathesis to the field of 3-D organic cage synthesis.^{42,44} In order to sufficiently synthesize 3-D cages, highly active catalysts are desired, because during the reaction process, long cross-linked oligomers will form in the early stage in light of the previous study of 2-D macrocycle synthesis, and to form the most thermodynamic favored product, extensive bond breaking and formation is needed. For the first time, the Zhang group designed and synthesized a shape-persistent rectangular prism molecular cage by using precipitation-driven alkyne metathesis and with high yield. This porphyrin-based molecular cage shows over 1000 times selectivity with fullerenes C₇₀ over C₆₀. The computational modeling showed that the height of the cage only decreased slightly comparing with the fullerene bound cage, indicating that the ethynylene-linked cage is highly shape-persistent.⁴² In the follow-up study, a two arm porphyrin-based macrocycle showed higher fullerene binding with C₈₄ vs C₇₀. It was observed that in the solution phase, this macrocycle tended to collapse (supported by variable-temperature NMR experiments) and in the presence of

guest molecules, the cages expanded to adapt the guests.⁴⁴ These results clearly showed that this macrocycle has more adapted size and favored to bind larger fullerenes.

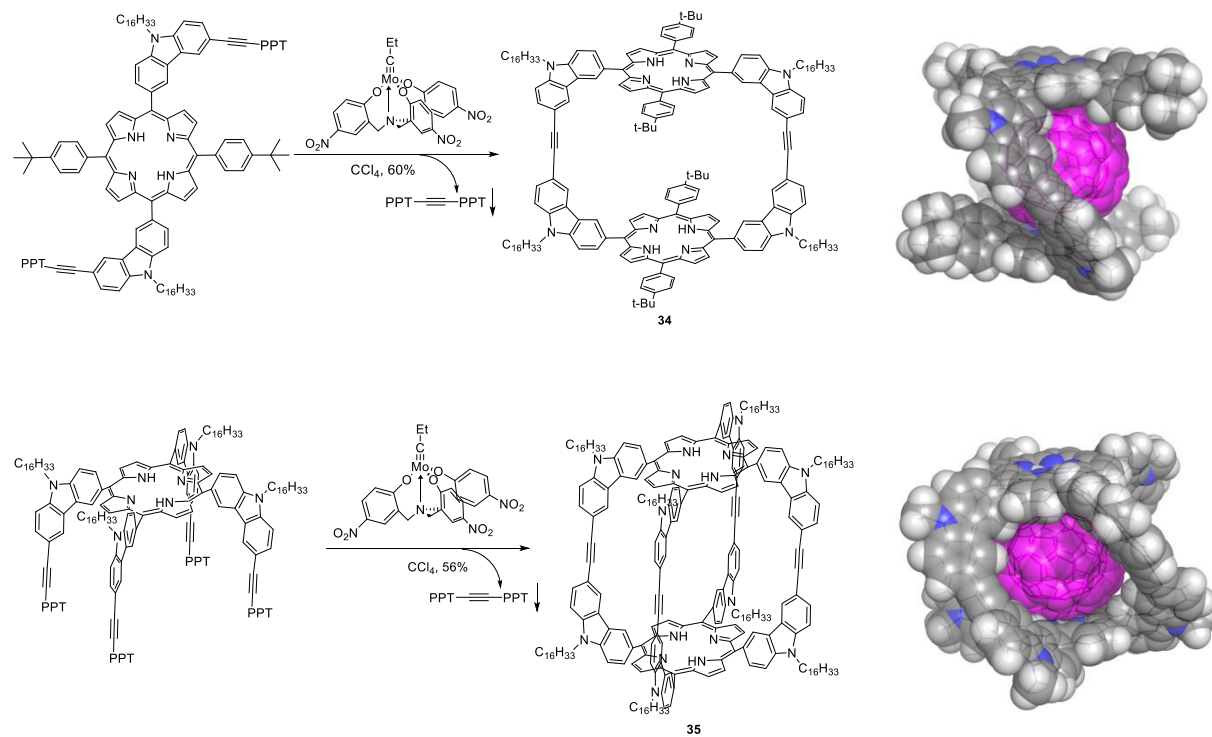


Figure 1.3. Synthesis of porphyrin-based macrocycle **34** and cage **35** and their molecular models of C₈₄@**34** and C₇₀@**35**.

Table 1.2. The association constants of **34**, **35** with different fullerenes.

	$K_{C_{60}} (M^{-1})$	$K_{C_{70}} (M^{-1})$	$K_{C_{84}} (M^{-1})$
34	1.3×10^4	2.0×10^6	2.2×10^7
35	1.4×10^5	1.5×10^8	2.4×10^7

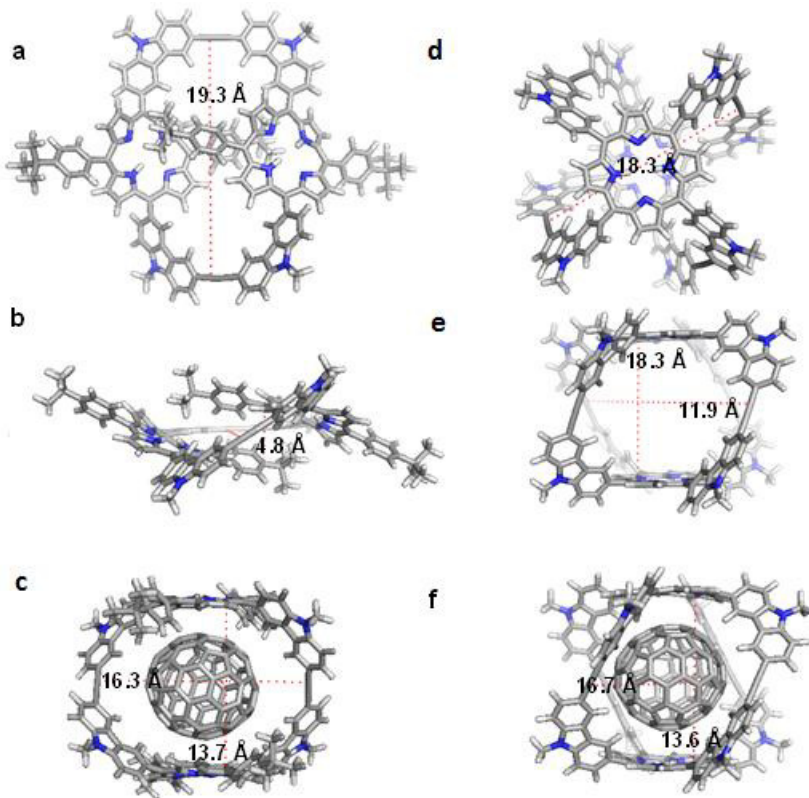


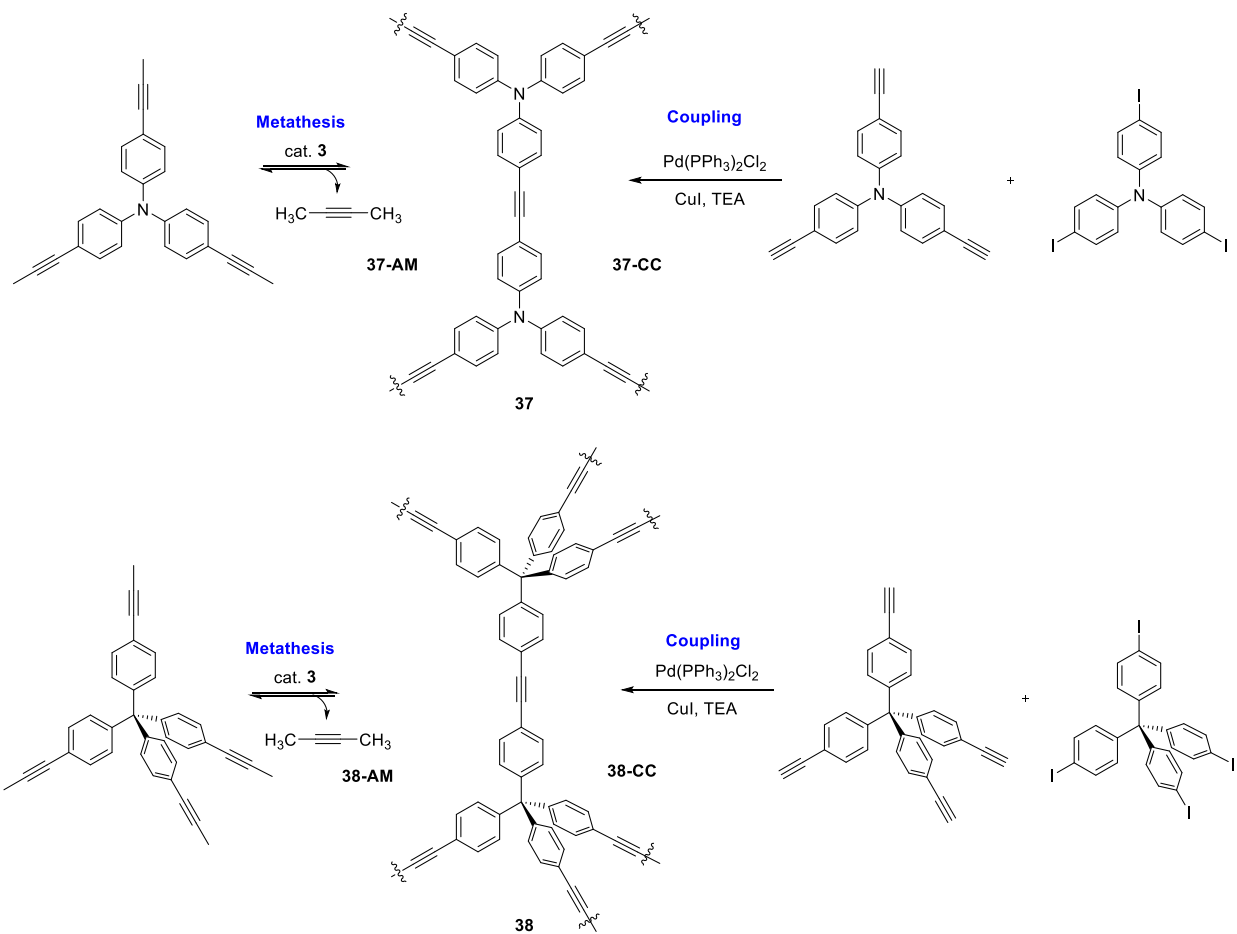
Figure 1.4. Molecular modeling of free **34** and **35** and $\text{C}_{84}@\text{34}$ and $\text{C}_{70}@\text{35}$. a, top view of free **34**; b, side view of free **34**; c, side view of $\text{C}_{84}@\text{34}$; d, top view of free **35**; e, side view of free **35**; f, side view of $\text{C}_{60}@\text{35}$.

1.2.2.3. Alkyne metathesis applications in the synthesis of poly(aryleneethynylene) networks.

There has been growing interest in purely organic porous materials over the past one decade because of their widespread applications in gas adsorption/separation, molecular recognition and so forth. The purely organic porous materials are generally constituted of C, H, O, N, B atoms with covalent bonds. The covalent organic frameworks (COFs) are great candidates for gas adsorption because of their high Brunauer–Emmett–Teller (BET) surface areas and low density. DC_vC, such as imine condensation/metathesis, boronic acid-diol condensation^{48–51} and boronic acid condensation^{51–52}, was utilized in synthesizing COFs. Under

reversible conditions, the materials can undergo “self-correction” mechanism so that the defects in the materials can be minimized to obtain more ordered structures.

Alkyne bond, considered as a robust and shape-persistent covalent bond, has great potentials in construction of COFs. Recently the Zhang group has explored the poly(aryleneethynylene) (PAE) network synthesis using alkyne metathesis for the first time and studied the materials performance difference between PAE synthesized via alkyne metathesis vs. Sonogashira coupling reactions.⁵³ The designed 2-D polymer and 3-D framework were synthesized using these two different methods and at three different temperatures for comparison. The PAEs synthesized from alkyne metathesis from 3 different temperatures all showed higher BET surface areas than that synthesized from irreversible Sonogashira coupling reactions. Although the researchers did not observe the crystallinity of the PEAs, the higher pore size analysis showed that the pore size of PEAs through alkyne metathesis is more uniformed. This finding proved that the reversibility of alkyne metathesis helped forming more ordered materials.



Scheme 1.14. Synthetic scheme of frameworks **37** and **38** using alkyne metathesis or cross coupling.

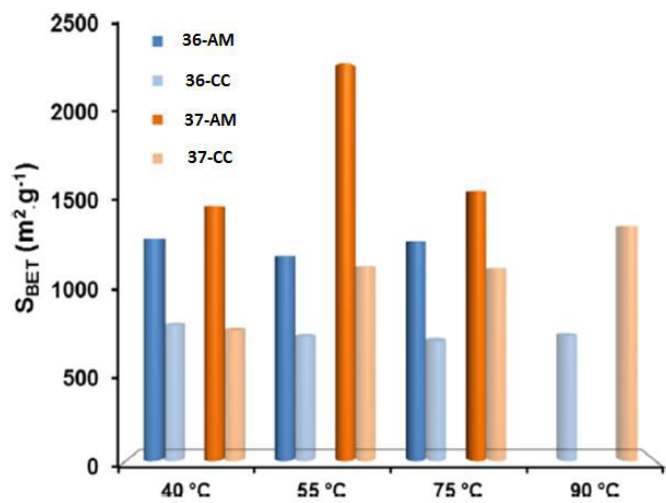


Figure 1.15. Comparation of BET surface areas of frameworks **37-AM**, **37-CC**, **38-AM** and **38-CC** synthesized using reversible alkyne metathesis or irreversible cross coupling at different temperatures.

1.3. Conclusion and Perspectives.

Alkyne metathesis has only been studied intensively recently. Great efforts have been invested in design of high activity, broadening functional groups tolerance and user friendly catalysts. Also living alkyne polymerization has achieved great success recently although it is quite monomer-dependent. It has been used in natural products, conjugated polymer synthesis. By utilizing the dynamic feature of metathesis, the synthetic difficulty of well-defined 2-D macrocycles and 3-D cage molecules were dramatically decreased. The reversibility was proved to be an important factor to synthesize more ordered structures and improve the BET surface areas of covalent organic frameworks. The rigidity and stability of alkyne bond helps resisting the collapse of hollow molecules. Thus the 2-D and 3-D frameworks built from ethynlenes showed high surface areas.

Well-defined 2-D, 3-D porous materials have potential applications in gas adsorption/separation, drug delivery, sensing, *etc.* Until now, only one paper of 3-D organic cage and one literature about 2-D and 3-D COFs synthesized through alkyne metathesis were reported. This area is still in its infant stage. Without the limitation of catalyst activity, scientists will be able to utilize alkyne metathesis to develop more 3-D organic architectures in the future.

1.4. References

1. Pennella, F.; Banks, R. L.; Bailey, G. C. *Chem. Commun.* **1968**, 1548.
2. Wengrovius, J. H.; Sancho, J.; Schrock, R. R. *J. Am. Chem. Soc.* **1981**, *103*, 3932-3934.
3. Pedersen, S. F.; Schrock, R. R.; Churchill, M. R.; Wasserman, H. J. *J. Am. Chem. Soc.* **1982**, *104*, 6808-6809.
4. Schrock, R. R. *Acc. Chem. Res.* **1986**, *19*, 342-348.
5. Schrock, R. R. *Chem. Rev.* **2002**, *102*, 145-179.
6. Zhang, W.; Kraft, S.; Moore, J. S. *J. Am. Chem. Soc.* **2004**, *126*, 329-335.

7. Jyothish, K.; Zhang, W. *Angew. Chem. Int. Ed.* **2011**, *50*, 3435-3438.
8. Jyothish, K.; Wang, Q.; Zhang, W. *Adv. Synth. Catal.* **2012**, *354*, 2073-2078.
9. Yang, H. S.; Liu, Z. N.; Zhang, W. *Adv. Synth. Catal.* **2013**, *355*, 885-890.
10. Bindl, M.; Stade, R.; Heilmann, E. K.; Picot, A.; Goddard, R.; Furstner, A. *J. Am. Chem. Soc.* **2009**, *131*, 9468-9470.
11. Heppekausen, J.; Stade, R.; Goddard, R.; Furstner, A. *J. Am. Chem. Soc.* **2010**, *132*, 11045-11057.
12. Prunet, J. *Eur. J. Org. Chem.* **2011**, 3634-3647.
13. Bunz, U. H. F. *Chem. Rev.* **2000**, *100*, 1605-1644.
14. Thomas, S. W.; Joly, G. D.; Swager, T. M. *Chem. Rev.* **2007**, *107*, 1339-1386.
15. Zhu, C. L.; Liu, L. B.; Yang, Q.; Lv, F. T.; Wang, S. *Chem. Rev.* **2012**, *112*, 4687-4735.
16. Goodson, F. E.; Wallow, T. I.; Novak, B. M. *J. Am. Chem. Soc.* **1997**, *119*, 12441-12453.
17. Weiss, K.; Michel, A.; Auth, E. M.; Bunz, U. H. F.; Mangel, T.; Mullen, K. *Angew. Chem. Int. Ed.* **1997**, *36*, 506-509.
18. Kloppenburg, L.; Song, D.; Bunz, U. H. F. *J. Am. Chem. Soc.* **1998**, *120*, 7973-7974.
19. Hu, K. D.; Yang, H. S.; Zhang, W.; Qin, Y. *Chem. Sci.* **2013**, *4*, 3649-3653.
20. Chen, X. Q.; Zhou, G. D.; Peng, X. J.; Yoon, J. *Chem. Soc. Rev.* **2012**, *41*, 4610-4630.
21. Jelinek, R.; Ritenberg, M. *Rsc Adv.* **2013**, *3*, 21192-21201.
22. Krouse, S. A.; Schrock, R. R.; Cohen, R. E. *Macromolecules* **1987**, *20*, 903-904.
23. Krouse, S. A.; Schrock, R. R. *Macromolecules* **1989**, *22*, 2569-2576.
24. Sedbrook, D. F.; Paley, D. W.; Steigerwald, M. L.; Nuckolls, C.; Fischer, F. R. *Macromolecules* **2012**, *45*, 5040-5044.
25. Paley, D. W.; Sedbrook, D. F.; Decatur, J.; Fischer, F. R.; Steigerwald, M. L.; Nuckolls, C. *Angew. Chem. Int. Ed.* **2013**, *52*, 4591-4594.
26. Staab, H. A.; Neunhoef. *K Synthesis-Stuttgart* **1974**, 424-424.
27. Ge, P. H.; Fu, W.; Herrmann, W. A.; Herdtweck, E.; Campana, C.; Adams, R. D.; Bunz, U. H. F. *Angew. Chem. Int. Ed.* **2000**, *39*, 3607-3610.
28. Miljanic, O. S.; Vollhardt, K. P. C.; Whitener, G. D. *Synlett* **2003**, 29-34.
29. Zhang, W.; Moore, J. S. *J. Am. Chem. Soc.* **2004**, *126*, 12796-12796.

30. Zhang, W.; Brombosz, S. M.; Mendoza, J. L.; Moore, J. S. *J. Org. Chem.* **2005**, *70*, 10198-10201.
31. Zhang, W.; Moore, J. S. *J. Am. Chem. Soc.* **2005**, *127*, 11863-11870.
32. Zhang, W.; Moore, J. S. *Angew. Chem. Int. Ed.* **2006**, *45*, 4416-4439.
33. Gross, D. E.; Moore, J. S. *Macromolecules* **2011**, *44*, 3685-3687.
34. Gross, D. E.; Discekici, E.; Moore, J. S. *Chem. Commun.* **2012**, *48*, 4426-4428.
35. Sisco, S. W.; Moore, J. S. *J. Am. Chem. Soc.* **2012**, *134*, 9114-9117.
36. Sisco, S. W.; Moore, J. S. *Chem. Sci.* **2014**, *5*, 81-85.
37. Mastalerz, M. *Angew. Chem. Int. Ed.* **2010**, *49*, 5042-5053.
38. Jin, Y. H.; Voss, B. A.; Jin, A.; Long, H.; Noble, R. D.; Zhang, W. *J. Am. Chem. Soc.* **2011**, *133*, 6650-6658.
39. Mastalerz, M.; Schneider, M. W.; Oppel, I. M.; Presly, O. *Angew. Chem. Int. Ed.* **2011**, *50*, 1046-1051.
40. Tozawa, T.; Jones, J. T. A.; Swamy, S. I.; Jiang, S.; Adams, D. J.; Shakespeare, S.; Clowes, R.; Bradshaw, D.; Hasell, T.; Chong, S. Y.; Tang, C.; Thompson, S.; Parker, J.; Trewin, A.; Bacsa, J.; Slawin, A. M. Z.; Steiner, A.; Cooper, A. I. *Nat. Mater.* **2009**, *8*, 973-978.
41. Francesconi, O.; Ienco, A.; Moneti, G.; Nativi, C.; Roelens, S. *Angew. Chem. Int. Ed.* **2006**, *45*, 6693-6696.
42. Zhang, C. X.; Wang, Q.; Long, H.; Zhang, W. *J. Am. Chem. Soc.* **2011**, *133*, 20995-21001.
43. Nishimura, N.; Kobayashi, K. *Angew. Chem. Int. Ed.* **2008**, *47*, 6255-6258.
44. Zhang, C. X.; Long, H.; Zhang, W. *Chem. Commun.* **2012**, *48*, 6172-6174.
45. McCaffrey, R.; Long, H.; Jin, Y.; Sanders, A.; Park, W.; Zhang, W. *J. Am. Chem. Soc.* **2014**, *136*, 1782-1785.
46. Jiang, S.; Jones, J. T. A.; Hasell, T.; Blythe, C. E.; Adams, D. J.; Trewin, A.; Cooper, A. I. *Nat. Commun.* **2011**, *2*.
47. Nishimura, N.; Yoza, K.; Kobayashi, K. *J. Am. Chem. Soc.* **2010**, *132*, 777-790.
48. El-Kaderi, H. M.; Hunt, J. R.; Mendoza-Cortes, J. L.; Cote, A. P.; Taylor, R. E.; O'Keeffe, M.; Yaghi, O. M. *Science* **2007**, *316*, 268-272.
49. Han, S. S.; Furukawa, H.; Yaghi, O. M.; Goddard, W. A. *J. Am. Chem. Soc.* **2008**, *130*, 11580-11581.
50. Wan, S.; Guo, J.; Kim, J.; Ihee, H.; Jiang, D. L. *Angew. Chem. Int. Ed.* **2008**, *47*, 8826-8830.

51. Furukawa, H.; Yaghi, O. M. *J. Am. Chem. Soc.* **2009**, *131*, 8875-8883.
52. Cote, A. P.; Benin, A. I.; Ockwig, N. W.; O'Keeffe, M.; Matzger, A. J.; Yaghi, O. M. *Science* **2005**, *310*, 1166-1170.
53. Zhu, Y. L.; Yang, H. S.; Jin, Y. H.; Zhang, W. *Chem. Mater.* **2013**, *25*, 3718-3723.

CHAPTER 2

Tetrameric Cage with an Unexpected D_{2h} Symmetry through Alkyne Metathesis

(Manuscript was submitted under the same title, co-authored with Zhang, C. X.; Noll, B. C.; Long, H.; Jin, Y., and Zhang, W.)

2.1. Abstract

Shape-persistent covalent organic polyhedrons (COPs) with ethynylene linkers are usually prepared through kinetically controlled cross-coupling reactions. Herein, we report high-yielding synthesis of ethynylene-linked rigid tetrameric cages via one-step alkyne metathesis from readily accessible triyne precursors. The tetrameric cage contains two macrocyclic panels and exhibits unique D_{2h} symmetry. The assembly of such a COP is a thermodynamically controlled process, which involves the initial formation of macrocycles as key intermediates followed by the connection of two macrocycles with ethynylene linkages. With a large internal cavity, the cage exhibits a high binding selectivity toward C₇₀ ($K = 3.9 \times 10^3$ L·mol⁻¹) over C₆₀ (no noticeable binding).

2.2. Introduction

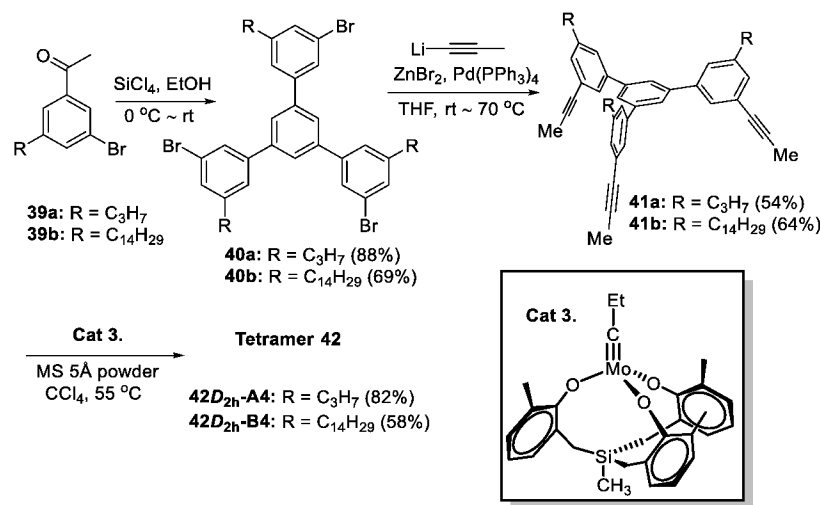
In recent years, discrete purely organic cage molecules, i.e. covalent organic polyhedrons (COPs) have attracted great attention due to their unique properties and interesting applications in gas adsorption/separation,¹⁻⁵ host-guest recognition⁶⁻¹¹ and as molecular “flasks”.¹²⁻¹³ Moreover, their great potential in emerging applications such as catalysis and drug delivery is highly attractive. Recent advances in dynamic covalent chemistry (DC_vC) have provided powerful thermodynamically controlled approaches towards COPs.¹⁴⁻¹⁸ Most COPs reported so far are assembled through dynamic imine chemistry or boronic acid condensation.^{16,19-21} Although these COPs have shown intriguing applications in chemistry and materials science, imine or B-O linkages are susceptible to hydrolysis in the presence of acid, base or even moisture,²²⁻²³ which leads to the decomposition of COPs and represents a potential drawback for certain applications. In this regard, COPs with more robust ethynylene linkages have attracted our attention. Besides the rigidity and high chemical and thermal stability, ethynylene linkages can enable electron conjugation if needed, which would be a valuable feature for electrical, optical, and sensing applications. To date, ethynylene-linked COPs have generally been prepared through Sonogashira, or Glaser-type coupling.²⁴⁻³¹ As coupling reactions are kinetically controlled, the target molecular cages are oftentimes obtained in low yields along with a large amount of oligomeric or polymeric side products. High-dilution (or pseudo high dilution) conditions with a large excess of catalysts are usually applied to minimize the “over-shooting” problem, however, with limited success. Alternatively, templates have been used to preorganize the monomers and direct the syntheses of nanorings or rotaxanes and cantenanes.³²⁻³⁵ Herein, we report template-free, dynamic covalent assembly of a purely hydrocarbon molecular cage through one-step alkyne metathesis. The tetrameric cage consists of two macrocyclic panels and

exhibits an unexpected D_{2h} symmetry. With a large internal cavity, the cage molecule serves as a fullerene receptor and shows a high binding selectivity for C₇₀ over C₆₀.

2.3. Results and discussion

Alkyne metathesis³⁶⁻³⁹ has emerged as an alternative viable dynamic covalent reaction. It has been widely practiced in the synthesis of natural products,^{37,40} shape-persistent macrocycles,⁴¹⁻⁴⁴ and polymers.⁴⁵⁻⁵⁰ However, only recently has alkyne metathesis been applied to more challenging COP synthesis which involves innumerable possible oligomeric and polymeric intermediates along the pathway to the target COP. In 2011, we reported the first application of dynamic alkyne metathesis in the synthesis of an ethynylene-linked shape-persistent rectangular prism.¹⁰ In our previous study, (benzoyldiphenyl)acetylene moiety had to be installed in the monomer unit to drive the equilibrium to the cage product by precipitation of bis(benzoylbiphenyl)acetylene byproducts. However, installation of the precipitating groups in the monomer requires additional synthetic steps, and their poor solubility causes difficult monomer purification and premature precipitation of oligomeric intermediates. Recently, we have developed triphenolsilane-based alkyne metathesis catalysts that are compatible with 5 Å molecular sieves, scavengers of small alkyne byproducts, e.g. 2-butyne.⁴⁴ In the presence of molecular sieves, simple propynyl substituted monomers can undergo alkyne metathesis with high conversion in a closed system using triphenolsilane-based catalysts. Therefore, in this study, simple triyne **41a** and **41b** are designed as the monomers of the tetrahedron-shaped tetrameric COP **42T_d** (Figure 2.1a). Compounds **41a** and **41b** are C_3 -symmetric with an edge-face angle of 60.0° which closely matches the edge-face angle of a tetrahedron (54.7°). The syntheses of **41a** and **41b** are straightforward starting from readily available acetyl benzene **39a** and **39b**. SiCl₄ catalyzed condensation reaction followed by Negishi coupling afforded **41a** and **41b** in good

overall yields. The alkyne metathesis of monomer **41a**/**41b** (27 mM) was then conducted at 55 °C for 16 h using triphenolsilane molybdenum alkylidene catalyst **3** (1 mol% per propyne moiety). GPC analysis of the crude product mixture showed the predominant formation of a single species. The metathesis products were obtained in good isolated yields and characterized by 1D ¹H, and ¹³C NMR, gCOSY, ROESY, GPC, and MALDI-TOF MS.



Scheme 2.1. Synthesis of tetrameric cage **42**.

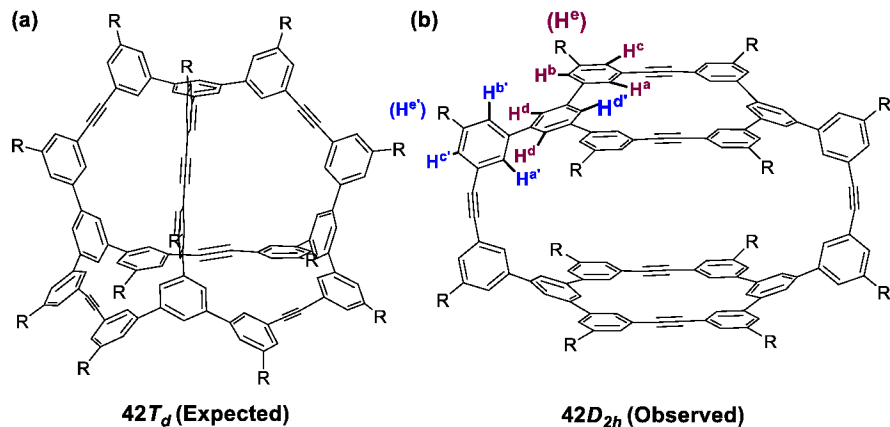


Figure 2.1. (a) Expected structure of tetramer **42T_d** with T_d symmetry; (b) Observed structure of tetramer **42D_{2h}** with D_{2h} symmetry.

As expected, MALDI-TOF MS of the metathesis product ($\text{R} = \text{C}_3\text{H}_7$) showed a strong signal at $m/z=1863$ (Figure 2.9), which corresponds to a tetramer. However, surprisingly, ¹H

NMR spectrum of the tetramer showed splitting of each set of originally chemically equivalent protons of the monomer unit into two signals in 2:1 ratio (total eight sets of aromatic proton signals, Figure 2.3i). This is inconsistent with the expected highly symmetrical tetrahedral structure **42T_d** (Figure 2.1a), which should show only four sets of aromatic proton signals. We excluded the possibility of two dimeric cages being interlocked, since (1) the dimeric cage of **41a** (or **41b**) would be highly strained and disfavored; (2) we did not observe any dimer species in the MALDI-MS; (3) The ¹H NMR spectra of the cage product at various temperatures consistently show sharp and distinct signals rather than broad and complicated ones. The tetrameric cage **42D_{2h}** (Figure 2.1b) with *D_{2h}* symmetry was then proposed, in which two macrocycle panels are connected by two diphenylacetylene side arms. This structure gives rise to the splitting of the three arms of a monomer into two types: two identical arms forming the macrocyclic panel with another monomer and a third arm bridging two macrocycles to form a cage. This agrees with the observed 2:1 ratio of two signals for each set of originally chemically equivalent protons of the monomer unit in ¹H NMR spectra of **42D_{2h}-A4** and **42D_{2h}-B4**.

The structure **42D_{2h}** was unambiguously determined by single crystal X-ray diffraction (Figure 2.2). Needle-like single crystals of **42D_{2h}-A4** were obtained through slow evaporation from a solution of **42D_{2h}-A4** in CH₂Cl₂ and acetonitrile co-solvent. **42D_{2h}-A4** was crystallized in the monoclinic space group *P12₁/c1*. It has been a challenge to obtain crystal structures of pure hydrocarbon cages due to their sensitivity to solvent loss and the easy collapse of the crystals.²⁴ After multiple failed trials, we finally succeeded in determining the structure and packing of the cage **42D_{2h}-A4** albeit with weak X-ray diffraction. The two macrocyclic panels (top and bottom of the cage) are slightly puckered and oriented in a slipped stack fashion relative to each other with the distance of 9.1 Å between them (Figure 2.2a, 2.2c). Two biphenyl acetylene arms

bridge the two panels with the face-to-edge angle of 49.4° , resulting in overall Z-shape geometry of the cage (Figure 2.2b). The dimension of the cage interior at the widest point is 19.4 Å. The packing structure shows that there are two stacks of parallel cages that are arranged at an angle of 141.7° to each other (Figure 2.2d, 2.2f). There is no connectivity between the cavities of the cages. The interior cavity of each cage is filled with one disordered acetonitrile molecule, and two propyl groups from the two neighboring cages. We did not observe any inter/intramolecular $\pi\text{-}\pi$ interactions. Due to the absence of functional groups with directing capability, the van der Waals interactions between neighboring molecules and C-H $\cdots\pi$ interactions between propyl chain and aromatic moieties appear to be the major forces to direct the crystal packing of the cage. This represents one of few purely hydrocarbon cage crystal structures.

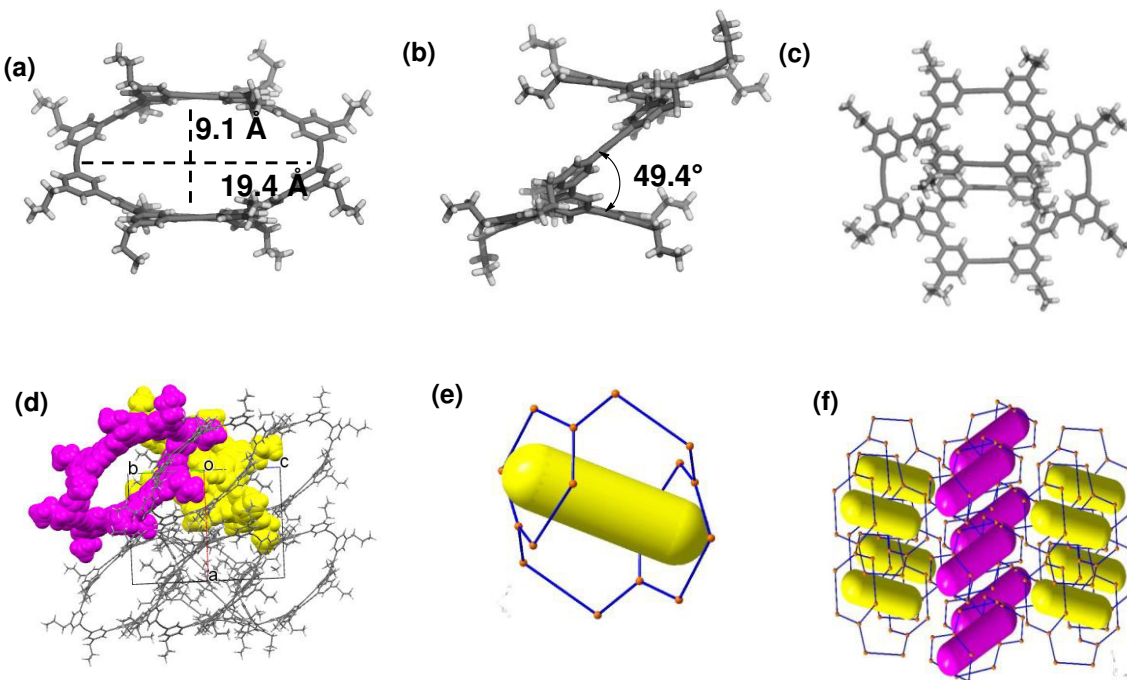


Figure 2.2. Crystal structure of **42D_{2h}-A4**: (a) Side view 1; (b) Side view 2; (c) Top view; (d) Crystal packing views along (011) direction; (e) Simplified view of **42D_{2h}-A4**; (f) Simplified view of the crystal packing, the two stacks of the cages oriented differently are color coded in yellow and magenta. Solvent molecules are omitted for clarification.

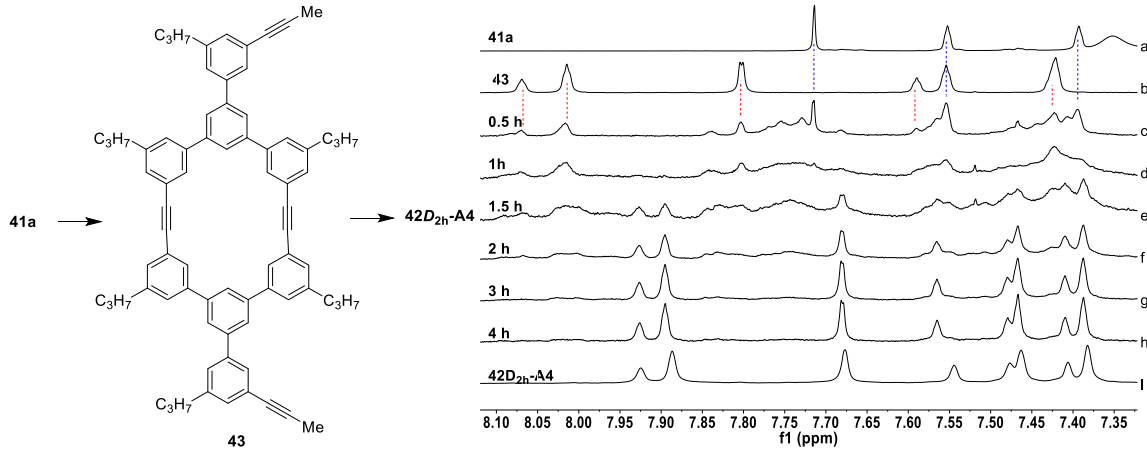
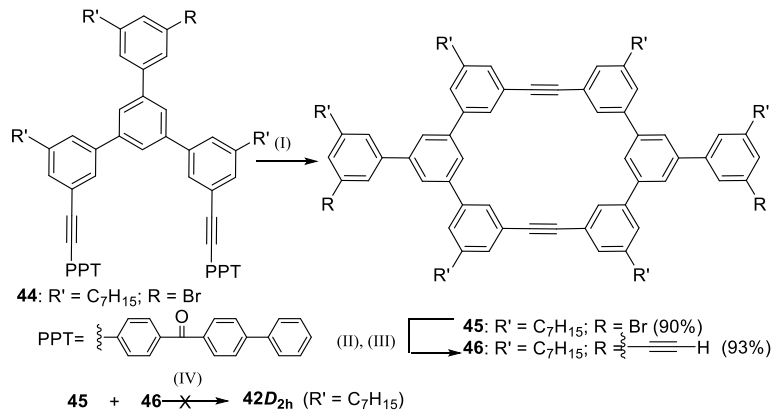


Figure 2.3. ¹H NMR spectra of monomer **41a** (a); Authentic sample of macrocyclic intermediate **43** (b); crude mixture after 0.5-4 h (c-h); cage product **42D_{2h}-A4** (i), in CDCl₃.

The formation of tetramer **42D_{2h}-A4** is quite unexpected. In order to gain better understanding of the cage formation process, we monitored the reaction progress. Aliquots of the reaction mixture were withdrawn at different time intervals, and analyzed by GPC and ¹H NMR spectroscopy. The GPC traces showed the initial formation of high molecular weight oligomers and their gradual conversion to **42D_{2h}-A4** (Figure 2.10). A closer look at the process through ¹H NMR data analysis revealed the initial conversion of monomer **41a** to a substantial amount of macrocycle **43** within 0.5 h (Figure 3). The authentic sample of macrocycle **43** was obtained by conducting alkyne metathesis of monomer **41a** in a closed system in the absence of molecular sieves that are typically used to scavenge 2-butyne byproduct. After stirring at 55 °C for 1 h, macrocycle **43** was isolated in 22% yield, together with unreacted monomer **41a**. This experiment supports the notion that the macrocycle **43** is present in a significant amount as a key intermediate during the formation of cage **42D_{2h}-A4**. The formation of a tetramer with *D_{2h}* symmetry is therefore likely guided by the initial predominant formation of macrocyclic panels (face-directed) rather than by the geometrical angle of the monomer arms (edge-directed). Intrigued by this observation, we attempted to prepare cage **42D_{2h}** (*R* = *n*-C₇H₁₅) through

kinetically controlled cross-coupling of two macrocyclic building blocks **45** and **46** (Scheme 2.2). Macrocycle **45** was obtained in excellent isolated yield (90%) through alkyne metathesis of compound **44**. This indicates the formation of **45** is a thermodynamically favored process and no significant angle strain is involved, further supporting the possibility that macrocyclic species **43** forms first and directs the assembly of **4D_{2h}**. Complementary macrocyclic building block **46** was then obtained via Sonogashira coupling of 8 with trimethylsilyl acetylene (TMSA) followed by desilylation. Kinetically controlled cross-coupling reactions have played an important role in the construction of well-defined, 2-D and 3-D molecular architectures.^{43,51-52} However, the attempted cross coupling of **45** and **46** failed to yield cage **4D_{2h}** under our tested reaction conditions (details see experimental section). MALDI-TOF MS, GPC and ¹H NMR analyses of the crude product mixtures in multiple trials showed the formation of oligomers and polymers without any noticeable amount of the cage products. More exotic reaction conditions that might lead to the desired cage formation were not further explored.



Scheme 2.2. Synthesis of **42D_{2h}** via kinetic control. (I) cat. **3**, CCl₄, 55 °C, 90%; (II) trimethylsilylacetylene, Pd(PPh₃)₂Cl₂, CuI, piperidine, THF, 80 °C; (III) K₂CO₃, MeOH, PhMe, 4 h, r.t.; (IV) Sonogashira cross-coupling reactions under various conditions.

In order to confirm that the cage **4D_{2h}** is a thermodynamically favored product and its formation is reversible, we conducted the scrambling experiment between **42D_{2h}-A4** and **42D_{2h}**.

B4. A 1:2 mixture of **42D_{2h}-A4** and **42D_{2h}-B4** were subjected to alkyne metathesis (55 °C, CCl₄, 16 h). The GPC trace of the crude reaction mixture showed a new peak with a broad shoulder (Figure 2.4). MALDI-MS of the crude reaction mixture showed all possible scrambled products, **A3B**, **A2B2**, **AB3** together with **A4** and **B4**, indicating that the system is dynamic and the cage **42D_{2h}** is not kinetically trapped.

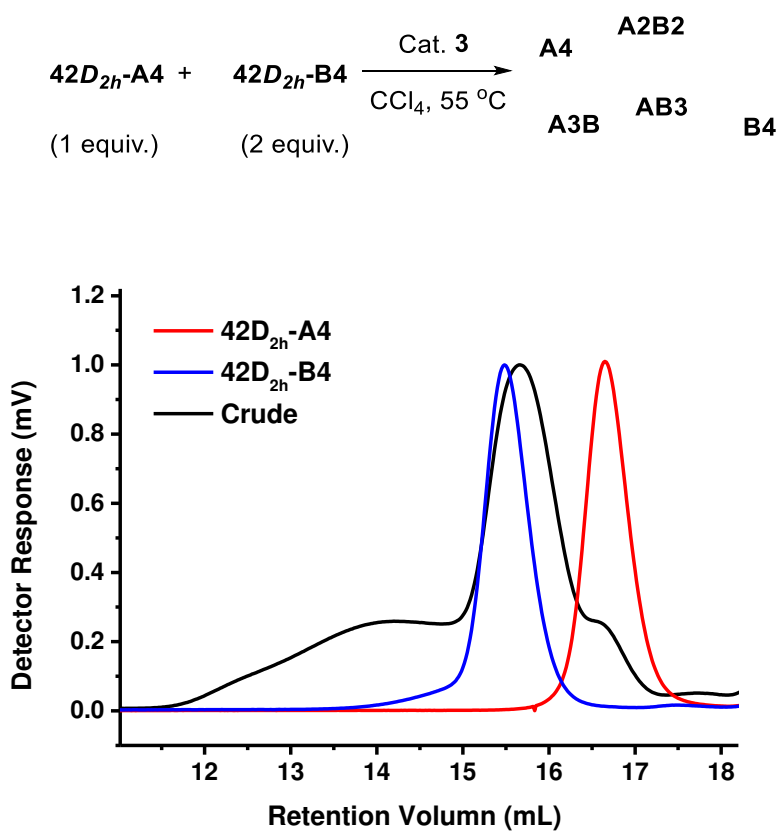


Figure 2.4. The GPC traces of the crude product from the cage scrambling experiment: **42D_{2h} - A4** (red); **42D_{2h} - B4** (blue); the crude mixture (black).

The cage **43D_{2h} - A4** has a large cavity with a distance between the top and bottom panels of ~9.0 Å based on the crystal structure. The shape-persistency and the rigid backbones consisting of aromatic moieties make cage **42D_{2h} - A4** an attractive host for guest molecules, such as fullerenes. In order to investigate the host-guest binding interactions between **42D_{2h} - A4** and

C_{60} or C_{70} , we conducted ^1H NMR titration experiments at 298 K in toluene- d_8 . Interestingly, **42D_{2h}-A4** showed a very weak binding interaction with C_{60} according to the ^1H NMR data obtained from the titration experiment. We did not observe any significant chemical shift changes of the cage protons when the solution of **42D_{2h}-A4** in toluene was titrated with increasing amount of C_{60} up to 6.2 equiv (Figure 2.24a). In contrast, the binding interaction between **42D_{2h}-A4** and C_{70} was evident. The addition of C_{70} (0-8.6 equiv.) to the solution of **42D_{2h}-A4** in toluene induced significant chemical shift changes of the aromatic and aliphatic protons that are in the close proximity to the fullerene guest (Figure 2.5a, Figure 2.24b). The protons H^{a} , $\text{H}^{\text{a}'}$, and H^{d} point toward the cavity and show pronounced upfield shifts upon fullerene binding.

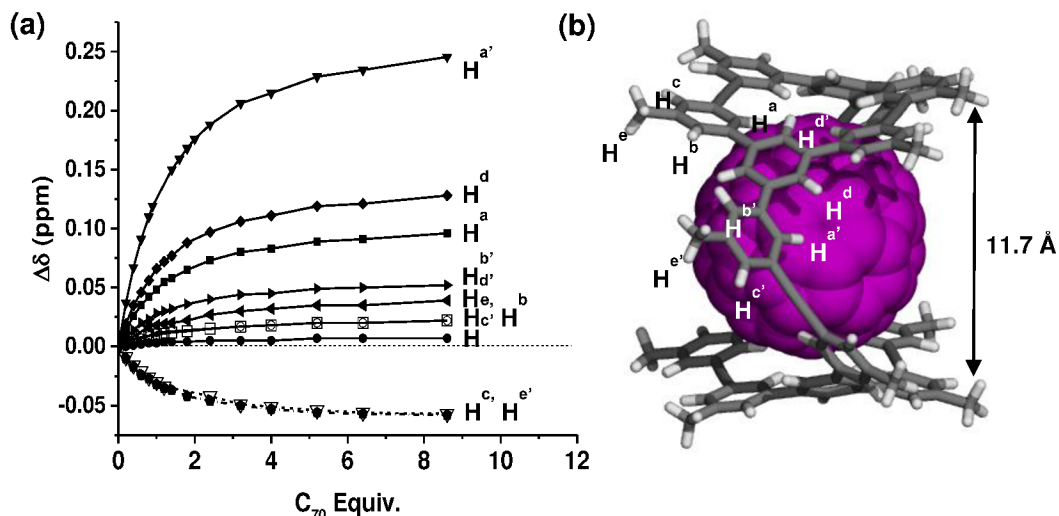


Figure 2.5. (a) The chemical shift changes in ^1H NMR spectra obtained during the titration of **42D_{2h}-A4** (0.14 mM) with increasing amount of C_{70} (0-8.6 equiv.) (b). The computational model (side view) of C_{70} @**42D_{2h}-A4**, Methyl groups are used for simplification. The NMR titrations were conducted in toluene- d_8 .

The $\text{H}^{\text{d}'}$ protons that are located at the inner side of the macrocyclic rings are pushed away from the cavity as the result of the puckered-shape of the macrocycles, leading to the small upfield shift of $\text{H}^{\text{d}'}$ signals upon fullerene binding. Aromatic proton H^{b} and the methylene

protons (H^e) are shielded in the presence of the fullerene guest. Analysis of the Job Plot (Figure 2.23) shows 1:1 binding stoichiometry between C_{70} and the cage **42D_{2h}-A4** with the binding constant of $3.9 \times 10^3 \text{ mol}^{-1}$. The energy-minimized structure of $\text{C}_{70}@\text{42D}_{2h}\text{-A4}$ shows that upon fullerene binding the bottom and top macrocyclic panels become perfectly co-facial rather than the original “slipped” conformation of the empty cage, with an enlarged interpanel distance about 11.7 Å (Figure 2.5b). Based on the computer modeling, the binding energy of **42D_{2h}-A4** with C_{70} is 10 kcal/mol lower than that of binding with C_{60} (-48.7 vs. -38.4 kcal/mol). Presumably C_{70} is bigger and more ellipsoidal than C_{60} , and resembles the shape of the cavity, thus providing a better fit inside the cage and stronger binding interaction.

We also attempted to synthesize the cage **42D_{2h}** with bromo group and methyl groups instead of propyl groups. However the metathesis reaction was not successful, resulting mainly oligomers. We believe that the inefficiency is due to the poor solubility of monomers and oligomer intermediates. Thus during the reaction, oligomers may precipitate out which cannot be further converted to desired cage product.

In conclusion, tetrameric cages **42D_{2h}** with an uncommon D_{2h} symmetry were obtained through one-step alkyne metathesis from readily accessible C_3 symmetrical propynyl-substituted monomers in good yields. The unexpected unique structure of the cage **42D_{2h}-A4** was fully characterized by 1D ^1H , and ^{13}C NMR, gCOSY, ROESY, GPC, MALDI-TOF MS and single crystal X-ray diffraction. The formation of the cage is likely a face-directed dynamic assembly process, which involves the formation of dimeric macrocycle panels as the key intermediates. Our attempts to synthesize the cage **42D_{2h}** through cross-coupling of two macrocyclic building blocks under various reaction conditions failed, showing that a dynamic covalent approach could be advantageous compared to kinetically controlled approaches for constructing complex

molecular architectures. Finally, the cage **42D_{2h}-A4** shows selective binding interactions for C₇₀ ($K_{\text{assoc}}=3.9\times10^3 \text{ mol}^{-1}$) over C₆₀ (no noticeable binding).

2.4. Experimental Section

2.4.1. Materials and general synthetic methods

Reagents and solvents were purchased from commercial suppliers and used without further purification, unless otherwise indicated. Tetrahydrofuran (THF), toluene, CH₂Cl₂ and dimethylformamide (DMF) were purified by the MBRAUN solvent purification systems.

All reactions were conducted under dry nitrogen in oven-dried glassware, unless otherwise specified. All the alkyne metathesis reactions were conducted in glovebox. The solvents used in alkyne metathesis were dried over 4 Å molecular sieves. Solvents were evaporated using a rotary evaporator after workup. Unless otherwise specified, the purity of the compounds was 195 % based on ¹H NMR spectral integration.

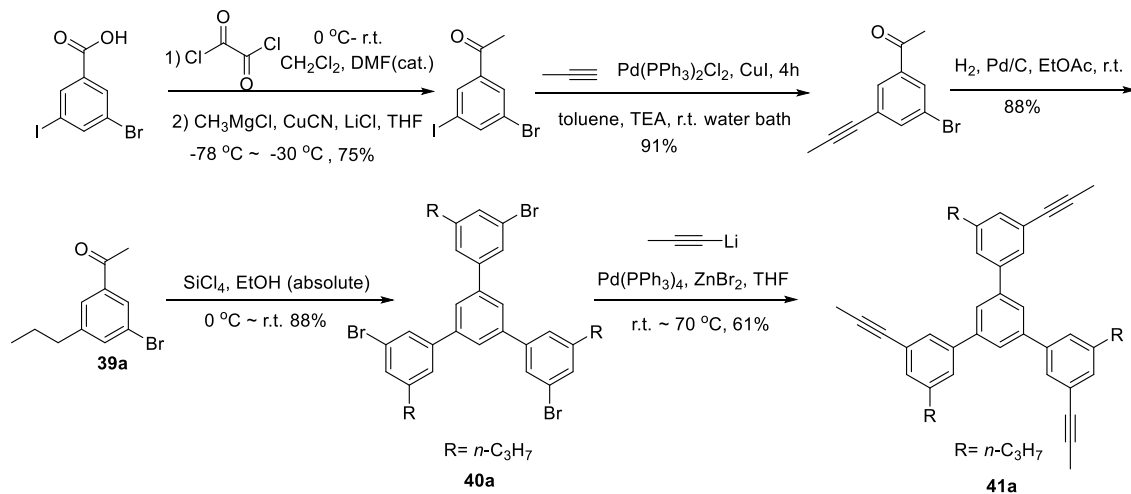
Flash column chromatography was performed by using a 100-150 times weight excess of flash silica gel 32-63 µm from Dynamic Absorbants Inc. Fractions were analyzed by TLC using TLC silica gel F254 250 µm precoated-plates from Dynamic Absorbants Inc. Analytical gel permeation chromatography (GPC) was performed using a Viscotek GPCmaxTM, a Viscotek Model 3580 Differential Refractive Index (RI) Detector, a Viscotek Model 3210 UV/VIS Detector and a set of two Viscotek Viscogel columns (7.8 × 30 cm, 1-MBLMW-3078, and 1-MBMMW-3078 columns) with THF as the eluent at 30 °C. The analytical GPC was calibrated using monodisperse polystyrene standards. UV-vis absorption measurements were carried out with Agilent 8453 spectrophotometer.

MALDI-TOF Mass spectra were obtained on the Voyager-DETM STR Biospectrometry Workstation using sinapic acid (SA) as the matrix. The high resolution mass spectra were obtained on Waters SYNAPT G2 High Definition Mass Spectrometry System. Analyte molecules were diluted into ESI solvents, methanol, chloroform or acetonitrile/water mixture, for final concentrations of 10 ppm or lower. The solution was injected into the electrospray ionization (ESI) source at a rate of 5 μ L/min. Either the ESI+ or ESI- mode was used in reference to the molecular properties. Accurate mass analysis was performed by using the Lock Mass calibration feature with the instrument.

NMR spectra were taken on Inova 400 and Inova 500 spectrometers. CHCl_3 (7.27 ppm), toluene- d_8 (2.09 ppm) were used as internal references in ^1H NMR, and CHCl_3 (77.00 ppm) for ^{13}C NMR. ^1H NMR data were reported in order: chemical shift, multiplicity (s, singlet; d, doublet; t, triplet; q, quartet; m, multiplet), coupling constants (J , Hz), number of protons.

2.4.2. Synthetic procedures

Reaction scheme:



1-(3-Bromo-5-iodophenyl)ethanone: The reported procedure in the literature was followed.⁵³ 3-Bromo-5-iodobenzoic acid (7.00 g, 21.4 mmol) and oxalyl chloride (5.4 g, 42.8 mmol) were dissolved in dry dichloromethane (35 mL) and the mixture was cooled to 0 °C. Then DMF (70 µL) was added to the reaction mixture and the reaction was allowed to warm up to room temperature slowly. After stirring for overnight, all the solvent was removed under vacuum and the product was directly subjected to the next step without further purification. CuCN (2.55 g, 28.5 mmol) and LiCl (2.41 g, 56.9 mmol) were added to a Schlenk tube, followed by THF (50 mL). The mixture was stirred for 10 min to form a clear solution. The resulting solution was cooled at -78 °C and a solution of CH₃MgCl in THF (3 M, 9.5 mL) was added slowly. The solution was allowed to warm up to -30 °C and stirred for 5 min before it was cooled to -78 °C again. A solution of the above acid chloride in THF (50 mL) was added to the above solution at -78 °C. The mixture was allowed to warm up to -20 °C and stirred at -20 °C overnight. The reaction mixture was poured into a mixture of saturated aqueous NH₄Cl (140 mL) and concentrated NH₃·H₂O (28 mL). The organic layer was extracted with EtOAc (2 x 140 mL) and the combined organic extracts were washed with brine (130 mL). After removing the volatiles, the residue was purified by flash column chromatography (eluting with hexane/CH₂Cl₂, 3/1, v/v) to provide the pure product as a white solid (5.21 g, 75% in two steps): ¹H NMR (500 MHz, CDCl₃) δ 8.19 (t, *J* = 1.5 Hz, 1H), 8.05 (t, *J* = 1.7 Hz, 1H), 8.04 (t, *J* = 1.6 Hz, 1H), 2.58 (s, 3H); ¹³C NMR (101 MHz, CDCl₃) δ 195.17, 143.78, 139.75, 135.94, 130.71, 123.46, 94.62, 26.58. HRMS (m/z): [M]⁺ calcd. for C₈H₆BrIO, 323.8647; found, 323.8651.

1-(3-Bromo-5-propynylphenyl)ethanone: The typical procedure for Sonogashira cross coupling reaction was followed.⁵⁴ To a Schlenk tube, 1-(3-bromo-5-iodophenyl)ethanone (2.0 g, 6.15 mmol), Pd(PPh₃)₂Cl₂ (129 mg, 0.18 mmol), and CuI (12 mg, 0.06 mmol) were added. After

vac/refill with N₂ three times, toluene (20 mL) and TEA (20 mL) were added into the reaction flask. Then the mixture was cooled to -20°C~30°C and propyne was bubbled into the solution for 10 min. The reaction was sealed, and the cooling bath was removed. The mixture was stirred at r.t. for 4 h. The reaction flask was opened slowly to release the pressure. The volatiles were removed and CH₂Cl₂ (50 mL) was added. After washing the reaction mixture with brine (70 mL) and satd. NH₄Cl (70 mL), the organic layer was dried over anhydrous Na₂SO₄. The solvent was removed under reduced pressure and the residue was purified by flash column chromatography (eluting with 10% CH₂Cl₂ in hexane) to provide the pure product as a white solid (1.33 g, 91%):
¹H NMR (400 MHz, CDCl₃) δ 7.91 – 7.87 (m, 1H), 7.80 – 7.76 (m, 1H), 7.63 – 7.59 (m, 1H), 2.52 (s, 3H), 2.01 (s, 3H); ¹³C NMR (101 MHz, CDCl₃) δ 195.86, 138.23, 138.10, 130.01, 129.95, 126.35, 122.43, 88.71, 77.50, 26.49, 4.23; HRMS (m/z): [M]⁺ calcd. for C₉H₁₁BrO, 235.9837; found, 235.9832.

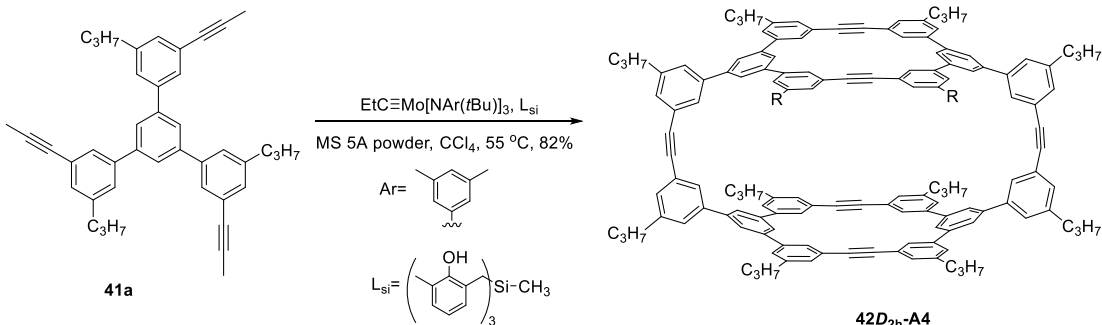
Compound 39a: To a round bottom flask, 1-(3-bromo-5-propynylphenyl)ethanone (4.00 g, 16.9 mmol) and Pd/C (5%) (3.6 g, 1.69 mmol) were added. After vac/refill with N₂ three times, EtOAc (30 mL) was added. After purging with H₂ three times, the reaction was stirred under H₂ (balloon) at r.t. for 3 h. The reaction was monitored by ¹H NMR spectroscopy. After all the starting material was consumed, the volatiles were removed and the residue was dissolved in EtOAc (40 mL). The solids were filtered and the solvent was removed. The crude product was purified by flash column chromatography (eluting with 10% CH₂Cl₂ in hexane) to give pure **39a** (3.50 g, 88%): ¹H NMR (500 MHz, CDCl₃) δ 7.90 (t, *J* = 1.7 Hz, 1H), 7.69 (t, *J* = 1.4 Hz, 1H), 7.53 (t, *J* = 1.7 Hz, 1H), 2.63 (t, *J* = 7.7 Hz, 2H), 2.59 (s, 3H), 1.72 – 1.61 (m, 2H), 0.95 (t, *J* = 7.3 Hz, 3H); ¹³C NMR (75 MHz, CDCl₃) δ 196.83, 145.32, 138.64, 135.89, 128.80, 126.89,

122.59, 37.47, 26.62, 24.22, 13.60; HRMS (m/z): [M]⁺ calcd. for C₁₁H₁₃BrO, 241.0310; found, 241.0317.

Compound 40a: To a Schlenck tube, compound **39a** (800 mg, 3.35 mmol) was added. Under nitrogen flow, EtOH (absolute, 20 mL) was added to the reaction flask. The reaction mixture was cooled at 0 °C, and SiCl₄ (4.44 mL, 33.5 mmol) was added dropwise to the reaction. The ice bath was removed and the reaction was stirred at r.t. overnight. A lot of precipitates were formed. The reaction mixture was poured into ice water (100 mL). The product was extracted with CH₂Cl₂ (3 x 50 mL). The organic extracts were combined and the volatiles were removed. The residue was purified by flash column chromatography (eluting with 10 % CHCl₃ in hexane) to give pure compound **40a** (655 mg, 88%): ¹H NMR (500 MHz, CDCl₃) δ 7.67 (s, 3H), 7.63 (t, *J* = 1.7 Hz, 3H), 7.40 – 7.38 (m, 3H), 7.38 – 7.37 (m, 3H), 2.67 (t, *J* = 7.7 Hz, 6H), 1.76 – 1.66 (m, 6H), 0.99 (t, *J* = 7.4 Hz, 9H); ¹³C NMR (101 MHz, CDCl₃) δ 145.49, 142.65, 141.36, 130.68, 127.67, 126.34, 125.50, 122.79, 37.79, 24.48, 13.80. MALDI-TOF(m/z): [M+Li]⁺ calcd. for C₃₃H₃₃Br₃Li, 675.0266; found, 675.0159.

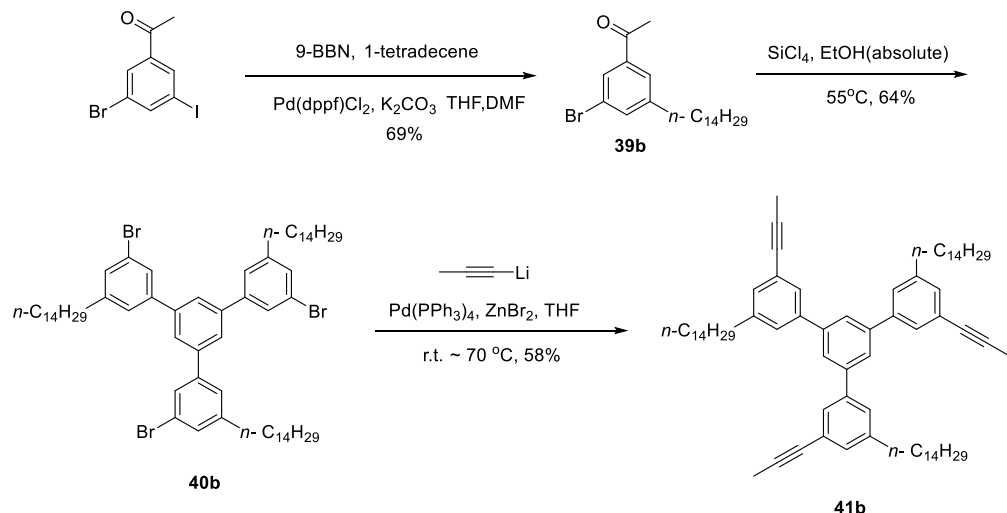
Compound 41a: To a Schlenk tube, propynyllithium (165 mg, 3.57 mmol), ZnBr₂ (743 mg, 3.29 mmol) and THF (4 mL) were added under nitrogen. After stirring for 30 min at r.t., a solution of the compound **40a** (400 mg, 0.60 mmol) and Pd(PPh₃)₄ (103 mg, 0.090 mmol) in THF (4 mL) was added to the mixture. The mixture was stirred at 70 °C overnight, and the solvent was removed under reduced pressure. The residue was redissolved in CH₂Cl₂ (25 mL), and the solution was washed with brine (60 mL). The organic layer was dried over anhydrous Na₂SO₄ and concentrated under vacuum. The residue was purified by flash column chromatography (eluting with hexane/CH₂Cl₂, 15/1, v/v) to give pure compound **41a** (200 mg, 61%): ¹H NMR (500 MHz, CDCl₃) δ 7.78 (s, 3H), 7.61 (s, 3H), 7.45 (s, 3H), 7.30 (s, 3H), 2.69 (t, *J* = 7.7 Hz,

6H), 2.12 (s, 9H), 1.80 – 1.69 (m, 6H), 1.02 (t, J = 7.4 Hz, 9H); ^{13}C NMR (101 MHz, CDCl_3) δ 143.18, 141.73, 140.91, 130.61, 127.74, 126.92, 125.02, 124.24, 85.61, 79.89, 37.81, 24.45, 13.77, 4.23. HRMS (m/z): [M]⁺ calcd. for $\text{C}_{42}\text{H}_{42}$, 546.3287; found, 546.3282.



42D_{2h}-A4: The monomer **41a** (800 mg, 1.65 mmol), 5 Å molecular sieves (4.0 g), and CCl_4 (58 mL) were added to a Schlenk tube in glovebox. In a separate flask, the multidentate ligand L_{si} (17.9 mg, 0.049 mmol) and the Mo(VI) carbyne precursor $\text{Et}\equiv\text{Mo}[\text{NAr}(t\text{Bu})]_3$ (29 mg, 0.049 mmol) were mixed in dry CCl_4 (2 mL) and the mixture was stirred for 10 minutes to generate the catalyst in situ. The catalyst solution was added to the above monomer solution and the mixture was stirred at 55 °C in a closed system. The reaction was monitored by GPC and ^1H NMR. After stirring for 16 h, the molecular sieves were filtered and the filtrate was concentrated. The residue was dissolved in THF (7 mL) and the solution was added to MeOH (70 mL) dropwise while stirring. A white precipitate formed immediately upon the addition. The precipitate was collected and washed with MeOH (2 × 50 mL) to provide pure cage **42D_{2h}-A4** (561 mg, 82 %): ^1H NMR (500 MHz, CDCl_3) δ 7.99 (s, 4H), 7.96 (s, 8H), 7.75 (s, 8H), 7.63 (s, 4H), 7.55 (s, 4H), 7.53 (s, 8H), 7.47 (s, 4H), 7.45 (s, 8H), 2.80 (t, J = 7.6 Hz, 8H), 2.74 (t, J = 7.6 Hz, 16H), 1.89 – 1.75 (m, 24H), 1.14 – 1.03 (m, 36H); ^{13}C NMR (75 MHz, CDCl_3) δ 143.42, 143.38, 142.42, 141.98, 141.62, 141.07, 130.15, 129.84, 129.82, 129.43, 127.67, 127.21, 125.73, 125.29, 123.58, 123.51,

89.88, 89.55, 38.00, 24.60, 24.49, 13.92, 13.89; MALDI-TOF(m/z): [M+H]⁺ calcd. for C₁₄₄H₁₃₃, 1863.04; found: 1862.96.



The cage **42D_{2h}-B4** was synthesized following the similar procedure as cage **42D_{2h}-A4**.

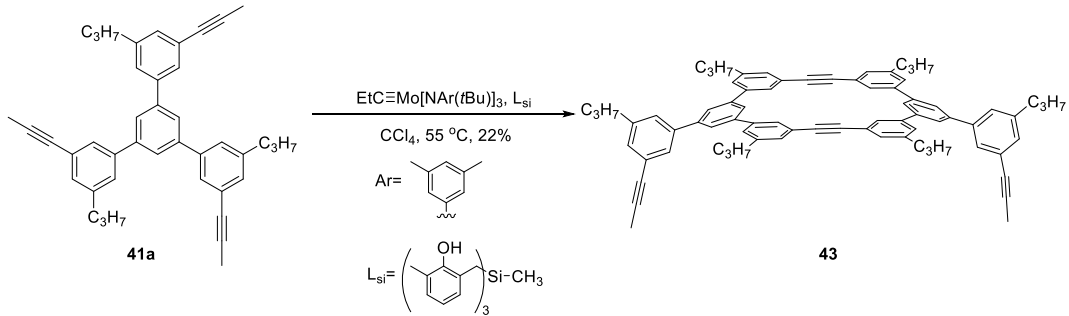
Compound 39b: To a seal tube, after vacuum and refill with N₂ three times, the 1-tetradecene (906 mg, 4.62 mmol) and THF (3 mL) were added under N₂. The solution was cooled in ice bath and 9-BBN (9.3 mL, 0.5M in THF) was added dropwise and the mixture was stirred for 10 min before removing ice bath. After stirring at room temperature for 4 h, to the above solution were added Pd(dppf)Cl₂ (112 mg, 0.154 mmol), 1-(3-Bromo-5-iodophenyl)ethanone (1.00 g, 3.08 mmol), K₂CO₃ (1.70 g, 12.3 mmol) in DMF (3 mL). The reaction was heated to 40 °C for overnight. The reaction was monitored by NMR. After the starting materials were fully converted, the solvent was removed under rotavap. The residue was redissolved in EtOAc (20 mL) and washed with brine (50 mL × 2) and the organic layer was dried over Na₂SO₄. After concentrated, the residue was purified by flash chromatography (eluting with 1% EtOAc in hexanes). Product (912 mg, 88%) was collected. ¹H NMR (500 MHz, CDCl₃): δ 7.89 (t, J = 1.8 Hz, 1H), 7.69 (s, 1H), 7.53 (t, J = 1.8 Hz, 1H), 2.67 – 2.61 (m, 2H), 2.59 (s, 3H), 1.66 – 1.56 (m,

2H), 1.37 – 1.20 (m, 22H), 0.88 (t, J = 6.9 Hz, 3H). ^{13}C NMR (101 MHz, CDCl_3): δ 197.09, 145.89, 138.89, 136.12, 129.04, 127.10, 122.88, 35.80, 32.17, 31.45, 29.94, 29.93, 29.90, 29.88, 29.88, 29.78, 29.66, 29.62, 29.42, 26.92, 22.95, 14.38.

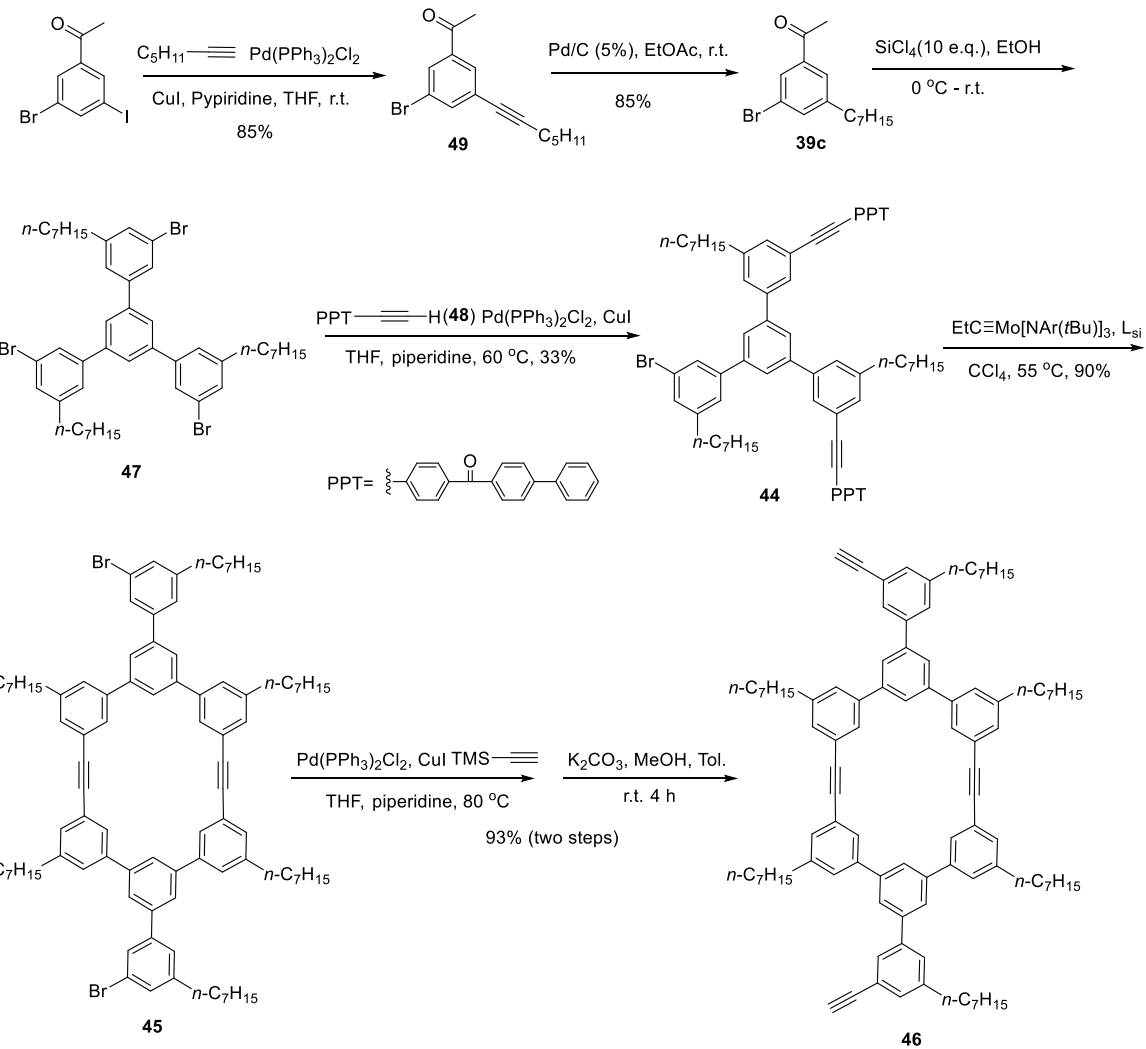
The physical data of **Compound 40b**: ^1H NMR (500 MHz, CDCl_3): δ 7.67 (s, 3H), 7.63 (t, J = 1.8 Hz, 3H), 7.39 (s, 3H), 7.38 (t, J = 1.7 Hz, 3H), 2.72 – 2.65 (m, 6H), 1.72 – 1.60 (m, 6H), 1.43 – 1.20 (m, 66H), 0.88 (t, J = 6.9 Hz, 9H). ^{13}C NMR (101 MHz, CDCl_3): δ 146.03, 142.90, 141.61, 130.87, 127.87, 126.53, 125.74, 123.07, 36.07, 32.19, 31.67, 29.96, 29.95, 29.93, 29.92, 29.85, 29.74, 29.63, 29.58, 22.96, 14.41.

The physical data of **Compound 41b**: ^1H NMR (400 MHz, CDCl_3): δ 7.70 (s, 3H), 7.53 (s, 3H), 7.37 (d, J = 1.7 Hz, 3H), 7.23 (s, 3H), 2.68 – 2.58 (m, 6H), 2.07 (s, 9H), 1.64 (p, J = 7.4 Hz, 6H), 1.23 (s, 66H), 0.86 (t, J = 6.7 Hz, 9H).

The physical data of cage **42D_{2h}-B4**: ^1H NMR (500 MHz, CDCl_3) δ 7.94 (s, 4H), 7.90 (s, 8H), 7.69 (s, 8H), 7.56 (s, 4H), 7.49 (s, 4H), 7.48 (s, 8H), 7.42 (s, 4H), 7.40 (s, 8H), 2.77 (t, J = 7.9 Hz, 8H), 2.71 (t, J = 7.9 Hz, 16H), 1.85 – 1.66 (m, 24H), 1.50 – 1.21 (m, 264H), 0.91 – 0.85 (m, 36H); ^{13}C NMR (101 MHz, CDCl_3) δ 143.68, 143.64, 141.99, 141.62, 141.05, 130.04, 129.75, 129.40, 127.60, 127.14, 125.72, 125.51, 125.28, 123.60, 123.56, 89.88, 89.55, 35.98, 31.95, 31.61, 31.58, 31.43, 29.74, 29.69, 29.67, 29.62, 29.56, 29.44, 29.40, 22.72, 14.15. MALDI-TOF(m/z): [M+H]⁺ calcd. for $\text{C}_{276}\text{H}_{397}$, 3714.11; found: 3714.22.



Macrocyclic 43: To a solution of monomer **41a** (20 mg, 0.036 mmol) in CCl_4 (5 mL) was added a newly generated catalyst solution (1 mL, generated from the precursor 2.4 mg, 0.0036 mmol and the ligand 1.5 mg, 0.0036 mmol as described above). The reaction mixture was stirred at 55°C for 1 h. The reaction was quenched by the addition of MeOH (1 mL). After removing the volatiles, the residue was purified by flash column chromatography (eluting with hexane/ CH_2Cl_2 , 10/1~7/1, v/v). The macrocycle **43** (4 mg, 22%) was obtained together with unreacted monomer **41a**. The physical data of macrocycle **43**: ^1H NMR (400 MHz, CDCl_3) δ 8.05 (s, 2H), 8.00 (s, 4H), 7.79 (d, $J = 1.6$ Hz, 4H), 7.57 (s, 2H), 7.54 (t, $J = 1.7$ Hz, 4H), 7.41 (q, $J = 1.4$ Hz, 6H), 7.26 (t, $J = 1.6$ Hz, 2H), 2.70 (t, $J = 7.7$ Hz, 8H), 2.65 (t, $J = 7.7$ Hz, 4H), 2.09 (s, 6H), 1.72 (m, 12H), 0.98 (m, 18H). ^{13}C NMR (101 MHz, CDCl_3) δ 143.57, 143.33, 142.14, 141.30, 141.14, 140.56, 130.82, 130.17, 129.08, 127.18, 125.23, 124.81, 124.19, 123.59, 89.74, 85.73, 79.91, 77.32, 77.00, 76.68, 38.01, 29.71, 24.56, 13.93; MALDI-TOF(m/z): $[\text{M}+\text{H}]^+$ calcd. for $\text{C}_{76}\text{H}_{72}$, 985.57; found: 986.83.



Compound 47 was synthesized following the similar synthetic route as **40a**. ^1H NMR (500 MHz, Chloroform-d): δ 7.63 (s, 3H), 7.39 (s, 3H), 7.37 (s, 3H), 2.73 – 2.63 (m, 6H), 1.72 – 1.63 (m, 6H), 1.44 – 1.21 (m, 24H), 0.89 (t, $J = 6.8$ Hz, 9H).

Compound 48 was synthesized following the reported procedures.¹⁰

The physical data of **Compound 49**: ^1H NMR (500 MHz, CDCl_3): δ 7.98 (t, $J = 1.8$ Hz, 1H), 7.87 (t, $J = 1.5$ Hz, 1H), 7.72 (t, $J = 1.7$ Hz, 1H), 2.59 (s, 3H), 2.42 (t, $J = 7.1$ Hz, 2H), 1.66 – 1.58 (m, 2H), 1.49 – 1.34 (m, 4H), 0.94 (t, $J = 7.2$ Hz, 3H).

The physical data of **Compound 39c**: ^1H NMR (500 MHz, CDCl_3): δ 7.89 (s, 1H), 7.69 (s, 1H), 7.53 (s, 1H), 2.69 – 2.62 (m, 2H), 2.59 (d, J = 0.8 Hz, 3H), 1.67 – 1.60 (m, 2H), 1.38 – 1.23 (m, 8H), 0.89 (t, J = 7.0 Hz, 3H).

Compound 44: To a Schlenk tube, compound **47** (200 mg, 0.239 mmol), PPT $\equiv\text{H}$ (148 mg, 0.52 mmol), $\text{Pd}(\text{PPh}_3)_2\text{Cl}_2$ (11.7 mg, 0.017 mmol) and CuI (1.2 mg, 0.013 mmol) were added. After vac/refill with N_2 three times, THF (2 mL) and piperidine (0.6 mL) were added. The reaction system was evacuated and refilled with N_2 three times. The mixture was stirred at 60 °C for 13 h. The solvent was removed under reduced pressure, and the residue was purified by flash column chromatography (eluting with hexane/ CH_2Cl_2 , 1/1~1/2.5, v/v) to give compound **44** (96 mg, 33%): ^1H NMR (500 MHz, CDCl_3) δ 7.92 (d, J = 8.3 Hz, 4H), 7.87 – 7.82 (m, 5H), 7.76 (d, J = 1.6 Hz, 2H), 7.76 – 7.72 (m, 6H), 7.72 – 7.66 (m, 9H), 7.65 – 7.60 (m, 2H), 7.56 – 7.49 (m, 6H), 7.48 – 7.44 (m, 3H), 7.39 (t, J = 1.6 Hz, 1H), 2.74 (t, J = 7.8 Hz, 4H), 2.70 (d, J = 7.8 Hz, 2H), 1.77 – 1.65 (m, 6H), 1.47 – 1.26 (m, 24H), 0.93 – 0.87 (m, 9H). ^{13}C NMR (101 MHz, CDCl_3) δ 196.19, 145.73, 144.20, 143.90, 142.88, 141.87, 141.24, 141.07, 139.58, 137.61, 136.46, 132.41, 132.21, 130.83, 130.77, 130.51, 129.97, 128.30, 127.90, 127.86, 127.63, 127.18, 126.79, 126.31, 125.58, 125.32, 123.46, 123.13, 122.77, 90.85, 89.01, 35.90, 35.81, 31.80, 31.77, 31.48, 31.41, 29.32, 29.27, 29.18, 29.13, 22.67, 22.64, 14.11, 14.09. MALDI-TOF(m/z): [M+H]⁺ calcd. for $\text{C}_{87}\text{H}_{84}\text{BrO}_2$, 1239.56; found, 1239.46.

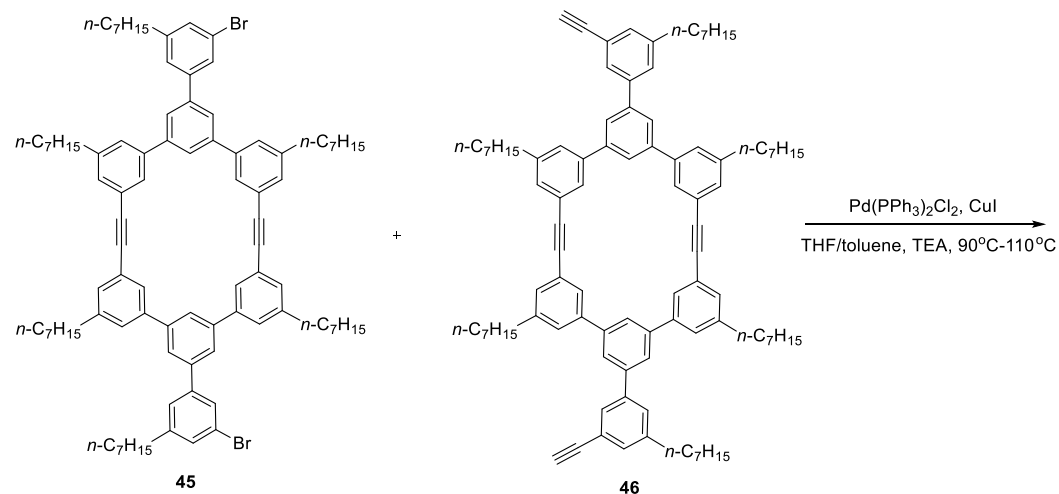
Compound 45: To a Schlenk tube, compound **44** (44 mg, 0.0355 mmol) and CCl_4 (1 mL) were added. In a separate flask, the multidentate ligand L_{si} (1.0 mg, 0.0025 mmol) and the Mo(VI) alkylidyne precursor $\text{Et}\equiv\text{Mo}[\text{NAr}(t\text{Bu})_3]$ (1.6 mg, 0.025 mmol) were mixed in dry CCl_4 (1 mL) and the mixture was stirred for 10 minutes to generate the catalyst in situ. The catalyst solution was added to the above solution of compound **44**. The mixture was stirred at 55 °C in a closed

system for 1 h. A white precipitate was formed during the reaction. The white solid was filtered, and the filtrate was concentrated. The residue was purified by flash column chromatography (eluting with hexane/CH₂Cl₂, 10/1, v/v) to give compound **45** (22.4 mg, 90 %): ¹H NMR (500 MHz, CDCl₃) δ 8.09 (s, 2H), 8.01 (s, 4H), 7.78 (d, *J* = 1.6 Hz, 4H), 7.69 (s, 2H), 7.56 (s, 4H), 7.44 (s, 6H), 7.39 (s, 2H), 2.75 (t, *J* = 7.8 Hz, 8H), 2.70 (d, *J* = 7.8 Hz, 4H), 1.79 – 1.66 (m, 12H), 1.46 – 1.28 (m, 48H), 0.92 – 0.88 (m, 18H). ¹³C NMR (101 MHz, CDCl₃) δ 145.70, 143.92, 143.21, 141.40, 141.28, 140.43, 130.46, 130.11, 129.09, 127.73, 127.01, 126.41, 125.55, 124.69, 123.65, 122.73, 89.76, 36.00, 35.81, 31.81, 31.78, 31.49, 31.40, 29.34, 29.27, 29.20, 29.14, 22.68, 22.66, 14.12, 14.10. MALDI-TOF(m/z): [M+H]⁺ calcd. for C₉₄H₁₁₄Br₂, 1402.73; found: 1402.58.

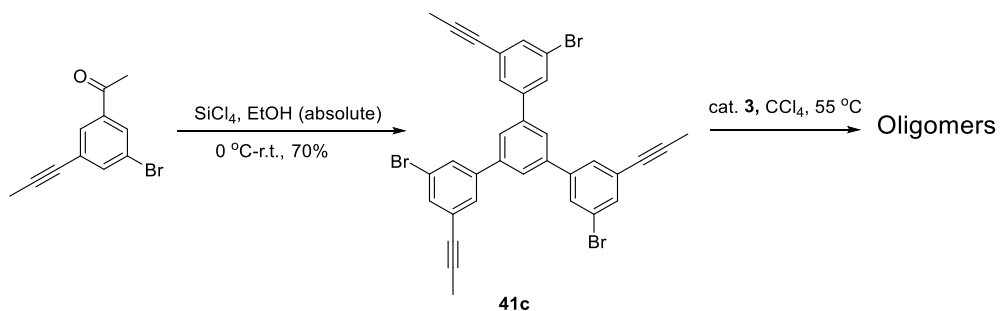
Compound 46: To a Schlenk tube, compound **45** (30.5 mg, 0.0217 mmol), Pd(PPh₃)₂Cl₂ (1.6 mg, 0.0022 mmol) and CuI (0.2 mg, 0.0022 mmol) were added. After vac/refill with N₂ three times, THF (0.5 mL), trimethylsilylacetylene (0.02 mL, 0.13 mmol) and piperidine (0.2 mL) were added. After vac/refill with N₂ three times, the reaction mixture was stirred at 80 °C for 16 h. The solvent was removed under reduced pressure, and the residue was purified by flash column chromatography (eluting with hexane/CH₂Cl₂, 15/1, v/v). The isolated product was dissolved in toluene (1 mL) and MeOH (1 mL), and K₂CO₃ (29 mg) was added. The reaction was stirred at r.t. for 4 h before the solvent was removed under reduced pressure. The residue was redissolved in CH₂Cl₂ (15 mL) and washed with brine (30 mL). After drying over Na₂SO₄, the solvent was removed and the crude was purified by flash column chromatography (eluting with hexane/CH₂Cl₂, 20/1, v/v) to give compound **46** (26 mg, 93% for two steps): ¹H NMR (500 MHz, CDCl₃) δ 8.09 (t, *J* = 1.7 Hz, 2H), 8.02 (t, *J* = 1.6 Hz, 4H), 7.81 (d, *J* = 1.7 Hz, 4H), 7.70 (t, *J* = 1.6 Hz, 2H), 7.56 (t, *J* = 1.6 Hz, 4H), 7.52 (t, *J* = 1.7 Hz, 2H), 7.44 (t, *J* = 1.4 Hz, 4H), 7.39 (t, *J* = 1.5 Hz, 2H), 3.15 (s, 2H), 2.81 – 2.67 (m, 12H), 1.80 – 1.65 (m, 12H), 1.46 – 1.23 (m, 48H),

0.94 – 0.87 (m, 18H). ^{13}C NMR (101 MHz, CDCl_3) δ 143.90, 143.80, 141.84, 141.47, 141.23, 140.51, 131.24, 130.07, 129.09, 128.51, 128.38, 127.03, 125.37, 124.71, 123.63, 122.33, 89.76, 83.91, 36.01, 35.82, 31.81, 31.79, 31.50, 31.42, 29.35, 29.28, 29.20, 29.16, 22.68, 22.66, 14.12, 14.10.

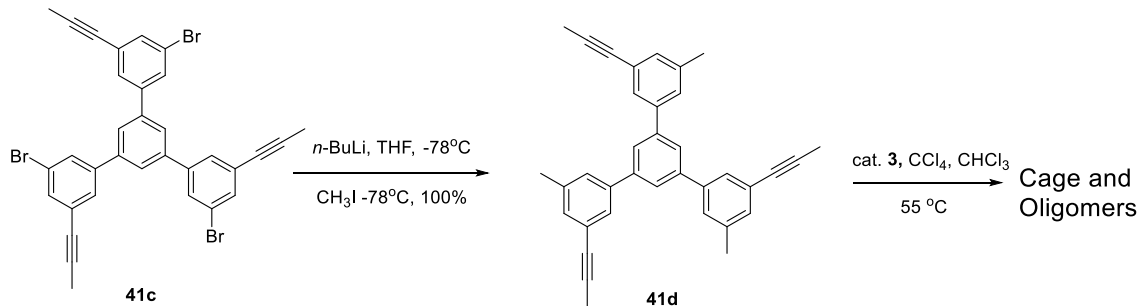
2.4.3. Attempted synthesis of $42D_{2h}$ through cross-coupling reactions



General Procedure: To a Schlenk tube, compound **45** and **46** in 1:1 molar ratio, $\text{Pd}(\text{PPh}_3)_4$, and CuI were added. After vac/refill with N_2 three times, the solvent (THF or toluene) and triethylamine (TEA) were added. After vac/refill with N_2 three times, the reaction mixture was stirred at $90\text{--}110\text{ }^\circ\text{C}$ for 16~40 h. The reaction progress was monitored using TLC, NMR, GPC and MALDI-TOF MS.



Compound 41c: To a seal tube, starting materials 1-(3-Bromo-5-propynylphenyl)ethanone (200 mg, 0.843 mmol) was added and vac/refill with N_2 for 3 times. Then EtOH (2.0 mL, absolute) was added and the reaction mixture was cooled at 0°C . The SiCl_4 (860 mg, 2.53 mmol) was added dropwise. After addition, the ice bath was removed and the reaction was stirred at room temperature for overnight. To workup this reaction, the reaction mixture was poured into cold water and extracted with CH_2Cl_2 (50 mL) for 3 times. After concentration of the organic phase, the residue was purified by column chromatography (eluting with hexanes/ CH_2Cl_2 , 20/1). Product (129 mg, 70%) was collected. ^1H NMR (500 MHz, CDCl_3) δ 7.72 (s, 3H), 7.69 (s, 3H), 7.63 (s, 3H), 7.58 (s, 3H), 2.10 (s, 9H).



Compound 41d: To a seal tube, starting materials **41c** (15 mg, 0.0228 mmol) was added. After vac/refill 3 times with N_2 , THF (1 mL) was added to the flask and cooled to -78°C . $n\text{-BuLi}$ (0.080 mmol) was added dropwise. The reaction mixture was stirred for 50 min at -78°C . Then CH_3I (13 μL , 0.205 mmol) was added to the reaction mixture at -78°C . Then the reaction was

allowed to slowly warm up to room temperature for overnight. The reaction was quenched by water and extracted with CH₂Cl₂ (50 mL × 3) and purified by column chromatography (hexane/CH₂Cl₂, 8/1~7/1). Product (11 mg, 100%) was isolated out. ¹H NMR (400 MHz, C₆D₆) δ 7.67 (s, 3H), 7.49 (s, 3H), 7.35 (s, 3H), 7.18 (s, 3H), 2.35 (s, 9H), 2.03 (s, 9H). ¹³C NMR (101 MHz, C₆D₆) δ 141.54, 140.83, 138.34, 131.11, 127.41, 124.92, 124.20, 85.66, 79.66, 21.23, 4.28.

Table 2.1. The attempted synthesis of **42D_{2h}** through cross coupling reactions under various conditions.

Entry	Amount of Monomer 45 (mmol)	Solvent	TEA	Pd(PPh ₃) ₄ mol%	Temperature	Reaction Time
1	0.004	THF (5 mL)	5 mL	10	90 °C	40 h
2	0.005	THF (3.5 mL)	3.5 mL	20	90 °C	18 h
3	0.005	THF (2.5 mL)	2.5 mL	10	90 °C	18 h
4	0.005	toluene (10 mL)	10 equiv.	10	110 °C	16 h
5*	0.005	toluene(10 mL)	110 equiv.	20	110 °C	20 h

* More TEA (100 e.q.) and palladium catalyst (10 %) were added to the reaction mixture of entry 4 and stirred for another 20 h after 16 h reaction of entry 4.

2.4.4. Scrambling experiment

Cage **42D_{2h}-A4** (2.0 mg, 0.0011 mmol) and cage **42D_{2h}-B4** (8.0 mg, 0.0022 mmol) and a solution of catalyst **3** (generated from precursor 0.39 mg, 0.00058 mmol; ligand 0.23 mg, 0.00058 mmol as described above) in CCl₄ (0.5 mL) were added to a dry Schlenk tube in glovebox. The reaction was stirred at 55 °C for 16 h.

2.4.5. Characterization of $4D_{2h}$ -A4

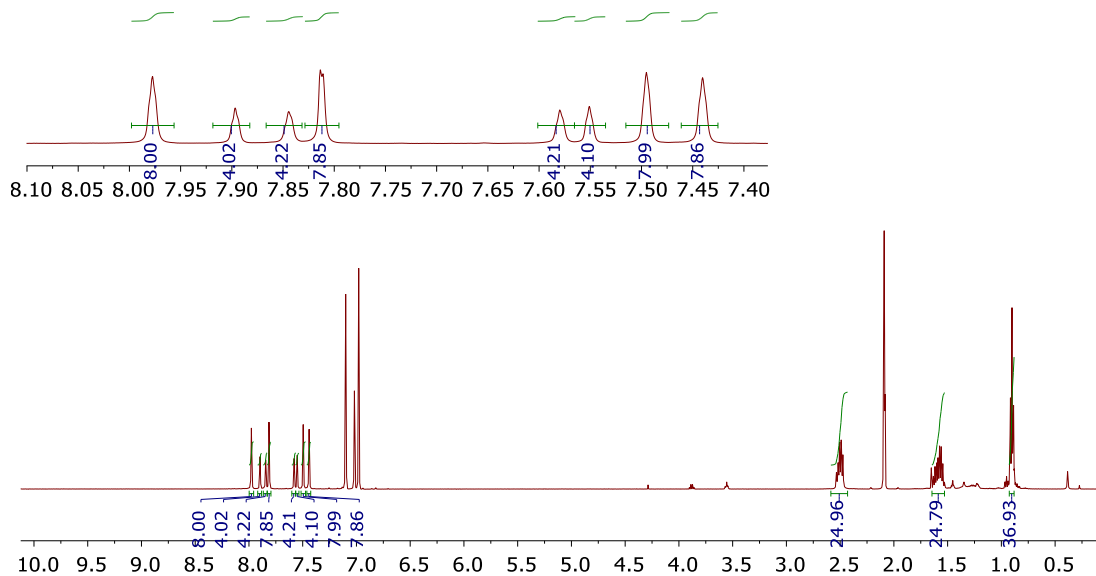


Figure 2.6. The ^1H NMR spectrum of cage **42D_{2h}-A4** in toluene- d_8 .

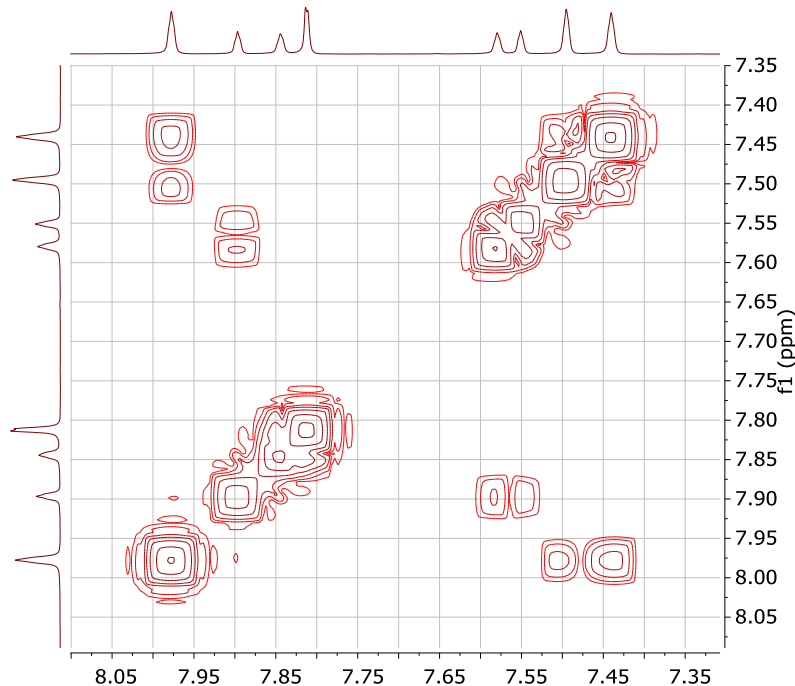


Figure 2.7. The aromatic region of gCOSY spectrum of cage **42D_{2h}-A4** in toluene- d_8 .

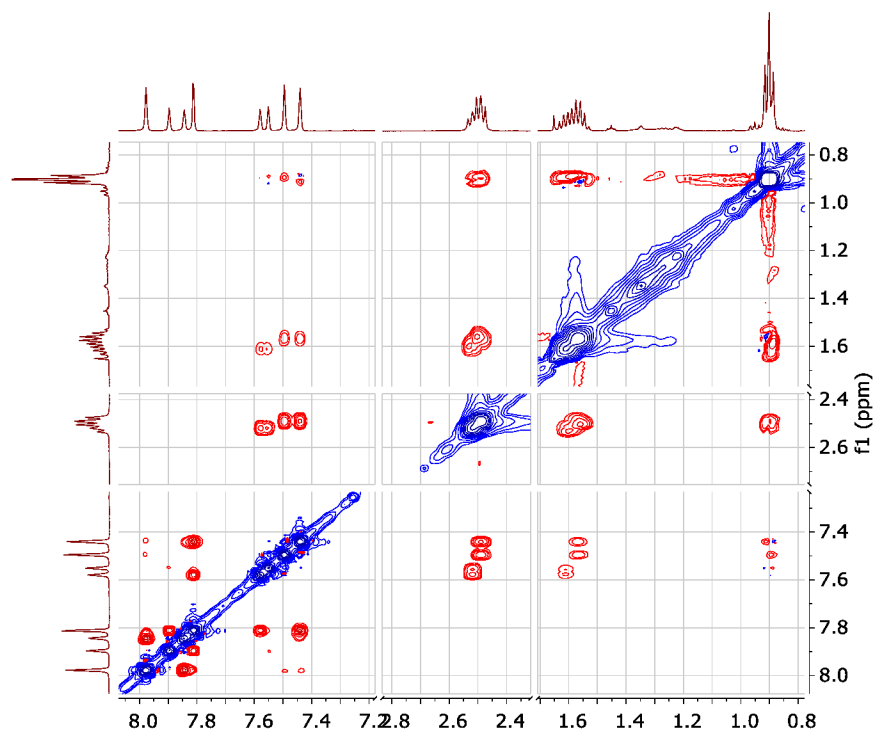


Figure 2.8. The ROESY experiment of cage **42D_{2h}-A4** in toluene-*d*₈.

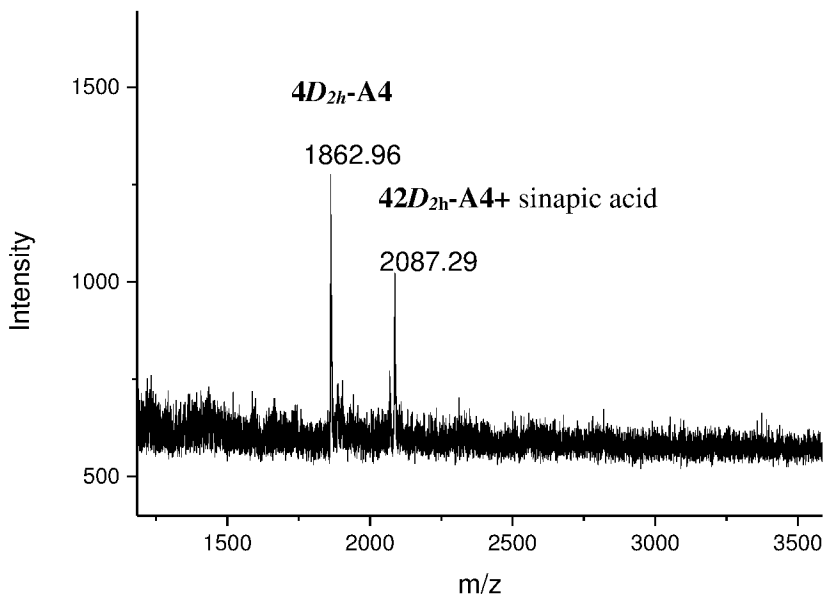


Figure 2.9. MALDI-TOF MS of cage **42D_{2h}-A4**.

2.4.6. GPC data of the kinetic study

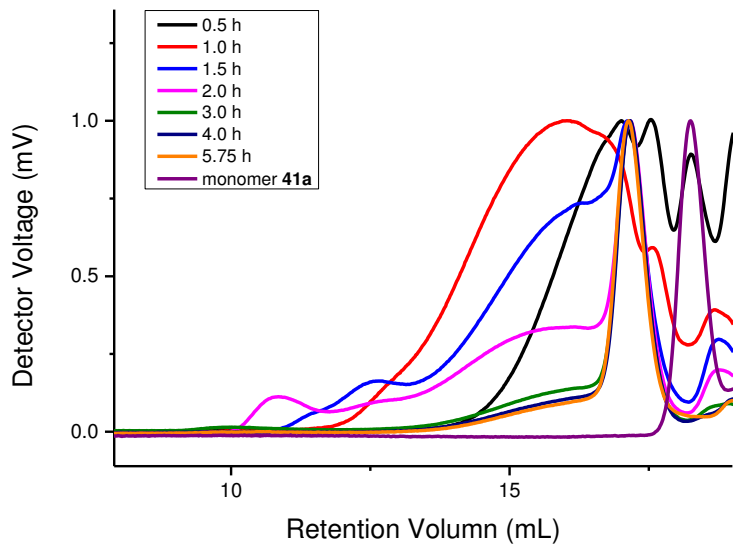


Figure 2.10. Kinetic study of the cage **42D_{2h}-A4** formation through alkyne metathesis: GPC traces of a crude product mixture after 0.5 h, 1.0 h, 1.5 h, 2.0 h, 3.0 h, 4.0 h, 5.75 h of the reaction time and the monomer **41a**. The GPC data showed the reaction was completed after 4 hours. The catalyst loading was 3 mol% per propynyl group.

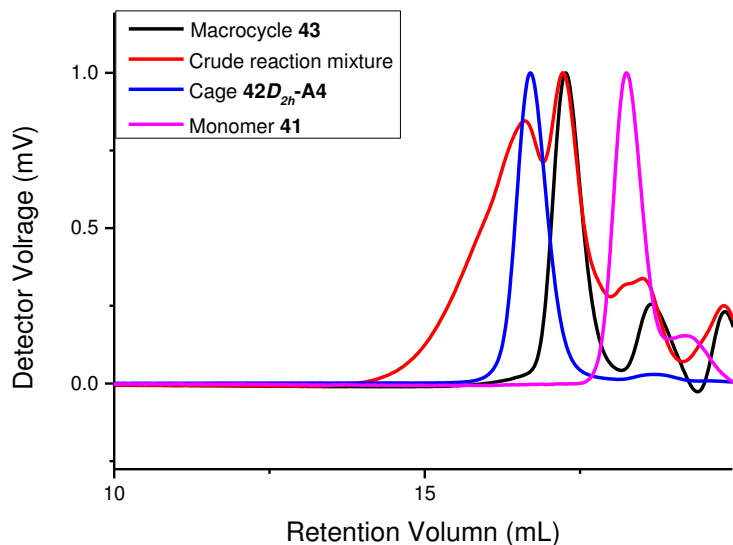


Figure 2.11. GPC traces of the crude reaction mixture of the macrocycle **43** formation (red), isolated macrocycle **43** (black), the monomer **41a** (magenta), and the cage **42D_{2h}-A4** (blue).

2.4.7. The binding study of cage **42D_{2h}-A4** with fullerene

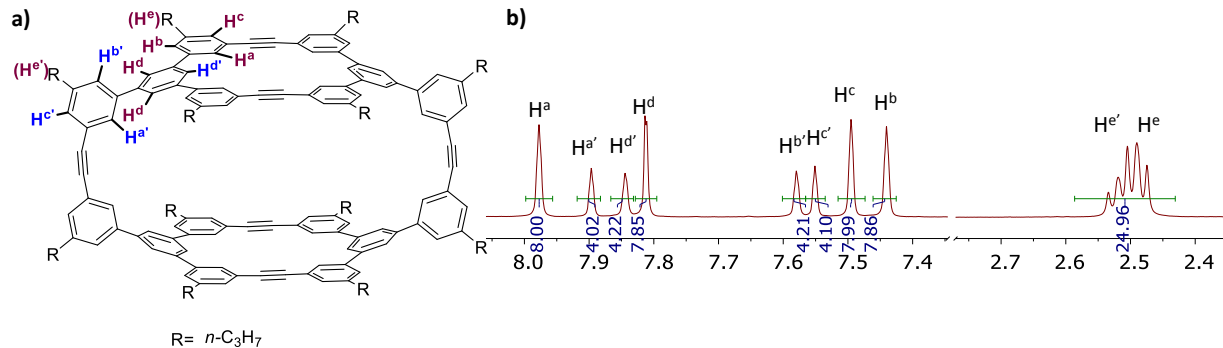


Figure 2.22. a) The structure of **42D_{2h}-A4** with the assigned proton peaks based on ¹H NMR, gCOSY and ROESY. b) The ¹H NMR spectrum of **42D_{2h}-A4** in toluene-*d*₈.

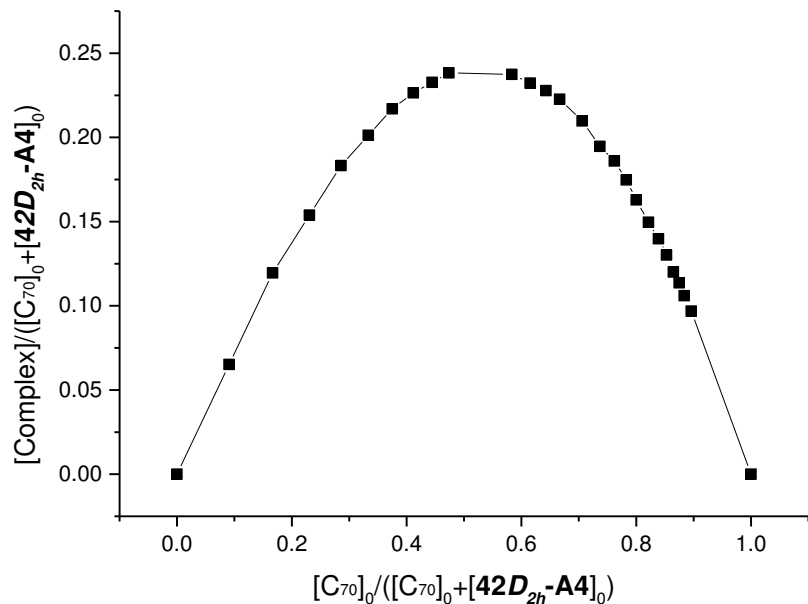


Figure 2.23. The Job Plot for the binding of C_{70} with cage **42D_{2h}-A4**, showing that the binding of C_{70} and cage **42D_{2h}-A4** is in 1:1 stoichiometry. The chemical shift changes of proton $H^{a'}$ were used for the calculation.

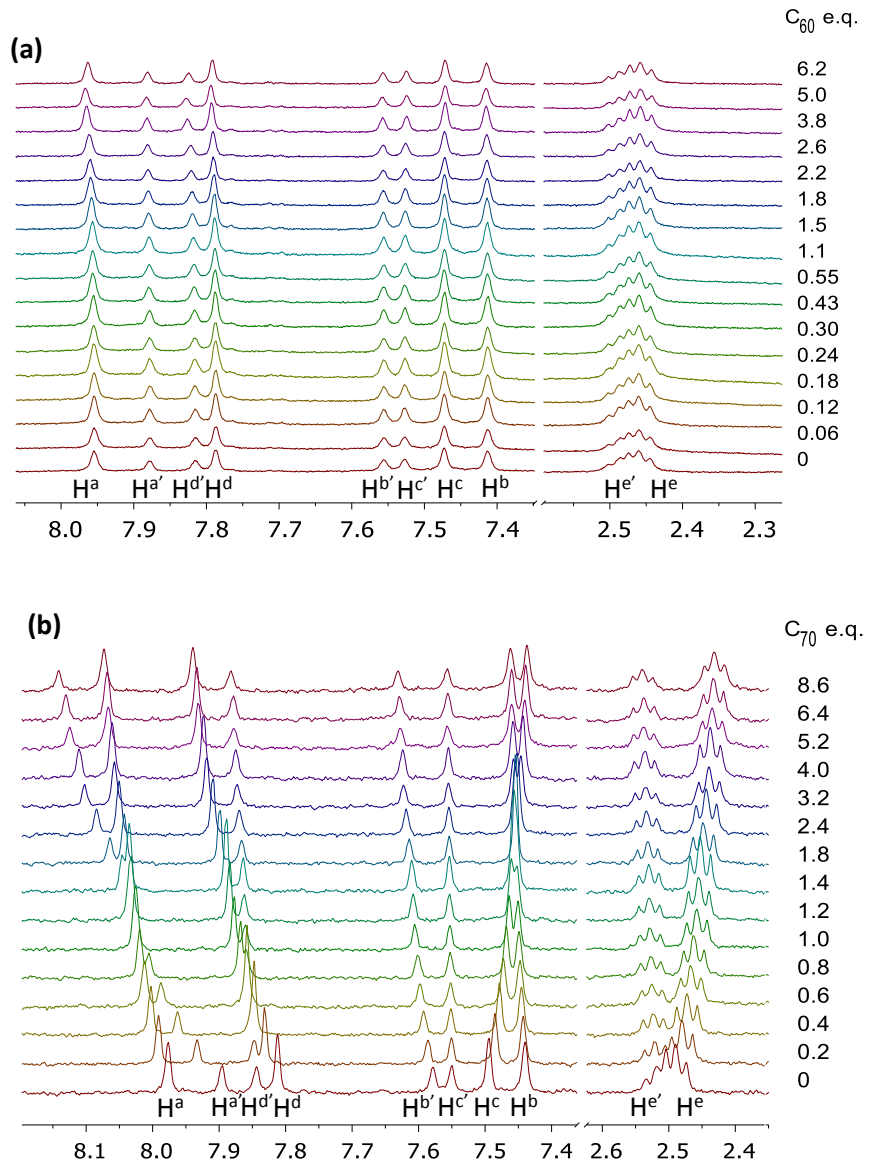


Figure 2.24. The ^1H NMR titration data of (a) cage **42D_{2h}-A4** (0.13 mM) with various amount of C_{60} (0-6.2 equiv), and (b) cage **42D_{2h}-A4** (0.14 mM) with various amount of C_{70} (0-8.6 equiv). The ^1H NMR titrations were done in toluene- d_8 .

2.4.8. Crystal structure report

A specimen of $C_{155.20}H_{149.80}Cl_4N_{4.60}$, approximate dimensions 0.032 mm x 0.117 mm x 0.159 mm, was used for the X-ray crystallographic analysis. The X-ray intensity data were measured on a Bruker D8 VENTURE diffractometer system equipped with a multilayer mirror monochromator and a Cu K α microfocus sealed tube ($\lambda = 1.54178 \text{ \AA}$). The XRD data of **42D_{2h}-A4** was deposited at Cambridge Crystallographic Data Centre with DDCD number 999558.

Table 2.2: Data collection details for 42D _{2h} -A4.												
Axis	dx/mm	2θ/°	ω/°	φ/°	χ/°	Width/ °	Frame s	Time/ s	Wavelength h/Å	Voltage e/kV	Current/m A	Temperature /K
Omega	34.975	90.68	346.95	45.00	61.50	0.50	211	45.00	1.54184	50	1.0	130
Phi	34.975	90.68	0.28	198.0 0	23.00	0.50	632	45.00	1.54184	50	1.0	130
Phi	34.974	75.68	77.65	0.00	-44.37	0.50	720	45.00	1.54184	50	1.0	130
Omega	34.974	-15.73	342.19	0.00	-61.50	0.50	147	20.00	1.54184	50	1.0	130
Omega	34.974	90.68	346.95	90.00	61.50	0.50	211	45.00	1.54184	50	1.0	130
Phi	34.974	90.68	90.39	0.00	-23.00	0.50	720	45.00	1.54184	50	1.0	130
Omega	34.974	90.68	346.95	180.0 0	61.50	0.50	211	45.00	1.54184	50	1.0	130
Omega	34.974	-45.68	213.62	360.0 0	44.87	0.50	198	30.00	1.54184	50	1.0	130
Phi	34.974	90.68	92.65	0.00	-44.38	0.50	720	45.00	1.54184	50	1.0	130
Omega	34.974	90.68	346.95	135.0 0	61.50	0.50	211	45.00	1.54184	50	1.0	130
Omega	34.974	-30.68	228.62	90.00	44.87	0.50	198	45.00	1.54184	50	1.0	130
Omega	34.974	-45.68	213.62	90.00	44.87	0.50	198	30.00	1.54184	50	1.0	130
Omega	34.974	90.68	346.95	225.0 0	61.50	0.50	211	45.00	1.54184	50	1.0	130
Omega	34.975	90.68	93.47	135.0	-44.87	0.50	194	45.00	1.54184	50	1.0	130

Axis	dx/mm	$2\theta/^\circ$	$\omega/^\circ$	$\phi/^\circ$	$\chi/^\circ$	Width/ °	Frame s	Time/ s	Wavelengt h/Å	Voltag e/kV	Current/m A	Temperature /K
		0										
Omega	34.975	-60.68	198.62	0.00	44.87	0.50	198	45.00	1.54184	50	1.0	130
Omega	34.975	90.68	346.95	$\frac{270.0}{0}$	61.50	0.50	211	45.00	1.54184	50	1.0	130
Omega	34.975	-60.68	198.62	90.00	44.87	0.50	198	45.00	1.54184	50	1.0	130
Omega	34.975	90.68	346.95	$\frac{315.0}{0}$	61.50	0.50	211	45.00	1.54184	50	1.0	130
Omega	34.975	90.68	93.47	45.00	-44.87	0.50	194	45.00	1.54184	50	1.0	130
Omega	34.975	-15.73	244.57	$\frac{144.0}{0}$	44.87	0.50	194	20.00	1.54184	50	1.0	130
Omega	34.975	90.68	346.95	0.00	61.50	0.50	211	45.00	1.54184	50	1.0	130

A total of 6199 frames were collected. The total exposure time was 73.47 hours. The frames were integrated with the Bruker SAINT software package using a narrow-frame algorithm. The integration of the data using a monoclinic unit cell yielded a total of 112997 reflections to a maximum θ angle of 50.43° (1.00 Å resolution), of which 6998 were independent (average redundancy 16.147, completeness = 99.8%, $R_{int} = 7.16\%$, $R_{sig} = 2.23\%$) and 5827 (83.27%) were greater than $2\sigma(F^2)$. No significant diffraction was observed beyond 1 Å, even with exposures of 120 s/°. The final cell constants of $a = 16.4702(12)$ Å, $b = 11.9661(8)$ Å, $c = 34.019(2)$ Å, $\beta = 91.009(3)$ °, volume = $6703.6(8)$ Å³, are based upon the refinement of the XYZ-centroids of 9962 reflections above 20 $\sigma(I)$ with 5.199° < 2θ < 108.6°. Data were corrected for absorption effects using the multi-scan method (SADABS). The ratio of minimum to maximum apparent transmission was 0.934. The calculated minimum and maximum transmission coefficients (based on crystal size) are 0.8340 and 0.9630.

The structure was solved and refined using the Bruker SHELXTL Software Package, using the space group $P12_1/c_1$, with $Z=2$ for the formula unit, $C_{155.20}H_{149.80}Cl_4N_{4.60}$ (Figure 2.25). The final anisotropic full-matrix least-squares refinement on F^2 with 765 variables converged at $R1 = 11.39\%$, for the observed data and $wR2 = 38.15\%$ for all data. The goodness-of-fit was 1.785. The largest peak in the final difference electron density synthesis was $1.234 \text{ e}^-/\text{\AA}^3$ and the largest hole was $-1.128 \text{ e}^-/\text{\AA}^3$ with an RMS deviation of $0.121 \text{ e}^-/\text{\AA}^3$. On the basis of the final model, the calculated density was 1.100 g/cm^3 and $F(000) = 2362 \text{ e}^-$.

The asymmetric unit, figure 2.26, contains $\frac{1}{2}$ -molecule of the cage compound, 2.3 molecules of acetonitrile, and 1 molecule of dichloromethane. The complete structure is generated by inversion. During refinement, F_{obs}^2 was observed to be consistently greater than F_{calc}^2 . The data were examined for indications of nonmerohedral twinning, and, although a few small, unindexed reflections exist, there is not strong evidence to support this idea (see Figure 2.27). Inspection for a pseudomerohedral twin was also unsuccessful. With such a large cavity in the center of the cage structure, it is possible that there is some randomly oriented solvent within the structure that might account for the observation, $F_{\text{obs}}^2 \gg F_{\text{calc}}$. Because of this unresolved electron density, the model is incomplete, and the agreement factors $R1$ and $wR2$ remain high. In addition, a suitable weighting scheme could not be calculated. The weight used for refinement was 0.2. The full SHEXL-2013 results file and all intensity data, formatted for SHELXL-2013, are appended to the CIF file.

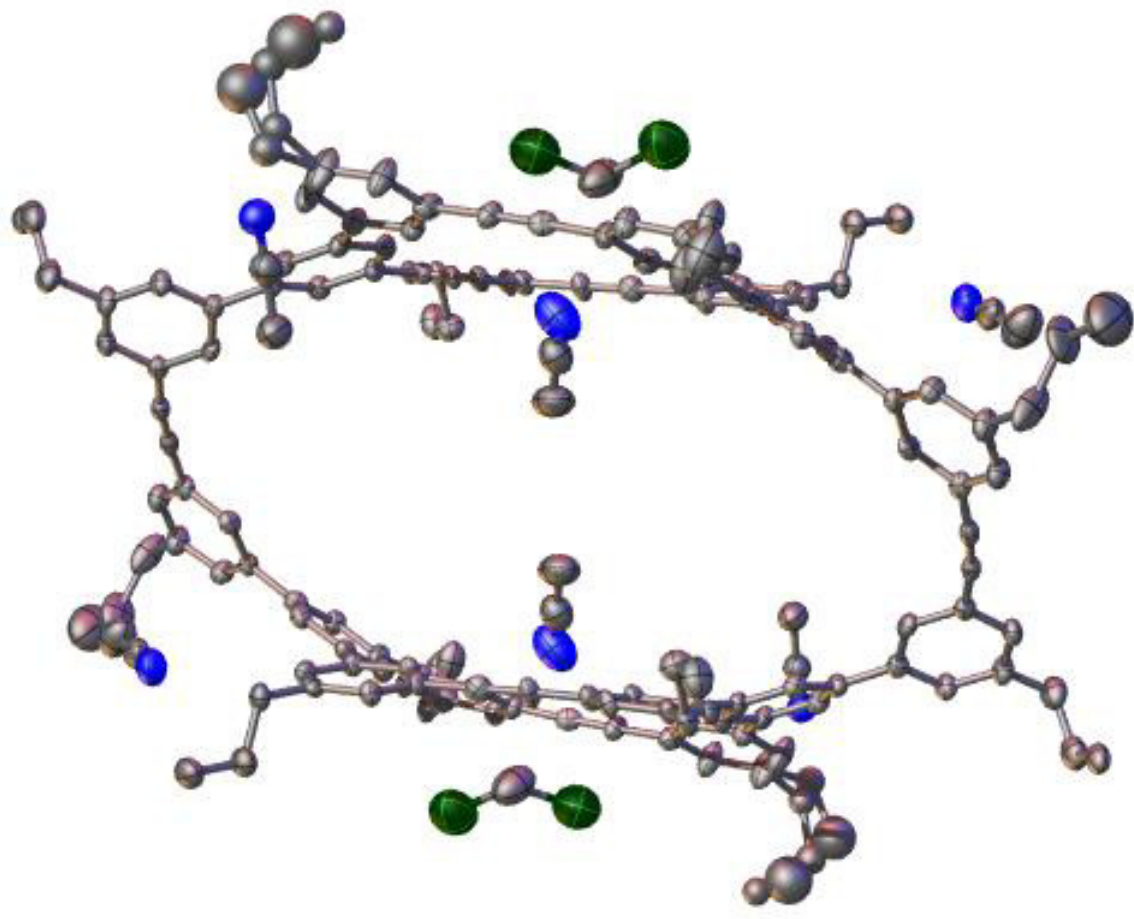


Figure 2.25. Image of complete structure after symmetry applied. H atoms omitted for clarity.

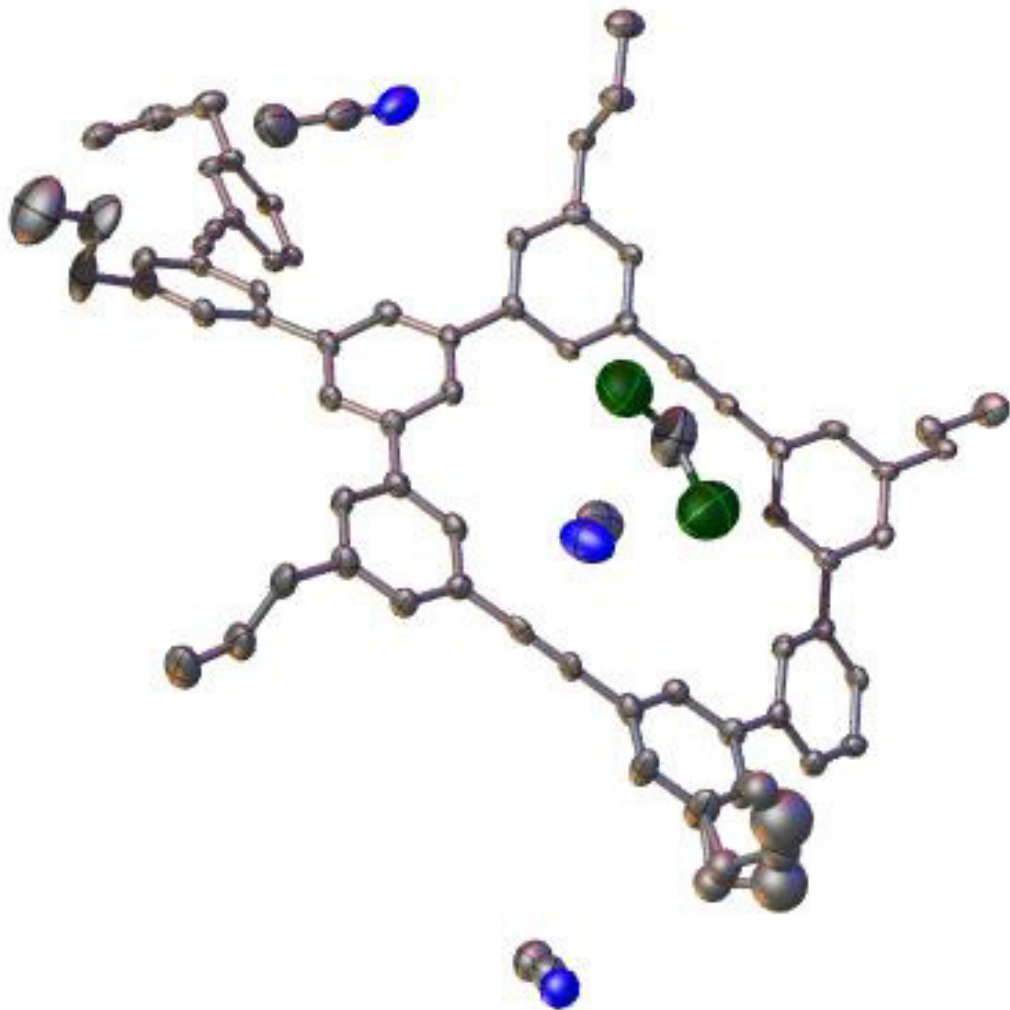


Figure 2.26. Image of asymmetric unit. H atoms omitted for clarity.

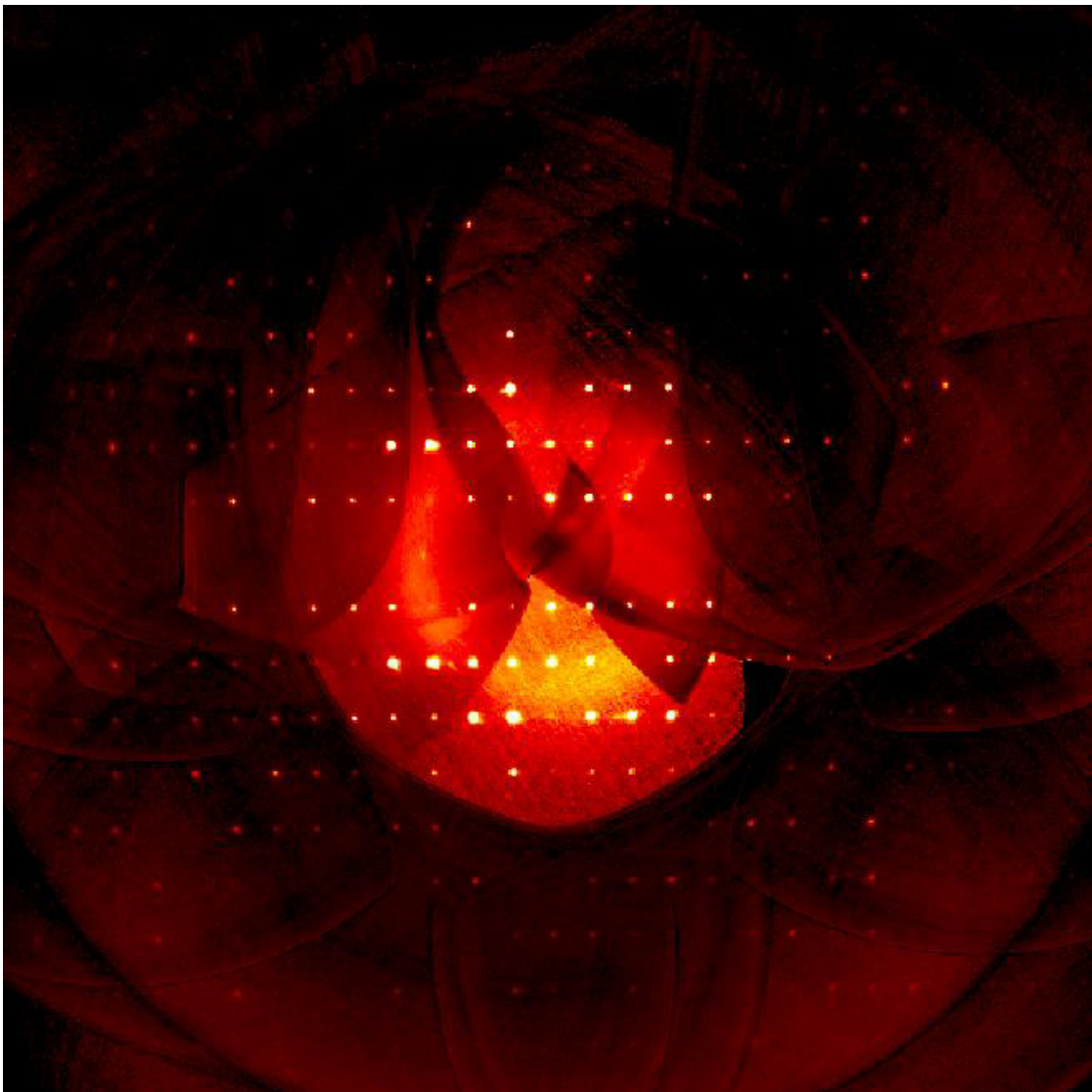


Figure 2.27. Generated precession image for layer hkl . There is little evidence for nonmerohedral twinning.

Table 2.3.	Sample and	crystal	data	for	42D_{2h}-A4.
Identification code	CU_IX57				
Chemical formula	C _{155.20} H _{149.80} Cl ₄ N _{4.60}				
Formula weight	2221.19				
Temperature	130(2) K				

Wavelength	1.54178 Å	
Crystal size	0.032 x 0.117 x 0.159 mm	
Crystal system	monoclinic	
Space group	<i>P</i> 1 2 ₁ /c 1	
Unit cell dimensions	a = 16.4702(12) Å	α = 90°
	b = 11.9661(8) Å	β = 91.009(3)°
	c = 34.019(2) Å	γ = 90°
Volume	6703.6(8) Å ³	
Z	2	
Density (calculated)	1.100 g/cm ³	
Absorption coefficient	1.188 mm ⁻¹	
F(000)	2362	

42D_{2h}-A4

Diffractometer	Bruker D8 VENTURE diffractometer
Radiation source	microfocus sealed tube, Cu K _α
Theta range for data collection	2.60 to 50.43°
Index ranges	-16<=h<=16, -11<=k<=11, -34<=l<=34
Reflections collected	112997
Independent reflections	6998 [R(int) = 0.0716]
Coverage of independent reflections	99.8%
Absorption correction	multi-scan
Max. and min. transmission	0.9630 and 0.8340
Structure solution technique	direct methods

Structure solution program	SHELXT v2014/1 (Sheldrcik, 2014)
Refinement method	Full-matrix least-squares on F^2
Refinement program	SHELXL-2014 (Sheldrick, 2014)
Function minimized	$\Sigma w(F_o^2 - F_c^2)^2$
Data / restraints / parameters	6998 / 48 / 765
Goodness-of-fit on F^2	1.785
Final R indices	5827 data; I>2σ(I) R1 = 0.1139, wR2 = 0.3684 all data R1 = 0.1265, wR2 = 0.3815
Weighting scheme	w=1/[$\sigma^2(F_o^2)+(0.2000P)^2$] where P=($F_o^2+2F_c^2)/3$
Largest diff. peak and hole	1.234 and -1.128 eÅ ⁻³
R.M.S. deviation from mean	0.121 eÅ ⁻³

2.5.Reference

1. Tozawa, T.; Jones, J. T.; Swamy, S. I.; Jiang, S.; Adams, D. J.; Shakespeare, S.; Clowes, R.; Bradshaw, D.; Hasell, T.; Chong, S. Y.; Tang, C.; Thompson, S.; Parker, J.; Trewin, A.; Bacsa, J.; Slawin, A. M.; Steiner, A.; Cooper, A. I. *Nat. Mater.* **2009**, *8*, 973-978.
2. Tian, J.; Thallapally, P. K.; McGrail, B. P. *CrystEngComm* **2012**, *14*, 1909-1919.
3. Cooper, A. I. *Angew. Chem. Int. Ed.* **2011**, *50*, 996-998.
4. Jin, Y.; Voss, B. A.; Jin, A.; Long, H.; Noble, R. D.; Zhang, W. *J. Am. Chem. Soc.* **2011**, *133*, 6650-6658.
5. Jin, Y.; Voss, B. A.; Noble, R. D.; Zhang, W. *Angew. Chem. Int. Ed.* **2010**, *49*, 6348-6351.
6. Francesconi, O.; Ienco, A.; Moneti, G.; Nativi, C.; Roelens, S. *Angew. Chem. Int. Ed.* **2006**, *45*, 6693-6696.
7. Mitra, T.; Jelfs, K. E.; Schmidtmann, M.; Ahmed, A.; Chong, S. Y.; Adams, D. J.; Cooper, A. I. *Nat. Chem.* **2013**, *5*, 276-281.

8. Schouwey, C.; Scopelliti, R.; Severin, K. *Chem. Eur. J.* **2013**, *19*, 6274-6281.
9. Ferrand, Y.; Crump, M. P.; Davis, A. P. *Science* **2007**, *318*, 619-622.
10. Zhang, C. X.; Wang, Q.; Long, H.; Zhang, W. *J. Am. Chem. Soc.* **2011**, *133*, 20995-21001.
11. Zhang, C. X.; Long, H.; Zhang, W. *Chem. Commun.* **2012**, *48*, 6172-6174.
12. McCaffrey, R.; Long, H.; Jin, Y.; Sanders, A.; Park, W.; Zhang, W. *J. Am. Chem. Soc.* **2014**, *136*, 1782-1785.
13. Lin, Z. H.; Sun, J. L.; Efremovska, B.; Warmuth, R. *Chem. Eur. J.* **2012**, *18*, 12864-12872.
14. Rowan, S. J.; Cantrill, S. J.; Cousins, G. R. L.; Sanders, J. K. M.; Stoddart, J. F. *Angew. Chem. Int. Ed.* **2002**, *41*, 898-952.
15. Corbett, P. T.; Leclaire, J.; Vial, L.; West, K. R.; Wietor, J. L.; Sanders, J. K. M.; Otto, S. *Chem. Rev.* **2006**, *106*, 3652-3711.
16. Belowich, M. E.; Stoddart, J. F. *Chem. Soc. Rev.* **2012**, *41*, 2003-2024.
17. Jin, Y.; Yu, C.; Denman, R. J.; Zhang, W. *Chem. Soc. Rev.* **2013**, *42*, 6634-6654.
18. Jin, Y.; Wang, Q.; Taynton, P.; Zhang, W. *Acc. Chem. Res.* **2014**, *47*, 1575-1586.
19. Rue, N. M.; Sun, J. L.; Warmuth, R. *Isr J Chem* **2011**, *51*, 743-768.
20. Severin, K. *Dalton Trans.* **2009**, 5254-5264.
21. Nishiyabu, R.; Kubo, Y.; James, T. D.; Fossey, J. S. *Chem. Commun.* **2011**, *47*, 1124-1150.
22. Dash, A. C.; Dash, B.; Praharaj, S. *J. Chem. Soc. Dalton* **1981**, 2063-2069.
23. Xu, J.; Duran, D.; Mao, B. *J. Liq. Chromatogr. R. T.* **2006**, *29*, 2795-2806.
24. Wu, Z. Y.; Lee, S.; Moore, J. S. *J. Am. Chem. Soc.* **1992**, *114*, 8730-8732.
25. Avellaneda, A.; Valente, P.; Burgun, A.; Evans, J. D.; Markwell-Heys, A. W.; Rankine, D.; Nielsen, D. J.; Hill, M. R.; Sumby, C. J.; Doonan, C. J. *Angew. Chem. Int. Ed.* **2013**, *52*, 3746-3749.
26. Zhang, C.; Chen, C. F. *J. Org. Chem.* **2007**, *72*, 9339-9341.
27. Anderson, H. L.; Gil-Ramirez, G.; Karlen, S. D.; Shundo, A.; Porfyrakis, K.; Ito, Y.; Briggs, G. A. D.; Morton, J. J. L. *Org. Lett.* **2010**, *12*, 3544-3547.
28. Rubin, Y.; Parker, T. C.; Khan, S. I.; Holliman, C. L.; McElvany, S. W. *J. Am. Chem. Soc.* **1996**, *118*, 5308-5309.
29. Rubin, Y.; Parker, T. C.; Pastor, S. J.; Jalisatgi, S.; Boulle, C.; Wilkins, C. L. *Angew. Chem. Int. Ed.* **1998**, *37*, 1226-1229.

30. Tobe, Y.; Nakagawa, N.; Naemura, K.; Wakabayashi, T.; Shida, T.; Achiba, Y. *J. Am. Chem. Soc.* **1998**, *120*, 4544-4545.
31. Tobe, Y.; Nakagawa, N.; Kishi, J. Y.; Sonoda, M.; Naemura, K.; Wakabayashi, T.; Shida, T.; Achiba, Y. *Tetrahedron* **2001**, *57*, 3629-3636.
32. Langton, M. J.; Matichak, J. D.; Thompson, A. L.; Anderson, H. L. *Chem. Sci.* **2011**, *2*, 1897-1901.
33. Kondratuk, D. V.; Perdigao, L. M. A.; Sullivan, M. C. O.; Svatek, S.; Smith, G.; Shea, J. N. O.; Beton, P. H.; Anderson, H. L. *Angew. Chem. Int. Ed.* **2012**, *51*, 6696-6699.
34. O'Sullivan, M. C.; Sprafke, J. K.; Kondratuk, D. V.; Rinfray, C.; Claridge, T. D. W.; Saywell, A.; Blunt, M. O.; O'Shea, J. N.; Beton, P. H.; Malfois, M.; Anderson, H. L. *Nature* **2011**, *469*, 72-75.
35. Sato, Y.; Yamasaki, R.; Saito, S. *Angew. Chem. Int. Ed.* **2009**, *48*, 504-507.
36. Schrock, R. R.; Czekelius, C. *Adv. Synth. Catal.* **2007**, *349*, 55-77.
37. Fürstner, A. *Angew. Chem. Int. Ed.* **2013**, *52*, 2794-2819.
38. Wu, X. A.; Tamm, M. *Beilstein J. Org. Chem.* **2011**, *7*, 82-93.
39. Jyothish, K.; Zhang, W. *Angew. Chem. Int. Ed.* **2011**, *50*, 8478-8480.
40. Fürstner, A.; Grela, K. *Angew. Chem. Int. Ed.* **2000**, *39*, 1234-1236.
41. Zhang, W.; Moore, J. S. *J. Am. Chem. Soc.* **2004**, *126*, 12796.
42. Zhang, W.; Moore, J. S. *J. Am. Chem. Soc.* **2005**, *127*, 11863-11870.
43. Zhang, W.; Moore, J. S. *Angew. Chem. Int. Ed.* **2006**, *45*, 4416-4439.
44. Yang, H.; Liu, Z.; Zhang, W. *Adv. Synth. Catal.* **2013**, *355*, 885-890.
45. Bunz, U. H. F. *Acc. Chem. Res.* **2001**, *34*, 998-1010.
46. Jyothish, K.; Wang, Q.; Zhang, W. *Adv. Synth. Catal.* **2012**, *354*, 2073-2078.
47. Hu, K. D.; Yang, H. S.; Zhang, W.; Qin, Y. *Chem Sci* **2013**, *4*, 3649-3653.
48. McGowan, K. P.; O'Reilly, M. E.; Ghiviriga, I.; Abboud, K. A.; Veige, A. S. *Chem. Sci.* **2013**, *4*, 1145-1155.
49. Paley, D. W.; Sedbrook, D. F.; Decatur, J.; Fischer, F. R.; Steigerwald, M. L.; Nuckolls, C. *Angew. Chem. Int. Ed.* **2013**, *52*, 4591-4594.
50. Yang, H.; Jin, Y.; Du, Y.; Zhang, W. *J. Mater. Chem. A* **2014**, *2*, 5986-5993.
51. Grave, C.; Schluter, A. D. *Eur. J. Org. Chem.* **2002**, 3075-3098.
52. Iyoda, M.; Yamakawa, J.; Rahman, M. J. *Angew. Chem. Int. Ed.* **2011**, *50*, 10522-10553.

53. Dominique, R.; Goodnow, R. A.; Kowalczyk, A.; Qiao, Q.; Sidduri, A.; Tilley, J. W. In *U.S. Pat. Appl. Publ.*; Google Patents: 2010; Vol. US20100240678 A1.
54. Sonogashira, K.; Tohda, Y.; Hagihara, N. *Tetra. Lett.* **1975**, 4467-4470.

CHAPTER 3

A Covalent Organic Polyhedron (COP) with an Unexpected Dumbbell Shape Constructed Through One-Step Alkyne Metathesis

3.1. Abstract

A well-defined 3-D organic cage molecule, with a unique dumbbell shape, was synthesized via one-step alkyne metathesis from readily accessible precursors in high yield. The unexpected formation of the tetrameric cage rather than the originally expected dimeric cage clearly shows the great importance of avoiding high angle strain in the design and synthesis of shape-persistent molecular cages via thermodynamically controlled alkyne metathesis reaction. The obtained cage molecule exhibits binding interactions with fullerenes, which opens the possibility for future development of novel cage-fullerene nanohybrid materials through self-assembly process.

3.2. Introduction

In recent years, discrete three-dimensional (3-D) covalent organic polyhedrons (COPs) have attracted great attention due to their unique properties and wide applications. With intrinsic porosity, shape-persistent 3-D cage compounds have been studied in gas adsorption, gas

separation (e.g., CO₂/N₂ or CO₂/CH₄ separation)¹⁻³, guest recognition⁴⁻⁷ and as reaction “flasks”⁸⁻¹¹. Moreover, their great potential in newly explored applications such as catalysis and drug delivery is highly attractive.

Supramolecular 3-D cages constructed via metal-ligand coordination have been well studied over the past few decades.¹²⁻¹³ By using certain metal ions and rigid organic ligands, well defined shape-persistent 3-D structures were efficiently assembled with designed geometry and functionality.⁴⁻⁶ In great contrast, covalent cage molecules, such as COPs with high thermal and chemical stability have rarely been reported in contrast to those supramolecular ones, which is mainly due to their great synthetic difficulty. Since the covalent bond formation is usually “irreversible” and does not have the “self-correction” mechanism, the desired products are usually synthesized in multiple steps with kinetic control and in low overall yields. To overcome such kinetic barriers and enable efficient synthesis of well-defined covalent organic molecular structures, dynamic covalent chemistry (DCC) has been developed as a thermodynamically controlled approach allowing the construction of 2-D and 3-D molecular architectures from simpler precursors in one step and high yield. With reversible formation of covalent bonds, the thermodynamically most stable product will be predominantly formed.

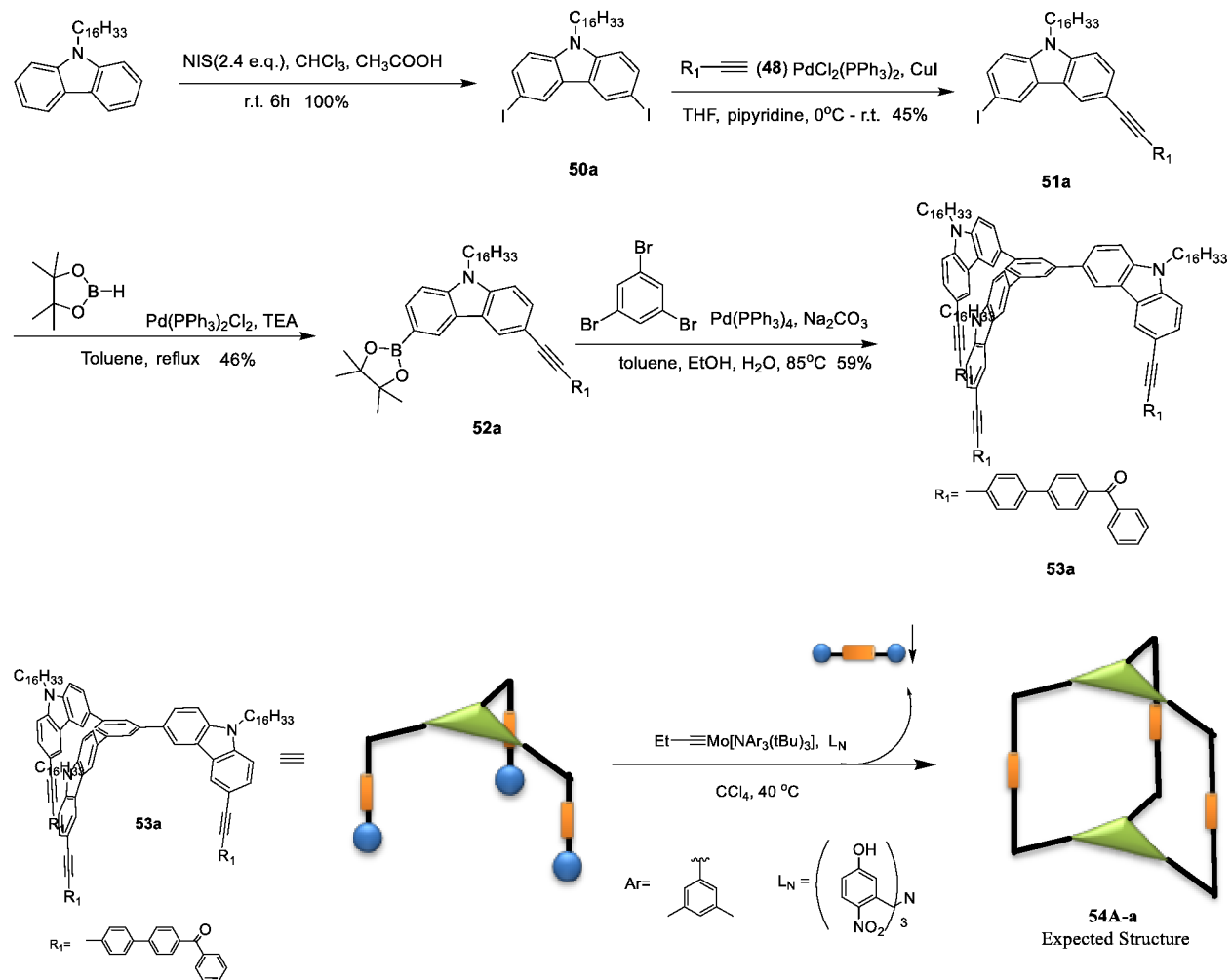
Currently the most commonly used dynamic covalent reaction is imine condensation/metathesis.^{1-2,14-17} Other DC_vC such as condensation reactions of boronic acids and diols have also been reported.¹⁸⁻²⁰ Although these reactions have shown a variety of applications in chemistry and materials science, the sensitivity of the imine or borate groups to acid or moisture represents a potential drawback for certain applications. It has been demonstrated that reduction of imine groups to amines can significantly increase the product stability, but the molecule generally loses some rigidity and conjugation, which sometimes are highly desired

properties. On the other hand, olefin metathesis and alkyne metathesis represent alternative DC_vC reactions, and they have been successfully utilized to construct shape-persistent 2-D macrocycles with high chemical and thermal stability.²¹ However, construction of well-defined 3-D cage molecules through olefin or alkyne metathesis has rarely been explored. Given the rigidity and linear geometry of acetylene bonds, we envisioned that alkyne metathesis would be an alternative viable approach for the synthesis of robust shape-persistent COPs. Moreover, the conjugated acetylene linkers render the cage potential in electrical, optical, and sensing applications. Very recently, our group has successfully synthesized a porphyrin-based 3-D COP in high yield through alkyne metathesis which, for the first time, demonstrated the feasibility of constructing 3-D architectures by using this type of DC_vC.²² Another ethynylene linked tetrameric COP was synthesized very recently, which exhibits a unique D_{2h} symmetry. (The results were discussed in Chapter 2 and the manuscript was submitted.) In this work, we report the alkyne metathesis of a tricarbazolyl-substituted benzene monomer that led to the formation of a unique, unexpected tetrameric cage molecule, which showed the critical role of angle strain in determining the shape-persistent COP formation. Such knowledge would guide future rational design and synthesis of 3-D shape-persistent COPs via alkyne metathesis.

3.3. Results and discussion

Our original goal of this work is to construct a 3-D shape-persistent COP with a small pore size through alkyne metathesis, and we proposed the tricarbazolyl-substituted benzene would be the smallest monomer that can be utilized. The monomer synthesis starts with the alkylation of carbazole, followed by iodination and Sonogashira cross-coupling, affording mono-substituted iodocarbazole **51a**. After converting the iodo group to pinacol borate, followed by Suzuki coupling with 1,3,5-tribromobenzene, tri-armed monomer **53a** was obtained, which was

subjected to the final step of alkyne metathesis. After reaction workup and chromatographic purification, a single species was isolated in 79% yield.



Scheme 3.1. Proposed synthetic scheme for dimeric cage **54A-a** via alkyne metathesis of monomer **53a**.

The isolated compound was then characterized by GPC ($M_n=4,866$, $M_w=5,069$, PDI=1.04, Figure 3.11), MALDI-TOF MS and NMR. Surprisingly, MALDI-MS (Figure 3.1) showed a strong signal at $m/z=5116.47$, corresponding to a tetrameric cage, rather than the expected dimeric one, and no dimer peak was observed. 1H NMR (Figure 3.2) showed two sets of peaks in both aromatic and aliphatic regions with the ratio close to 2:1, which is also inconsistent with our

expected dimer structure. To rule out the possibility that the species we isolated contains a mixture of two compounds, a gCOSY experiment was conducted (Figure 3.8). The spectrum clearly showed that the two peaks corresponding to the protons on the central benzenes are coupled to each other, which indicated these two sets of signals are indeed from one compound. Since the MALDI-MS showed the formation of a tetrameric cage, there are three possible product structures with different topology: 1) a tetrahedron-shaped tetrameric cage, 2) a tetrameric cage containing two interlocked dimer cages, or 3) a tetrameric cage consisting of two dimer cages covalently connected to each other side by side, with a “dumbbell” shape (Figure 3.3). In order to rule out the possibility that two sets of signals resulted from conformational locked structure on the NMR time scale, a high temperature (59 °C) NMR was conducted (Figure 3.11). The spectrum showed only a little shift and relatively sharper peaks, without observing coalescence, which means that these two sets of peaks are indeed from different structural isomers (with different bond connections). Since a tetrahedral cage (Figure 3.3, **54C-a**) should only exhibit one set of proton signals on the NMR spectrum due to its high symmetry, which is inconsistent with our experimental observation,¹⁶ the possibility of formation of a tetrahedral cage can be ruled out. Given the observed two sets of proton signals on the ¹H NMR spectrum, two of six bicarbazolylacetylene arms are likely in different chemical environment from the other four. Both the interlocked cage (Figure 3.3, **54B-a**) and dumbbell-shaped cage (Figure 3.3, **54D-a**) have two different sets of protons (1:2 ratio) in their structures. However, non-covalently interlocked dimers are known to usually give much broader and more complex proton peaks than a single non-interlocked molecule and high temperature NMR should show peak coalescence because of higher exchange rate at higher temperature.¹⁷ Therefore, the formation of the interlocked cage can be ruled out, and the isolated tetrameric cage compound was finally

assigned to the dumbbell-shape structure **54D-a** (Figure 3.4), in which the bond connection can be considered as follows: a cage dimer is formed first with two arms covalently connected, then the unreacted two acetylene end groups point outside and are covalently connected with the two acetylene groups of the other dimer to form the final tetrameric cage. In such configuration, the two inside “bridging” arms are in different chemical environment from the other four outside, which also causes the asymmetry of the protons on the four benzene rings.

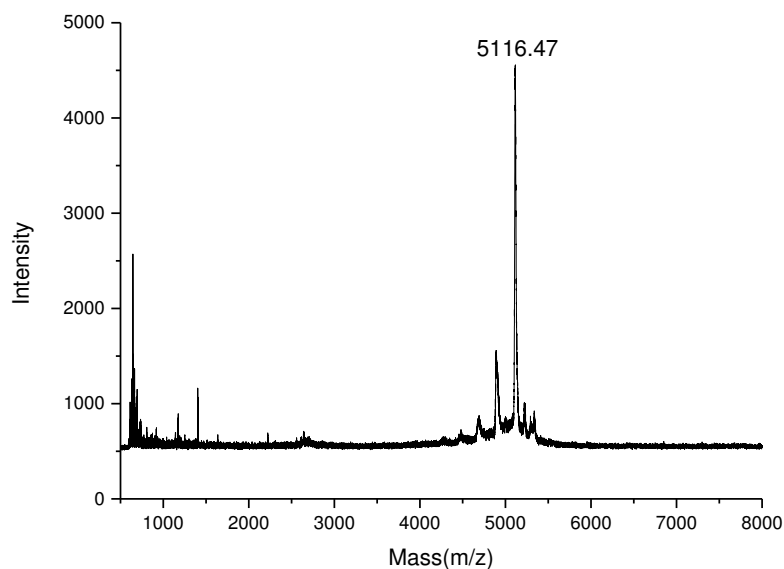


Figure 3.1. The MALDI-MS of the crude reaction mixture from the metathesis of monomer **53a**.

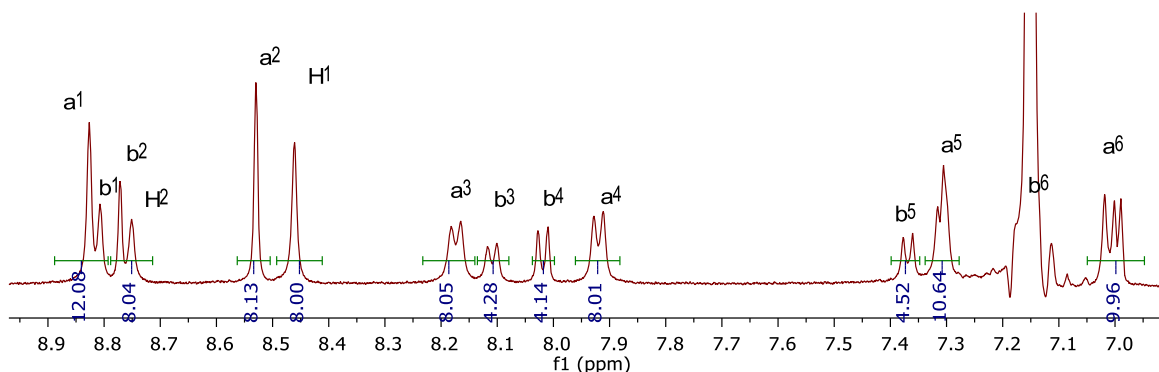


Figure 3.2. Expanded aromatic region of ^1H NMR of cage **54D-a** in C_6D_6 . The label of each peak is consistent with the label on Figure 3.5. Assignment is based on gCOSY, ROESY and NOESY experiments (Figure 3.11-3.13).

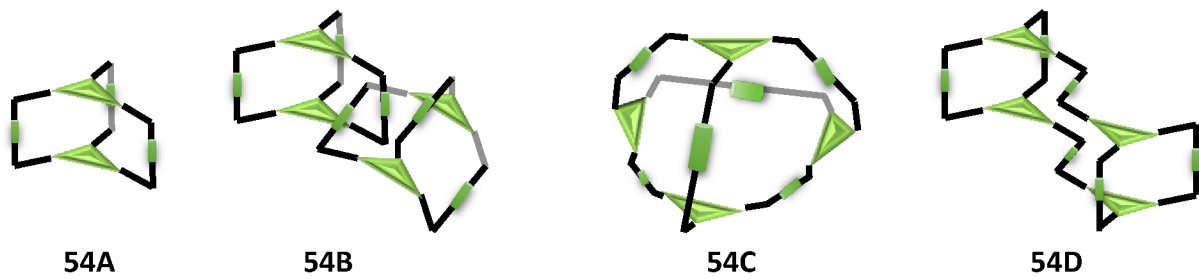


Figure 3.3. **54A:** dimeric cage; **54B:** interlocked dimers; **54C:** tetrahedral cage; **54D:** dumbbell-shaped cage

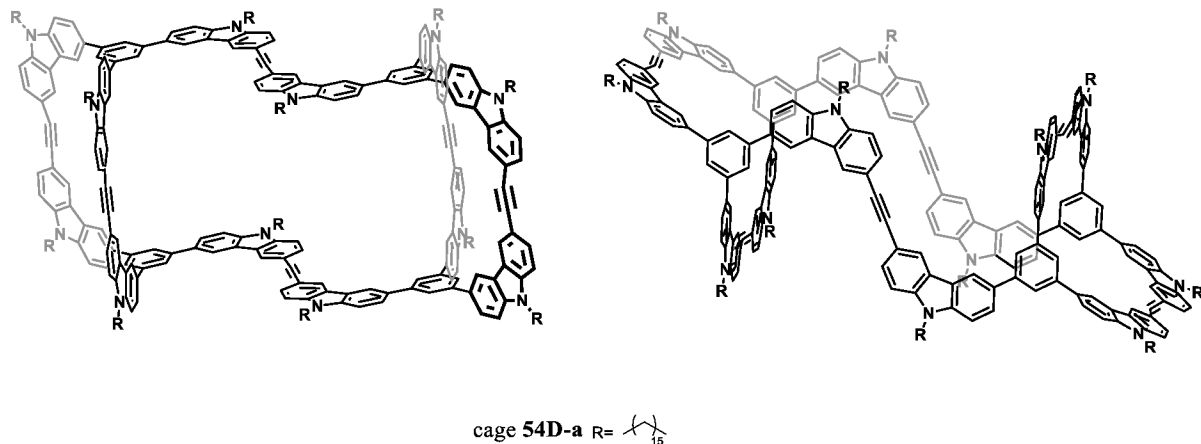


Figure 3.4. Chemical structure of cage **54D-a**, side view (left) and top view (right).

The favored formation of the “dumbbell” shaped tetrameric cage over the dimeric one is supported by the computer modeling study, which shows that the tetramer formation is energetically much more favored (~17.4 kcal/mol) than the formation of two highly strained dimers. In the energy-minimized conformation of **54D** (Figure 3.5), four outer bicarbazolylacetylene arms form one “claw” (bowl-shaped concave face) on each end, and the other two arms in the middle are closely packed to each other. The four outer arms take almost planar conformation, in which two carbazoles and one ethynylene moieties on each arm are

conjugated to achieve a large π -surface area. In contrast, on the inner two arms, in order to avoid the steric hindrance between hydrogens on the 2, 4-position on carbazole and those on the phenyl groups, the carbazoles and central benzenes cannot be in the same plane. Also the bicarbazolylacetylene arm is a little bit twisted to minimize the distance to the other arm. Such close proximity may offer some favored π - π interaction between those two arms to gain further stabilization. The computer calculation indicates that a significant angle strain is built up upon the covalent bonding of the third arm in the dimer case. Since the angle between the two substitutions of a carbazole (3 & 6 positions, acetylene group & central benzene) is not perfect 90° (calcd. 87.4°), in spite of small angle difference away from the desired one, the third arm in a very rigid dimer cage could suffer significant strain. Thus it is conceivable that the first two dicarbazolylacetylene arms in the dimer cage can be formed relatively easily. However the unreacted third acetylene end groups left on both sides of the dimer cannot easily take the favored conformation to get the third arm covalently connected through metathesis, and they just point outside to minimize the steric hindrance. Finally, two unclosed dimers get close to each other and react to form the two bridging arms, thus affording the final tetrameric cage structure.

The formation of such an unexpected, unique dumbbell-shaped tetrameric cage instead of the originally expected dimeric one clearly demonstrates the critical role of angle strain in determining the product distribution. To enable the predominant formation of certain shape-persistent molecular cages via reversible alkyne metathesis, the target structures should be the thermodynamically most favored and have minimal angle strain, which represents an important criterion for rational design of 2-D and 3-D shape-persistent molecular architectures.

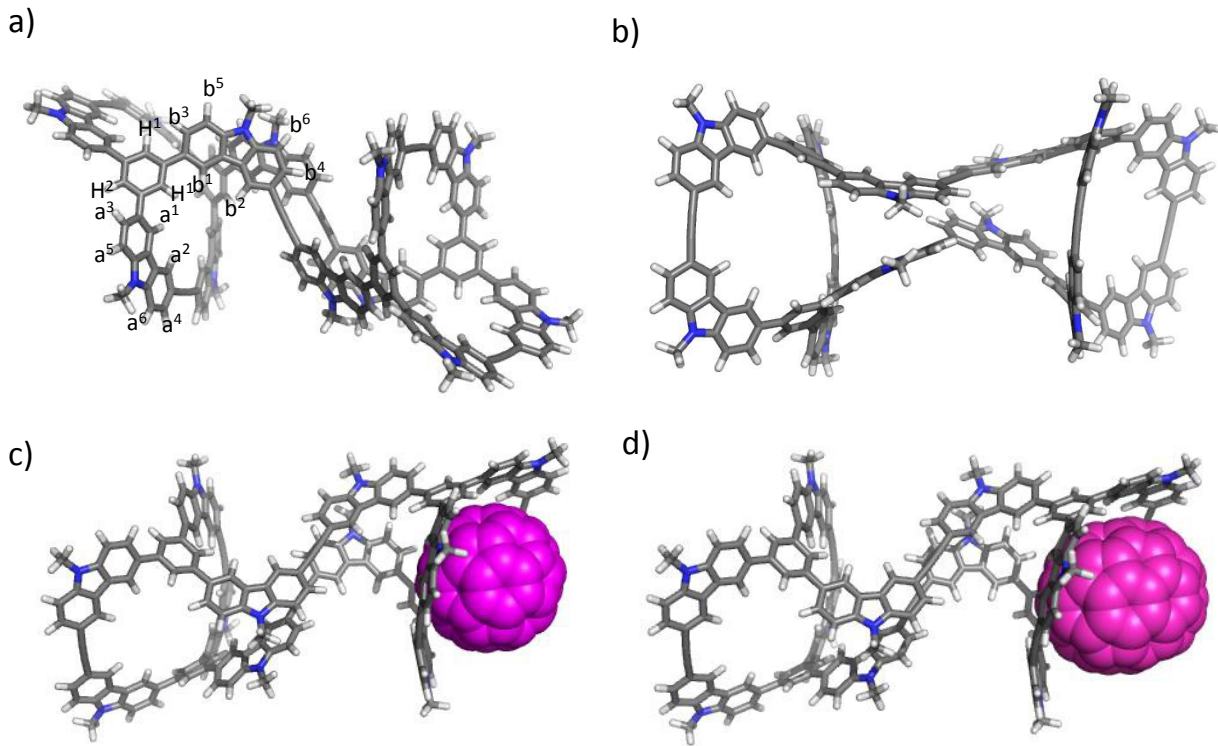


Figure 3.5. Calculated molecular modeling structure of cage **54D**, top view (a) and side view (b), **54D@C₆₀**(c), **54D@C₇₀**(d). Methyl groups were used in the calculation instead of alkyl chains for simplicity.

To further understand the reaction process, a kinetic study was conducted. Aliquots of the reaction mixture were withdrawn at different time intervals, and analyzed by GPC, MALDI and ¹H NMR spectroscopy. The GPC traces showed the initial formation of high molecular weight oligomers and their gradual conversion to cage **54D-a** (Figure 3.6.a). The precipitation driven reaction was very fast. Only after 5 min, the reaction already gave a large amount of oligomers (Figure 3.6.a), and the cage formation completed after 2 h and 10 min. Based on MALDI-TOF MS, the dimeric macrocyclic intermediate was observed clearly in the first 5 min of the reaction (Figure 3.6.b).

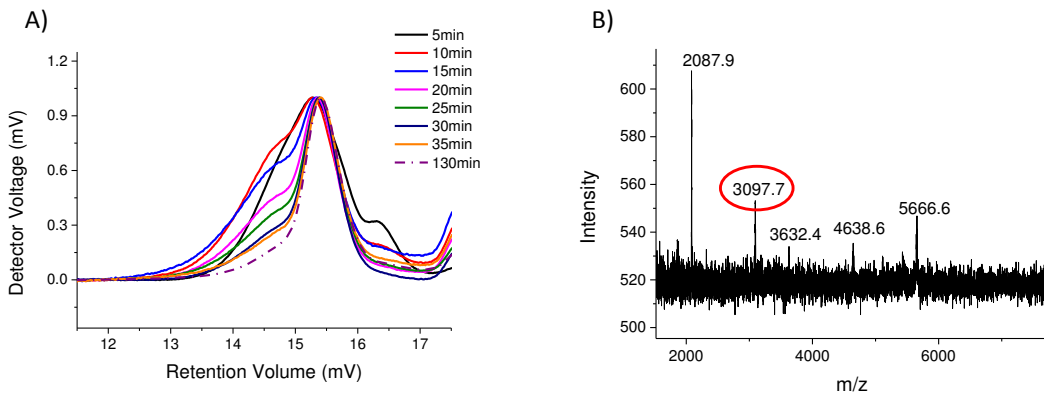


Figure 3.6. a) Kinetic study of the cage **54D-a** formation through alkyne metathesis: GPC traces of a crude product mixture after 5 min, 10 min, 15 min, 20 min, 25 min, 30 min, 35 min and 130 min of the reaction time. The GPC data showed the reaction was completed after 2 hours and 10 min. b) MALDI-TOF MS of the crude reaction mixture of 5 min. The m/z peak 3097.7 is corresponding to the dimeric macrocycle intermediate.

Since the tetrameric cage **54D** has two open ends (bowl-shape) exhibiting a fully conjugated π -surface and the carbazole is known as a good electron donor moiety, we next studied the binding interaction of this cage with fullerene electron acceptors, C_{60} and C_{70} . The 1H NMR titration was performed in both CS_2 and toluene- d_8 . The shift of proton signals was observed in both solvents, which clearly indicates the binding interaction of the cage with fullerenes. It was also found that the binding affinity of the cage with a given fullerene in the good solvent CS_2 is weaker than that in the poor solvent toluene, which is consistent with the previously reported case.²³ NMR titration shows that the peaks of the protons on the outer carbazoles shift more significantly than other protons on the inner carbazoles (Figure 3.7). This indicates the fullerene binding sites of cage **54D** are on the two bowl-shaped ends rather than the bridging arms, which is consistent with the computational simulation result (Figure 3.5, c&d). Unfortunately, given the poor solubility of fullerenes and the relatively weak binding interactions, the binding constants cannot be calculated. However, the shift of the proton signals for the C_{70} -bound cage was larger than that for the C_{60} -bound cage, given the same equivalent loading of C_{70}

and C₆₀ (Figure 3.7). Such an observation qualitatively indicates the binding of the cage with C₇₀ is likely stronger than that with C₆₀, presumably due to the increased π-π stacking between the cage and C₇₀. Again computer modeling supports the notion of more favored C₇₀ binding for cage **54D** (5.0 kcal/mol more stable). Although cage **54D** doesn't exhibit very strong fullerene binding affinity in the current study, it is conceivable that changing the carbazole moieties into some other electron more rich donor groups could significantly increase the cage-fullerene binding, which would open the possibility for future fabrication of 2-D or 3-D functional materials based on cage-fullerene nanohybrid composites.

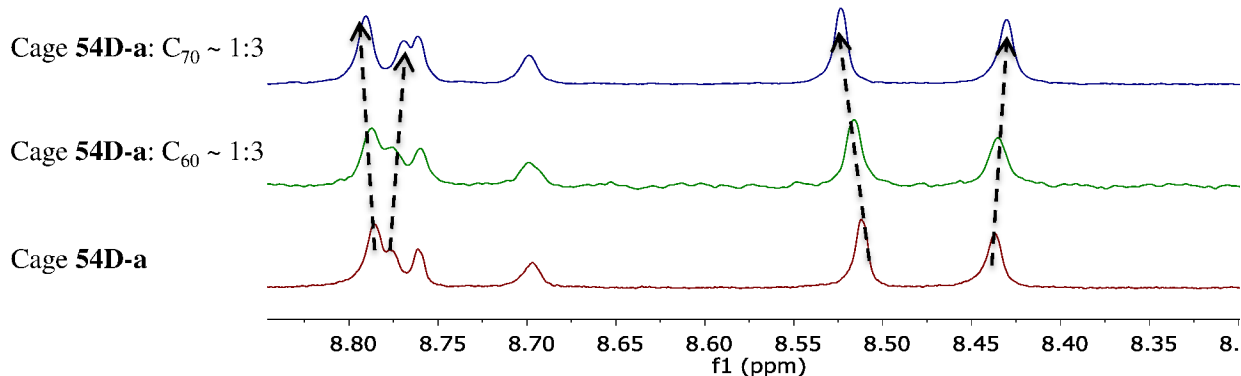


Figure 3.7. Titration study of cage **54D-a** with C₆₀ and C₇₀ in toluene-*d*₈. The concentration of **54D-a** was 0.14 mmol/L. At the ratio of 3:1 (fullerenes to **54D-a**), the peaks in aromatic region (labeled with arrows) showed dramatic difference in its chemical shift between the cage-fullerene complexes (with either C₆₀ or C₇₀ bound inside).

In order to further confirm the structure of cage **54D**, great efforts were devoted to growing single crystals. Cage **54D** with different side chains were synthesized to tune its solubility to facilitate crystal growth. Alkyl chains with different length were incorporated into monomers and the cage syntheses were all successful (based on NMR and MALDI-TOF MS) except the cage with linear hexyl groups. It was found that the solubility of cage **54D-b** monomer was too poor, and the alkyne metathesis reaction ended up with oligomer side products.

Therefore later, long linear chains and branched alkyl chains were used. Unfortunately, the single crystal was not successfully obtained.

We also designed a series of monomers with cleavable side chains. Their potential applications, besides tuning the solubility, are that the free carbazole sites can be further functionalized with other functional groups for different purposes, such as attaching active groups for growing frameworks, attaching specific molecular recognition sites for specific target binding. The carbamate groups are able to be cleaved under basic/acidic conditions. The synthesis of the monomers was straight forward. However, during the synthesis of cage **54D**, it was found that the reactions of monomers with carbamate groups were much slower than the cage synthesis with alkyl chains, always resulting in oligomers based on GPC data. We believe that the electron withdrawing groups, e.g. carbamate group, likely decrease the electron density of the ethynlenes, thus slowing down the reaction of alkyne metathesis. Very recently, by using the silane based alkyne metathesis catalyst **3**, the boc-protected cage **54D-j** was synthesized and isolated successfully. These observations also illustrate the importance of development of highly reactive catalysts.

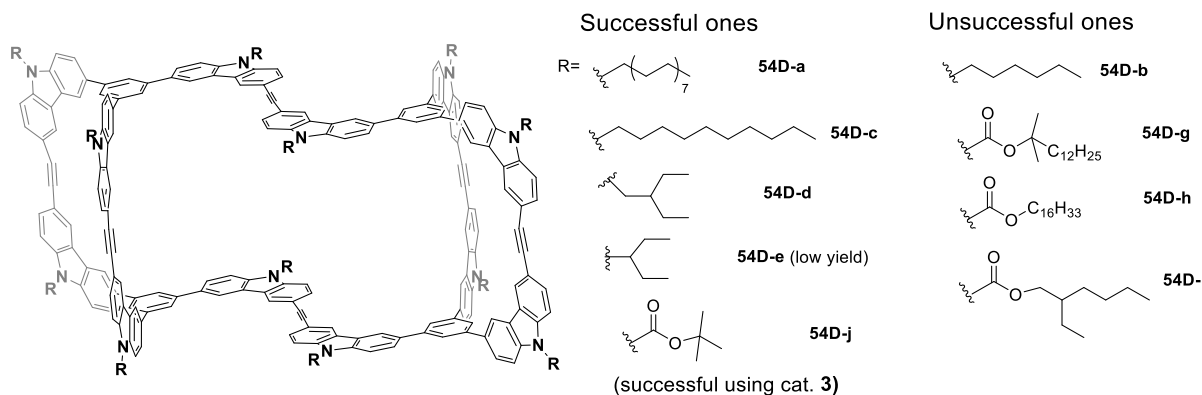


Figure 3.8. The cage **54D** with different side chains.

3.4. Conclusion

In conclusion, a shape-persistent COP with a dumbbell shape was obtained in one step from readily accessible monomers in high yield through alkyne metathesis. The unexpected unique cage structure was fully characterized by $^1\text{H}/^{13}\text{C}$ NMR, gCOSY, ROESY, GPC and MALDI-TOF mass spectrometry. The computer modeling study also supported that the dumbbell-shaped tetrameric cage was energetically favored, with -17.4 kcal/mol lower energy than the formation of two dimers. In addition, without purposely incorporating strong donor moieties, this cage compound showed binding interactions with electron poor guest molecules C_{60} and C_{70} , which opens new possibilities for fabrication of cage-fullerene composite materials. Alkyne metathesis as a dynamic covalent chemistry represents a novel highly efficient synthetic approach to shape-persistent 3D architectures. But the target structure should be thermodynamically favored and has minimal angle strain, which should be taken into consideration in rational molecular design. It should also be noted that the shape, size and functionality of cage molecules could be easily tuned in a modular fashion by varying the building blocks to achieve novel physical (e.g., electrical, optical) properties or high selectivity in guest recognition.

3.5. Experimental Section

3.5.1. Materials and general synthetic methods

Reagents and solvents were purchased from commercial suppliers and used without further purification, unless otherwise indicated. Tetrahydrofuran (THF), toluene, CH_2Cl_2 and dimethylformamide (DMF) were purified by the MBRAUN solvent purification systems.

All reactions were conducted under dry nitrogen in oven-dried glassware, unless otherwise specified. All the alkyne metathesis reactions were conducted in glovebox. The solvents used in alkyne metathesis were dried over 4 Å molecular sieves. Solvents were evaporated using a rotary evaporator after workup. Unless otherwise specified, the purity of the compounds was 195 % based on ¹H NMR spectral integration.

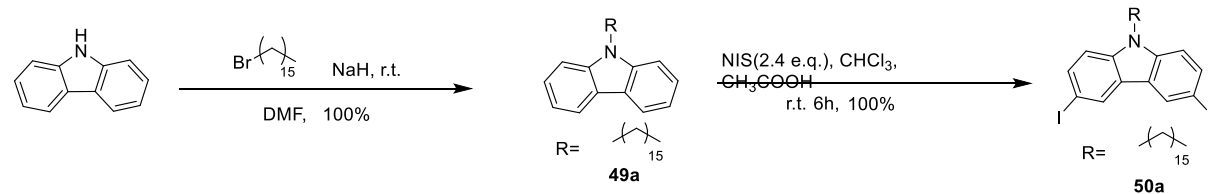
Flash column chromatography was performed by using a 100-150 times weight excess of flash silica gel 32-63 µm from Dynamic Absorbants Inc. Fractions were analyzed by TLC using TLC silica gel F254 250 µm precoated-plates from Dynamic Absorbants Inc. Analytical gel permeation chromatography (GPC) was performed using a Viscotek GPCmaxTM, a Viscotek Model 3580 Differential Refractive Index (RI) Detector, a Viscotek Model 3210 UV/VIS Detector and a set of two Viscotek Viscogel columns (7.8 × 30 cm, 1-MBLMW-3078, and 1-MBMMW-3078 columns) with THF as the eluent at 30 °C. The analytical GPC was calibrated using monodisperse polystyrene standards.

MALDI-TOF Mass spectra were obtained on the Voyager-DE™ STR Biospectrometry Workstation using sinapic acid (SA) as the matrix. The high resolution mass spectra were obtained on Waters SYNAPT G2 High Definition Mass Spectrometry System. Analyte molecules were diluted into ESI solvents, methanol, chloroform or acetonitrile/water mixture, for final concentrations of 10 ppm or lower. The solution was injected into the electrospray ionization (ESI) source at a rate of 5 µL/min. Either the ESI+ or ESI- mode was used in reference to the molecular properties. Accurate mass analysis was performed by using the Lock Mass calibration feature with the instrument.

NMR spectra were taken on Inova 400 and Inova 500 spectrometers. CHCl_3 (7.27 ppm), toluene- d_8 (2.09 ppm) were used as internal references in ^1H NMR, and CHCl_3 (77.00 ppm) for ^{13}C NMR. ^1H NMR data were reported in order: chemical shift, multiplicity (s, singlet; d, doublet; t, triplet; q, quartet; m, multiplet), coupling constants (J , Hz), number of protons.

The Amber 11.0 molecular dynamics program package²⁴ was used to optimize the structures of cages **54A**, **54D** and cage **54D**@C₆₀ and **54D**@C₇₀ by energy minimization for 1000 steps. The force field used for the cages **54A**, **54D** and fullerenes was the general Amber force field (GAFF)²⁵ with the charge parameters computed by the AM1-BCC method.

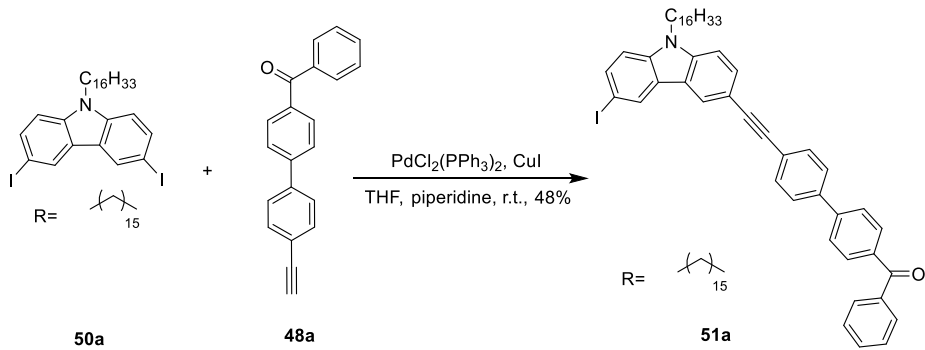
3.5.2. Synthetic procedures



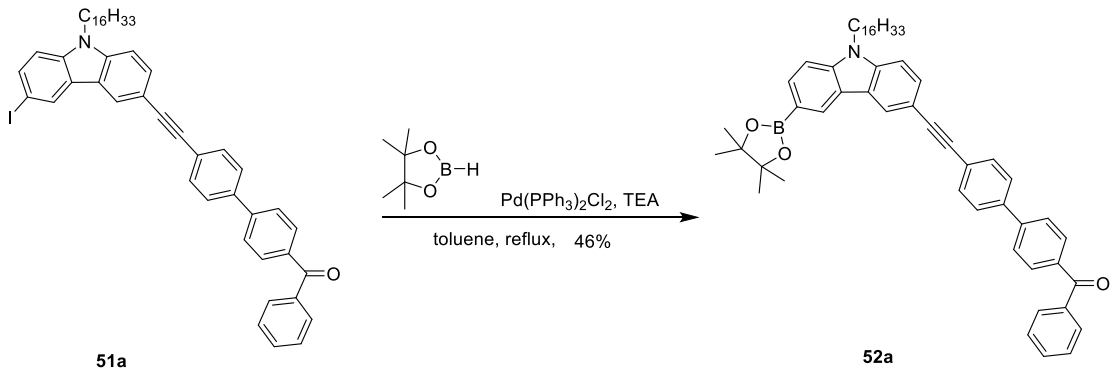
9-hexadecyl-9H-carbazole (**49a**) and 9-hexadecyl-3,6-diiodo-9H-carbazole (**50a**) were made following reported procedure²¹.

9-hexadecyl-9H-carbazole (49a): ^1H NMR (500 MHz, CDCl_3) δ 8.12 (d, $J = 7.8$ Hz, 2H), 7.48 (dd, $J = 8.0, 7.3$ Hz, 2H), 7.42 (d, $J = 8.1$ Hz, 2H), 7.26 – 7.22 (m, 2H), 4.31 (t, $J = 7.3$ Hz, 2H), 1.96 – 1.80 (m, 2H), 1.51 – 1.17 (m, 27H), 0.90 (t, $J = 6.9$ Hz, 3H).

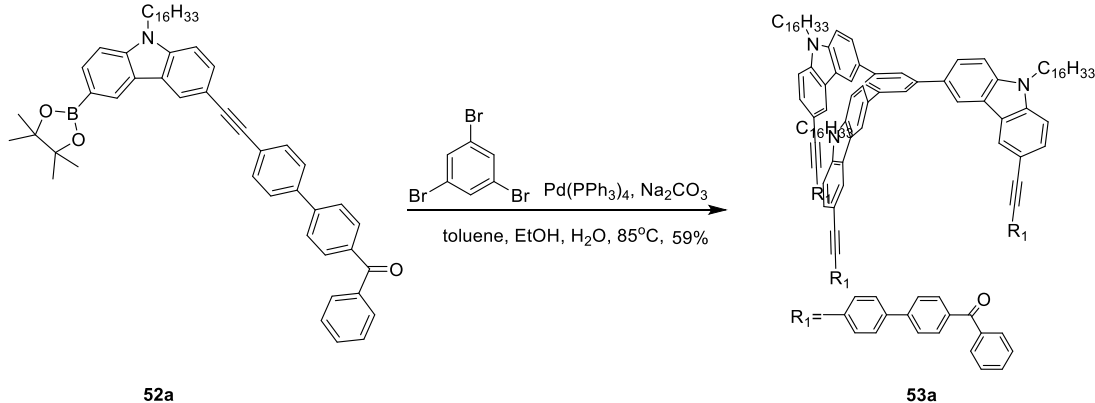
9-hexadecyl-3,6-diiodo-9H-carbazole (50a): ^1H NMR (500 MHz, CDCl_3) δ 8.34 (d, $J = 1.6$ Hz, 2H), 7.72 (dd, $J = 8.6, 1.7$ Hz, 2H), 7.19 (d, $J = 8.6$ Hz, 2H), 4.23 (t, $J = 7.2$ Hz, 2H), 1.91 – 1.70 (m, 2H), 1.45 – 1.14 (m, 27H), 0.89 (t, $J = 7.0$ Hz, 3H).



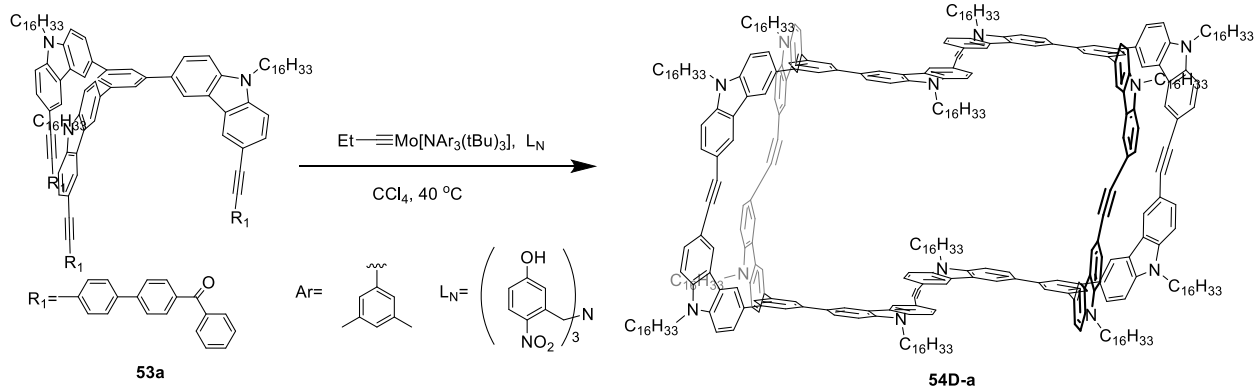
51a: To a Schlenk tube was added 9-hexadecyl-3,6-diiodo-9H-carbazole (**50a**) (2.028 g, 3.153 mmol), **48** (1.00 g, 3.47 mmol), CuI (4.7 mg, 0.025mmol) and Ph(PPh₃)₂Cl₂ (44 mg, 0.063 mmol). Then the flask was degassed and refilled with N₂ three times. With N₂ bubbling, add THF (20 mL) and piperidine (10 mL) to the tube and degas and refill with N₂ three time. After the mixture was reacted at room temperature overnight, it was washed with sat. NH₄Cl. The aqueous layer was discarded. The organic layer was dried by Na₂SO₄ and the solvent was removed under reduced pressure. The reaction mixture was purified by column chromatography (with eluting solvent hexane/CH₂Cl₂, 1/8~1/2) and gave the light yellow solid 1.20 g (48%). ¹H NMR (500 MHz, CDCl₃) δ 8.40 (d, *J* = 1.6 Hz, 1H), 8.27 – 8.22 (m, 1H), 7.95 – 7.89 (m, 2H), 7.86 (dt, *J* = 8.4, 1.6 Hz, 2H), 7.77 – 7.71 (m, 3H), 7.70 – 7.65 (m, 6H), 7.64 – 7.60 (m, 1H), 7.56 – 7.50 (m, 2H), 7.36 (d, *J* = 8.5 Hz, 1H), 7.18 (d, *J* = 8.6 Hz, 1H), 4.24 (t, *J* = 7.1 Hz, 2H), 1.94 – 1.73 (m, 2H), 1.48 – 1.14 (m, 27H), 0.90 (t, *J* = 8.9 Hz, 3H). ¹³C NMR (101 MHz, CDCl₃) δ 196.5, 144.6, 140.3, 140.1, 139.3, 137.9, 136.6, 134.5, 132.7, 132.3, 131.1, 130.3, 130.1, 129.6, 128.6, 127.4, 127.0, 125.1, 124.5, 124.0, 121.8, 113.9, 111.2, 109.2, 92.2, 87.9, 82.1, 43.5, 32.2, 30.0, 29.9, 29.8, 29.7, 29.6, 29.1, 27.5, 23.0, 14.5. HRMS (ESI, *m/z*) calcd. for C₄₉H₅₂INO: 797.3112, found: 797.3112.



52a: **51a** (278 mg, 0.284 mmol) and $\text{Pd}(\text{PPh}_3)_2\text{Cl}_2$ (7 mg, 0.01 mmol) were charged in a Schlenk tube. Then the tube was degassed and refill with N_2 three times. With N_2 bubbling, add toluene (5 mL) and TEA (1mL) to the tube and degas and refill three times and then add 4,4,5,5-tetramethyl-1,3,2-dioxaborolane (0.1 mL, 0.693 mmol). Then the mixture was heated to 85 °C overnight. After the mixture was cooled down to room temperature, it was washed with NH_4Cl (sat., 50 mL) and dried over Na_2SO_4 , then concentrated down. The reaction mixture was purified by column chromatography (with solvent hexane/ CH_2Cl_2 , 1/1~0/1) and gave 115 mg product (46%). ^1H NMR (400 MHz, CDCl_3) δ 8.63 (d, J = 10.7 Hz, 1H), 8.38 (s, 1H), 7.95 (t, J = 6.5 Hz, 1H), 7.92 (d, J = 8.3 Hz, 2H), 7.85 (dd, J = 5.2, 3.4 Hz, 2H), 7.74 (d, J = 8.1 Hz, 2H), 7.71 – 7.64 (m, 6H), 7.64–7.58 (m, 1H), 7.55–7.48 (m, 2H), 7.41 (d, J = 8.3 Hz, 1H), 7.38 (d, J = 8.5 Hz, 1H), 4.29 (t, J = 6.9 Hz, 2H), 1.93 – 1.77 (m, 2H), 1.42 (s, 12H), 1.40 – 1.16 (m, 27H), 0.89 (t, J = 6.6 Hz, 3H). ^{13}C NMR (101 MHz, CDCl_3) δ 196.5, 144.7, 143.2, 140.5, 139.2, 137.9, 136.6, 132.7, 132.6, 132.2, 131.0, 130.2, 129.5, 128.6, 128.2, 127.4, 127.0, 124.6, 124.2, 123.4, 122.4, 113.7, 109.1, 108.6, 92.5, 87.6, 83.9, 43.5, 32.2, 30.0, 29.9, 29.8, 29.7, 29.6, 29.2, 27.5, 25.2, 22.9, 14.4. HRMS (ESI, m/z) calcd for $\text{C}_{55}\text{H}_{64}\text{BNO}_3$: 797.4991, found: 797.4991.



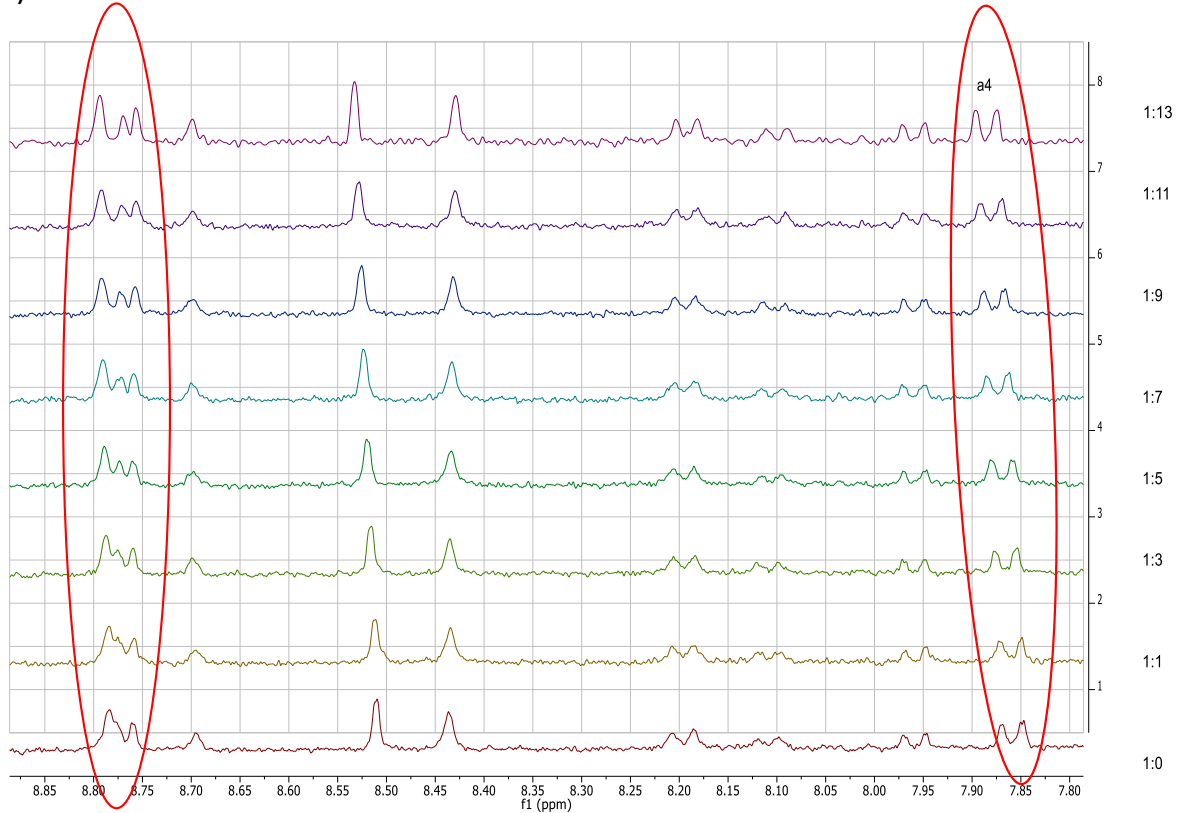
53a: To a Schlenk tube was added **52a** (290 mg, 0.363 mmol), 1,3,5-tribromobenzene (27.2 mg, 0.0865 mmol), Na₂CO₃ (82.5 mg, 0.778 mmol) and Ph(PPh₃)₄ (10 mg, 0.0086 mmol). Then the flask was degassed and refill with N₂ three times. With N₂ bubbling, add toluene (10 mL), H₂O (4mL) and EtOH (4 mL) to the tube and degas and refill three times. Then the mixture was heated to 85°C overnight. After the mixture was cooled down to room temperature, it was washed with sat. NH₄Cl (50 mL). The aqueous layer was discarded. The organic layer was dried by Na₂SO₄ and the solvent was removed under reduced pressure. The reaction mixture was purified by column chromatography (with eluting solvent hexane/CH₂Cl₂, 1/1~1/4) and gave 115 mg product (59%). ¹H NMR (500 MHz, CDCl₃) δ 8.56 (d, *J* = 1.5 Hz, 3H), 8.48 (d, *J* = 1.4 Hz, 3H), 8.07 (s, 3H), 7.98 (dd, *J* = 8.5, 1.6 Hz, 3H), 7.89 – 7.84 (m, 6H), 7.84 – 7.80 (m, 6H), 7.71 (dd, *J* = 8.4, 1.5 Hz, 3H), 7.70 – 7.64 (m, 12H), 7.63 – 7.59 (m, 9H), 7.56 (d, *J* = 8.6 Hz, 3H), 7.53 – 7.48 (m, 6H), 7.44 (d, *J* = 8.5 Hz, 3H), 4.36 (t, *J* = 7.0 Hz, 6H), 1.98 – 1.88 (m, 6H), 1.49 – 1.40 (m, 6H), 1.38-1.34 (m, 6H), 1.34 – 1.18 (m, 66H), 0.87 (t, *J* = 7.0 Hz, 9H). ¹³C NMR (101 MHz, CDCl₃) δ 196.4, 144.6, 143.3, 140.9, 140.7, 139.1, 137.9, 136.5, 133.3, 132.6, 132.2, 131.0, 130.2, 129.7, 128.5, 127.4, 126.9, 126.2, 125.0, 124.6, 124.2, 123.3, 123.3, 119.5, 113.5, 109.6, 109.2, 92.6, 87.7, 43.7, 32.1, 29.9, 29.8, 29.8, 29.7, 29.6, 29.3, 27.6, 22.9, 14.4. MALDI-TOF MS: calcd. for C₁₅₃H₁₅₉O₃N₃: 2087.24, found: 2088.36 (MH⁺).



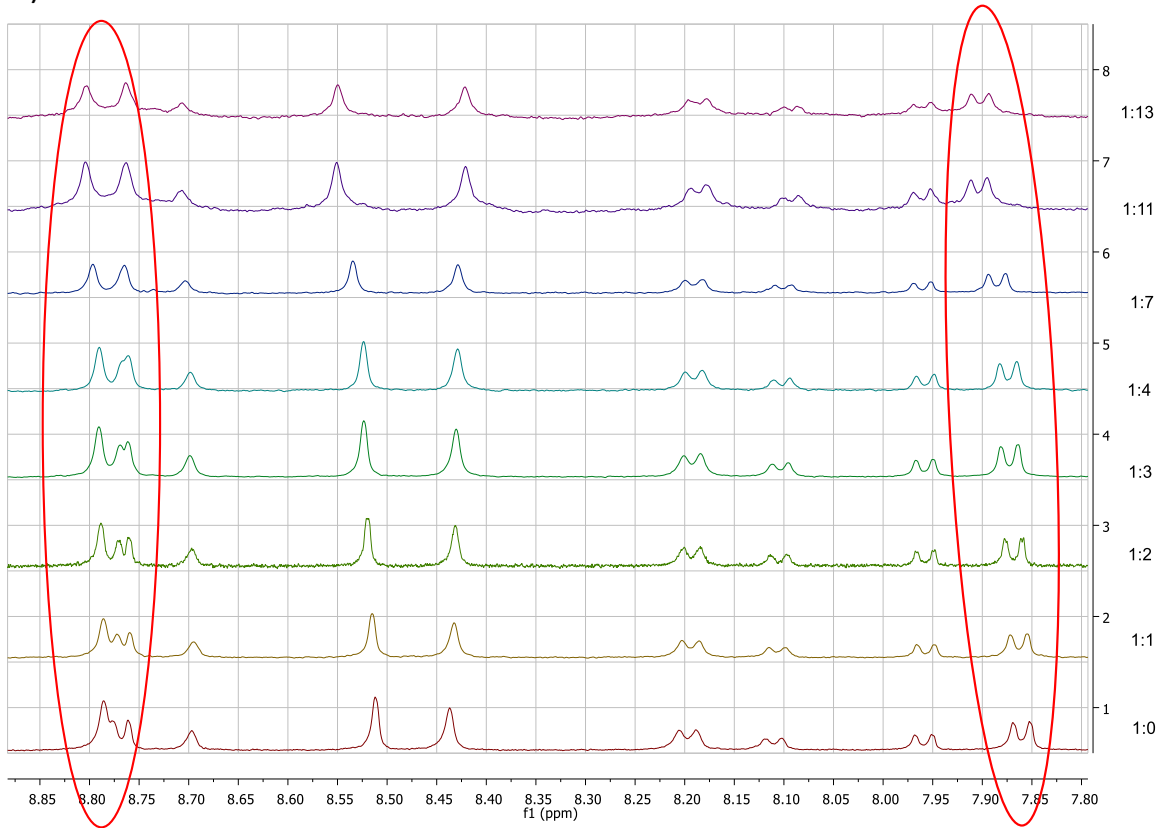
Cage 54D-a: The ligand L_N (14.5 mg, 0.0303 mmol) and the molybdenum precursor (20.2 mg, 0.0303 mmol) were premixed in dry carbon tetrachloride (1.5 mL) for 20 minutes to generate the catalyst *in situ*. Then the monomer **53a** (115 mg, 0.055 mmol) was added and the stirring was continued overnight. The reaction was monitored by GPC. After GPC showed sharp single peak in reasonable range, the reaction was taken out of the glovebox and the precipitates were filtered by vacuum filtration. The filtrate was concentrated down and purified by column chromatography (with eluting solvent hexane/CH₂Cl₂, 4/1) and 56 mg (79%) light yellow solid was collected. ¹H NMR (500 MHz, CDCl₃) δ 8.61 (s, 4H), 8.60 (s, 8H), 8.58(s, 4H), 8.41(s, 8H), 8.29(s, 4H), 8.11(s, 8H), 8.08(d, J=10 Hz, 8H), 7.98 (d, J=10Hz, 4H), 7.74 (d, J = 8.5, 8H), 7.66 (d, J = 8.2, 8H), 7.57 (d, J = 8.6, 4H), 7.49 (d, J = 8.7 Hz, 8H), 7.45 (d, J = 8.7 Hz, 4H), 7.28 (d, 4H), 4.40(s, 8H), 4.09(s, 16H), 1.98(m, 8H), 1.77(m, 16H), 1.27-1.15(m, 348H), 0.90-0.82(m, 87H). ¹³C NMR (101 MHz, CDCl₃) δ 143.0, 142.4, 140.4, 140.3, 133.1, 131.9, 129.7, 128.7, 125.6, 125.2, 124.3, 124.0, 123.3, 123.2, 123.1, 122.8, 119.4, 118.5, 114.2, 114.0, 109.3, 109.1, 108.7, 89.2, 88.0, 43.4, 43.1, 31.9, 29.7, 29.6, 29.5, 29.6, 29.1, 29.0, 27.4, 27.3, 22.7, 14.1. MALDI-TOF MS: calcd. for C₃₇₂H₄₈₀N₁₂: 5115.79, found: 5115.66 (M⁺).

3.5.3. Host guest study of Cage **54D-a** with Fullerenes in toluene-*d*₈ and CS₂

A)



B)



C)

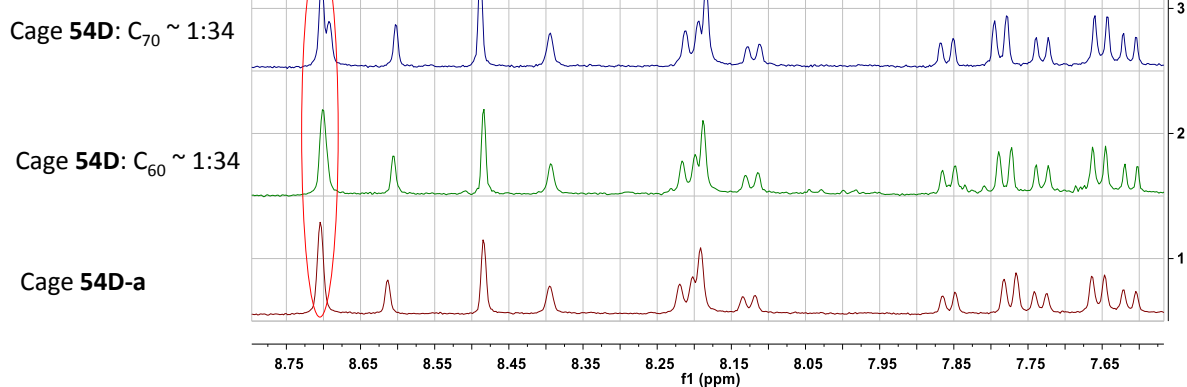


Figure 3.9. NMR Titration study of cage **54D-a** with C_{60} (A) and C_{70} (B) in toluene- d_8 . The concentration of cage **54D-a** was 0.14 mmol/L. C) cage **54D-a** with C_{60} and C_{70} in CS_2 .

3.5.4. NMR characterization of cage **54D-a**

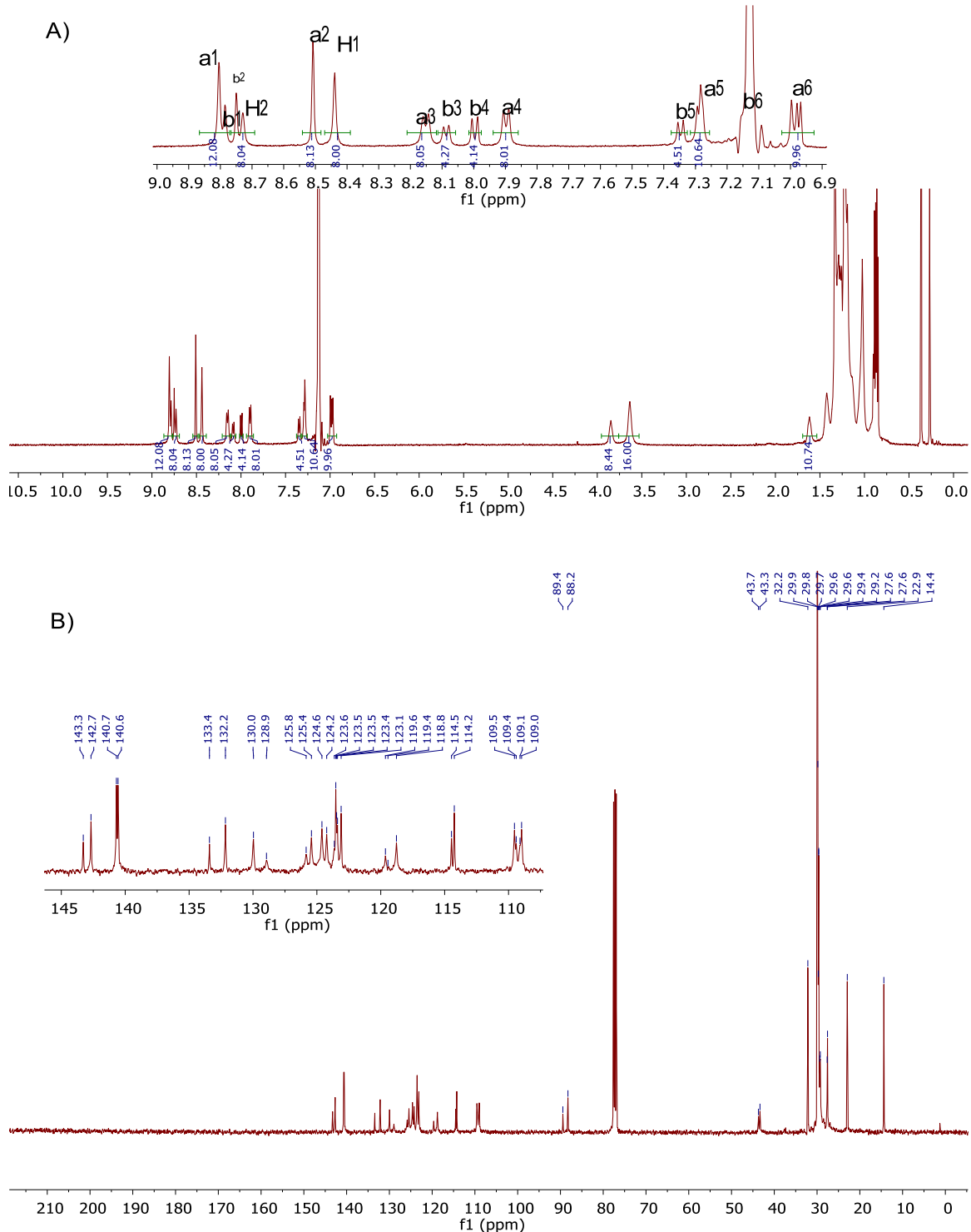


Figure 3.10. ^1H NMR of cage **54D-a** in C_6D_6 (A) and ^{13}C NMR in CDCl_3 (B). Proton b^6 was hidden by benzene peak in ^1H NMR.

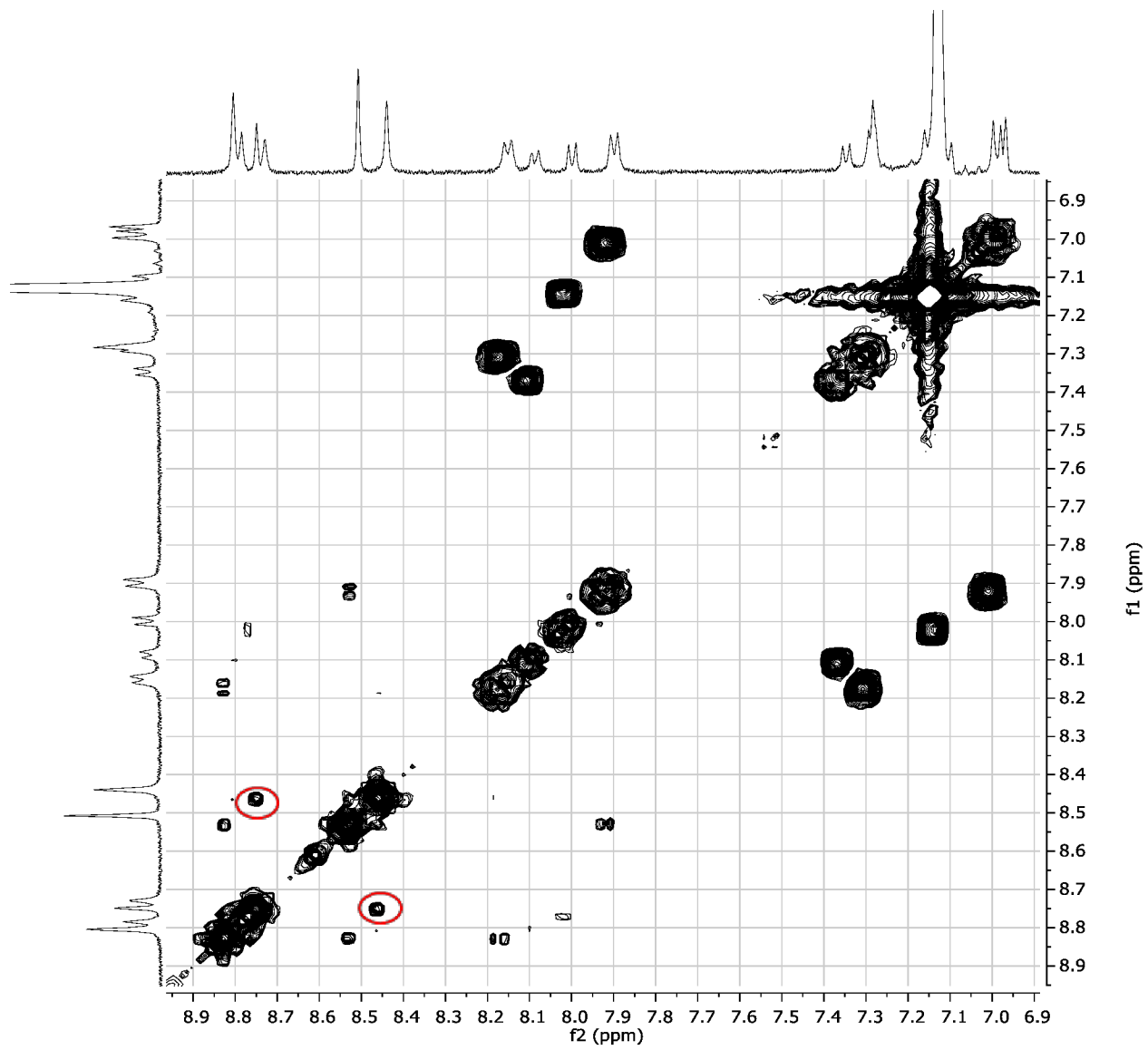


Figure 3.11. gCOSY of cage **54D-a** in C_6D_6 . The cross peak labeled (belonging to center benzene protons H^1 and H^2) proved that the two sets of peaks are from one molecule instead of two different species.

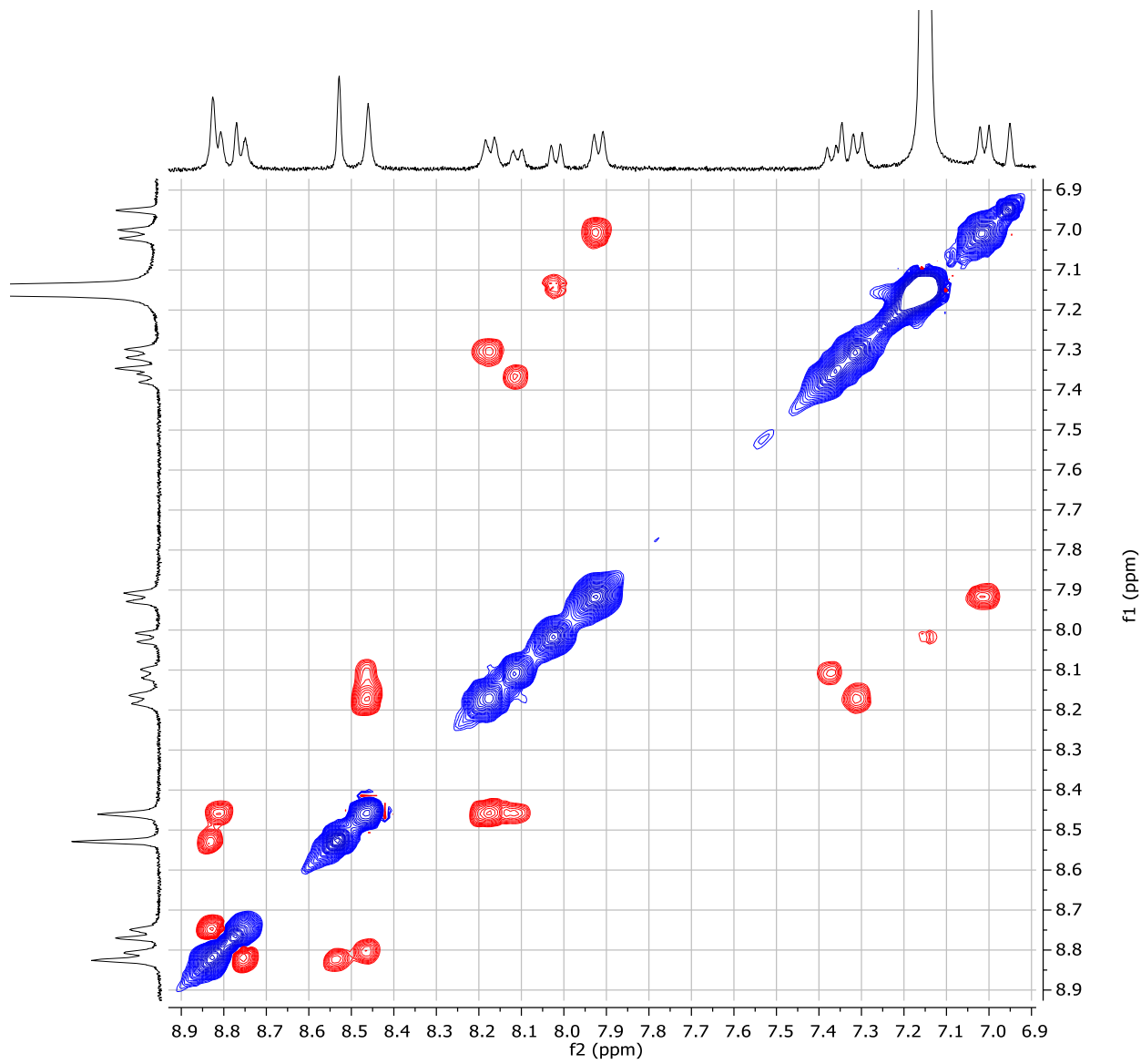


Figure 3.12. ROESY of cage **54D-a** in C_6D_6 .

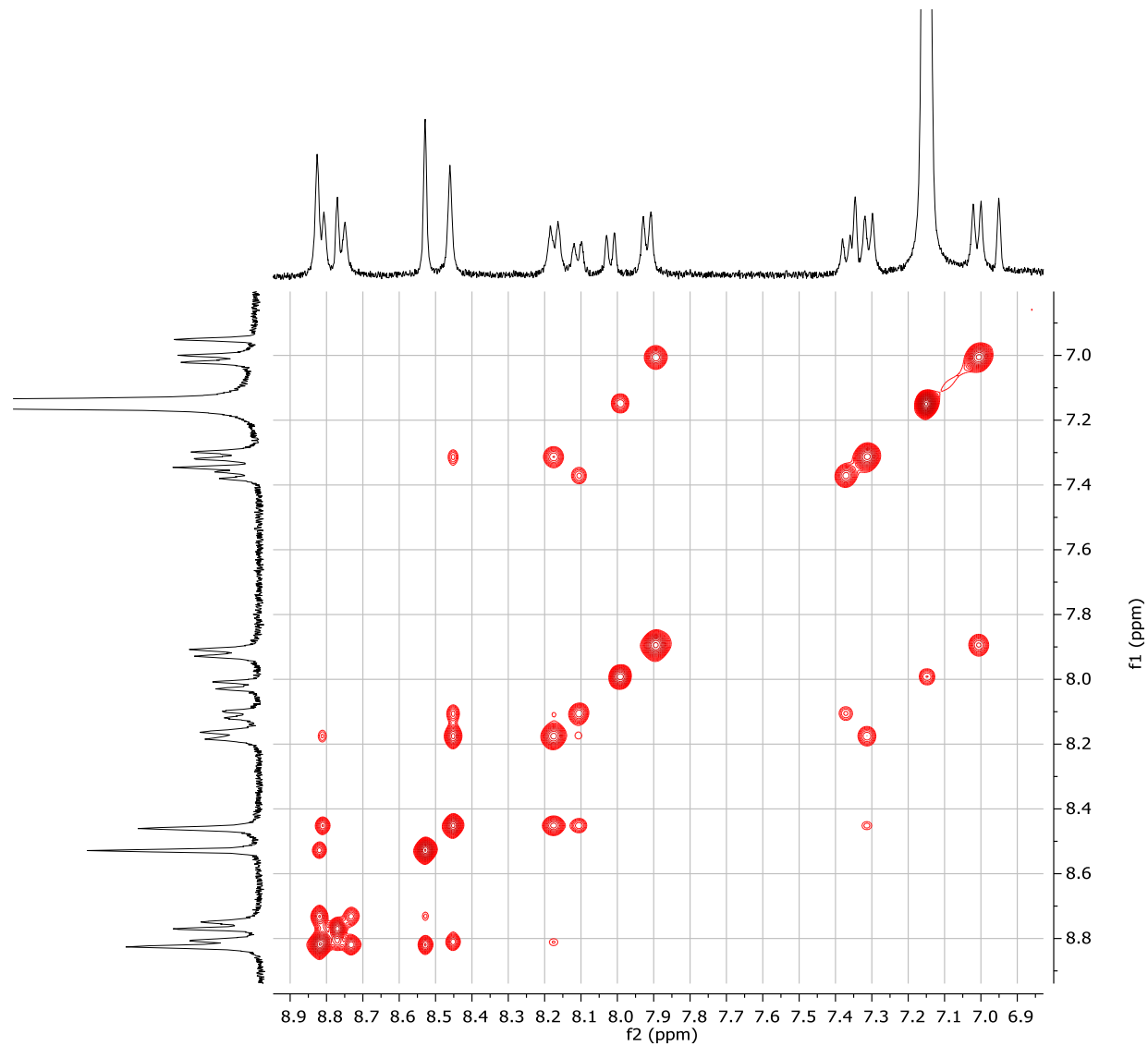


Figure 3.13. NOESY of cage **54D-a** at room temperature in C_6D_6 .

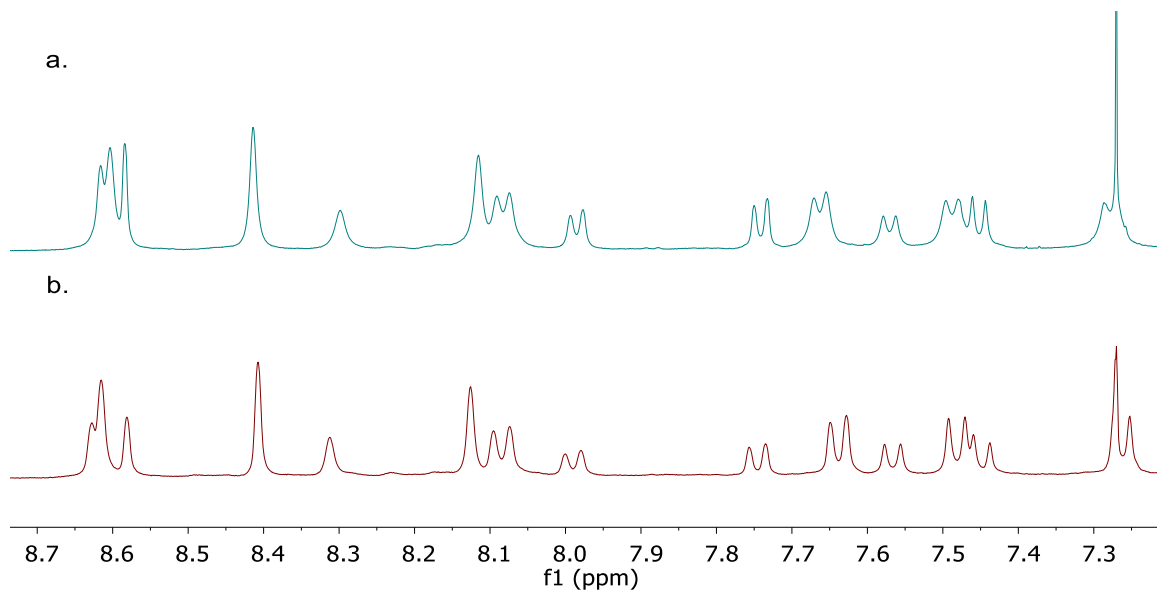


Figure 3.14. The aromatic region of ¹H NMR of cage **54D-a** at 20 °C (a) and 59 °C (b) in CDCl₃.

3.5.5. GPC characterization

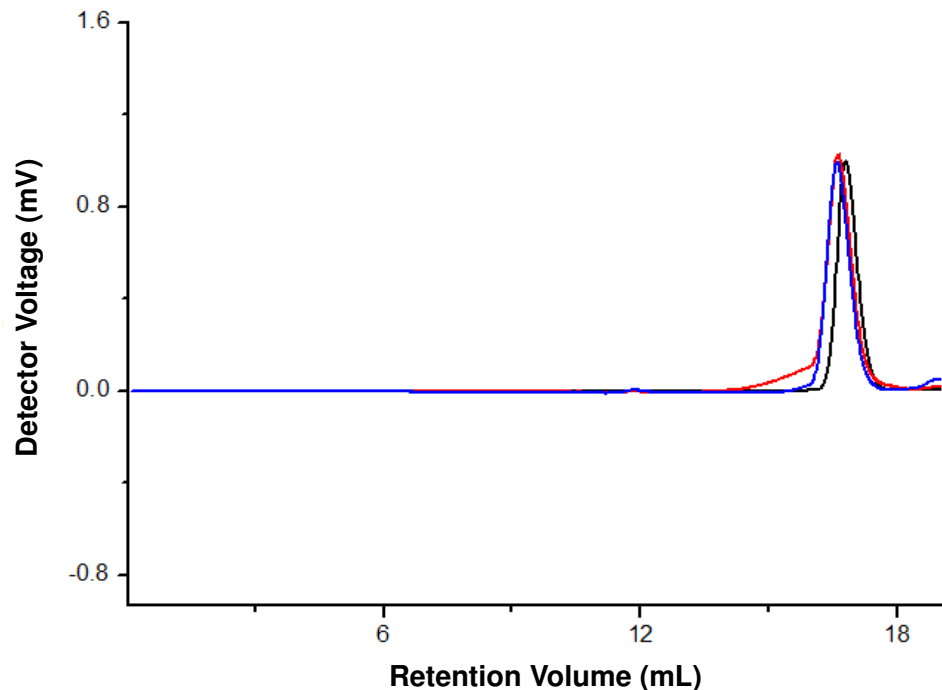
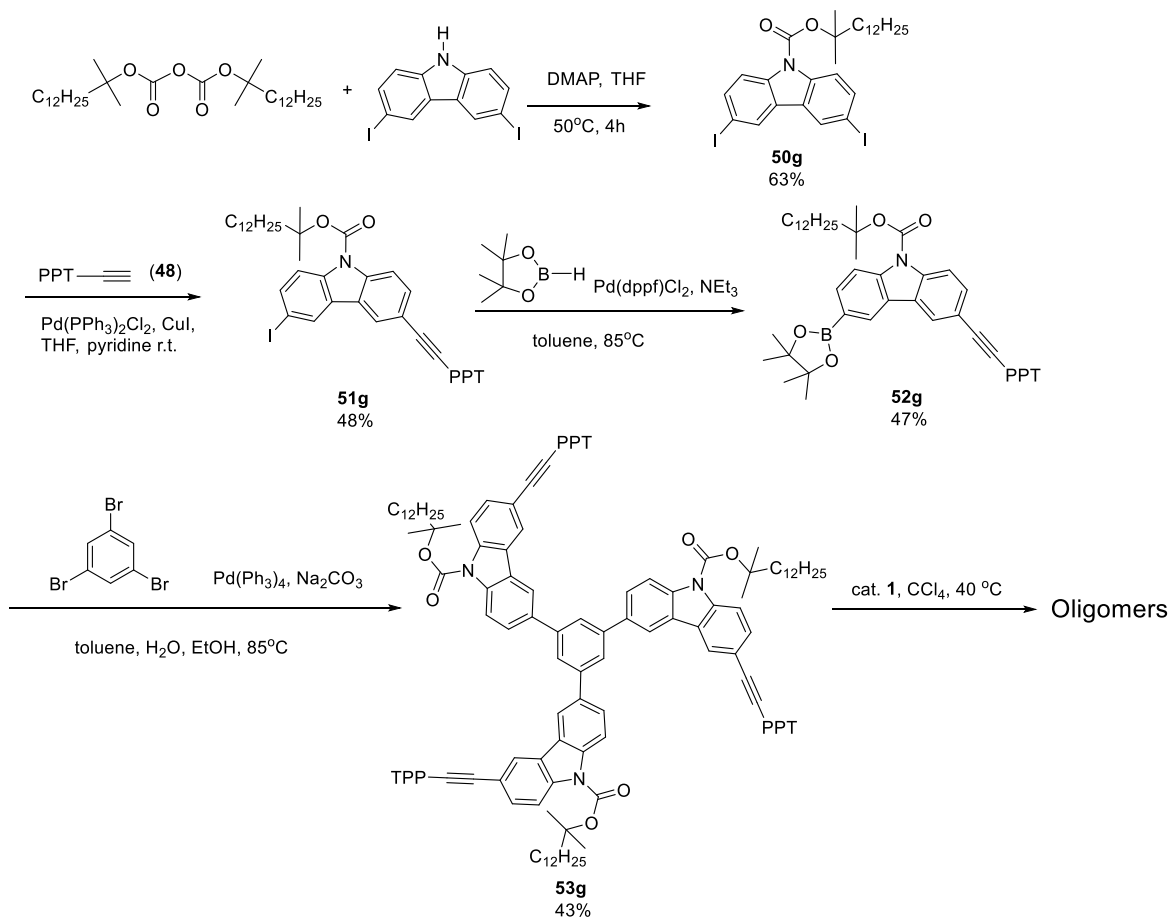


Figure 3.15. Normalized GPC traces of monomer **53** (black), crude reaction mixture after workup (red) and pure cage **54D-a** (blue).

3.5.6. Synthetic procedures of 53b, 54D-c, 54D-d, 53h, 53g, 53i, 54D-j.



Bis(1,1-dimethyltridecyl) dicarbonate was synthesized following literature procedure.²⁶

3,6-diiodo-9H-carbazole was synthesized following literature procedure.²⁷ To a solution of carbazole (20.0 g, 120 mmol) in acetic acid (500 mL) was added potassium iodide (25.8 g, 155 mmol). With stirring, potassium iodate (33.8 g, 192 mmol) was slowly added to the mixture and refluxed for 15 min. The reaction mixture was cooled to room temperature, and then quenched with NaHSO₃ (aq.) until the purple color disappeared. CH₂Cl₂ (200 mL) was added to the mixture. After separation, the organic layer was collected. The aqueous layer was washed with CH₂Cl₂ (100 mL × 2), and the organic layers were combined and washed with NaHCO₃ (aq. 200

mL) and brine (150 mL). The organic phase was dried over Na_2SO_4 and the solvent was removed under vacuum. The product (31.0 g, 62%) was crystallized from CHCl_3 (250 mL).

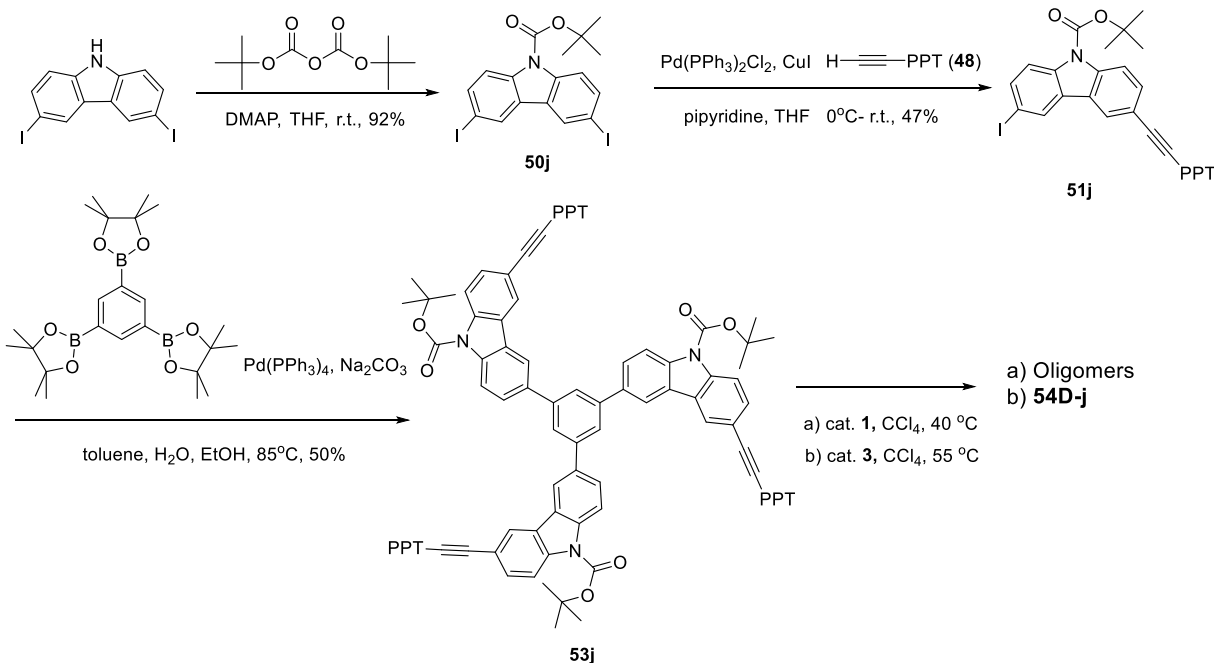
52g were synthesized following similar procedure as **52a**.

Physical data for **50g**: ^1H NMR (500 MHz, CDCl_3) δ 8.21 (d, J = 1.7 Hz, 2H), 8.03 (d, J = 8.8 Hz, 2H), 7.74 (dd, J = 8.8, 1.8 Hz, 2H), 2.08 – 2.02 (m, 2H), 1.72 (s, 6H), 1.51 – 1.20 (m, 20H), 0.94 – 0.86 (m, 3H).

Physical data for **51g**: ^1H NMR (500 MHz, CDCl_3) δ 8.31 (d, J = 1.8 Hz, 1H), 8.27 (d, J = 8.6 Hz, 1H), 8.13 (d, J = 1.5 Hz, 1H), 8.06 (d, J = 8.8 Hz, 1H), 7.93 (d, J = 8.3 Hz, 2H), 7.86 (dd, J = 8.3, 1.4 Hz, 2H), 7.79 – 7.72 (m, 3H), 7.72 – 7.66 (m, 5H), 7.65 – 7.60 (m, 1H), 7.53 (t, J = 7.7 Hz, 2H), 2.11 – 2.02 (m, 2H), 1.74 (s, 6H), 1.53 – 1.19 (m, 20H), 0.88 (t, J = 7.0 Hz, 3H).

Physical data for **52g**: ^1H NMR (400 MHz, CDCl_3) δ 8.50 (d, J = 1.0 Hz, 1H), 8.29 (s, 1H), 8.26 (s, 1H), 7.97 – 7.90 (m, 3H), 7.88 – 7.82 (m, 2H), 7.79 – 7.71 (m, 2H), 7.71 – 7.58 (m, 6H), 7.52 (t, J = 7.3 Hz, 1H), 2.12 – 2.00 (m, 2H), 1.74 (d, J = 1.0 Hz, 6H), 1.55 – 1.18 (m, 32H), 0.87 (t, J = 6.8 Hz, 3H).

Physical data for **53g**: ^1H NMR (400 MHz, CDCl_3) δ 8.47 – 8.39 (m, 6H), 8.38 – 8.32 (m, 6H), 8.07 (s, 3H), 7.98 – 7.93 (m, 3H), 7.90 – 7.78 (m, 12H), 7.75 – 7.57 (m, 24H), 7.55 – 7.46 (m, 6H), 2.18 – 2.07 (m, 6H), 1.78 (s, 18H), 1.57 – 1.14 (m, 60H), 0.84 (t, J = 6.9 Hz, 9H).



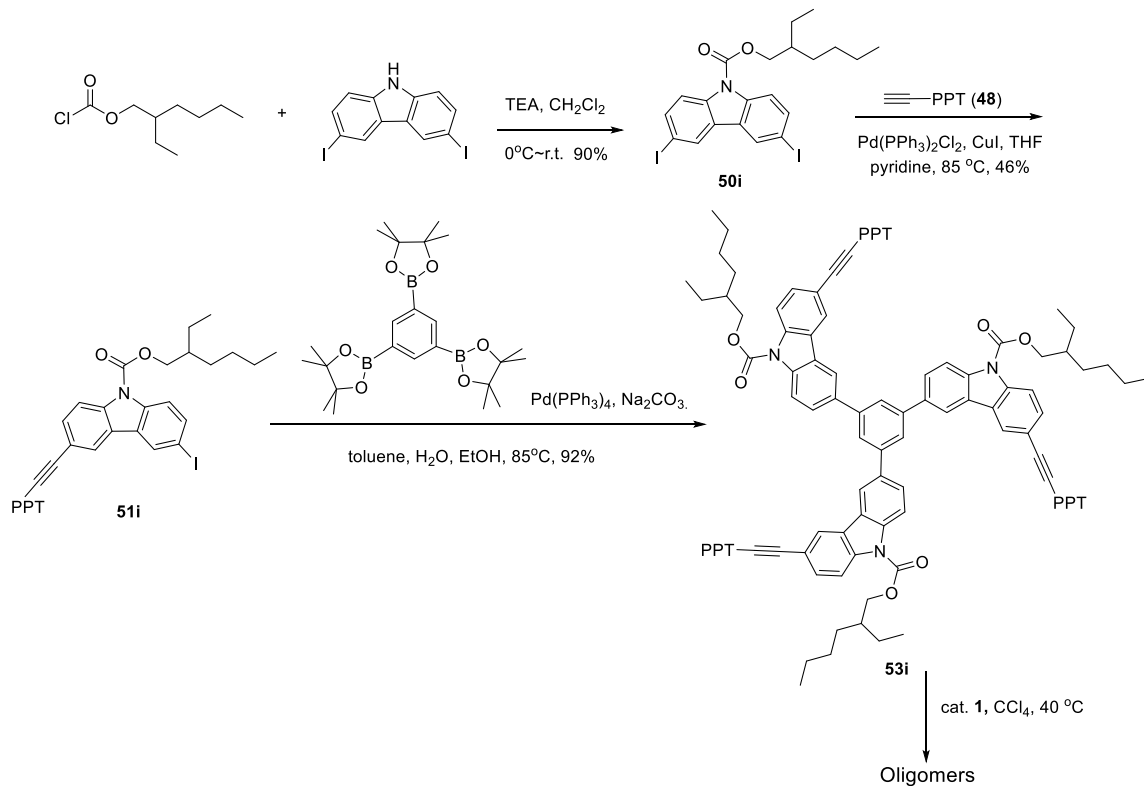
9-Boc-3,6-diiodocarbazole (50j): To a round bottom flask, 3,6-diiodo-9*H*-carbazole (10.0 g, 23.8 mmol), n 4-dimethylaminopyridine (2.66 g, 23.8 mmol) and di-*tert*-butyl dicarbonate (10.4 g, 47.6 mmol) were dissolved in dry THF (300 mL). The reaction was stopped after stirring at r.t. for 3 h by removing all solvent under vacuum. The residue was redissolved in CH₂Cl₂ (200 mL) and washed with 1M HCl (150 mL), NaHCO₃ (aq. 150 mL) and brine (150 mL) separately. Then the organic phase was concentrated down after dried over Na₂SO₄. The white product (11.4 g, 92%) was collected after purified by column chromatography (hexanes/CH₂Cl₂, 2/1, v/v). The NMR characterization was the same as the reported.²⁷

Compound 51j: To a Schlenk tube 9-boc-3,6-diiodocarbazole (1.730 g, 3.33 mmol), compound **48** (1.13 g, 4 mmol), Pd(PPh₃)₂Cl₂ (70 mg, 0.1 mmol) and CuI (7 mg, 0.08 mmol) were charged. THF (20 mL) and piperidine (7 mL) were added under N₂ flow. The reaction was stirred at r.t. for 16 h. The solvent was removed by vacuum evaporation, the crude reaction mixture was dissolved in CH₂Cl₂ (50 mL) and washed with NH₄Cl (sat., 70 mL) and brine (70 mL). The organic extracts were dried over Na₂SO₄, and concentrated. The residue was purified by flash

column chromatography ($\text{CH}_2\text{Cl}_2/\text{hexane}$, 1/1~1.5/1, v/v) to give the product as a yellow solid (1.05 g, 47 %). ^1H NMR (500 MHz, CDCl_3) δ 8.29 (d, $J = 1.8$ Hz, 1H), 8.27 (d, $J = 8.7$ Hz, 1H), 8.11 (d, $J = 1.8$ Hz, 1H), 8.06 (d, $J = 8.8$ Hz, 1H), 7.92 (d, $J = 8.2$ Hz, 2H), 7.86 (d, $J = 7.3$ Hz, 1H), 7.78 – 7.72 (m, 3H), 7.71 – 7.66 (m, 5H), 7.65 – 7.60 (m, 1H), 7.55 – 7.50 (m, 2H), 1.78 (s, 9H). ^{13}C NMR (126 MHz, CDCl_3) δ 195.90, 150.20, 143.92, 139.15, 137.89, 137.76, 137.45, 136.23, 135.69, 132.27, 131.99, 130.92, 130.64, 129.85, 128.40, 128.17, 127.05, 126.98, 126.56, 124.13, 123.13, 122.88, 118.00, 117.73, 116.11, 90.79, 88.63, 86.79, 84.53, 28.18.

1,3,5-Tris(4,4,5,5-tetramethyl-1,3,2-dioxaborolan-2-yl)benzene was synthesized following reported procedure.²⁸

53j is synthesized following the general Suzuki coupling procedure. ^1H NMR (500 MHz, CDCl_3) δ 8.47 – 8.41 (m, 6H), 8.40 – 8.33 (m, 6H), 8.08 (s, 3H), 7.97 (dd, $J = 8.7, 1.9$ Hz, 3H), 7.91 – 7.79 (m, 12H), 7.76 – 7.57 (m, 24H), 7.55 – 7.48 (m, 6H), 1.83 (s, 27H).



3,6-Diiodo-9H-carbazole was synthesized following the reported procedure.²⁹

3,6-Diiodo-9-(2-ethyl)hexyloxycarbonyl-carbazole (50i) was synthesized following the modified synthetic procedure.³⁰ ¹H NMR (500 MHz, CDCl₃) δ 8.26 (d, *J* = 1.8 Hz, 2H), 8.07 (d, *J* = 8.8 Hz, 2H), 7.78 (dd, *J* = 8.8, 1.8 Hz, 2H), 4.54 – 4.43 (m, 2H), 1.86 (hept, *J* = 6.3 Hz, 1H), 1.55 – 1.31 (m, 8H), 1.00 (t, *J* = 7.5 Hz, 3H), 0.93 (t, *J* = 7.0 Hz, 3H).

51i and **53i** were synthesized following similar procedure as synthesis of **51a** and **53a**.

Physical data of **51i**: ¹H NMR (500 MHz, CDCl₃) δ 8.28 – 8.22 (m, 2H), 8.08 (t, *J* = 1.9 Hz, 1H), 8.04 (d, *J* = 8.7 Hz, 1H), 7.95 – 7.90 (m, 2H), 7.88 – 7.83 (m, 2H), 7.77 – 7.71 (m, 3H), 7.70 – 7.59 (m, 6H), 7.56 – 7.50 (m, 2H), 4.58 – 4.37 (m, 2H), 1.88 (hept, *J* = 6.3 Hz, 1H), 1.60 – 1.33 (m, 8H), 1.02 (t, *J* = 7.5 Hz, 3H), 0.94 (t, *J* = 7.0 Hz, 3H).

Physical data of **53i**: ¹H NMR (500 MHz, CDCl₃) δ 8.47 (d, *J* = 8.7 Hz, 3H), 8.43 (d, *J* = 1.7 Hz, 3H), 8.37 (d, *J* = 1.9 Hz, 6H), 8.08 (s, 3H), 7.98 (dd, *J* = 8.7, 1.9 Hz, 3H), 7.89 – 7.86 (m, 6H), 7.84 – 7.81 (m, 6H), 7.74 (dd, *J* = 8.7, 1.7 Hz, 3H), 7.70 – 7.64 (m, 12H), 7.64 – 7.59 (m, 9H), 7.51 (t, *J* = 7.7 Hz, 6H), 4.56 (dd, *J* = 5.7, 3.9 Hz, 6H), 1.94 (dt, *J* = 12.3, 6.0 Hz, 3H), 1.67 – 1.57 (m, 6H), 1.41 (tt, *J* = 14.8, 7.5 Hz, 18H), 1.05 (t, *J* = 7.5 Hz, 9H), 0.95 (t, *J* = 7.1 Hz, 9H). ¹³C NMR (101 MHz, CDCl₃) δ 196.35, 152.50, 144.31, 142.28, 139.47, 138.48, 138.35, 137.83, 136.60, 132.66, 132.35, 130.97, 130.21, 128.55, 127.34, 126.90, 126.10, 126.00, 123.59, 123.22, 118.39, 118.16, 116.78, 116.48, 91.34, 88.95, 70.10, 39.17, 30.74, 29.17, 24.18, 23.28, 14.38, 11.31.

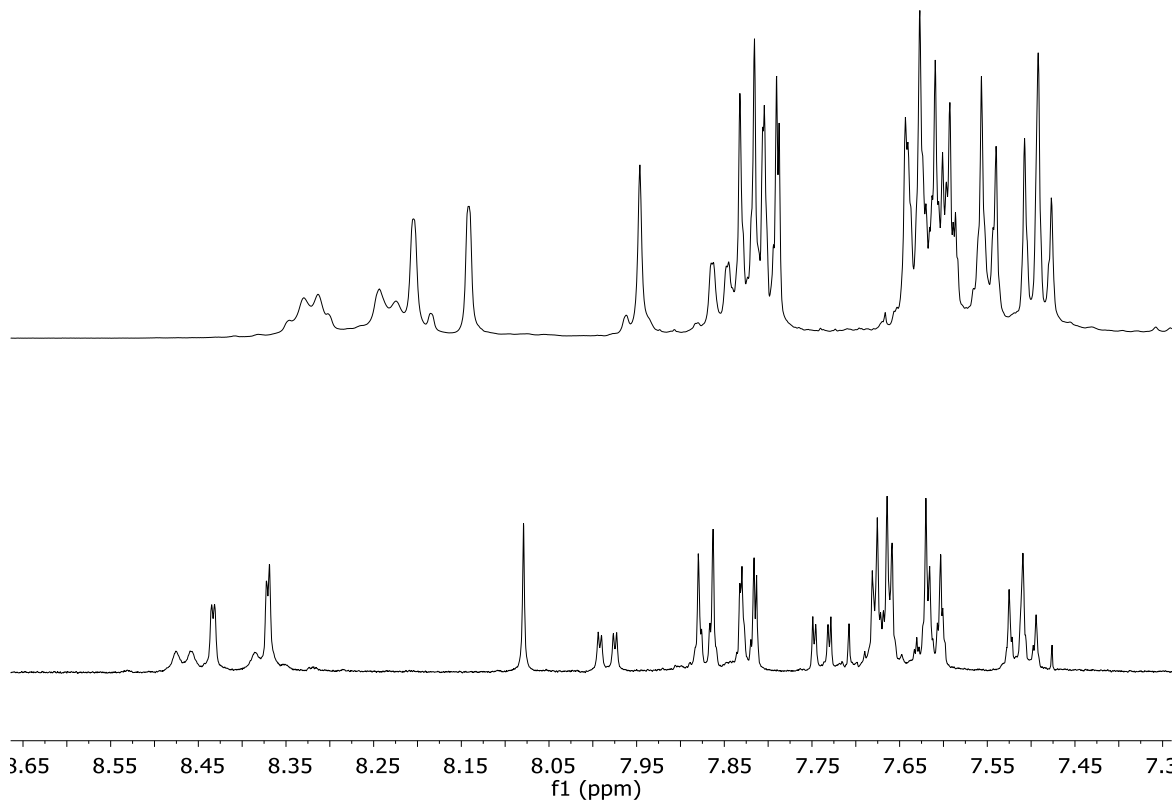
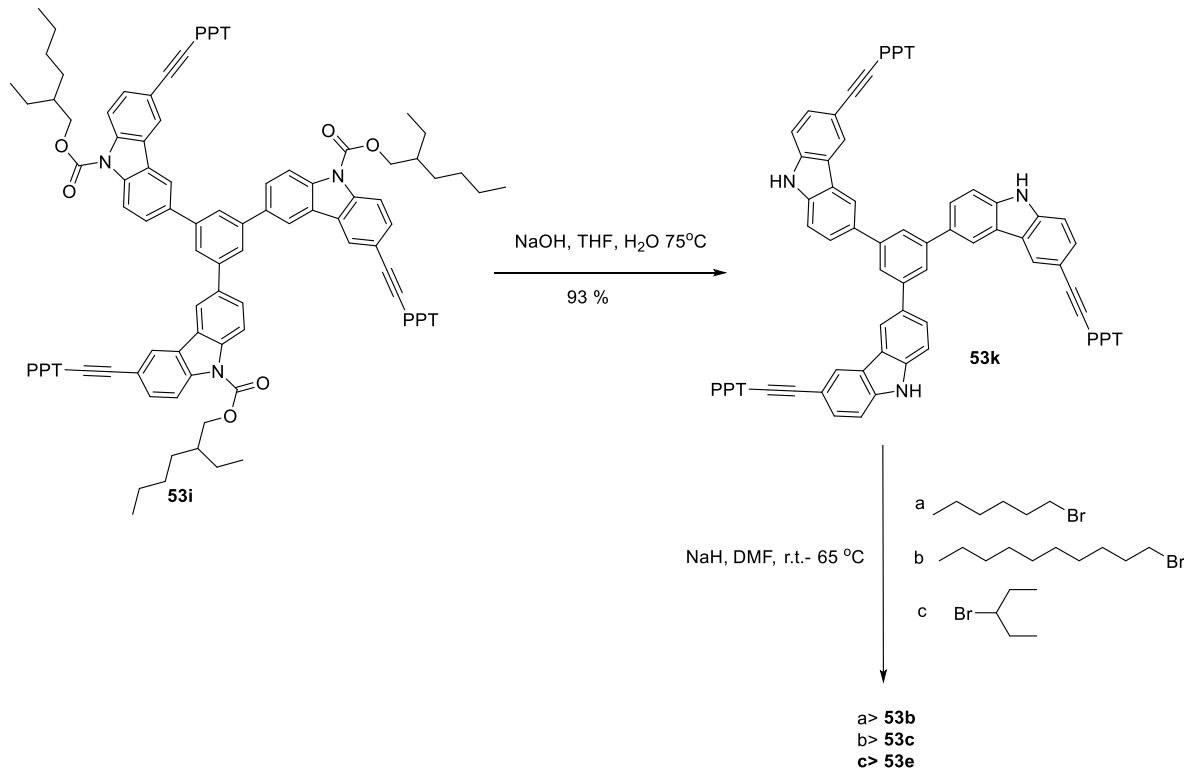


Figure 3.16. The ^1H NMR spectra of dilute (bottom) and concentrated (top) **53i**, showing that the **53i** has strong aggregation in solution.



53k: 53i (144 mg, 0.076 mmol) was dissolved in THF (3 mL). Then a NaOH (150 mg in 3 mL) solution was added. The mixture was heated to 75 °C overnight. Then the solvent was removed under reduced pressure. The resulting solids were washed with EtOAc (10 mL × 2) and hexanes (10 mL × 2). Then the solids (101 mg, 93 %) were collected as pure product. ^1H NMR (500 MHz, THF- d_8) δ 8.79 (d, J = 1.7 Hz, 3H), 8.58 (d, J = 1.4 Hz, 3H), 8.23 (s, 3H), 8.07 (dd, J = 8.4, 1.8 Hz, 3H), 7.90 (d, J = 8.3 Hz, 6H), 7.88 – 7.81 (m, 12H), 7.78 (d, J = 8.3 Hz, 6H), 7.71 (d, J = 8.3 Hz, 6H), 7.69 – 7.63 (m, 9H), 7.59 – 7.53 (m, 9H).

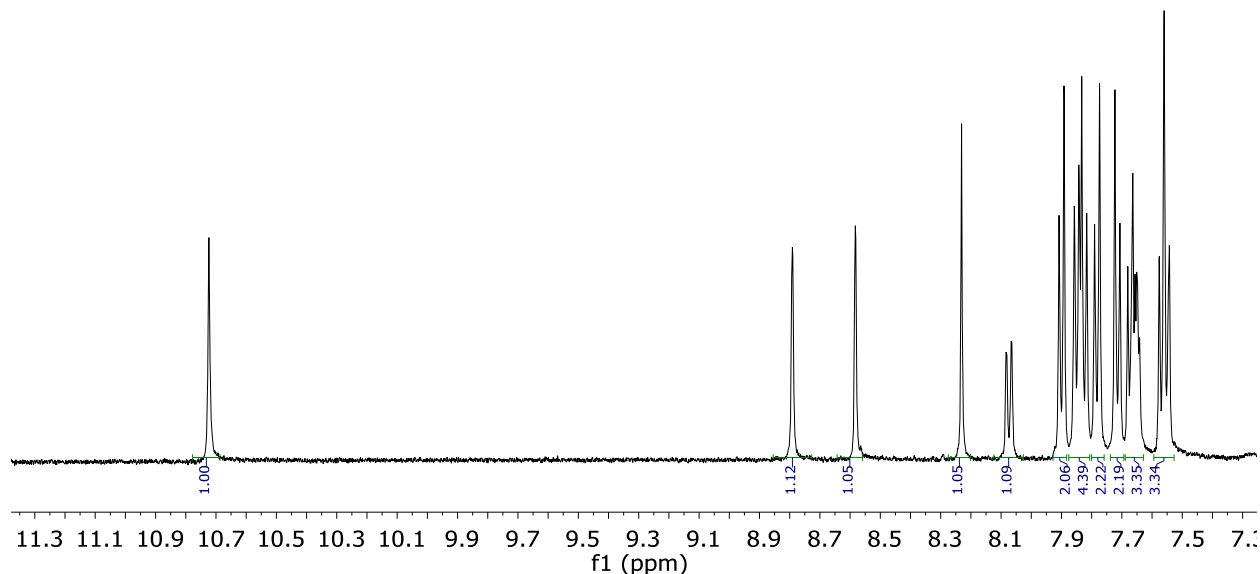


Figure 3.17. The ^1H NMR of chain cleaved **53k**.

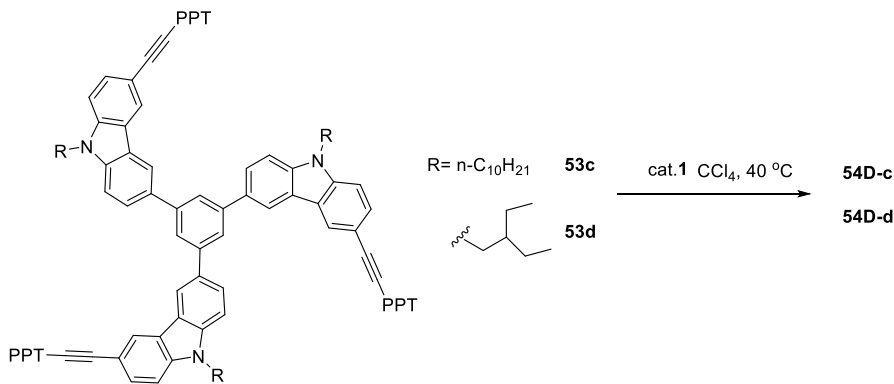
53b, **53c**, and **53e** were synthesized following general procedure for attaching bromo-alkane to carbazole. The yield of synthesizing **53d** is low, mainly due to steric hinderance. Thus elevated temperature 65 °C is needed.

Physical data of **53b** ^1H NMR (500 MHz, CDCl_3) δ 8.57 (d, J = 1.7 Hz, 3H), 8.49 (d, J = 1.5 Hz, 3H), 8.07 (s, 3H), 7.99 (dd, J = 8.5, 1.8 Hz, 3H), 7.90 – 7.85 (m, 6H), 7.85 – 7.79 (m, 6H), 7.71 (dd, J = 8.4, 1.6 Hz, 3H), 7.70 – 7.65 (m, 9H), 7.65 – 7.55 (m, 15H), 7.51 (t, J = 7.7 Hz, 9H),

7.45 (d, $J = 8.5$ Hz, 3H), 4.39 (t, $J = 7.2$ Hz, 6H), 1.96 (p, $J = 7.3$ Hz, 6H), 1.51 – 1.23 (m, 18H), 0.90 (t, $J = 7.0$ Hz, 9H).

Physical data of **53c** ^1H NMR (400 MHz, CDCl_3) δ 8.55 (d, $J = 1.7$ Hz, 3H), 8.47 (d, $J = 1.4$ Hz, 3H), 8.06 (s, 3H), 7.97 (dd, $J = 8.5, 1.8$ Hz, 3H), 7.89 – 7.83 (m, 6H), 7.84 – 7.78 (m, 6H), 7.73 – 7.58 (m, 24H), 7.56 (d, $J = 8.6$ Hz, 3H), 7.53 – 7.47 (m, 6H), 7.43 (d, $J = 8.6$ Hz, 3H), 4.37 (t, $J = 7.2$ Hz, 6H), 1.94 (p, $J = 7.4$ Hz, 7H), 1.50 – 1.16 (m, 42H), 0.93 – 0.82 (m, 9H).

Physical data of **53e** ^1H NMR (500 MHz, CDCl_3) δ 8.57 (s, 3H), 8.48 (s, 3H), 8.08 (s, 3H), 7.93 (d, $J = 7.4$ Hz, 3H), 7.89 – 7.84 (m, 6H), 7.84 – 7.79 (m, 6H), 7.70 – 7.63 (m, 15H), 7.63 – 7.56 (m, 12H), 7.50 (t, $J = 7.6$ Hz, 9H), 4.60 – 4.37 (m, 3H), 1.35 – 1.25 (m, 12H), 0.83 (t, $J = 7.3$ Hz, 18H).

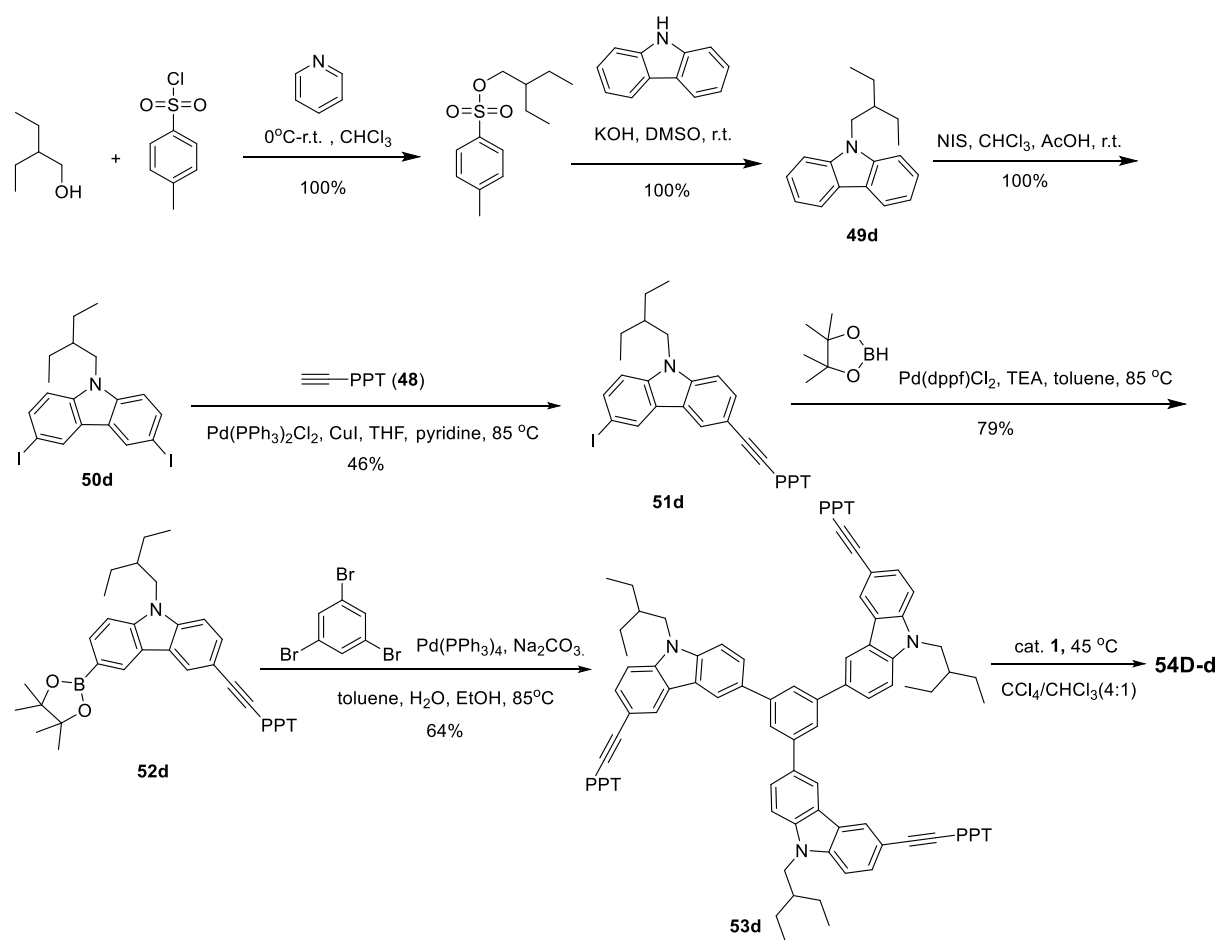


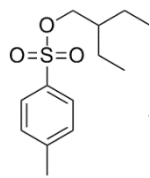
Physical data of **54D-c**: ^1H NMR (500 MHz, CDCl_3) δ 8.64 – 8.56 (m, 16H), 8.40 (d, $J = 1.5$ Hz, 8H), 8.29 (s, 4H), 8.11 (s, 8H), 8.08 (d, $J = 8.7$ Hz, 8H), 7.98 (d, $J = 7.1$ Hz, 4H), 7.74 (d, $J = 8.4$ Hz, 4H), 7.65 (d, $J = 9.1$ Hz, 8H), 7.57 (d, $J = 8.4$ Hz, 4H), 7.49 (d, $J = 8.7$ Hz, 8H), 7.45 (d, $J = 8.7$ Hz, 4H), 7.29 (d, $J = 7.2$ Hz, 8H), 4.58 – 4.33 (m, 8H), 4.23 – 3.94 (m, 16H), 2.02 – 1.92 (m, 8H), 1.84 – 1.72 (m, 16H), 1.58 – 1.20 (m, 168H), 0.79 (t, $J = 7.0$ Hz, 36H). MALDI-TOF(m/z): $[\text{M} + \text{H}]^+$ calcd. for $\text{C}_{300}\text{H}_{336}\text{N}_{12}$, 4108.68; found: 4111.08.

Physical data of **54D-d**: ^1H NMR (500 MHz, CDCl_3) δ 8.64 (s, 4H), 8.60 (s, 12H), 8.38 (d, $J = 1.6$ Hz, 8H), 8.30 (s, 4H), 8.13 (s, 8H), 8.10 (d, $J = 8.1$ Hz, 8H), 8.00 (d, $J = 8.2$ Hz, 4H), 7.60 – 7.53 (m, 12H), 7.51 – 7.42 (m, 12H), 7.19 (d, $J = 8.5$ Hz, 8H), 4.28 (d, $J = 7.4$ Hz, 8H), 3.91 (d, $J = 7.4$ Hz, 16H), 2.15 – 2.07 (m, 4H), 1.96 – 1.88 (m, 8H), 1.51 – 1.28 (m, 48H), 1.02 (t, $J = 7.4$ Hz, 72H). MALDI-TOF(m/z): [M] $^+$ calcd. for $\text{C}_{252}\text{H}_{240}\text{N}_{12}$, 3435.92; found, 3436.04.

Due to purification difficulty, **54D-e** was not successfully purified.

The synthetic route for **54D-d** from the free carbazole:





The reported synthetic procedure was followed. ^{31}H NMR (500 MHz, CDCl_3) δ 7.80 (d, $J = 8.3$ Hz, 2H), 7.35 (d, $J = 8.0$ Hz, 2H), 3.94 (d, $J = 5.5$ Hz, 2H), 2.46 (s, 3H), 1.48 (q, $J = 6.0$ Hz, 1H), 1.40 – 1.26 (m, 4H), 0.80 (t, $J = 7.5$ Hz, 6H).

49d: The reported synthetic procedure was followed. ^{32}H NMR (500 MHz, CDCl_3) δ 8.24 (d, $J = 7.8$ Hz, 2H), 7.59 (td, $J = 7.6, 6.7, 1.5$ Hz, 2H), 7.52 (d, $J = 8.3$ Hz, 2H), 7.37 (t, $J = 7.4$ Hz, 2H), 4.25 (d, $J = 7.5$ Hz, 2H), 2.14 (hept, $J = 6.6$ Hz, 1H), 1.70 – 1.40 (m, 4H), 1.06 (t, $J = 7.4$ Hz, 6H). ^{13}C NMR (101 MHz, CDCl_3) δ 141.19, 125.84, 123.06, 120.58, 119.03, 118.97, 109.25, 47.31, 41.12, 24.15, 11.24.

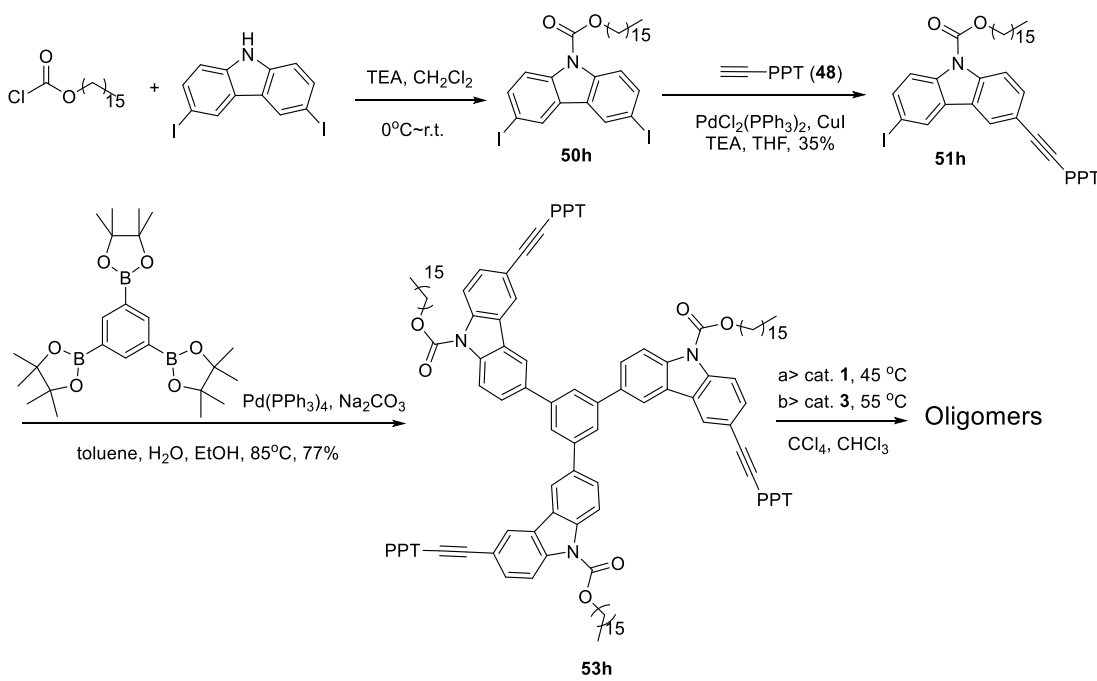
Physical data of **50d**: ^1H NMR (500 MHz, CDCl_3) δ 8.33 (d, $J = 1.7$ Hz, 2H), 7.71 (dd, $J = 8.6, 1.7$ Hz, 2H), 7.16 (d, $J = 8.6$ Hz, 2H), 4.09 (d, $J = 7.5$ Hz, 2H), 1.93 (hept, $J = 6.7$ Hz, 1H), 1.49 – 1.23 (m, 4H), 0.92 (t, $J = 7.5$ Hz, 6H). ^{13}C NMR (101 MHz, CDCl_3) δ 140.13, 134.68, 129.52, 124.14, 111.40, 81.88, 47.41, 40.93, 24.00, 11.10.

Physical data of **51d**: ^1H NMR (500 MHz, CDCl_3) δ 8.37 (d, $J = 1.7$ Hz, 1H), 8.22 (d, $J = 1.6$ Hz, 1H), 7.95 – 7.89 (m, 2H), 7.89 – 7.84 (m, 2H), 7.77 – 7.59 (m, 9H), 7.52 (dd, $J = 8.3, 7.0$ Hz, 2H), 7.33 (d, $J = 8.5$ Hz, 1H), 7.14 (d, $J = 8.6$ Hz, 1H), 4.07 (d, $J = 7.5$ Hz, 2H), 1.94 (d, $J = 7.5$ Hz, 1H), 1.45 – 1.26 (m, 4H), 0.93 (t, $J = 7.5$ Hz, 6H).

Physical data of **52d**: ^1H NMR (500 MHz, CDCl_3) δ 8.64 (s, 1H), 8.38 (d, $J = 1.5$ Hz, 1H), 7.95 (dd, $J = 8.3, 1.1$ Hz, 1H), 7.94 – 7.91 (m, 2H), 7.88 – 7.84 (m, 2H), 7.76 (d, $J = 8.3$ Hz, 2H), 7.71 – 7.60 (m, 6H), 7.53 (t, $J = 7.7$ Hz, 2H), 7.43 – 7.36 (m, 2H), 4.20 (d, $J = 7.5$ Hz, 2H), 2.01 (p, $J = 6.8$ Hz, 1H), 1.40 – 1.31 (m, 4H), 0.94 (t, $J = 7.4$ Hz, 6H). ^{13}C NMR (101 MHz, CDCl_3) δ 196.47, 144.64, 143.63, 140.91, 139.19, 137.96, 136.58, 132.77, 132.67, 132.28, 131.05,

130.26, 129.50, 128.59, 128.23, 127.40, 127.01, 124.53, 124.22, 123.39, 122.40, 113.78, 109.43, 108.94, 92.56, 87.70, 83.90, 47.38, 40.96, 25.22, 25.14, 24.03, 11.14.

Physical data of **53d**: ^1H NMR (500 MHz, CDCl_3) δ 8.57 (d, $J = 1.8$ Hz, 3H), 8.48 (d, $J = 1.1$ Hz, 2H), 8.07 (s, 3H), 7.98 (dd, $J = 8.5, 1.8$ Hz, 3H), 7.90 – 7.85 (m, 6H), 7.85 – 7.80 (m, 6H), 7.73 – 7.66 (m, 18H), 7.65 – 7.59 (m, 6H), 7.57 (d, $J = 8.5$ Hz, 3H), 7.54 – 7.48 (m, 6H), 7.44 (d, $J = 8.6$ Hz, 3H), 4.27 (d, $J = 7.4$ Hz, 6H), 2.09 (hept, $J = 6.7$ Hz, 3H), 1.55 – 1.39 (m, 12H), 1.00 (t, $J = 7.4$ Hz, 18H).



50h was synthesized following the similar procedure of synthesis of **50i**. ^1H NMR (500 MHz, CDCl_3) δ 8.24 (d, $J = 1.8$ Hz, 2H), 8.05 (d, $J = 8.8$ Hz, 2H), 7.77 (dd, $J = 8.8, 1.8$ Hz, 2H), 4.53 (t, $J = 6.7$ Hz, 2H), 1.91 (p, $J = 6.9$ Hz, 2H), 1.45 – 1.20 (m, 27H), 0.89 (t, $J = 6.9$ Hz, 3H).

Physical data of **51h**: ^1H NMR (500 MHz, CDCl_3) δ 8.34 (d, $J = 1.8$ Hz, 1H), 8.30 (d, $J = 8.7$ Hz, 1H), 8.16 (d, $J = 1.8$ Hz, 1H), 8.10 (d, $J = 8.7$ Hz, 1H), 7.93 (d, $J = 8.3$ Hz, 2H), 7.89 – 7.84 (m, 2H), 7.79 (dd, $J = 8.8, 1.8$ Hz, 1H), 7.76 (d, $J = 8.4$ Hz, 2H), 7.69 (s, 5H), 7.53 (t, $J = 7.6$ Hz,

2H), 4.57 (t, J = 6.7 Hz, 2H), 1.93 (tt, J = 13.5, 7.2 Hz, 2H), 1.55 – 1.23 (m, 26H), 0.95 – 0.87 (m, 3H).

Physical data of **53h**: ^1H NMR (500 MHz, CDCl_3) δ 8.49 – 8.42 (m, 3H), 8.40 (d, J = 1.8 Hz, 3H), 8.38 – 8.32 (m, 6H), 8.06 (s, 3H), 7.96 (dd, J = 8.7, 1.9 Hz, 3H), 7.90 – 7.85 (m, 6H), 7.82 (dd, J = 8.2, 1.4 Hz, 6H), 7.72 (dd, J = 8.6, 1.7 Hz, 3H), 7.71 – 7.64 (m, 12H), 7.64 – 7.58 (m, 9H), 7.51 (t, J = 7.7 Hz, 6H), 4.61 (t, J = 6.8 Hz, 6H), 1.98 (q, J = 7.1 Hz, 6H), 1.48 – 1.41 (m, 6H), 1.40 – 1.17 (m, 72H), 0.89 (t, J = 7.0 Hz, 9H). MALDI-TOF MS: calcd. for $[\text{M}+\text{H}]^+$ $\text{C}_{105}\text{H}_{60}\text{N}_3\text{O}_3$: 1412.48, found: 1413.39.

3.6. References

1. Jin, Y. H.; Voss, B. A.; Noble, R. D.; Zhang, W. *Angew. Chem. Int. Ed.* **2010**, *49*, 6348-6351.
2. Mastalerz, M.; Schneider, M. W.; Oppel, I. M.; Presly, O. *Angew. Chem. Int. Ed.* **2011**, *50*, 1046-1051.
3. Mastalerz, M. *Angew. Chem. Int. Ed.* **2010**, *49*, 5042-5053.
4. Murase, T.; Otsuka, K.; Fujita, M. *J. Am. Chem. Soc.* **2010**, *132*, 7864-+.
5. Sato, S.; Morohara, O.; Fujita, D.; Yamaguchi, Y.; Kato, K.; Fujita, M. *J. Am. Chem. Soc.* **2010**, *132*, 3670-3671.
6. Meng, W. J.; Breiner, B.; Rissanen, K.; Thoburn, J. D.; Clegg, J. K.; Nitschke, J. R. *Angew. Chem. Int. Ed.* **2011**, *50*, 3479-3483.
7. Francesconi, O.; Ienco, A.; Moneti, G.; Nativi, C.; Roelens, S. *Angew. Chem. Int. Ed.* **2006**, *45*, 6693-6696.
8. Heinz, T.; Rudkevich, D. M.; Rebek, J. *Nature* **1998**, *394*, 764-766.
9. Yoshizawa, M.; Klosterman, J. K.; Fujita, M. *Angew. Chem. Int. Ed.* **2009**, *48*, 3418-3438.
10. Lin, Z. H.; Sun, J. L.; Efremovska, B.; Warmuth, R. *Chem. Eur. J.* **2012**, *18*, 12864-12872.
11. Yang, H. W.; Kong, X.; Wei, J. F.; Liu, C. C.; Song, W. J.; Zhang, W.; Wei, W.; He, S. H. *Cell. Physiol. Biochem.* **2012**, *29*, 561-570.
12. Tranchemontagne, D. J. L.; Ni, Z.; O'Keeffe, M.; Yaghi, O. M. *Angew. Chem. Int. Ed.* **2008**, *47*, 5136-5147.

13. Zhang, W.; Jyothish, K.; Yang, H. S.; Wang, Q. *Abstr. Pap. Am. Chem. Soc.* **2013**, 246.
14. Jin, Y. H.; Voss, B. A.; Jin, A.; Long, H.; Noble, R. D.; Zhang, W. *J. Am. Chem. Soc.* **2011**, 133, 6650-6658.
15. Skowronek, P.; Gawronski, J. *Org. Lett.* **2008**, 10, 4755-4758.
16. Tozawa, T.; Jones, J. T. A.; Swamy, S. I.; Jiang, S.; Adams, D. J.; Shakespeare, S.; Clowes, R.; Bradshaw, D.; Hasell, T.; Chong, S. Y.; Tang, C.; Thompson, S.; Parker, J.; Trewin, A.; Bacsa, J.; Slawin, A. M. Z.; Steiner, A.; Cooper, A. I. *Nat. Mater.* **2009**, 8, 973-978.
17. Hasell, T.; Wu, X. F.; Jones, J. T. A.; Bacsa, J.; Steiner, A.; Mitra, T.; Trewin, A.; Adams, D. J.; Cooper, A. I. *Nat. Chem.* **2010**, 2, 750-755.
18. Kataoka, K.; James, T. D.; Kubo, Y. *J. Am. Chem. Soc.* **2007**, 129, 15126-15127.
19. Yang, H. S.; Liu, Z. N.; Zhang, W. *Adv. Synth. Catal.* **2013**, 355, 885-890.
20. Furstner, A.; Radkowski, K.; Grabowski, J.; Wirtz, C.; Mynott, R. *J. Org. Chem.* **2000**, 65, 8758-8762.
21. Zhang, W.; Moore, J. S. *J. Am. Chem. Soc.* **2004**, 126, 12796-12796.
22. Zhang, C. X.; Wang, Q.; Long, H.; Zhang, W. *J. Am. Chem. Soc.* **2011**, 133, 20995-21001.
23. Hosseini, A.; Taylor, S.; Accorsi, G.; Armaroli, N.; Reed, C. A.; Boyd, P. D. W. *J. Am. Chem. Soc.* **2006**, 128, 15903-15913.
24. Case, D. A. e. a. *AMBER 11*; University of California, San Francisco.
25. Wang, J.; Wolf, R. M.; Caldwell, J. W.; Kollman, P. A.; Case, D. A. *J. Comput. Chem.* **2004**, 25, 1157-1174.
26. Naddo, T.; Che, Y.; Zhang, W.; Balakrishnan, K.; Yang, X.; Yen, M.; Zhao, J.; Moore, J. S.; Zang, L. *J. Am. Chem. Soc.* **2007**, 129, 6978-6979.
27. Albrecht, K.; Yamamoto, K. *J. Am. Chem. Soc.* **2009**, 131, 2244-2251.
28. Liu, Y.; Niu, F.; Lian, J.; Zeng, P.; Niu, H. *Synthetic Met.* **2010**, 160, 2055-2060.
29. Prachumrak, N.; Pansay, S.; Namuangruk, S.; Kaewin, T.; Jungsuttiwong, S.; Sudyoadsuk, T.; Promarak, V. *Eur. J. Org. Chem.* **2013**, 2013, 6619-6628.
30. Butler, K. V.; Kalin, J.; Brochier, C.; Vistoli, G.; Langley, B.; Kozikowski, A. P. *J. Am. Chem. Soc.* **2010**, 132, 10842-10846.
31. Sworen, J. C.; Smith, J. A.; Berg, J. M.; Wagener, K. B. *J. Am. Chem. Soc.* **2004**, 126, 11238-11246.
32. Belletête, M.; Blouin, N.; Boudreault, P.-L. T.; Leclerc, M.; Durocher, G. *J. Phys. Chem. A* **2006**, 110, 13696-13704.

CHAPTER 4

A Dimeric Triangular Prism and Its Interlocked Cages Synthesized via Alkyne Metathesis

4.1. Introduction

Interlocked molecules, by definition, are molecules that are mechanically linked and have to break at least one covalent bond to divide into two or more molecular components.¹⁻² These molecules, such as rotaxanes, knots, catenanes, are mechanically interlocked to each other that only have noncovalent interactions. Apparently, these molecules with interesting topologies endowed great synthetic difficulty. The first 2-D catenane designed and synthesized using ion-templated method was reported by Sauvage in 1983³. This work inspired a tremendous amount of topologically interesting molecules being designed and synthesized via metal-ion, e.g. catenanes, rotaxanes, knots and links, and increased the synthetic yields dramatically.⁴⁻⁵ However, 3-D interlocked cages were discovered much later in 1999 by the Fujita group. The triply interlocked metal organic dimeric cages quickly formed and existed as the main product in the system. More interestingly, there was no strong directing effect or template effect in the system.⁶ Later, more metal organic interlocked cages were reported with different topologies by Kuroda⁷, Hardie⁸ and Clever⁹⁻¹⁰. The metal-organic polycatenanes **56** were also discovered by

Lu^{11} . With the development of covalent organic polyhedrons, interlocked covalent 3-D cages were also discovered but more rarely. The first three covalent interlocked 3-D cages were reported by the Cooper group in 2010¹². They observed the tetrahedral monomeric cages can slowly transform into triply interlocked dimeric cages in solution and crystallize out to drive the transformation equilibrium. Very recently in 2014, Mastalerz and coworkers crystallized out another interlocked giant COPs from its mono-cage compound solution¹³. To our best knowledge, these two works are the only reported interlocked covalent cages by now. In this work, a carbazole based covalent organic triangular prism and its interlocked cages synthesized through one-step alkyne metathesis will be discussed.

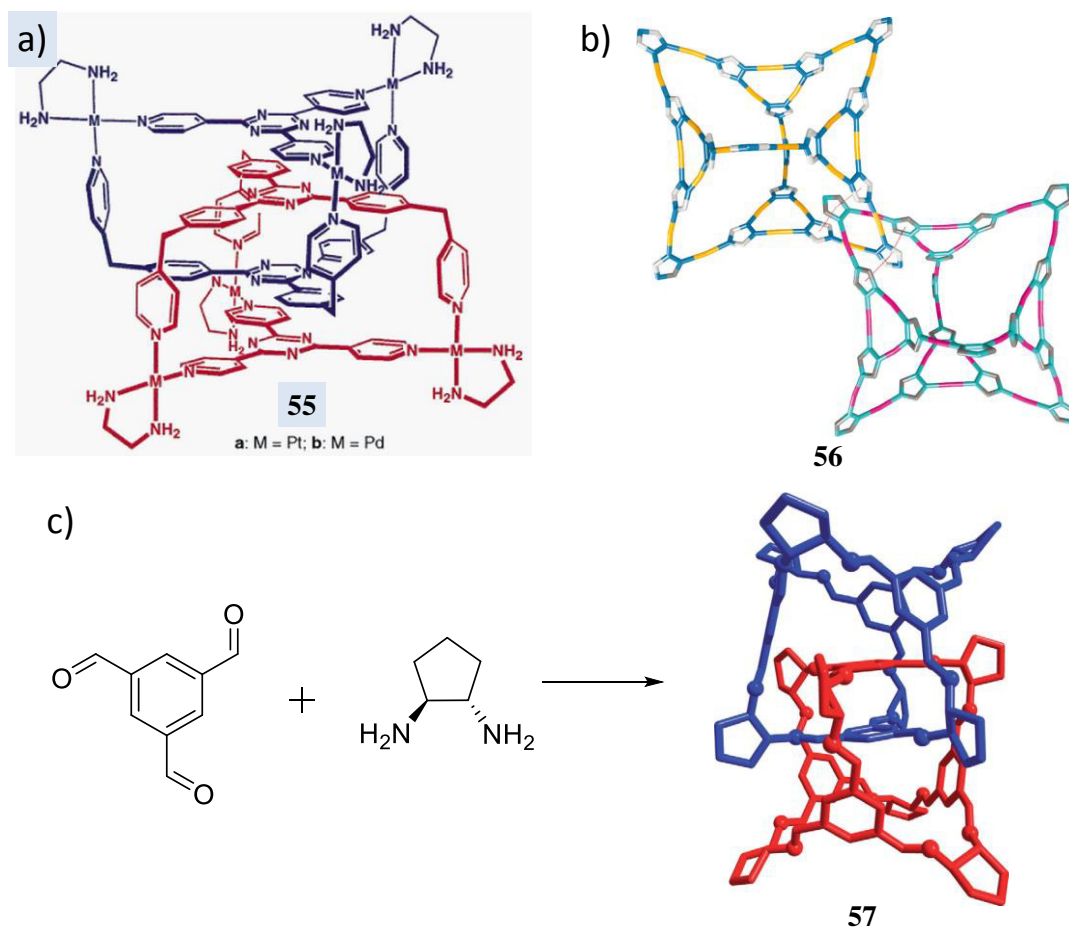


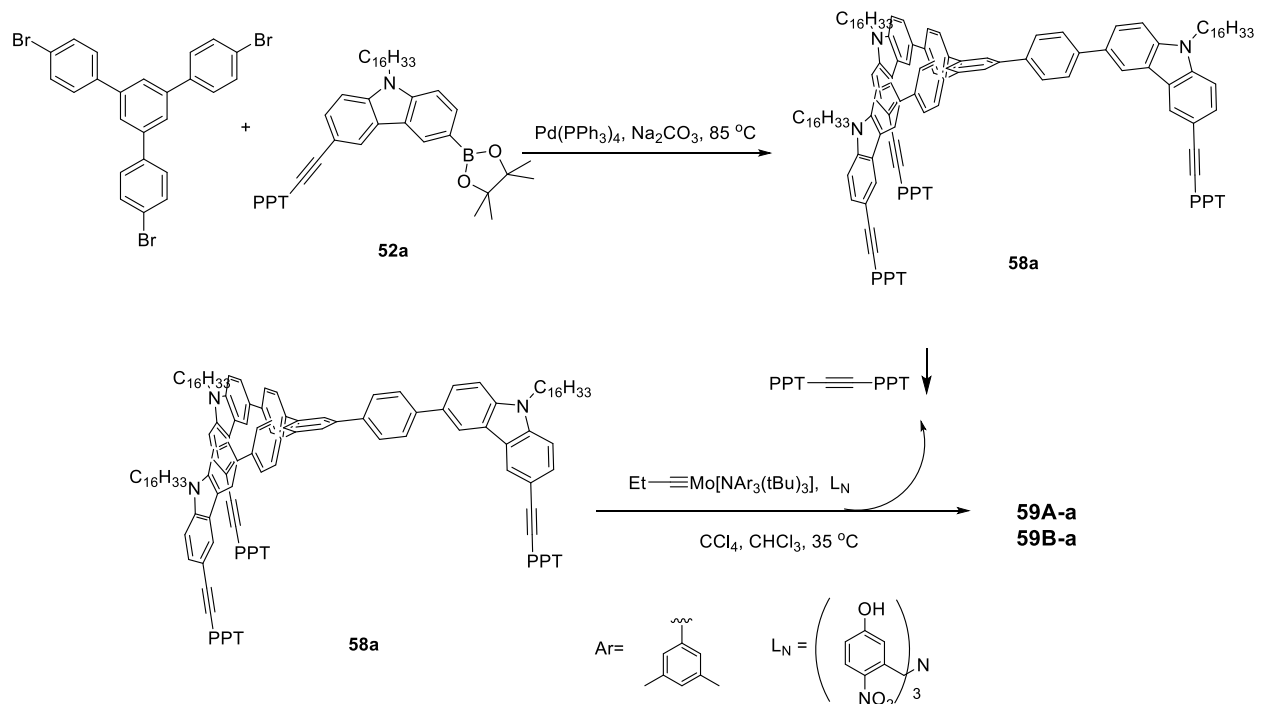
Figure 4.1. a) The crystal structure of interlocked MOP cage **56** reported by the Fujita group; b) the two interlocked cages in the polycatenane **56** reported by the Lu group; c) the synthetic scheme and crystal structure of one interlocked COP cage **57** reported by the Cooper group.

4.2. Results and Discussion

Given the dynamic nature of alkyne metathesis (a newly emerged DC_vC reaction for COP synthesis), its final product is usually the most thermodynamically favored. This is the key factor that leads to the formation of the dumbbell-shaped cage **54D** through alkyne metathesis as described in Chapter 3. The computational modeling result supports that the energy of two dimeric cages **54A** is indeed much higher than one dumbbell-shaped cage **54D**. We believe that the 87.4° angle of 3,6-disubstituted carbazole, which is less than the ideal 90° angle, induces angle strain thus elevating the energy of the dimeric cage. However, interestingly, with the same carbazole motif to provide a roughly the 90° vertex on a flat top piece, the reported porphyrin-based dimeric cage **35** showed high yield through alkyne metathesis.¹⁴ This observation leads us to the further investigation of the rules in construction of the shape-persistent covalent organic polyhedrons.

The main differences between the dumbbell-shaped cage and the porphyrin-based cage are 1) the center of dumbbell-shaped cage **54D** is a phenyl group and the center of **35** is a porphyrin; 2) **54D** contains 3 arms, and **35** contains 4 arms. The number of arms could affect the shape-persistency of one compound (e.g., 4-arm porphyrin cage **35**¹⁴ vs. 2-arm porphyrin macrocycle **36**¹⁵), but cage compounds with 3 arms vs. 4 arms should have similar shape-persistency and conformational stability. Given such consideration, we doubt that only the difference in the number of arms could induce the formation of cage structures with totally different topology. Therefore the size of the center piece of the monomer drew our attention. We speculate that the larger center piece would have relatively larger out-of-plane bending vibration that can release the angle strain introduced by the carbazole building block to certain extent, thus decreasing the enthalpy of the cage compound.

In order to study the dependence of cage formation on different building blocks, we designed the extended monomer **58a** with one more phenyl group installed on each arm (Scheme 4.1). Using catalyst **1** in CCl_4 and CHCl_3 mixed solvent at 35 °C, alkyne metathesis of monomer **58a** was conducted, after which, one major peak was observed on GPC. MALDI-TOF MS showed mainly a tetrameric species formed, along with dimer and even hexamer and octamer signals. TLC mainly showed two spots. Because of the difficulty in separating these two fractions using flash chromatography, prep TLC was used and two pure fractions were successfully obtained. The first fraction was confirmed by NMR and MALDI-TOF MS to be dimeric cage **59A-a**. In contrast to the NMR spectrum of the dumbbell-shaped cage **54D**, the ^1H NMR (Figure 4.2) of this dimeric cage only shows one set of signals corresponding the cage backbones and side chains instead of two sets with 2:1 ratio (Figure 3.1), which indicates that all three arms are identical. Compared with previously described dumbbell shape cage **54D**, we believe that the larger bending vibration of the extended center piece helped with the release of side arm strain caused by not fully matched geometry angle. Thus during the dimer formation, enthalpy was not sacrificed to a significant degree. In this case, the dimeric cage formed favorably. This observation supported the previous assumption that a larger center piece would provide more out-of-plane bending vibrations, thus lowering the enthalpy of dimeric product, which will result in dimer cages with higher entropy contribution.



Scheme 4.1. The synthetic scheme of cage **59A-a** and **59B-a**.

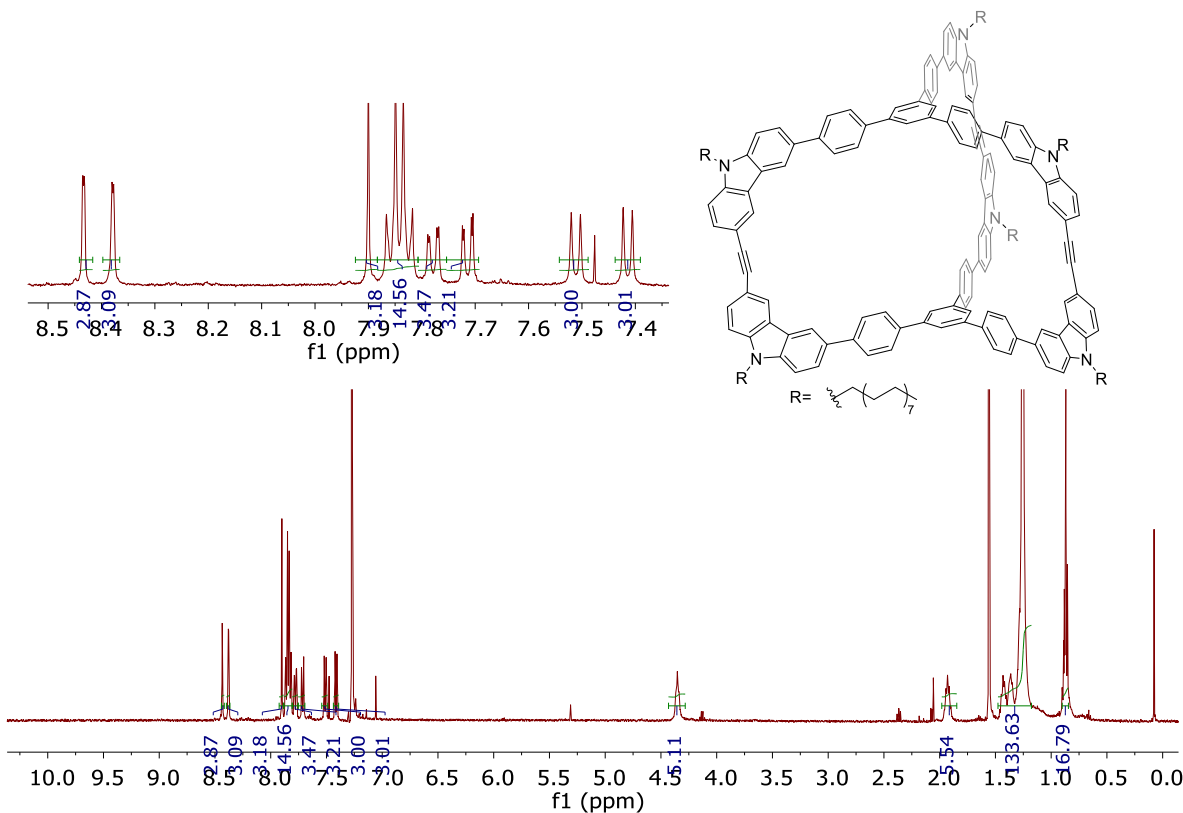


Figure 4.2. The structure of dimeric cage **59A-a** and its ^1H NMR spectrum in CDCl_3 .

However, the main product of this reaction was the second isolated fraction which was proved to be a tetramer by MALDI-TOF MS. The possible configurations of a tetrameric cage include 1) tetrahedral cage; 2) dumbbell-shaped cage; 3) interlocked cages. Thus, further NMR characterization was conducted. Surprisingly, the room temperature ¹H NMR signal is very broad (Figure 4.3) compared to both the dumbbell shape cage **54D** and the dimeric cage **59A-a**. Variable-temperature NMR and low temperature ROESY experiments were taken in order to investigate if the broad signals come from conformational change or configurational complexity. It is well known that if it is induced by configuration complexity (bond connection complexity), there should be no significant change on NMR signals at various temperatures. But if it is due to conformation exchange, the shape of the NMR peaks should change upon varying temperatures since the rate of conformation exchange depends on temperature. The variable-temperature NMR spectra (Figure 4.3) showed a dramatic change of both chemical shift and the shape of peaks at high or low temperatures. At -50 °C, the broad peaks observed at room temperature NMR spectrum were much sharper and well resolved, which means lower temperature slows down the conformation exchange. After increasing the temperature to 58 °C, a large number of peaks coalesced, giving fewer peak numbers, which is due to faster exchange rate at elevated temperature. This represents a strong evidence indicating that the conformation exchange contributed to peak broadening and complexity. ROESY experiment (Figure 4.11) also supported that chemical/conformational exchange existed in the **59B-a** sample at -50 °C. Since the cages were covalently bonded, there was no chemical exchange. These ROESY cross peaks were from conformational exchange. Given these characterization data, we believe that the tetrameric species **59B-a** 1) does not take the similar configuration as the dumbbell-shaped cage or tetrahedral cage, since the symmetry of the NMR signal was much lower than the dumbbell-

shaped or tetrahedral one; 2) should have low energy barrier on conformation exchange which can be observed at NMR time scale.

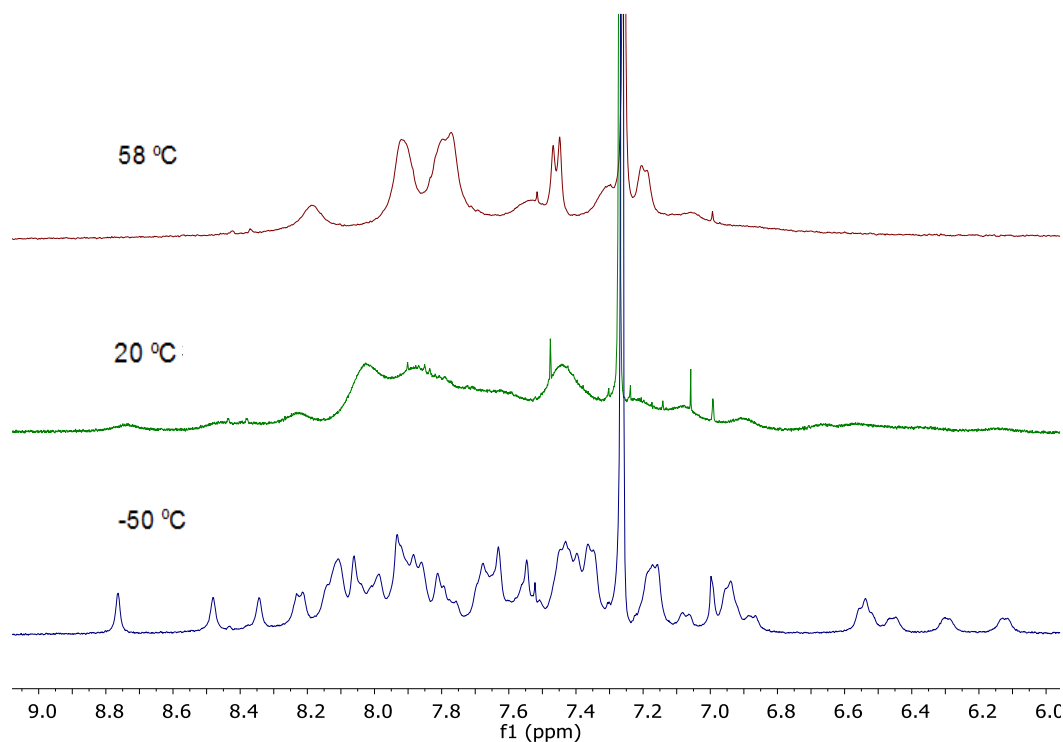
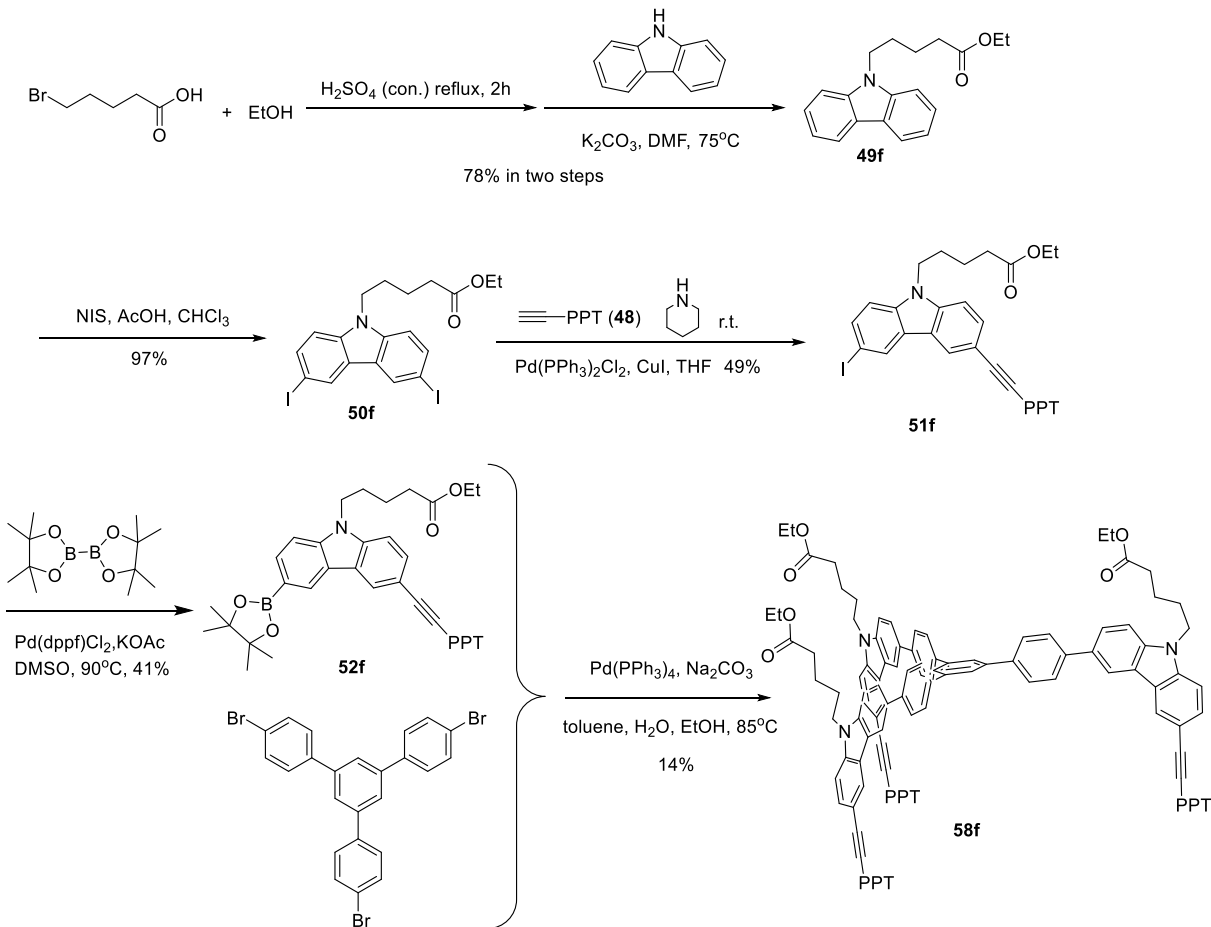


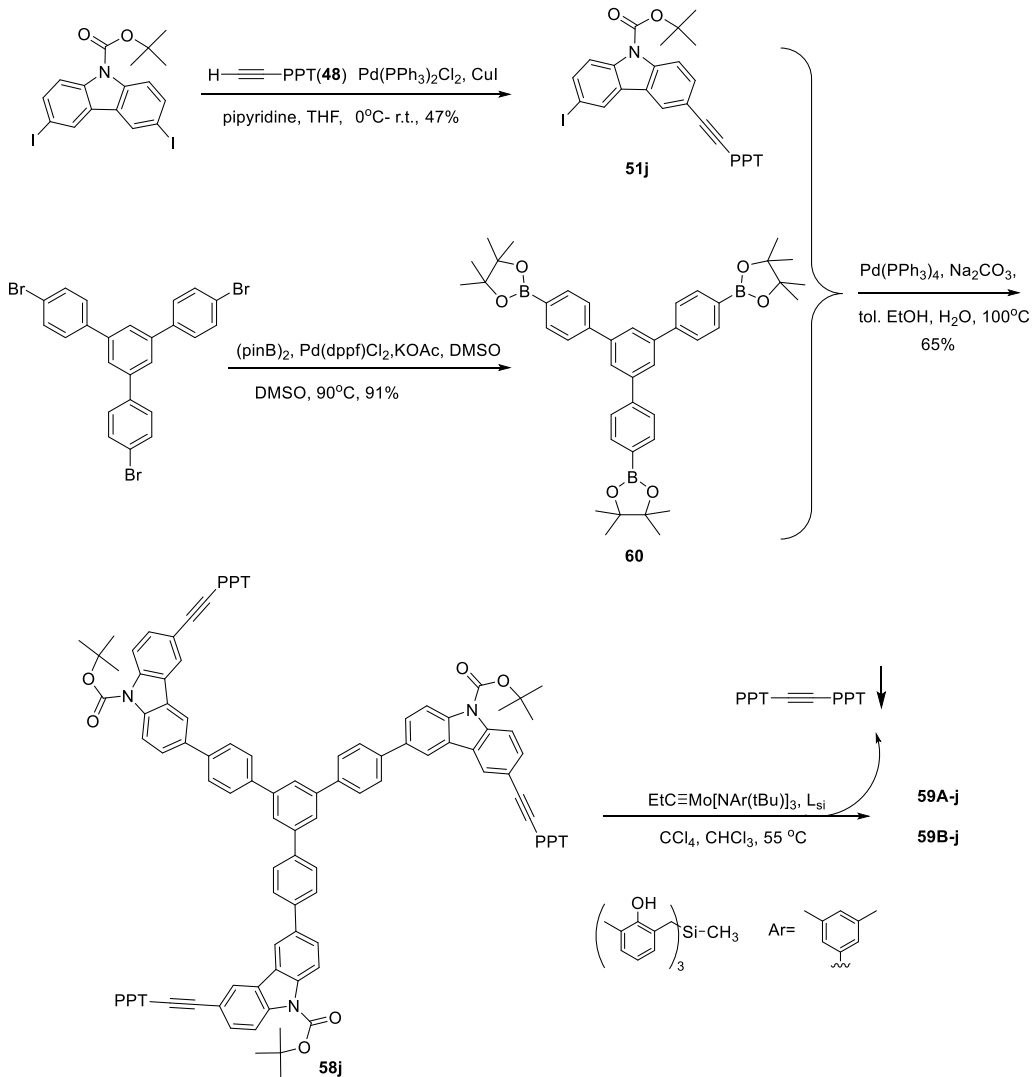
Figure 4.3. The variable-temperature NMR spectra of product **59B-a** at 58 °C (top), 20 °C (middle) and -50 °C (bottom).

However, given the difficulty in separation **59a-A** from **59B-a**, only limited amount of pure materials can be obtained from prep TLC separation. In order to synthesize **59A** and **59B** more efficiently and study the structure of **59B**, later, a carbazole based cage substituted with ester groups was synthesized (scheme 4.2). The resulting dimeric and tetrameric cages exhibit very different polarity, which makes the purification much easier. However, although the cage products can be easily purified, the yield of the Suzuki coupling reaction to synthesize monomer **58f** is very low. Therefore another carbazole based cage substituted with Boc group was designed. The synthetic route worked out in good overall yield as shown in scheme 4.3. 9-Boc-3,6-diiodocarbazole was obtained following a reported procedure¹⁶, followed by the Sonagashira

coupling with the compound **48** to give the carbazole arm **51j**. The center piece **60** was synthesized from the coupling of 1,3,5-tris(*p*-bromophenyl)benzene with bis(pinacolato)diboron, followed by Suzuki coupling with arm **51j**, affording the final monomer **58j**.



Scheme 4.2. The synthetic scheme of monomer **58f**.



Scheme 4.3. The synthetic scheme of cage **59A-j** and **59B-j**.

After alkyne metathesis, one major peak showed up on GPC (Figure 4.4) with a polydispersity index (PDI) of 1.13. Similar as what we observed for **59-a** cage formation, MALDI-TOF MS analysis of crude reaction mixture showed mainly tetramers with a small amount of dimers, and even a trace of hexamers and octamers were detected. The ¹H NMR of the crude mixture was very complicated, drifted baseline with sharp peaks on top of it was observed (Figure 4.5). After purification through column chromatography, two fractions were collected. The first fraction was identified as dimeric cage **59A-j** after full characterization using ¹H, ¹³C NMR, GPC and MALDI-TOF MS. As expected, the ¹H NMR is very similar as **59A-j**.

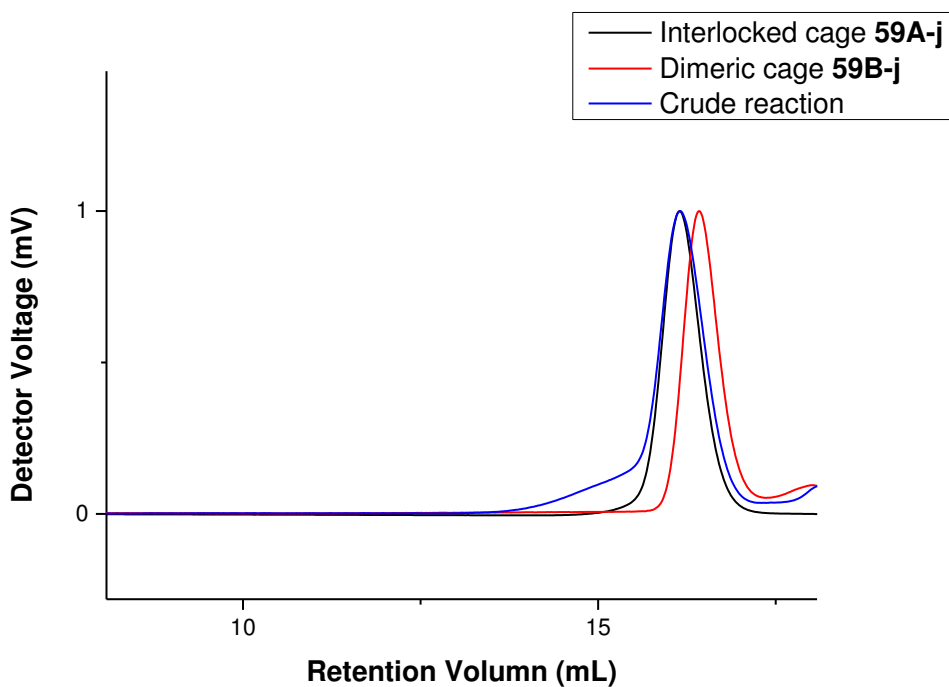


Figure 4.4. Normalized GPC data of the crude reaction mixture of cage formation (blue), isolated dimeric cage **59A-j** (red, PDI=1.04, M_n =2445, M_w =2539) and isolated interlocked cage **59B-j** (black, PDI=1.05, M_n =3000, M_w =3164).

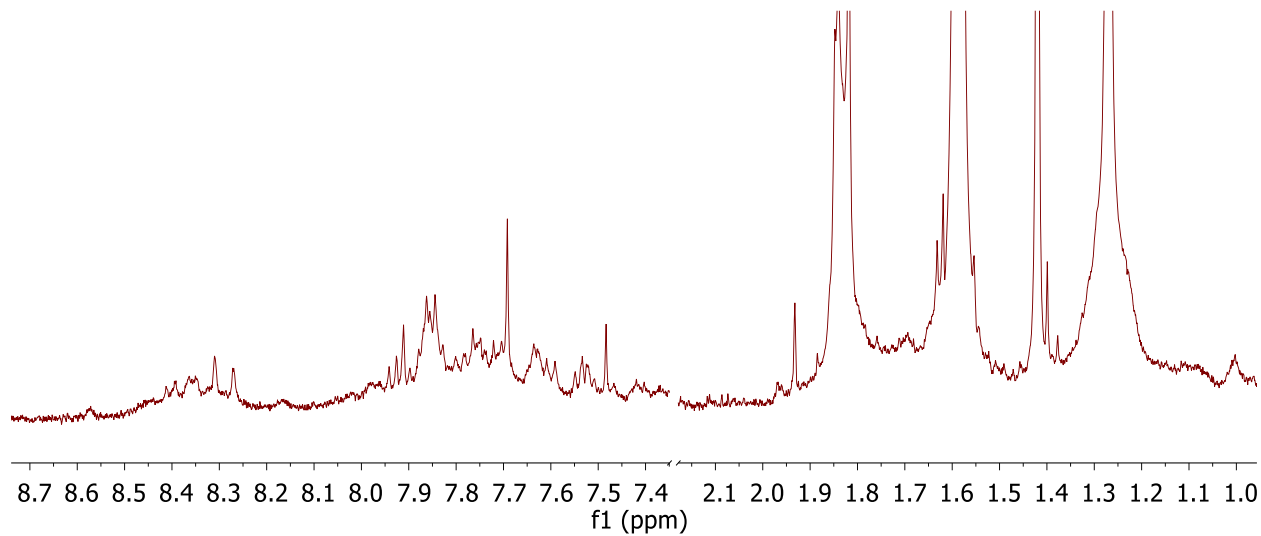


Figure 4.5. The ^1H NMR of crude reaction mixture of cage **59-j** formation in CDCl_3 .

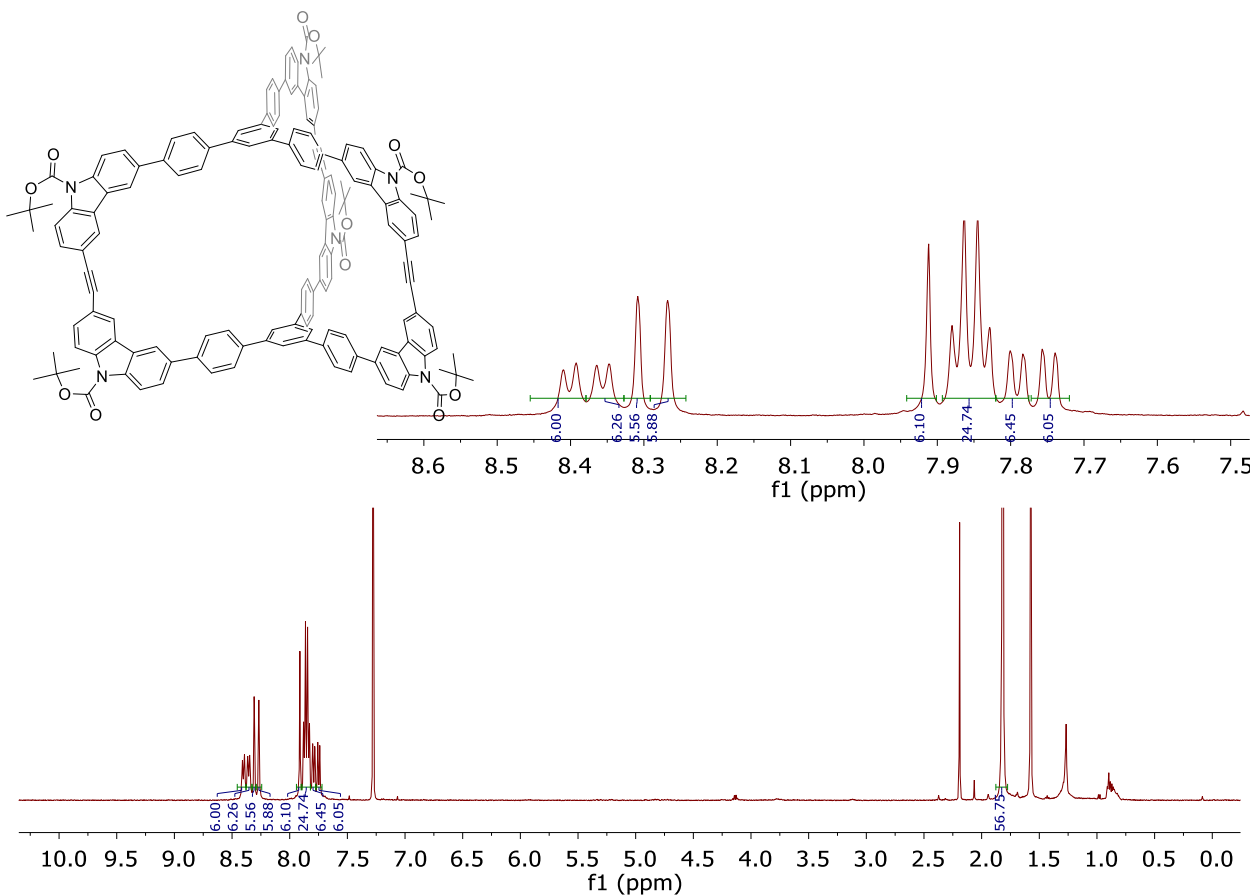


Figure 4.6. The structure of dimeric cage **59A-j** and its ^1H NMR spectrum in CDCl_3 .

The main product of this reaction was the second isolated fraction which was proved to be a tetramer by GPC and MALDI-TOF MS. Surprisingly, the room temperature ^1H NMR signal (Figure 4.7) was not as broad as that of **59B-a** (Figure 4.3, middle), and it is more comparable with the NMR spectrum of **59B-a** at -50 °C. This observation suggests that the Boc protected interlocked-cage compound **59B-j** may have higher energy barrier to the relative movement of two cage units in one interlocked-cage complex and slow down the conformational exchange, indicating that the side arms could affect the relative motion rate of two cage units in one interlocked-cage complex. One possible reason is that the Boc group containing a bulky *tert*-butyl group provided more steric hinderance compared to a linear alkyl chain. Variable-temperature NMR experiments were also conducted (Figure 4.10). Elevated temperature

accelerated the conformation exchange, so the higher temperature NMR showed some coalesced peaks with similar trend as the cage **59B-a**. However, different from **59B-a**, some peaks were getting broader in lower temperature NMR. One possible reason is that the solubility of cage **59B-j** with Boc groups is poor, thus at low temperature, the aggregation occurs, resulting in signal broadening.

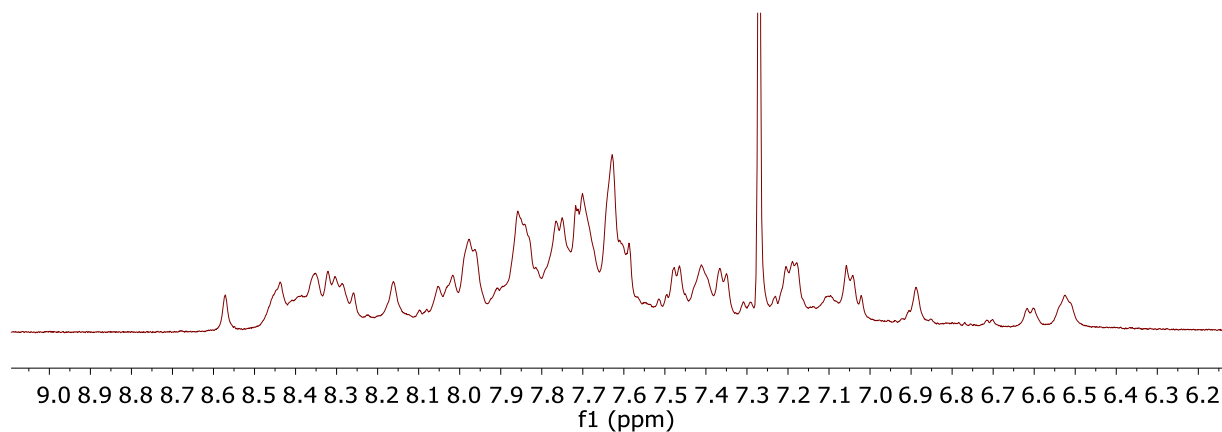


Figure 4.7. Aromatic region of ^1H NMR spectrum of product **59B-j** at 20 °C.

Based on NMR and MALDI-TOF MS characterization, the product **59B** are likely the interlocked cages. Although the possibility of this product is narrowed down to interlocked cages, there is still more than one possible structure. As shown in figure 4.8, two cages have two possible ways to interlock, side-by-side or face-to-face. The interlocked cages reported by Fujita, Cooper and Kuroda claimed that the π - π stacking interactions stabilized the face-to-face dimer cages based on their XRD data. However, another face-to-face interlocked-cage complex reported by Hardie and coworkers showed weak hydrogen bonding instead of π - π stacking. Interestingly, among all reported cases, only the polycatenanes reported by the Lu group intercalated in a side-by-side fashion¹¹. All the other interlocked cages were face-to-face interconnected based on the XRD data. In our case, unfortunately, the single crystal of the

products was not obtained. Therefore, there is no direct evidence illustrating which type of intercatenation this is.

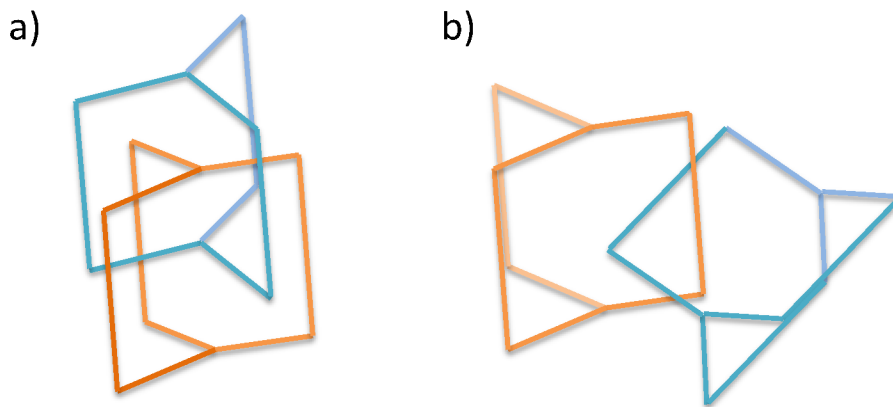


Figure 4.8. The two possible interlocked cage structures, a) face-to-face; b) side-by-side.

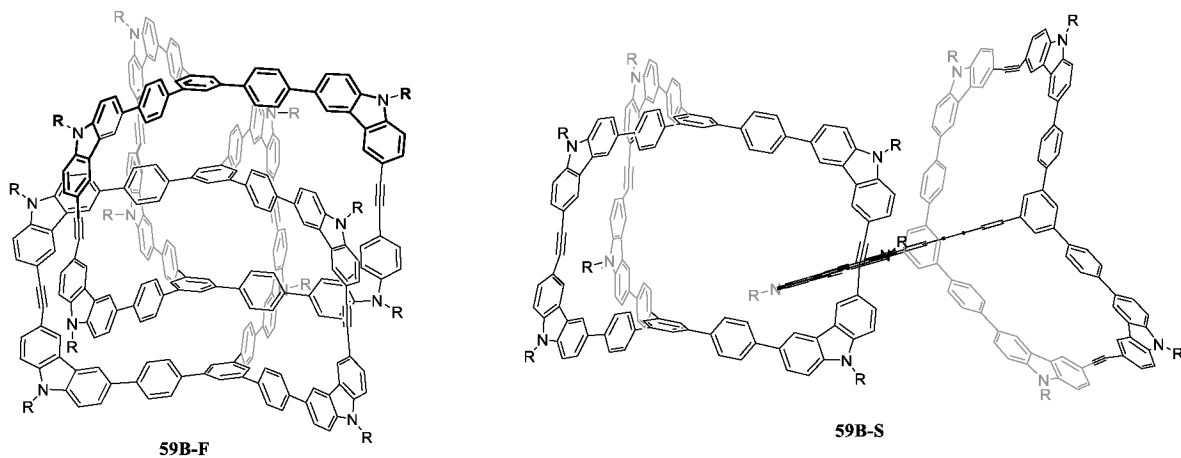


Figure 4.9. The product structures of interlocked cages **59B-F** and **59B-S**.

Diffusion-ordered NMR spectroscopy (DOSY) experiments of dimeric cage **59A-j** and interlocked cages **59B-j** were conducted in order to 1) compare the size of **59A-j** and **59B-j**; 2) verify whether or not fraction **59B-j** is a mixture of molecules with different sizes. DOSY experiments of both **59A-j** (Figure 4.14) and **59B-j** (Figure 4.15) exhibited only one diffusion rate, which indicated that both hydrodynamic sizes are uniform for dimeric cage **59A-j** and interlocked cages **59B-j**. Comparing the hydrodynamic radii of both **59A-j** and **59B-j**, the hydrodynamic radius of **59A-j** is half of that of **59B-j** (Equation 4.4), which is consistent with

the size difference of dimeric cage **59A-j** and interlocked cages **59B-j**. Although based on these results, it is still inconclusive that whether the **59B-j** is pure face-to-face or side-by-side interlocked cages or a mixture of both, it further supported that fraction **59B-j** is an interlocked species.

A kinetic study of the cage formation of **59A-j** and **59B-j** was conducted in order to understand the alkyne metathesis process. Aliquots of the reaction mixture were withdrawn after 0.5 h, 1 h, 4 h, 8 h and 23 h and 48 h (new batch of catalyst was added after 24 h), and analyzed by GPC, MALDI-TOF MS and ¹H NMR spectroscopy. Interestingly, the GPC data indicated that there was no much change from 0.5 h to 23 h, and the 48 h data showed the peak shifted to higher molecular weight direction with decreased shoulder peak (Figure 4.12). MALDI-TOF MS clearly indicated that both dimeric cage and tetrameric cages formed at 0.5 h of the reaction. Qualitatively, the intensity of dimer cage peak is stronger than the tetrameric cage peak from 0.5 h to 23 h. While the 48 h MALDI-TOF MS shows reversed result. The m/z intensity of tetrameric cage is much stronger, which is consistent with the GPC data at 48 h. However, NMR data showed continuous change in the first 4 h of the reaction. During this period, the baselines turned flatter and the dimeric cage peaks were sharper. It indicated that the cage species were forming mainly in the first 4 h. No obvious change on NMR after 4 h with clear dimeric cage **59A-j** peaks showed up, indicating the cage formation completed after 4 h. This observation indicates that both the dimeric cage and tetrameric cage formations are very fast. But the transformation from dimeric cage to tetrameric interlocked cages is relatively slow based on the GPC and MALDI-TOF MS results. (The NMR signal of interlocked cages was broad, so it is difficult to identify the ratio of dimeric cage vs. interlocked cages.)

4.3. Conclusion

We designed and synthesized dimeric cages **59A-a** and **59A-j** and their interlocked cages **59B-a** and **59B-j** with different side chains through alkyne metathesis. The extended center piece of monomer **58** promoted the dimer cage **59A** formation instead of the dumbbell-shaped cage which proved that more out-of-plane bending vibration of a flat center piece could release the angle strain of a cage product to certain extent, thus lowering the enthalpy of dimer products. The interlocked cages **59B-a** and **59B-j** exhibited different rate of conformation exchange which suggests that the side chains could affect the relative motion of two cage units in one interlocked cages. However, whether the interlocked cages **59B** take the face-to-face or side-by-side intercalated motif is still open to speculation.

4.4. Experimental Section

4.4.1. Materials and general synthetic methods

Reagents and solvents were purchased from commercial suppliers and used without further purification, unless otherwise indicated. Tetrahydrofuran (THF), toluene, CH₂Cl₂ and dimethylformamide (DMF) were purified by the MBRAUN solvent purification systems.

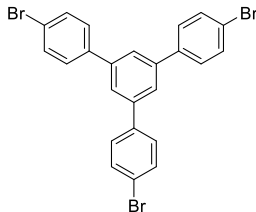
All reactions were conducted under dry nitrogen in oven-dried glassware, unless otherwise specified. All the alkyne metathesis reactions were conducted in glovebox. The solvents used in alkyne metathesis were dried over 4 Å molecular sieves. Solvents were evaporated using a rotary evaporator after workup. Unless otherwise specified, the purity of the compounds was 195 % based on ¹H NMR spectral integration.

Flash column chromatography was performed by using a 100-150 times weight excess of flash silica gel 32-63 μ m from Dynamic Absorbants Inc. Fractions were analyzed by TLC using TLC silica gel F254 250 μ m precoated-plates from Dynamic Absorbants Inc. Analytical gel permeation chromatography (GPC) was performed using a Viscotek GPCmaxTM, a Viscotek Model 3580 Differential Refractive Index (RI) Detector, a Viscotek Model 3210 UV/VIS Detector and a set of two Viscotek Viscogel columns (7.8 \times 30 cm, 1-MBLMW-3078, and 1-MBMMW-3078 columns) with THF as the eluent at 30 °C. The analytical GPC was calibrated using monodisperse polystyrene standards. UV-vis absorption measurements were carried out with Agilent 8453 spectrophotometer.

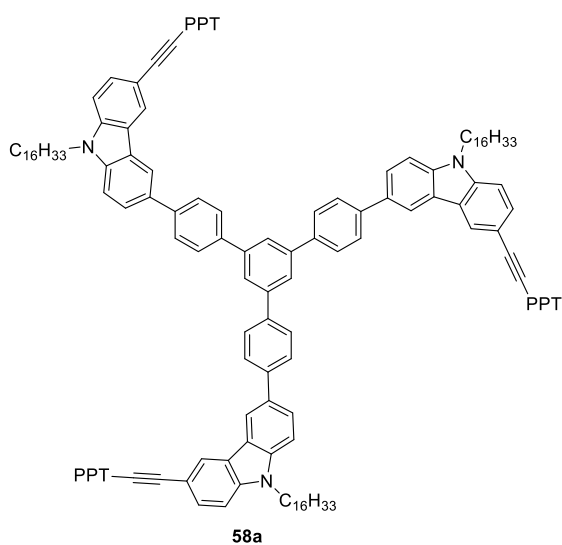
MALDI-TOF Mass spectra were obtained on the Voyager-DE™ STR Biospectrometry Workstation using sinapic acid (SA) as the matrix. The high resolution mass spectra were obtained on Waters SYNAPT G2 High Definition Mass Spectrometry System. Analyte molecules were diluted into ESI solvents, methanol, chloroform or acetonitrile/water mixture, for final concentrations of 10 ppm or lower. The solution was injected into the electrospray ionization (ESI) source at a rate of 5 μ L/min. Either the ESI+ or ESI- mode was used in reference to the molecular properties. Accurate mass analysis was performed by using the Lock Mass calibration feature with the instrument.

NMR spectra were taken on Inova 400 and Inova 500 spectrometers. CHCl₃ (7.27 ppm), toluene-*d*₈ (2.09 ppm) were used as internal references in ¹H NMR, and CHCl₃ (77.00 ppm) for ¹³C NMR. ¹H NMR data were reported in order: chemical shift, multiplicity (s, singlet; d, doublet; t, triplet; q, quartet; m, multiplet), coupling constants (*J*, Hz), number of protons.

4.4.2. Compounds Preparation



1,3,5-Tri(4-bromophenyl)benzene was synthesized following the reported procedure. ^{17}H NMR (500 MHz, CDCl_3) δ 7.70 (s, 3H), 7.62 (d, $J = 8.5$ Hz, 5H), 7.55 (d, $J = 8.5$ Hz, 6H).

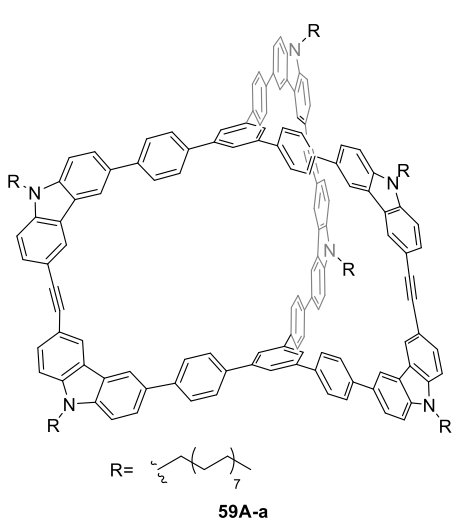


58a was synthesized following general Suzuki coupling reaction procedure. **52a** (965 mg, 1.21 mmol), 1,3,5-tri(4-bromophenyl)benzene (146 mg, 0.269 mmol), $\text{Pd}(\text{PPh}_3)_4$ (32 mg, 0.027 mmol) and Na_2CO_3 (0.3 M, 10 mL aqueous solution) were used. Product (480 mg, 77%) was purified by column chromatography (hexanes/ CH_2Cl_2 , 1/1~0/1, v/v). ^1H NMR (500 MHz, CDCl_3) δ 8.42 (d, $J = 1.5$ Hz, 6H), 7.98 (s, 3H), 7.95 – 7.82 (m, 27H), 7.79 – 7.65 (m, 21H), 7.64 – 7.59 (m, 3H), 7.51 (tt, $J = 7.4, 5.3$ Hz, 9H), 7.42 (d, $J = 8.5$ Hz, 3H), 4.34 (t, $J = 7.2$ Hz, 6H), 1.93 (p, $J = 7.5$ Hz, 6H), 1.48 – 1.15 (m, 78H), 0.88 (t, $J = 6.9$ Hz, 9H).

Synthesis of **59A-a** and **59B-a**:

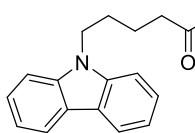
Following the typical alkyne metathesis reaction procedure. To a monomer **58a** (391 mg, 0.167 mmol) in CHCl_3 (5mL) and CCl_4 (13 mL) solution was added newly prepared catalyst **1** solution (precursor 10.1 mg, 0.0152 mmol and amine ligand 7.1 mg, 0.0152 mmol). The reaction was heated to 35 °C overnight. The reaction was monitored by GPC. After normal workup, the

product was purified by column chromatography (hexanes/CH₂Cl₂, 2.5/1, v/v). The unseparated mixture were further purified using prep TLC (eluting with hexanes/CH₂Cl₂, 2.5/1, v/v).



Dimeric cage 59A-a: ^1H NMR (500 MHz, CDCl_3) δ 8.43 (d, $J = 1.6$ Hz, 6H), 8.38 (d, $J = 1.7$ Hz, 6H), 7.90 (s, 6H), 7.88 – 7.81 (m, 24H), 7.78 (dd, $J = 8.6, 1.8$ Hz, 6H), 7.71 (dd, $J = 8.4, 1.6$ Hz, 6H), 7.51 (d, $J = 8.6$ Hz, 6H), 7.41 (d, $J = 8.5$ Hz, 6H), 4.35 (s, 12H), 2.00 – 1.87 (m, 12H), 1.51 – 1.14 (m, 156H), 0.87 (t, $J = 6.9$ Hz, 16H). MALDI-TOF(m/z): $[\text{M}]^+$ calcd. for $\text{C}_{222}\text{H}_{263}\text{N}_6$, 3016.09; found, 3015.08.

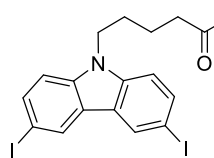
Interlocked cages 59B-a: MALDI-TOF(m/z): $[M]^+$ calcd. for $C_{444}H_{526}N_{12}$, 6032.18; found, 6033.60.



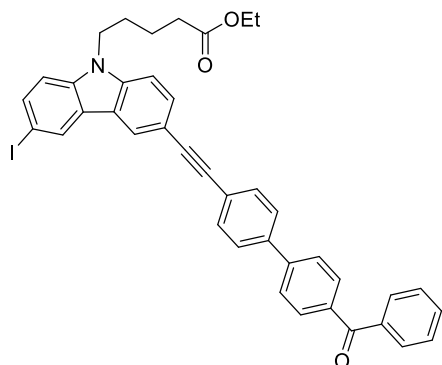
Ethyl 5-(9H-carbazol-9-yl)pentanoate (49f): 5-Bromopentanoic acid (5.00 g, 27.6 mmol), EtOH (25 mL) and concentrated H₂SO₄ (0.12 mL)

were added to a seal tube. The reaction was reflux for 2 h and solvent was removed under vacuum to get the crude product (5.01 g). The crude product was used directly in the next step. To a seal tube, ethyl 5-bromopentanoate (5.01 g, 24 mmol), carbazole (2.00 g, 12 mmol) and K₂CO₃ (4.80 g, 34.5mmol) and dry DMF (30 mL) were added, and the mixture was heated to 80 °C for 2 days. Then the reaction was quenched by cold water (50 mL). Then the product was extracted by hexanes (100 mL × 3) and dried over Na₂SO₄. After removing the solvent, the crude product was purified by flash column chromatography (hexanes/EtOAc/CHCl₃, 7/1/7, v/v/v). 3.184 g pure product was collected (78% yield in two steps). ¹H NMR (400 MHz, CHCl₃) δ 8.09

(d, $J = 7.7$ Hz, 2H), 7.49 – 7.42 (m, 2H), 7.39 (d, $J = 8.2$ Hz, 2H), 7.22 (t, $J = 7.7$ Hz, 2H), 4.32 (t, $J = 7.1$ Hz, 2H), 4.08 (q, $J = 7.1$ Hz, 2H), 2.30 (t, $J = 7.3$ Hz, 2H), 1.97 – 1.83 (m, 2H), 1.78 – 1.66 (m, 2H), 1.20 (t, $J = 7.1$ Hz, 3H). HRMS (m/z): [M+Li]⁺ calcd. for C₁₉H₂₂NO₂, 296.1645; found, 296.1655.

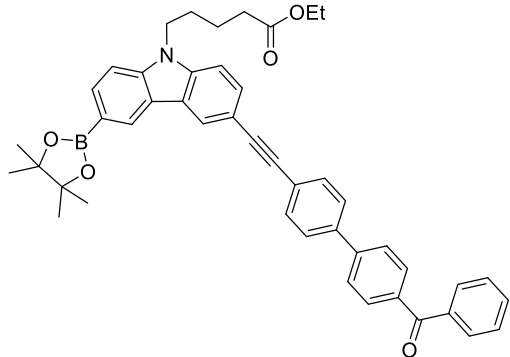


Ethyl 5-(3,6-diiodo-9H-carbazol-9-yl)pentanoate (50f): To a round bottom flask, ethyl 5-(9H-carbazol-9-yl)pentanoate (**49f**) (2.18 g, 7.39 mmol), NIS (3.66g, 16.2 mmol) were dissolved in CHCl₃ (50 mL) and HOAc (11 mL). The reaction mixture was stirred at room temperature for 4.5 h. After the reaction, the solvent was reduced under rotavap to 15 mL and filter to collect the precipitates. The precipitates were washed with cold hexanes. The white solids (3.94 g, 97%) were collected as pure product. ¹H NMR (500 MHz, CHCl₃) δ 8.34 (d, $J = 1.7$ Hz, 2H), 7.72 (dd, $J = 8.6, 1.7$ Hz, 2H), 7.19 (d, $J = 8.6$ Hz, 2H), 4.27 (t, $J = 7.1$ Hz, 2H), 4.10 (q, $J = 7.1$ Hz, 2H), 2.30 (t, $J = 7.2$ Hz, 2H), 1.92 – 1.83 (m, 2H), 1.73 – 1.62 (m, 2H), 1.21 (t, $J = 7.1$ Hz, 3H). ¹³C NMR (101 MHz, CHCl₃) δ 173.13, 140.23, 125.58, 122.76, 120.31, 118.76, 108.51, 60.31, 42.59, 33.84, 28.36, 22.61, 14.14. HRMS (m/z): [M]⁺ calcd. for C₁₉H₁₉LiI₂NO₂, 552.9634; found, 552.9656. HRMS (m/z): [M+Li]⁺ calcd. for C₁₉H₁₉LiI₂NO₂, 552.9659; found, 552.9634.



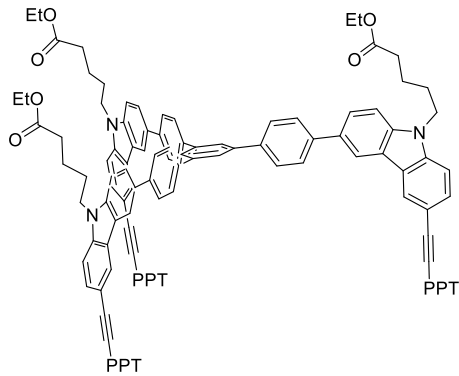
51f: Follow normal Sonagashia coupling reaction procedure. Ethyl 5-(3,6-diiodo-9H-carbazol-9-yl)pentanoate (**50f**) (3.77 g, 7.20 mmol), PPT —— H (**48**) (2.33 g, 8.63 mmol), Pd(PPh₃)₂Cl₂ (150 mg, 0.29 mmol) and CuI (5 mg, 0.026 mmol), THF (15 mL) and piperidine (4 mL) were used. After purified by flash chromatography eluting with (hex/EA/CHCl₃, 7/1/7~5/1/5, v/v/v), pure product (2.363 g, 49 %) was collected. ¹H NMR (500

MHz, CHCl₃) δ 8.41 (d, *J* = 1.6 Hz, 1H), 8.26 (d, *J* = 1.5 Hz, 1H), 7.93 (d, *J* = 8.3 Hz, 2H), 7.88 – 7.83 (m, 2H), 7.79 – 7.71 (m, 3H), 7.71 – 7.66 (m, 5H), 7.65 – 7.60 (m, 1H), 7.53 (dd, *J* = 8.3, 7.0 Hz, 2H), 7.39 (d, *J* = 8.5 Hz, 1H), 7.21 (d, *J* = 8.6 Hz, 1H), 4.31 (t, *J* = 7.1 Hz, 2H), 4.11 (q, *J* = 7.2 Hz, 2H), 2.33 (t, *J* = 7.2 Hz, 2H), 1.98 – 1.84 (m, 2H), 1.79 – 1.64 (m, 2H), 1.23 (t, *J* = 7.2 Hz, 3H). ¹³C NMR (101 MHz, CHCl₃) δ 196.16, 172.94, 144.24, 139.83, 139.73, 139.02, 137.58, 136.29, 134.31, 132.36, 131.95, 130.72, 129.92, 129.32, 128.26, 127.10, 126.69, 124.80, 124.16, 123.64, 121.53, 113.71, 110.84, 108.84, 91.78, 87.62, 81.91, 60.38, 42.85, 40.92, 33.69, 28.24, 22.48, 14.15. HRMS (m/z): [M+Li]⁺ calcd. for C₄₀H₃₂LiINO₂, 708.1588; found, 708.1591.



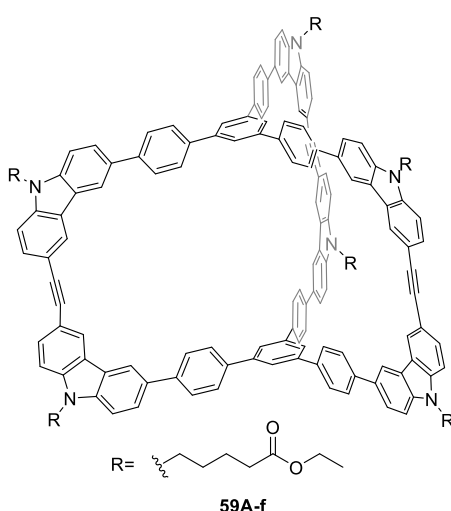
52f: To a seal tube, **51f** (1.965 g, 2.80 mmol), bis(pinacolato)diboron (1.067 g, 4.2 mmol), Pd(dppf)Cl₂ (61 mg, 0.084 mmol) and KOAc (824 mg, 8.4 mmol) were added. After vacuum and refill with N₂ three times, DMSO (20 mL) was added under N₂ flow. Then the reaction was heated to 90 °C. After stirring for 18 h, the reaction mixture was cooled to room temperature and ethyl acetate (50 mL) was added to the mixture and the mixture was washed with water (100 mL × 3). The organic layer was collected and washed with brine (50 mL). After drying over Na₂SO₄, solvent was removed under reduced pressure and the residue was purified by flash chromatography (eluting with hexanes/EtOAc/CHCl₃, 5/1/3) yielding yellow product (805 mg, 41%). ¹H NMR (500 MHz, CHCl₃) δ 8.63 (s, 1H), 8.37 (d, *J* = 1.5 Hz, 1H), 7.95 (dd, *J* = 8.2, 1.1 Hz, 1H), 7.94 – 7.91 (m, 2H), 7.86 (dd, *J* = 8.3, 1.4 Hz, 2H), 7.76 (d, *J* = 8.3 Hz, 2H), 7.68 (s, 4H), 7.67 (dd, *J* = 8.5, 1.7 Hz, 1H), 7.65 – 7.60 (m, 1H), 7.53 (dd, *J* = 8.3, 7.1 Hz, 2H), 7.41 (d, *J* = 8.3 Hz, 1H), 7.39 (d, *J* = 8.5 Hz, 1H), 4.35 (t, *J* = 7.1 Hz, 2H), 4.11 (q, *J* = 7.1 Hz, 2H), 2.32 (t, *J* = 7.2 Hz, 2H), 1.98 –

1.89 (m, 2H), 1.76 – 1.68 (m, 2H), 1.22 (t, J = 7.1 Hz, 3H). HRMS (m/z): [M+Li]⁺ calcd. for C₄₆H₄₂LiBINO₂, 708.3481; found, 708.3519.



Monomer 58f: To a Schlenk tube **52f** (270 mg, 0.385 mmol), 1,3,5-tri(4-bromophenyl)benzene (52.2 mg, 0.096 mmol), Pd(PPh₃)₄ (16.7 mg, 0.0144 mmol) were charged. Toluene (2 mL), Na₂CO₃ solution (1M, 0.8 mL) and EtOH (0.8 mL) were added under N₂ flow. The reaction was stirred at 110 °C for 16 h. The aqueous phase was discarded after separation. The organic phase was washed with NH₄Cl (sat. 50 mL) and brine (50 mL). The organic extracts were dried over Na₂SO₄, and concentrated. The residue was purified by flash column chromatography (hexanes/CHCl₃/EtOAc, 4/4/1~2/3/1) to give the product as a yellow solid (27.6 mg, 14 %). ¹H NMR (400 MHz, CDCl₃) δ 8.38 (d, *J* = 1.0 Hz, 6H), 7.95 (s, 3H), 7.92 – 7.76 (m, 27H), 7.74 – 7.55 (m, 24H), 7.53 – 7.43 (m, 9H), 7.37 (d, *J* = 8.5 Hz, 3H), 4.32 (t, *J* = 7.0 Hz, 6H), 4.10 (q, *J* = 7.1 Hz, 6H), 2.33 (t, *J* = 7.2 Hz, 6H), 2.03 – 1.85 (m, 6H), 1.80 – 1.62 (m, 6H), 1.22 (t, *J* = 7.2 Hz, 9H). ¹³C NMR (101 MHz, CDCl₃) δ 196.23, 173.10, 132.39, 131.99,

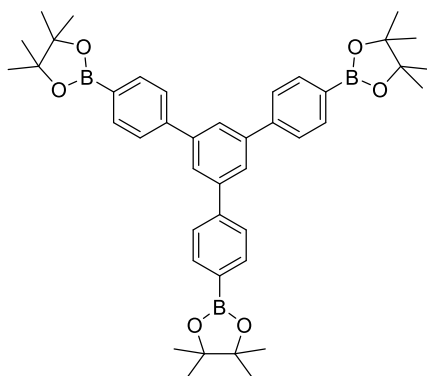
130.78, 129.98, 128.30, 127.81, 127.65, 127.16, 126.74,
124.25, 123.85, 123.06, 118.95, 113.37, 109.23, 92.21,
87.53, 60.44, 33.83, 29.71, 28.45, 22.63, 14.22.



Physical data of **59A-f**: ^1H NMR (500 MHz, CDCl_3) δ 8.43 (d, $J = 1.6$ Hz, 6H), 8.37 (d, $J = 1.7$ Hz, 6H), 7.90 (s, 6H), 7.89 – 7.81 (m, 24H), 7.78 (dd, $J = 8.5$, 1.8 Hz, 6H), 7.72 (dd, $J = 8.5$, 1.7 Hz, 6H), 7.51 (d, $J = 8.6$ Hz, 6H), 7.42 (d, $J = 8.6$ Hz, 6H).

= 8.5 Hz, 6H), 4.47 – 4.31 (m, 5H), 4.12 (q, J = 7.2 Hz, 12H), 2.41 – 2.33 (m, 12H), 2.06 – 1.94 (m, 12H), 1.86 – 1.72 (m, 12H), 1.23 (t, J = 7.1 Hz, 18H). MALDI-TOF MS: calcd. for [M]⁺ C₁₆₈H₁₄₄N₆O₁₂: 2438.09, found: 2438.34.

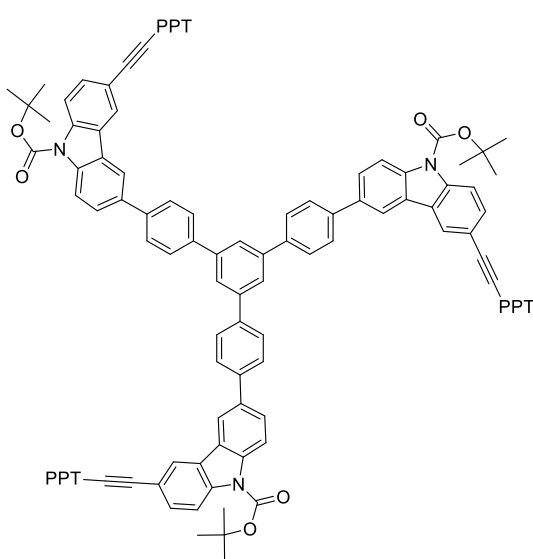
Physical data of **59B-f**: MALDI-TOF MS: calcd. for [M]⁺ C₃₃₆H₂₈₈N₁₂O₂₄: 4876.18, found: 4871.97 .



60: To a Schlenk tube 1,3,5-tris(*p*-bromophenyl)benzene (680 mg, 1.252 mmol), bis(pinacolato)diboron (1.00 g, 3.94 mmol), Pd(dppf)Cl₂ (91.5 mg, 0.125 mmol) and KOAc (1.47 g, 15.0 mmol) were charged. DMF (15 mL) was added under N₂ flow. The reaction was stirred at 80 °C for 16 h. The solvent was removed by vacuum evaporation, the crude reaction mixture

was dissolved in CH₂Cl₂ (40 mL) and washed with NH₄Cl (sat., 60 mL) and brine (70 mL). The organic extracts were dried over Na₂SO₄, and concentrated. The residue was purified by flash column chromatography (1% MeOH in CH₂Cl₂) to give the product as a white solid (778 mg, 91 %). ¹H NMR (400 MHz, CDCl₃) δ 7.94 (d, J = 7.9 Hz, 6H), 7.83 (s, 3H), 7.72 (d, J = 7.9 Hz, 6H), 1.39 (s, 36H). ¹³C NMR (101 MHz, CDCl₃) δ

143.67, 142.22, 135.32, 126.66, 125.54, 109.99, 83.84, 24.87.



Monomer 58j: To a Schlenk tube **60** (255 mg, 0.373 mmol), **51j** (1.25 g, 1.86 mmol), Pd(PPh₃)₄ (55 mg, 0.048 mmol) were charged. Toluene (65 mL), Na₂CO₃ solution (1M, 8 mL) and EtOH (8 mL)

were added under N₂ flow. The reaction was stirred at 90 °C for 12 h. The aqueous phase was discarded after separation. The organic phase was washed with NH₄Cl (sat. 100 mL) and brine (100 mL). The organic extracts were dried over Na₂SO₄, and concentrated. The residue was purified by flash column chromatography (hexanes/CHCl₃/EtOAc, 30:10:1) to give the product as a yellow solid (469 mg, 65 %). ¹H NMR (500 MHz, CDCl₃) δ 8.41 (d, *J* = 8.7 Hz, 3H), 8.36 (d, *J* = 8.7 Hz, 3H), 8.34 – 8.30 (m, 6H), 7.99 (s, 3H), 7.96 – 7.88 (m, 18H), 7.88 – 7.83 (m, 9H), 7.75 (d, *J* = 8.3 Hz, 6H), 7.74 – 7.67 (m, 15H), 7.65 – 7.59 (m, 3H), 7.52 (t, *J* = 7.7 Hz, 6H), 1.83 (s, 27H). ¹³C NMR (101 MHz, CDCl₃) δ 196.10, 150.62, 144.12, 141.84, 140.08, 139.70, 139.26, 138.48, 138.18, 137.56, 136.33, 135.69, 132.35, 132.07, 130.72, 130.64, 129.92, 128.25, 127.75, 127.58, 127.11, 126.68, 126.52, 125.74, 125.61, 124.82, 123.35, 122.95, 117.83, 117.59, 116.57, 116.29, 91.17, 88.51, 84.36, 28.33, 28.33. MALDI-TOF(m/z): [M–C₁₅H₂₄O₂+H]⁺ calcd. for C₁₂₃H₇₅N₃O₃, 1642.58; found: 1643.49.*

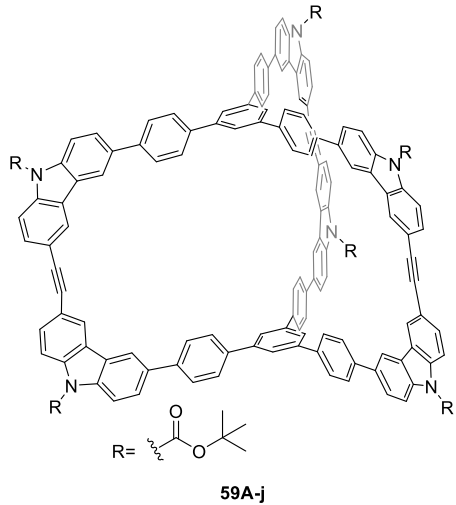
Preparation of dimer cage **59A-j** and interlocked cages **59B-j**

Trial 1: The monomer **58j** (190 mg, 0.0979 mmol), CCl₄ (8 mL) and CHCl₃ (10 mL) were added to a dry Schlenk tube in glovebox. The multidentate ligand L_{si} (4.8 mg, 0.012 mmol) and the Mo(VI) carbyne precursor (7.8 mg, 0.012 mmol) were premixed in dry carbon tetrachloride (2 mL) for 10 minutes to generate the catalyst in situ. After the generation, the catalyst solution was added to the monomer solution and stirred at 55 °C in close system. The reaction was monitored by GPC and NMR. After overnight, the precipitates were filtered off and the liquid was concentrated down. The residue was washed with brine and dried over Na₂SO₄. The solution was concentrated down under reduced pressure. The residue was purified by column

*The Boc groups were cleaved under MALDI-TOF MS conditions.

(hexane/CHCl₃/EtOAc, 30/20/1, v/v/v) and dimer cage **59A-j** (7.0 mg, 6%) and interlocked **59B-j** cages (65.6, 59%) were collected.

Trial 2: Follow the general alkyne metathesis procedure. Monomer **58j** (102 mg, 0.0525 mmol), the multidentate ligand L_{si} (2.5 mg, 0.0063 mmol) and the Mo(VI) carbyne precursor (4.2 mg, 0.0063 mmol), CCl₄ (10 mL) and CHCl₃ (10 mL) were used. Dimer cage **59A-j** (7.9 mg, 13%) and interlocked cage **59B-j** (19.8 mg, 33%) were collected.



Dimeric cage 59A-j: ¹H NMR (500 MHz, CDCl₃) δ 8.40 (d, *J* = 8.8 Hz, 6H), 8.35 (d, *J* = 8.7 Hz, 6H), 8.32 – 8.28 (m, 6H), 8.26 (d, *J* = 1.9 Hz, 6H), 7.91 (s, 6H), 7.85 (q, *J* = 8.3 Hz, 24H), 7.78 (dd, *J* = 8.8, 1.8 Hz, 6H), 7.74 (dd, *J* = 8.7, 1.7 Hz, 6H), 1.81 (s, 54H). ¹³C NMR (125 MHz, CDCl₃) δ 181.87, 142.72, 140.89, 140.34, 138.40, 138.30, 136.55, 130.96, 130.84, 128.18, 128.02, 127.12, 125.89, 125.68, 122.62, 118.28, 118.16, 116.66, 116.47, 84.42, 28.38. Due

to poor solubility of cage **59A-j**, the ¹³C NMR was determined using indirect method (HSQC figure 4.16 and HMBC figure 4.17). MALDI-TOF(m/z): [M–C₃₀H₄₈O₁₂+H]⁺ calcd. for C₁₂₆H₇₂N₆, 1670.59; found: 1668.06. *

Interlocked cage 59B-j: For ¹H and ¹³C NMR see figure 4.18b and 4.19. MALDI-TOF(m/z): [M–C₆₀H₉₆O₂₄+H]⁺ calcd. for C₂₅₂H₁₄₅N₁₂, 3340.18; found: 3335.53. *

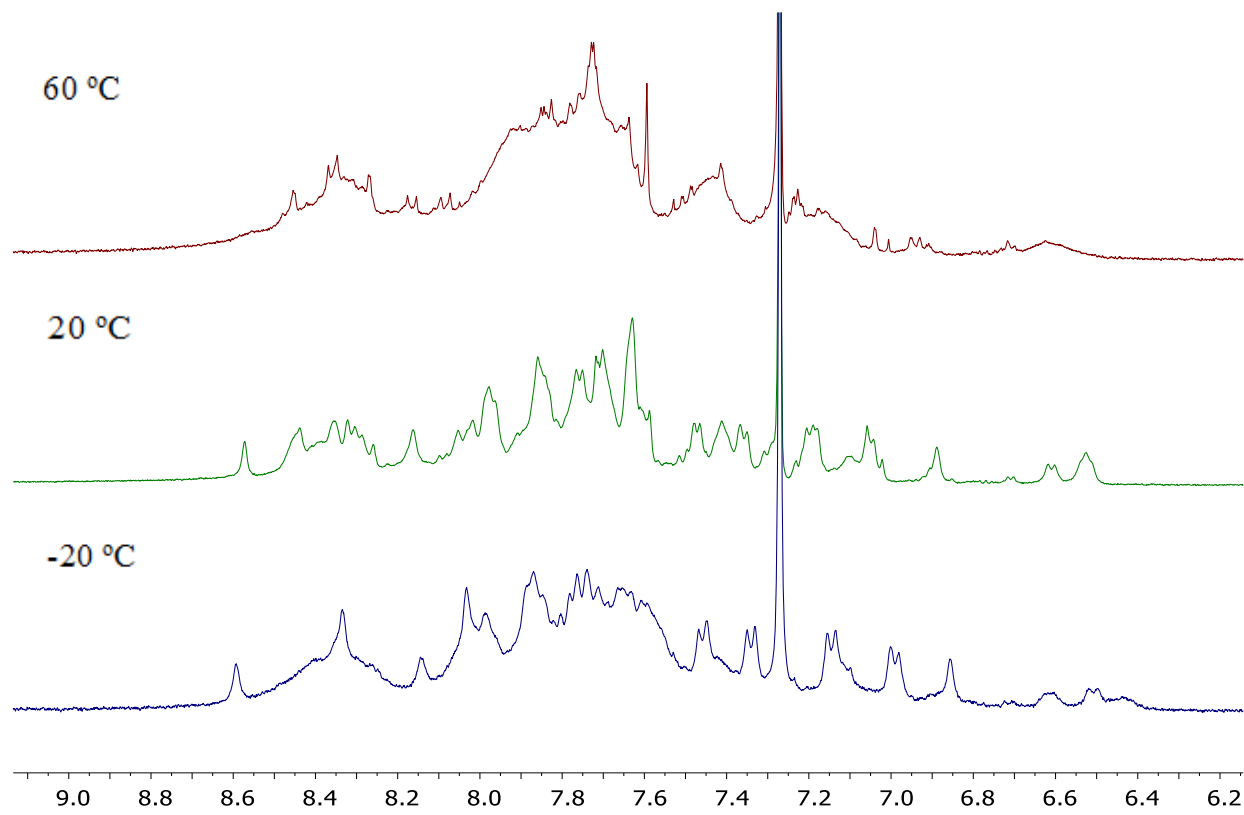


Figure 4.10. The aromatic region of variable-temperature NMR spectra of product **59B-j** at 60 °C (top), 20 °C (middle), -20 °C (bottom). The broadening of the spectrum at -20 °C may be due to aggregation.

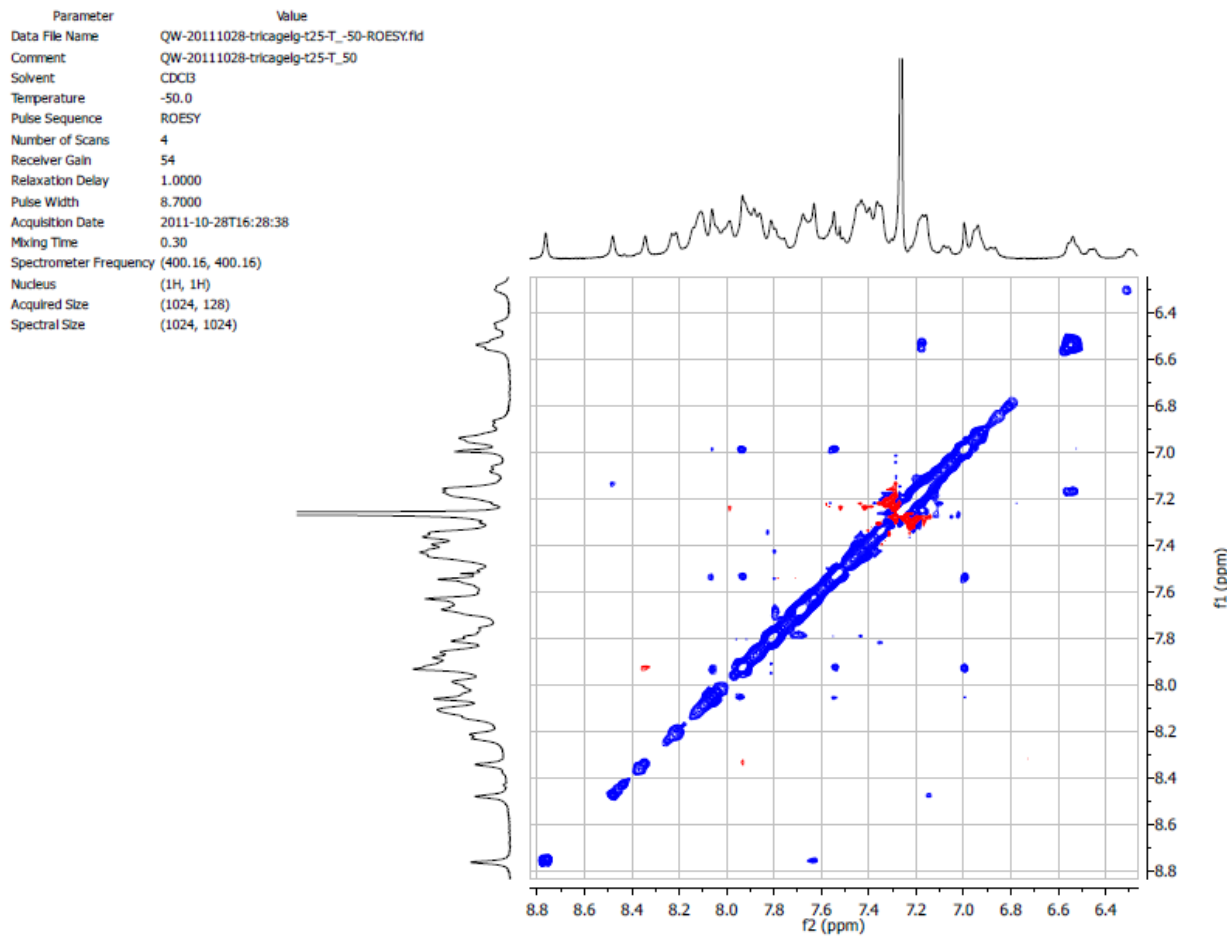


Figure 4.11. ROESY experiment of **59B-a** in CDCl₃ at -50 °C with mixing time 0.3 s. The blue cross peaks (except for the diagonal peaks) are due to chemical/conformational exchange.

4.4.3. Kinetic study of cage formation

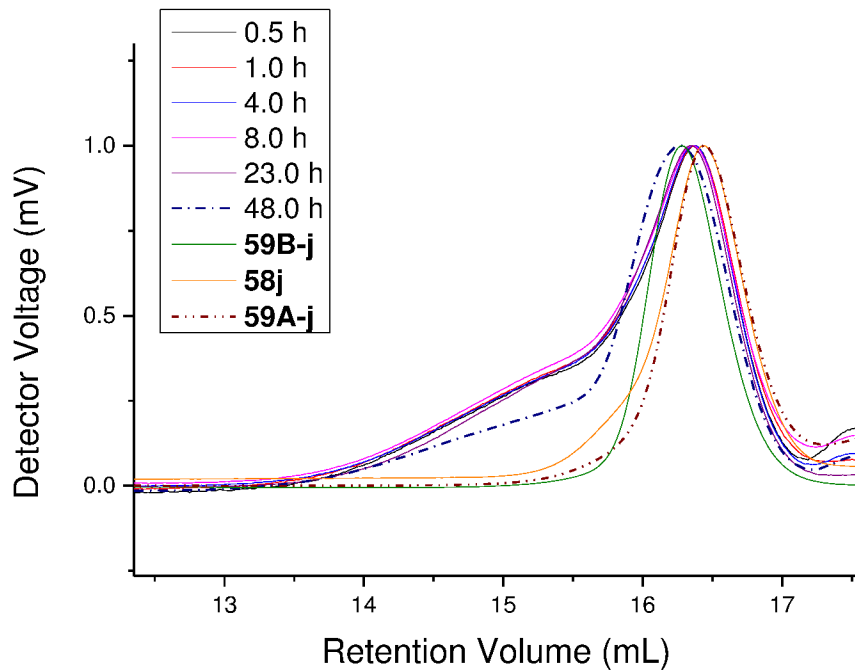


Figure 4.12. Kinetic study of the cage **59A-j** and **59B-j** formation through alkyne metathesis. Normalized GPC traces of a crude product mixture after 0.5 h, 1.0 h, 4.0 h, 8.0 h, 23 h and 48 h of the reaction time and the purified cages **59A-j**, **59B-j** and monomer **58j**.

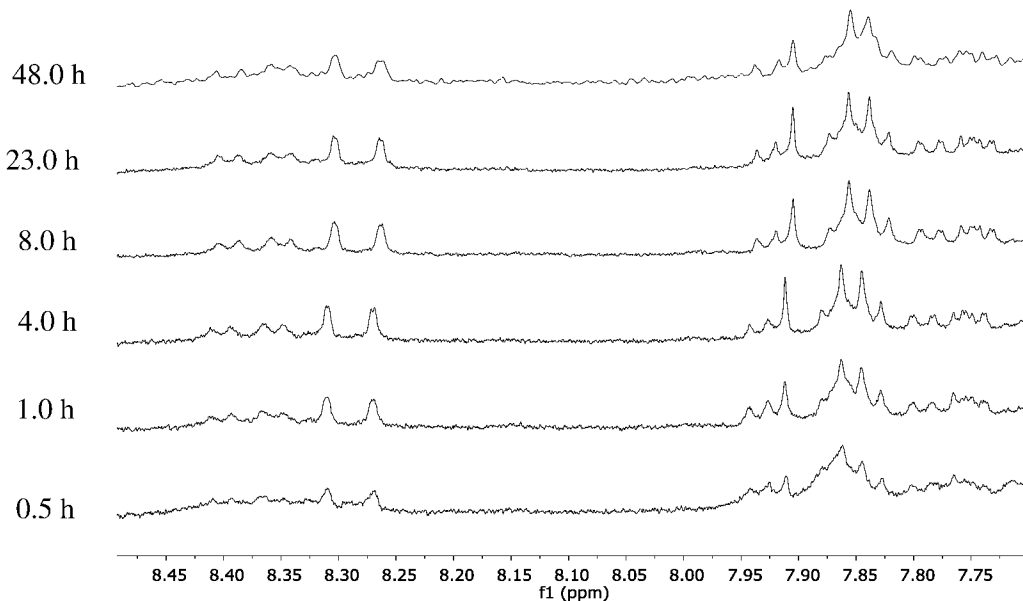


Figure 4.13 Kinetic study of the cage **59A-j** and **59B-j** formation through alkyne metathesis. ¹H NMR spectra of a crude product mixture after 0.5 h, 1.0 h, 4.0 h, 8.0 h, 23.0 h and 48 h (as labeled on the left of the spectrum) of alkyne metathesis.

4.4.4. DOSY experiment

DOSY experiments of **59A-j** and **59B-j** were conducted respectively in order to study their relative size difference. Based on Stokes-Einstein equation (Equation 4.1), the thermodynamic radius of a particle is correlative with solution temperature and viscosity. In order to minimize the uncertain factors, DOSY experiments were done in the same solvent (CDCl_3) and temperature (296 K), and CHCl_3 solvent residue was used as internal standard. The DOSY experiments show very narrow diffusion constants results for both **59A-j** and **59B-j**. The measured diffusion constant of the dimeric cage **59A-j** is $3.09 \times 10^{-10} \text{ m}^2\text{s}^{-1}$ and that of CHCl_3 is $24.0 \times 10^{-10} \text{ m}^2\text{s}^{-1}$; the diffusion constant of interlocked cage **59B-j** is $1.83 \times 10^{-10} \text{ m}^2\text{s}^{-1}$ and that of CHCl_3 is $19.8 \times 10^{-10} \text{ m}^2\text{s}^{-1}$.

To calculate the relative size of thermodynamic radius of dimeric cage and interlocked cage, Stokes-Einstein equation was used:

$$D = \frac{k_B T}{6\pi\eta r} \quad (\text{Equation 4.1})$$

D is the diffusion constant.

T is temperature.

k_B is the Boltzmann's constant.

η is the viscosity of the solution.

r is the thermodynamic radius of the particle.

Since the experiments were conducted under same temperature, thus

$$\frac{r_{dimer}}{r_{interlk}} = \frac{\eta_{interlk}}{\eta_{dimer}} \frac{D_{interlk}}{D_{dimer}} \quad (\text{Equation 4.2})$$

CHCl_3 as the internal standard was used to determine the relative viscosity difference of these two solutions:

$$\frac{\eta_{dimer}}{\eta_{interlk}} = \frac{D_{interlk-\text{CHCl}_3}}{D_{dimer-\text{CHCl}_3}} = \frac{19.8 \text{ } m^2\text{s}^{-1}}{24.0 \text{ } m^2\text{s}^{-1}} = 0.825 \quad (\text{Equation 4.3})$$

So the relative thermodynamic radiiuses of the dimeric cage and interlocked cage can be determined:

$$\frac{r_{dimer}}{r_{interlk}} = \frac{\eta_{interlk}}{\eta_{dimer}} \frac{D_{interlk}}{D_{dimer}} = \frac{1}{0.825} \frac{1.83 \text{ } m^2\text{s}^{-1}}{4.09 \text{ } m^2\text{s}^{-1}} = 0.54 \quad (\text{Equation 4.4})$$

The relative thermodynamic volume of of dimeric cage and interlocked cage is:

$$\frac{V_{dimer}}{V_{interlk}} = \left(\frac{r_{dimer}}{r_{interlk}} \right)^3 = (0.54)^3 = 0.16 \quad (\text{Equation 4.5})$$

The DOSY experiments indicated that the thermodynamic radius of dimeric cage **59A-j** is about half of the second isolated species **59B-j**, which is a strong evidence showing that the second isolated species is indeed twice of the dimeric cage, thus very likely an interlocked species. But the narrow diffusion constant measured result of **59B-j** still cannot prove whether there is only one interlocked species or two different ones since there are no big difference for the face-to-face and side-by-side interlocked products.

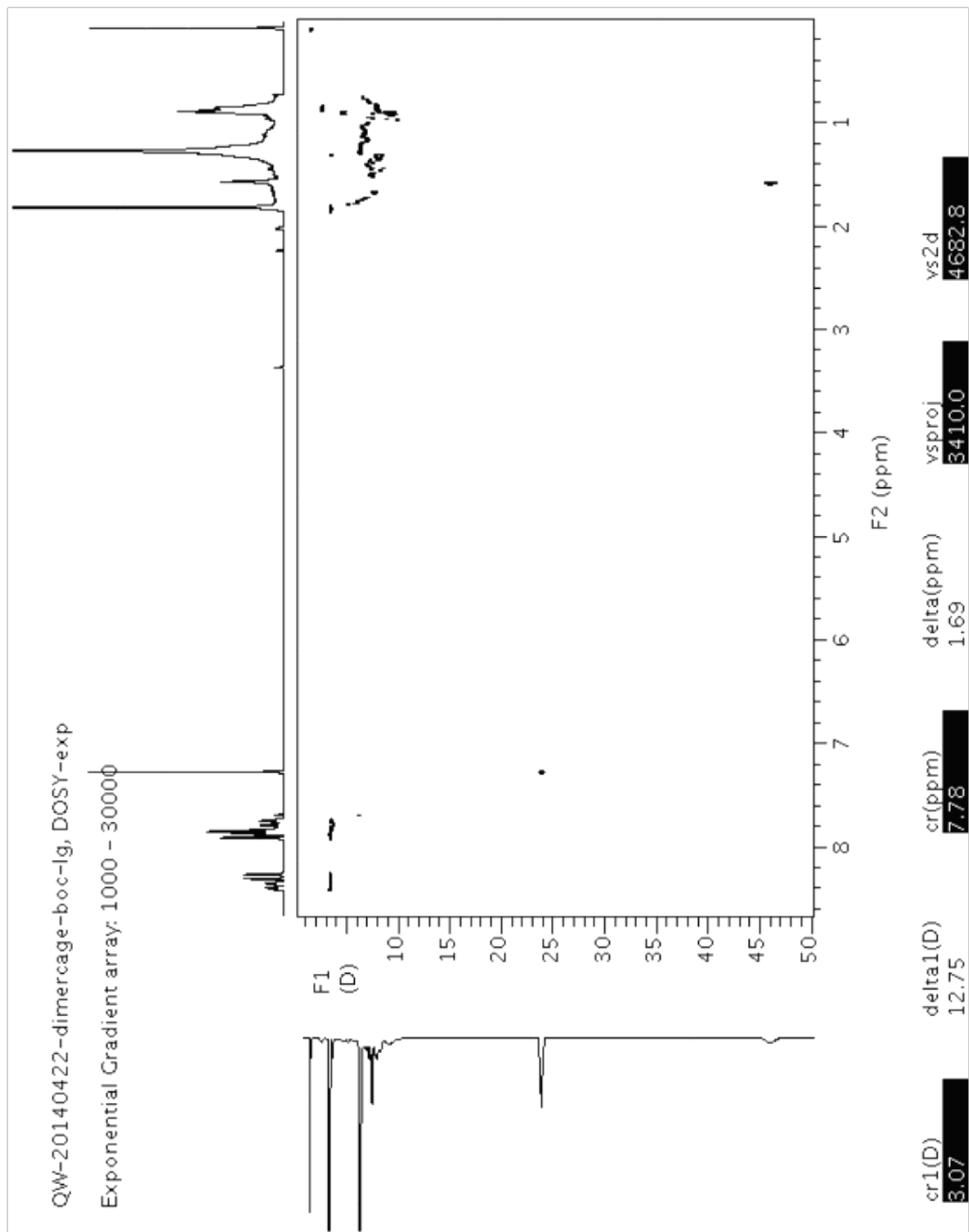


Figure 4.14. DOSY experiment of dimeric cage **59A-j**.

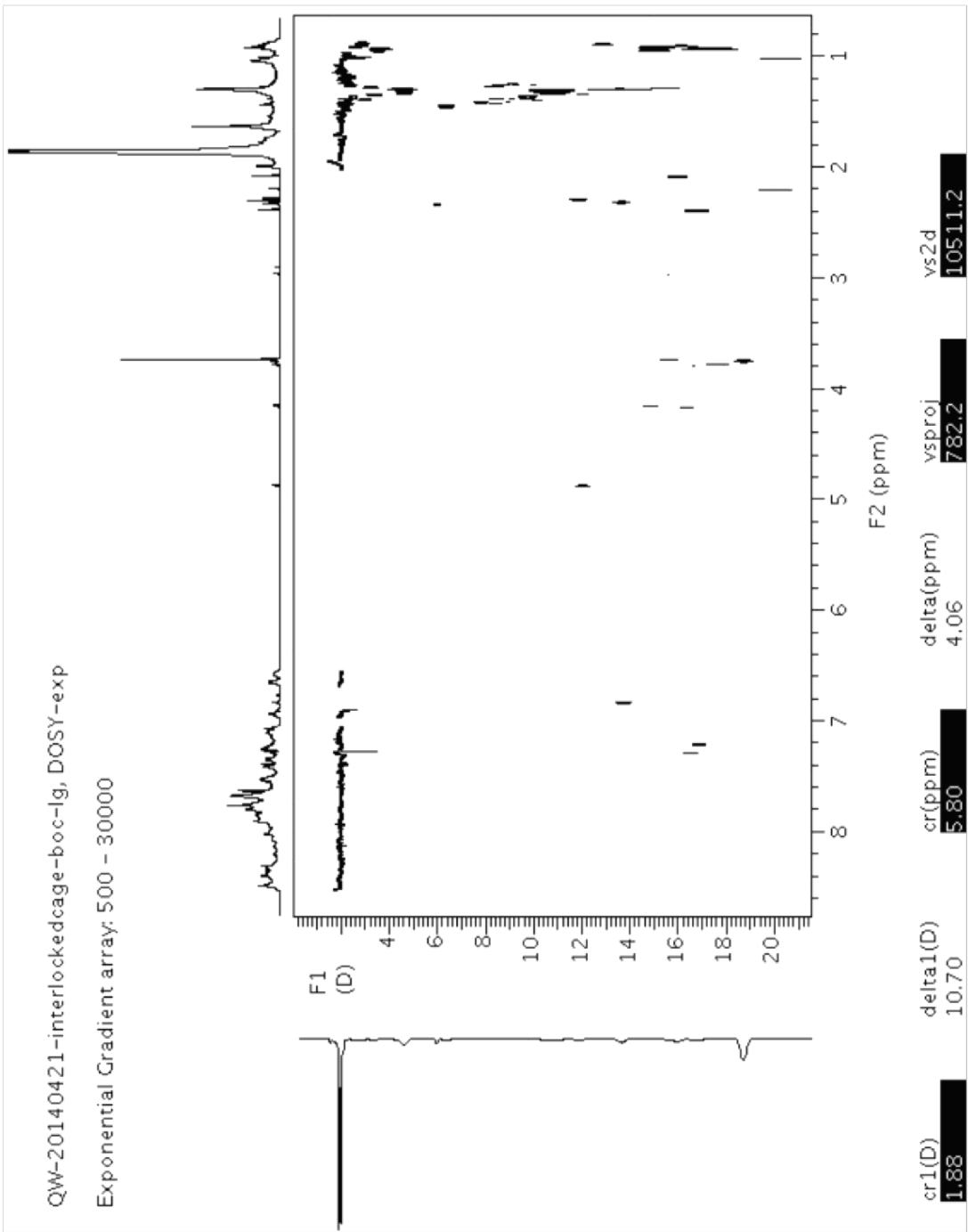


Figure 4.15. DOSY experiment of interlocked cage **59B-j**.

4.4.5. Determination of ^{13}C NMR of cage **59A-j**.

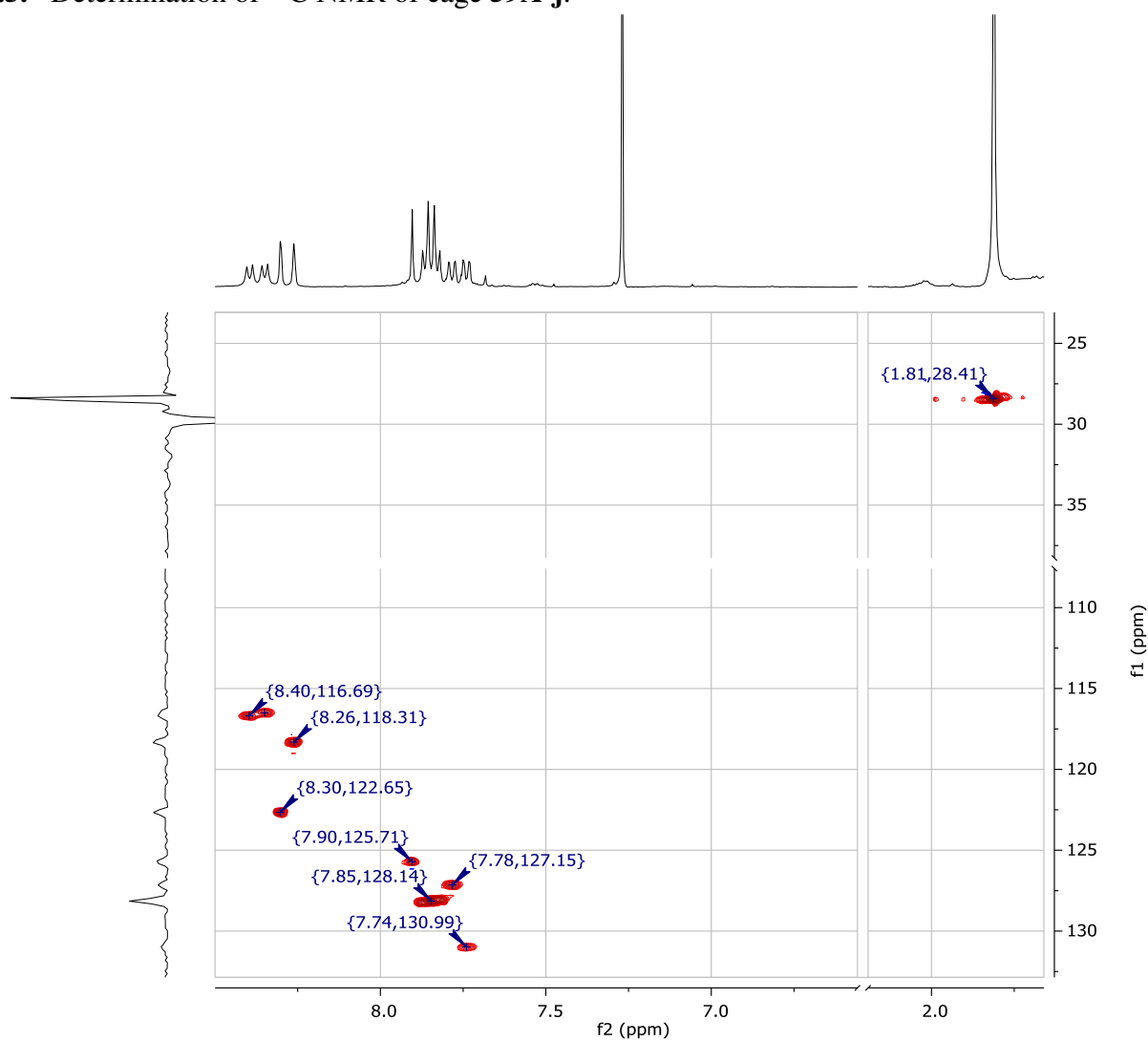


Figure 4.16. The HSQC spectrum of cage **59A-j**.

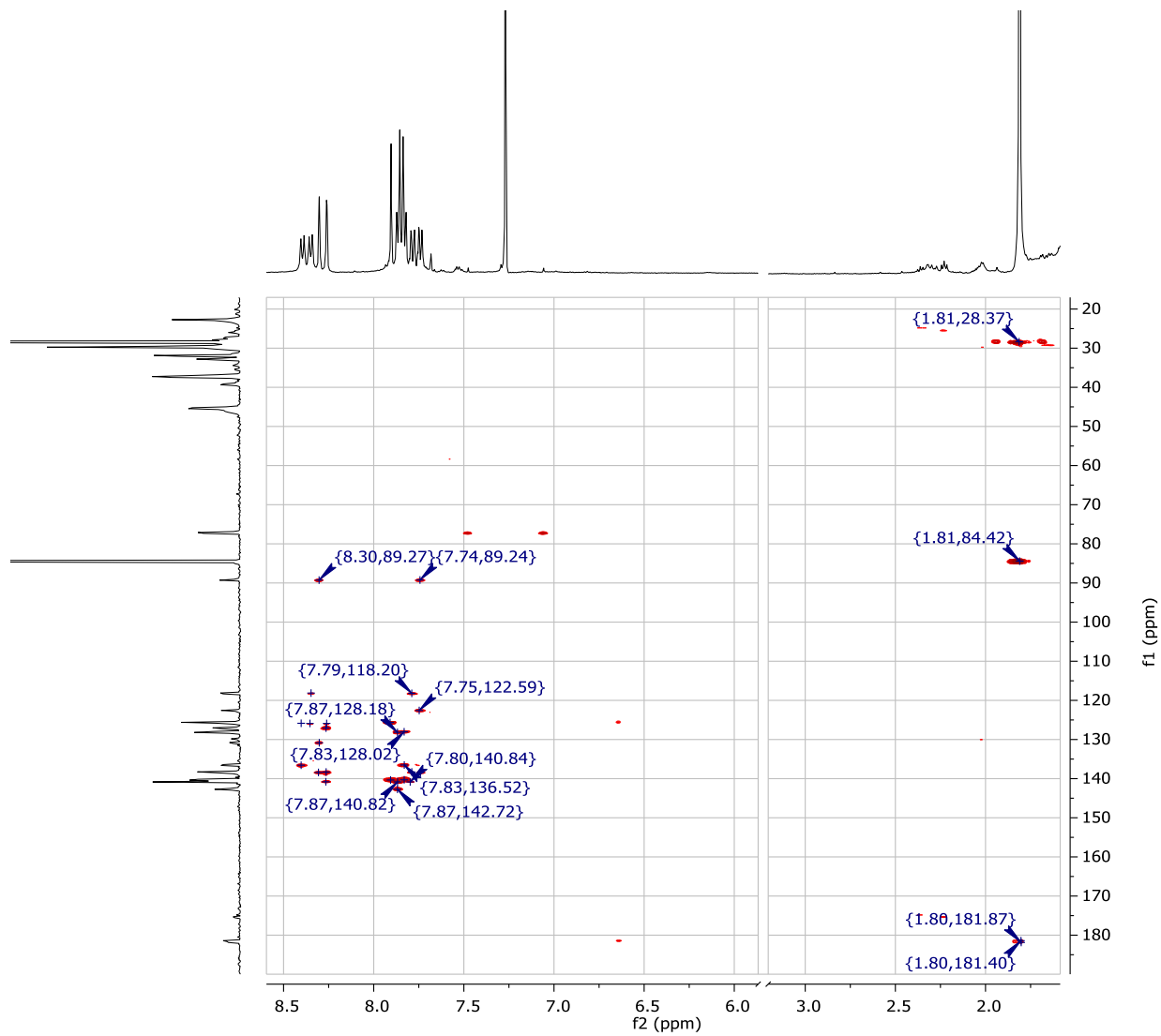


Figure 4.17. The HMBC spectrum of cage **59A-j**.

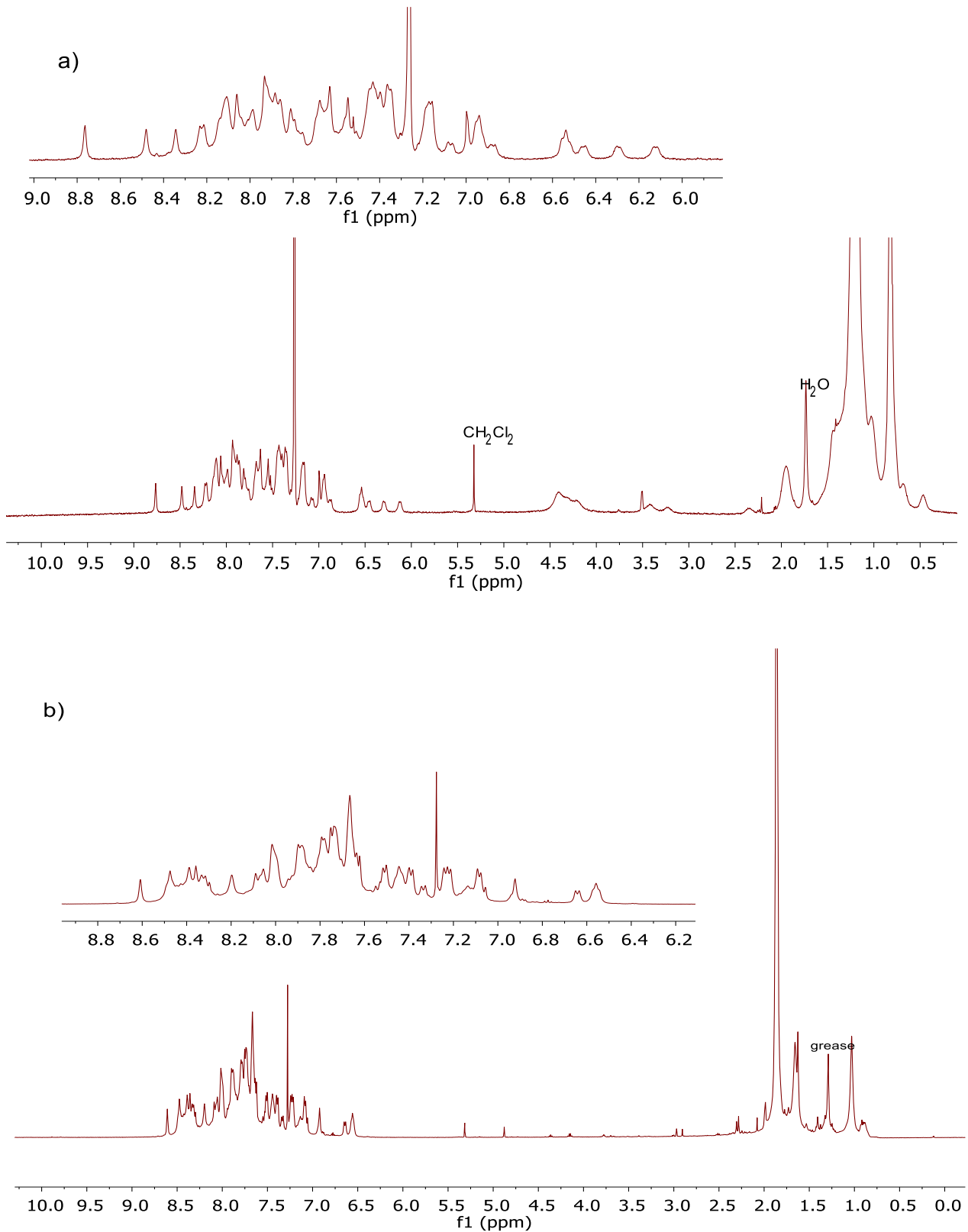


Figure 4.18. The ^1H NMR spectra of cage **59B-a** (a) and **59B-j** (b).

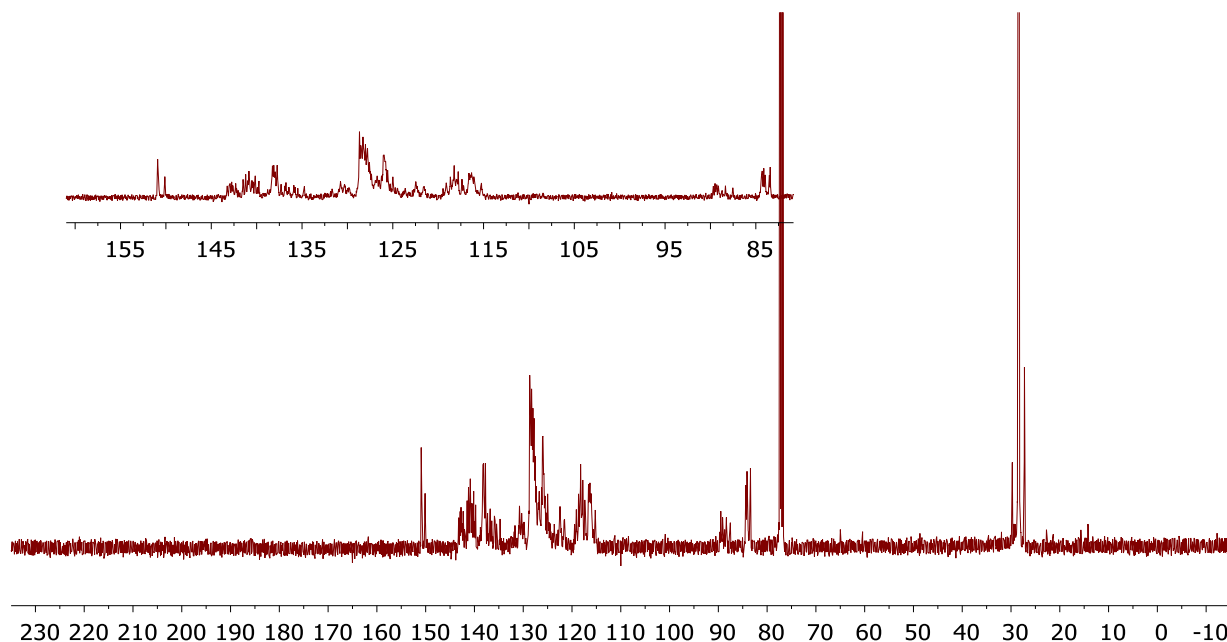


Figure 4.19. The ^{13}C NMR spectra of cage **59B-j**.

4.5. References

1. Forgan, R. S.; Sauvage, J. P.; Stoddart, J. F. *Chem. Rev.* **2011**, *111*, 5434-5464.
2. Barin, G.; Forgan, R. S.; Stoddart, J. F. *P Roy. So.c a-Math. Phy.* **2012**, *468*, 2849-2880.
3. Dietrichbuchecker, C. O.; Sauvage, J. P.; Kintzinger, J. P. *Tetrahedron Lett.* **1983**, *24*, 5095-5098.
4. Breault, G. A.; Hunter, C. A.; Mayers, P. C. *Tetrahedron* **1999**, *55*, 5265-5293.
5. Beves, J. E.; Blight, B. A.; Campbell, C. J.; Leigh, D. A.; McBurney, R. T. *Angew. Chem. Int. Ed.* **2011**, *50*, 9260-9327.
6. Fujita, M.; Fujita, N.; Ogura, K.; Yamaguchi, K. *Nature* **1999**, *400*, 52-55.
7. Fukuda, M.; Sekiya, R.; Kuroda, R. *Angew. Chem. Int. Ed.* **2008**, *47*, 706-710.
8. Westcott, A.; Fisher, J.; Harding, L. P.; Rizkallah, P.; Hardie, M. J. *J. Am. Chem. Soc.* **2008**, *130*, 2950-2951.
9. Freye, S.; Hey, J.; Torras-Galan, A.; Stalke, D.; Herbst-Irmer, R.; John, M.; Clever, G. H. *Angew. Chem. Int. Ed.* **2012**, *51*, 2191-2194.
10. Frank, M.; Hey, J.; Balcioglu, I.; Chen, Y.-S.; Stalke, D.; Suenobu, T.; Fukuzumi, S.; Frauendorf, H.; Clever, G. H. *Angew. Chem. Int. Ed.* **2013**, *52*, 10102-10106.

11. Kuang, X. F.; Wu, X. Y.; Yu, R. M.; Donahue, J. P.; Huang, J. S.; Lu, C. Z. *Nat. Chem.* **2010**, 2, 461-465.
12. Hasell, T.; Wu, X. F.; Jones, J. T. A.; Bacsa, J.; Steiner, A.; Mitra, T.; Trewin, A.; Adams, D. J.; Cooper, A. I. *Nat. Chem.* **2010**, 2, 750-755.
13. Zhang, G.; Presly, O.; White, F.; Oppel, I. M.; Mastalerz, M. *Angew. Chem. Int. Ed.* **2014**, 53, 5126-5130.
14. Zhang, C. X.; Wang, Q.; Long, H.; Zhang, W. *J. Am. Chem. Soc.* **2011**, 133, 20995-21001.
15. Zhang, C. X.; Long, H.; Zhang, W. *Chem. Commun.* **2012**, 48, 6172-6174.
16. Albrecht, K.; Yamamoto, K. *J. Am. Chem. Soc.* **2009**, 131, 2244-2251.
17. Kotha, S.; Kashinath, D.; Lahiri, K.; Sunoj, Raghavan B. *Eur. J. Org. Chem.* **2004**, 2004, 4003-4013.

CHAPTER 5

Ethyneylene Linked Pyrene-based Shape-Persistent COPs: Research Progress and Outlook

5.1. Introduction

The past couple of decades have witnessed tremendous efforts devoted to the area of cancer cell imaging, drug delivery and targeting. Various controlled drug delivery systems have been developed, such as protein self-assembly cages,¹⁻² quantum dots,³⁻⁷ polymers,⁸⁻¹¹ and lipids^{10,12-14}. Recently, metal organic polyhedrons and frameworks have also been applied to the field of drug delivery.¹⁵⁻¹⁹ One great advantage of these large-sized carriers is their selective accumulation into cancer cells due to “enhanced permeability and retention effect”,²⁰ thus facilitating the imaging and reducing the general toxicity and the side effects of the active compound. As an alternative class of cage molecules, covalent organic polyhedrons (COPs) are seeking their applications beyond the well-established fields such as gas adsorption/separation²¹⁻²⁵, host-guest chemistry²⁶⁻³⁰. COPs, usually with discrete and tunable pore size and easily

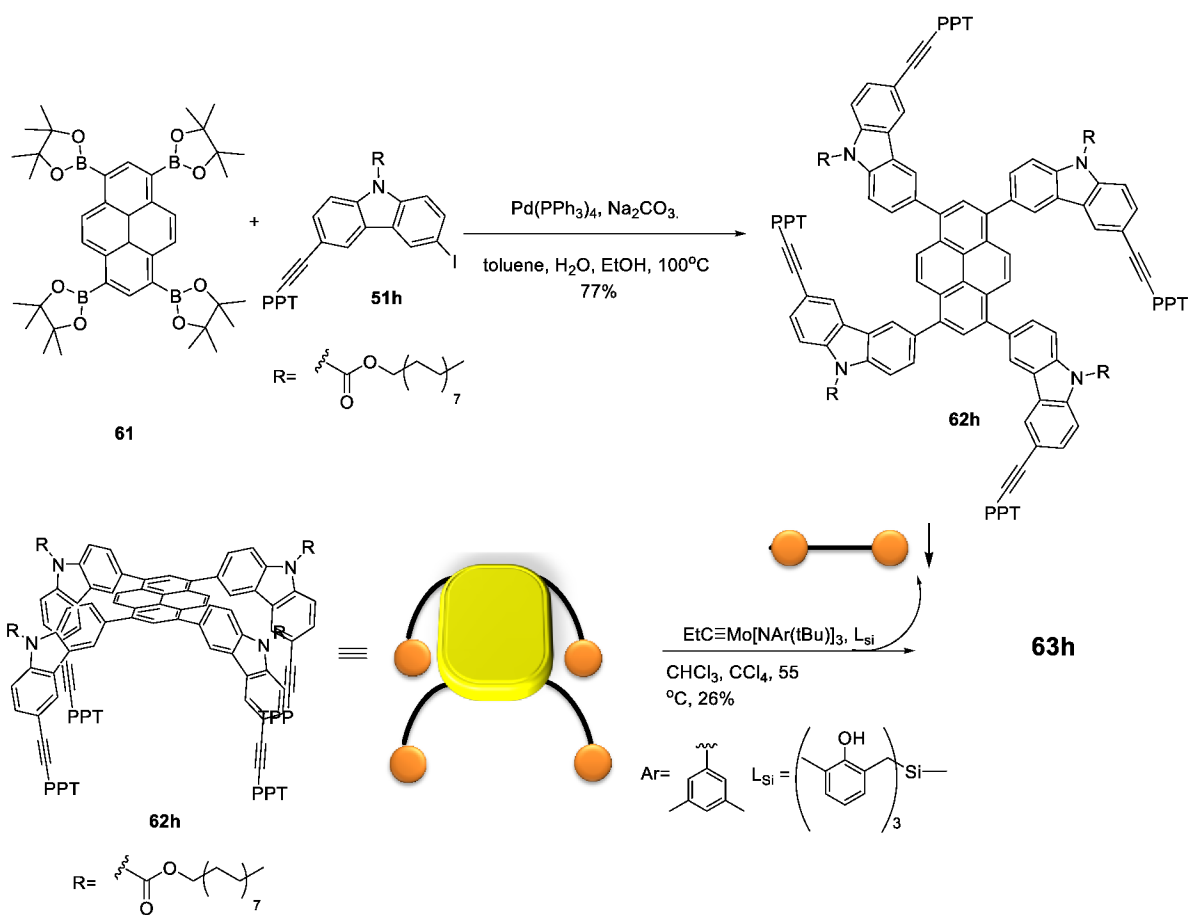
functionalized surface, could provide a novel platform for cell imaging, drug delivery and targeting.

Pyrene moiety is a well-known chromophore, which has been widely used in cell imaging, molecular sensing and diagnosis, etc.³¹⁻³⁶ It has also been shown that pyrene can bind with fullerenes via π - π stacking interactions.³⁷ Therefore, COPs comprising pyrene moieties could be potentially used in fullerene separation and delivery. On the other hand, metallofullerenes, such as Gd@C₆₀ and Gd₃N@C₆₀ with Gd³⁺ or Gd₃N⁶⁺ encapsulated in the fullerene cage, have been explored as magnetic resonance imaging (MRI) contrast agents.³⁸⁻⁴⁰ One great advantage of these metallofullerenes is their significantly enhanced biological safety since their “cage” structure completely prevents the release of highly toxic Gd³⁺ ion into biological environment. Given the above consideration, we envision the pyrene-based shape-persistent molecular cages could serve as a “vehicle” to deliver the metallofullerenes into biosystems for imaging/diagnostic application.

5.2. Preliminary results and discussion

In this chapter, the design and synthesis of an ethynylene linked COP with pyrene moieties incorporated will be discussed. The target monomer has four arms, containing one carbazole on each arm to act as a vertex. The monomer was synthesized via Suzuki coupling of a pyrene-based center piece **61** and an iodo substituted carbazole side arm **51h**. Then the monomer **62h** was subjected to alkyne metathesis catalyzed by catalyst **1** or **3** in a mixed solvent of CCl₄ and chloroform to provide the cage product. The dimeric cage formation was proved by MALDI-TOF MS and GPC. However, the cage synthesis was not very efficient with catalyst **1** or **3**. A large amount of oligomer byproduct remained in the reaction mixture even after 2 times of addition of newly generated catalyst solution, after 16 h time interval. Although the yield is low,

cage **63h** was successfully isolated and characterized with NMR and MALDI-TOF MS. The MALDI-TOF MS showed clear and clean dimeric cage formation. However, the NMR showed more proton signals than expected (Figure 5.1). Specifically, two sets of signals in the aromatic region with similar peak shapes and chemical shift were observed, but the integration ratio of these two sets of peaks varied between different fractions after column separation (Figure 5.5). This observation indicated that there are likely two different cages formed in the metathesis reaction, with slightly different polarity. Given the fact that both products were dimeric cages, we believe that these are two isomers. The pyrene moiety in a monomer unit contains both a major axis and a minor axis. When forming a dimeric cage, there are two ways to connect two monomers together (Figure 5.2), forming two isomers, in which the two monomer units can be connected with each other in a parallel or a vertical fashion. It was observed that before any workup and purification right after alkyne metathesis, the ratio of these two isomers is about 1:1. This observation indicates that there is no much energy difference between the isomers, which is presumably due to the small length difference between the long axis and the short one (30% difference). Moreover, the carbazole arms can easily rotate along single bonds, resulting in similar angle strain generated in either way of connection. All the arms on each isomer are all identical, so each isomer exhibits one set of signal on NMR with slightly different chemical shift.



Scheme 5.1. The synthetic route for cage **63h**.

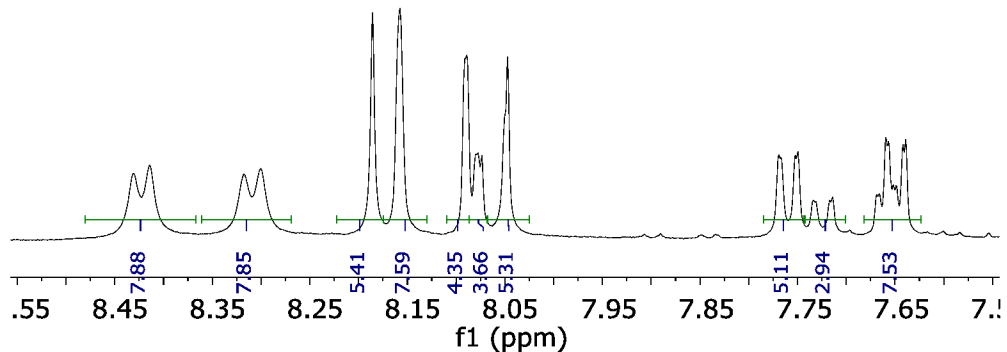


Figure 5.1. The aromatic region of ^1H NMR spectrum of cage **63h** after column purification (mixture of two isomers with a rough ratio of 5:3).

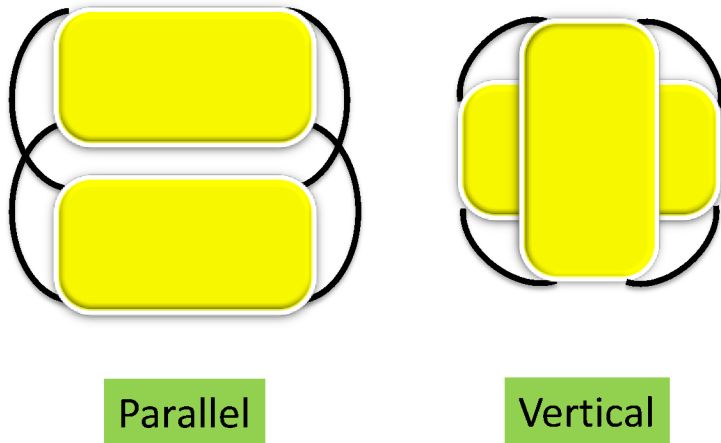


Figure 5.2. The topology of two isomers of cage **63h**, two pyrene moieties taking either parallel (left) or vertical (right) connections.

The binding study of cage **63h** and fullerenes was conducted. Interestingly, the fluorescence titration indicated cage **63h** exhibited much stronger binding affinity with C₆₀ rather than C₇₀ (Figure 5.3). The binding constant for C₆₀@**63h** is 2.9×10^6 L·mol⁻¹, while the binding constant for C₇₀@**63h** is 2.1×10^5 L·mol⁻¹, although the fitting curve for calculating the binding constants did not fit the data very well, which is likely due to the presence of some inseparable oligomer impurities in the cage sample. Nonetheless, it is fair to draw at least a qualitative conclusion that a much weaker binding affinity of cage **63h** with C₇₀ is observed than C₆₀ case.

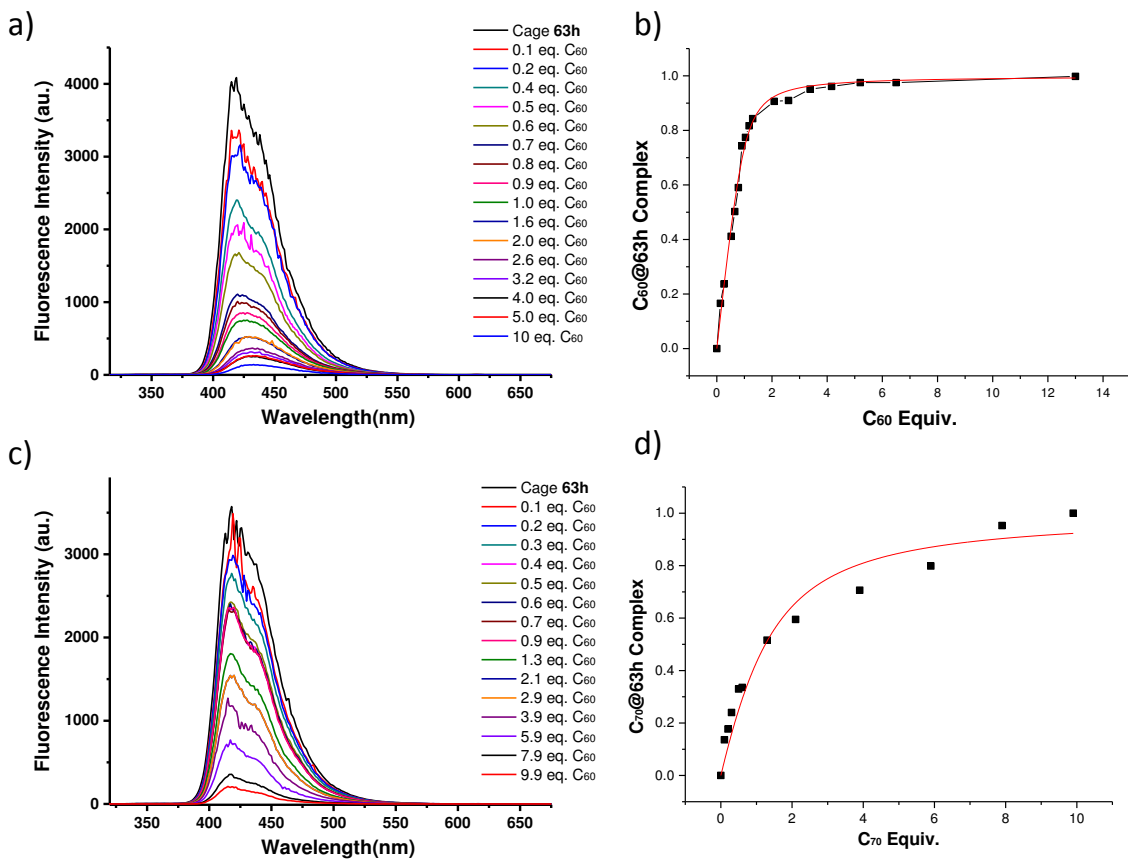
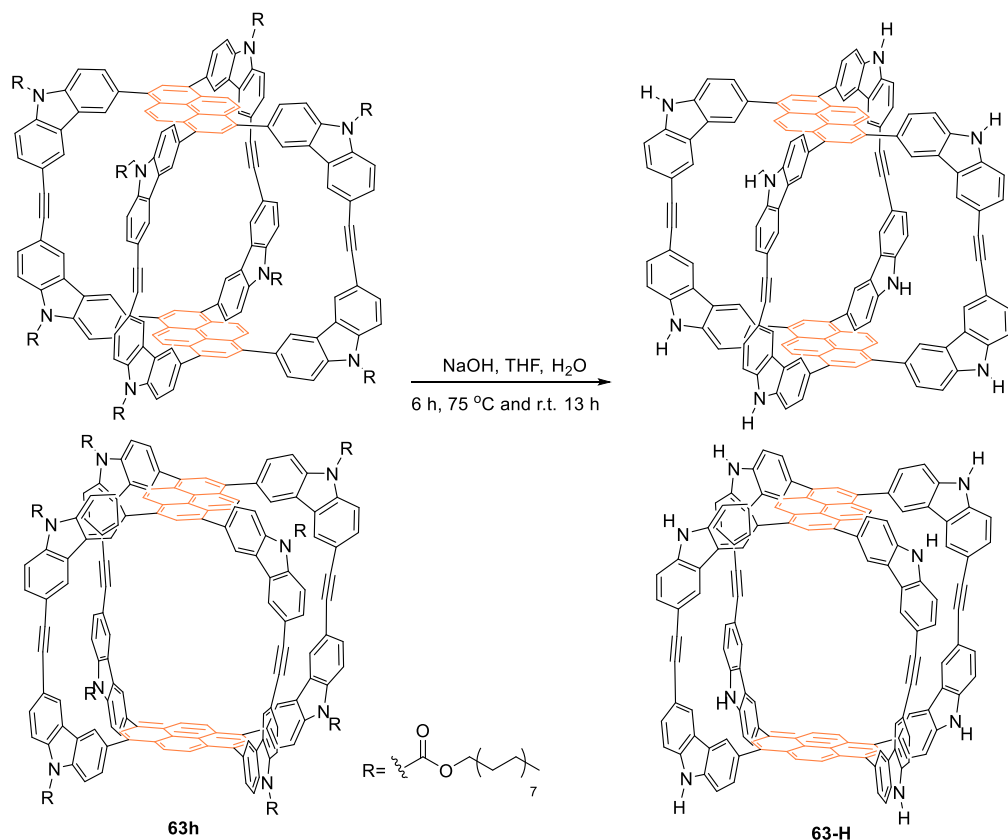


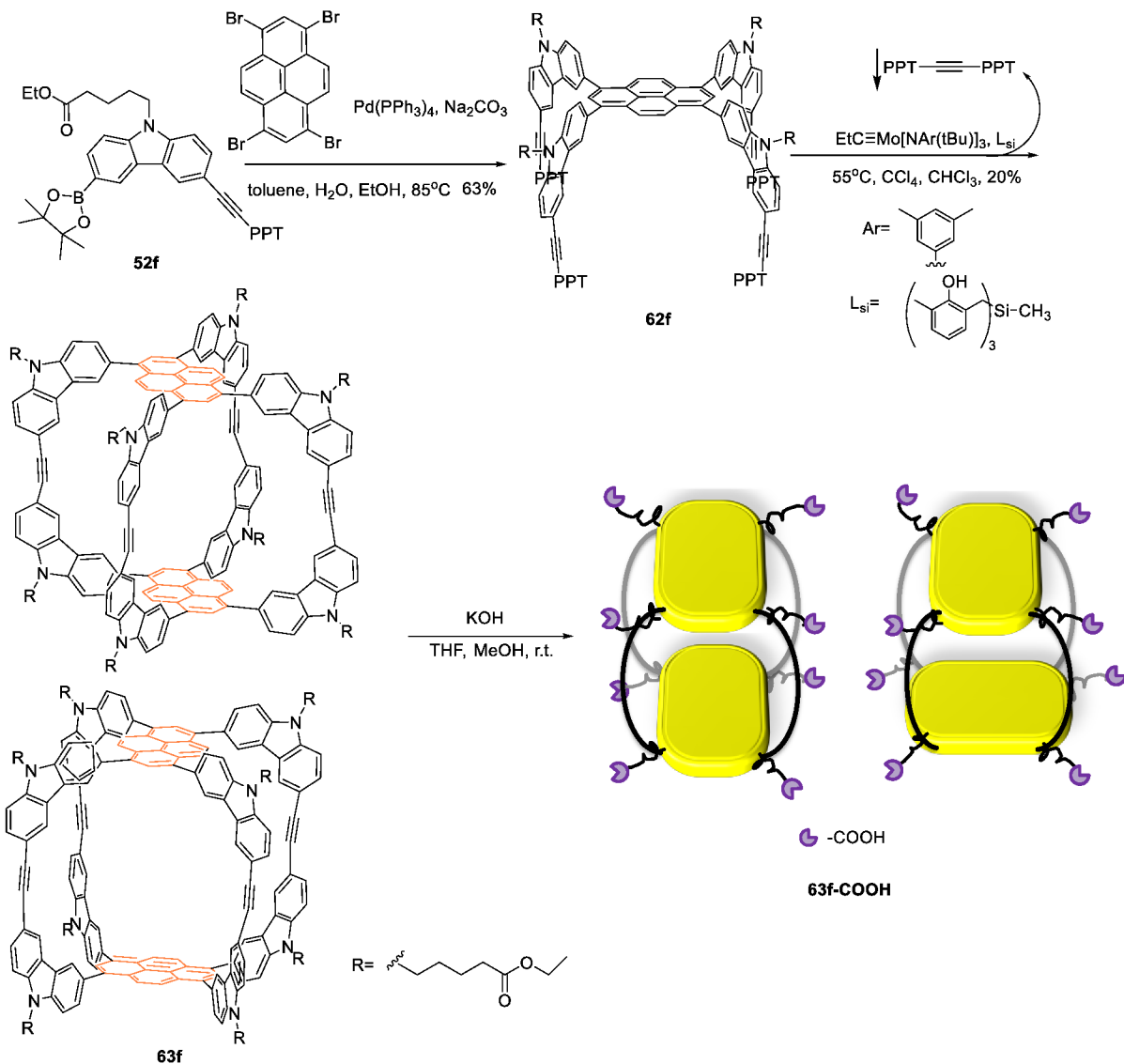
Figure 5.3. The fluorescence titration experiments of cage **63h** with C₆₀ and C₇₀ (excited at 306 nm). The concentration of **63h** in toluene is 3.63×10^{-6} mol/L. Fluorescence titration spectra of cage **63h** with addition of C₆₀ (a) and C₇₀ (c). (b) and (d) are plots of normalized FL at 420 nm vs. equivalent of fullerene (C₆₀ and C₇₀) added. The red curves are the fitting curves.

Given the pyrene cage molecules in hand and the demonstrated strong fullerene binding, next we would like to study the behaviors of cage **63h** in biological environment. However, it turned out working with cage **63h** in biosystems is very challenging due to its highly hydrophobic nature. To overcome the poor solubility issue, the free carbazole based cage **63-H** was synthesized by cleaving the long alkyl chains in basic condition (Scheme 5.2). However, the unsubstituted cage molecule still showed very poor solubility in aqueous solution. Later, we designed and synthesized another cage **63f** with cleavable ester side chains (Scheme 5.3), which can provide carboxylic acid groups after hydrolysis, thus increasing the cage solubility in

aqueous solution. The synthetic route for **63f** followed the similar procedure as for the synthesis of cage **63h**.



Scheme 5.2. Condition for cleavage of carbamate side chains to generate free carbazole based cage **63-H**.



Scheme 5.3. The synthetic route of cage **63f** and **63f-COOH**.

The cage **63f** also showed binding affinity with fullerenes C_{60} and C_{70} based on the fluorescence titration experiments (Figure 5.6). The titration study showed that the binding of **63f** with C_{70} is stronger than with C_{60} , which is in contrast to the binding behavior of **63h** with fullerenes. It is still not clear what could cause the different fullerene binding preference between cage **63h** vs. **63f**. More experiments are needed to further study the binding behavior of the pyrene-based cages **63** with fullerenes.

The carboxylic acid substituted cage **63f-COOH** was successfully obtained after hydrolysis under basic condition. It was found that the solubility of cage **63f-COOH** in water is indeed significantly improved, particularly in basic conditions. However, this acid-functionalized cage showed decreased fluorescence in aqueous solutions compared to those cases in organic solvent, such as DMSO and THF. Nonetheless, even with weaker fluorescence, the biological study showed the cellular uptake of cage **63f-COOH** (Figure 5.4).

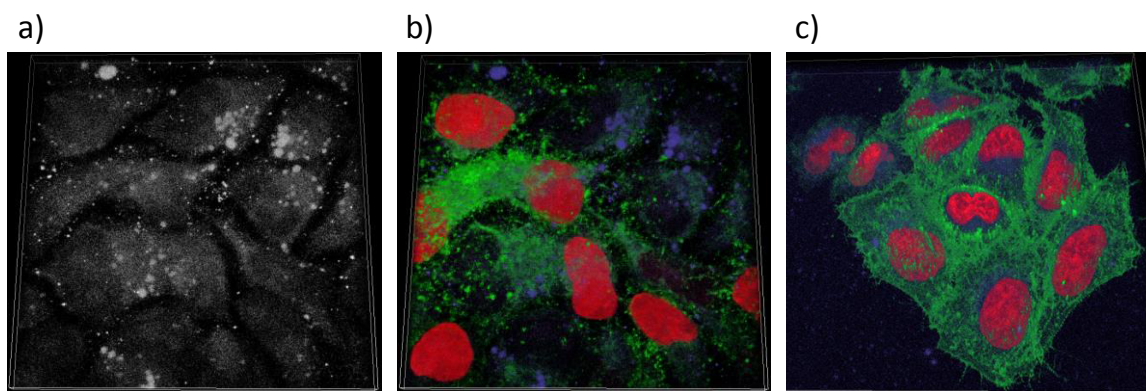


Figure 5.4. Cellular uptake of cage **63f-COOH** in HeLa C9 cells as determined by TIRF microscopy. a) cage **63f-COOH** only; b) and c) **63f-COOH** with H2B-mCherry (nucleus) and YFP-H-ras (membrane).

5.3. Perspectives and recommendations for future

5.3.1. Cage and Gd-metallofullerene complexation study for MRI contrast agent

The pyrene-based cages **63h** and **63f** showed significant binding with fullerenes. The next step will be testing the binding behavior of cage **63** with Gd-metallofuleres. It is known that the metallocfullerenes have quite different electronic properties compared to regular fullerenes. Therefore, more studies need to be conducted on the host-guest binding. If the result is promising, certain tumor targeting groups can be installed on the exterior of the cage to achieve selective targeting and imaging.

Nevertheless, not limited to the pyrene-based cages, other COPs can also be candidates for serving as the “delivering vehicle” for Gd- metallofullerenes.

5.3.2. Application of pyrene-labeled COP in the mechanism study of cellular uptake of COPs

The mechanism of how the COPs are transferred into cells is still unknown. With pyrene-labeled COP, the mechanism can be studied by monitoring the process with fluorescence microscopy. This work will be helpful for future rational design of COP-based drug carrier.

5.4. Experimental Section

5.4.1. Materials, general synthetic methods and biological study condition

Reagents and solvents were purchased from commercial suppliers and used without further purification, unless otherwise indicated. Tetrahydrofuran (THF), toluene, CH₂Cl₂ and dimethylformamide (DMF) were purified by the MBRAUN solvent purification systems.

All reactions were conducted under dry nitrogen in oven-dried glassware, unless otherwise specified. All the alkyne metathesis reactions were conducted in glovebox. The solvents used in alkyne metathesis were dried over 4 Å molecular sieves. Solvents were evaporated using a rotary evaporator after workup. Unless otherwise specified, the purity of the compounds was 195 % based on ¹H NMR spectral integration.

Flash column chromatography was performed by using a 100-150 times weight excess of flash silica gel 32-63 µm from Dynamic Absorbants Inc. Fractions were analyzed by TLC using TLC silica gel F254 250 µm precoated-plates from Dynamic Absorbants Inc. Analytical gel permeation chromatography (GPC) was performed using a Viscotek GPCmaxTM, a Viscotek Model 3580 Differential Refractive Index (RI) Detector, a Viscotek Model 3210 UV/VIS

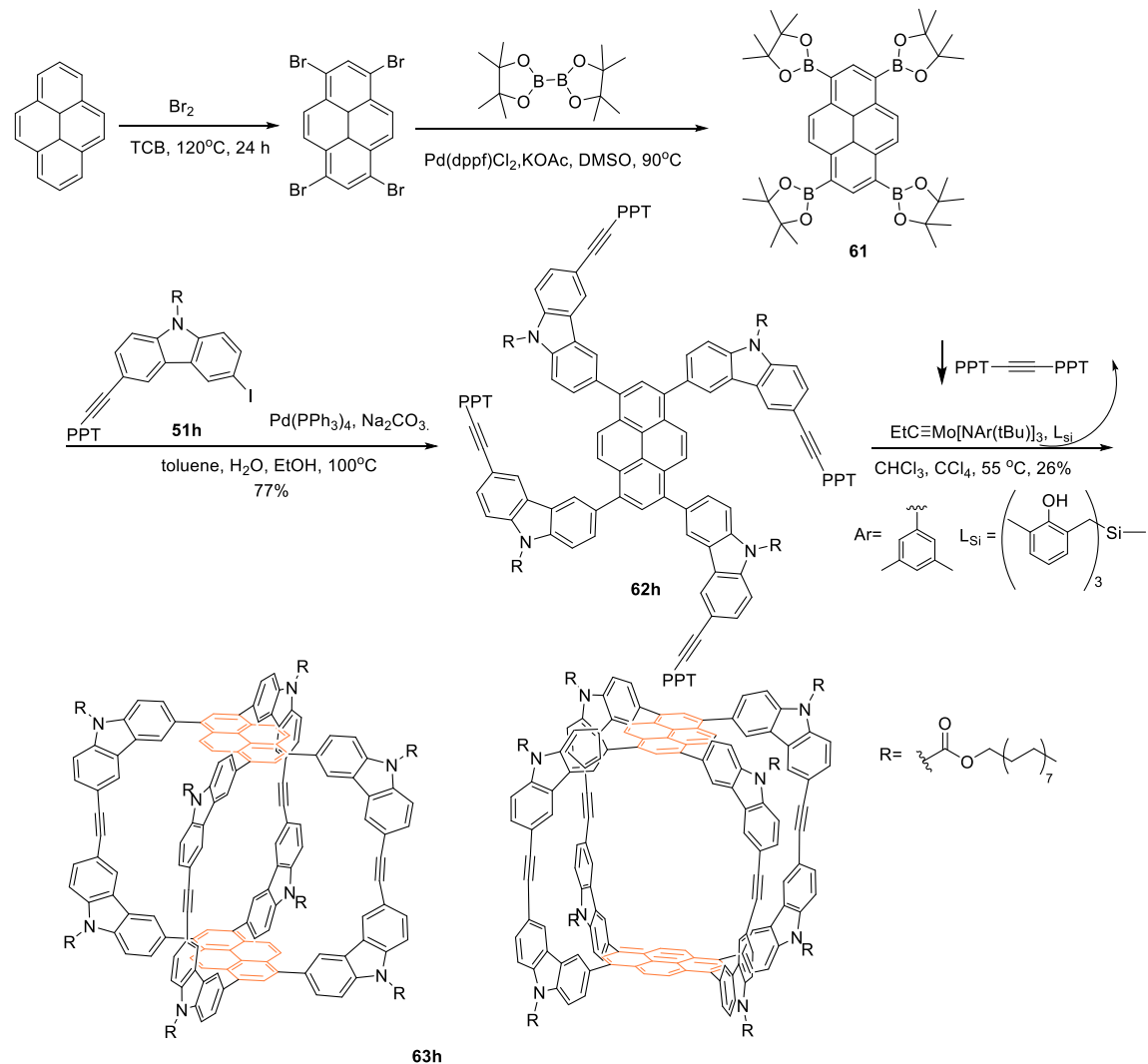
Detector and a set of two Viscotek Viscogel columns (7.8 × 30 cm, 1-MBLMW-3078, and 1-MBMMW-3078 columns) with THF as the eluent at 30 °C. The analytical GPC was calibrated using monodisperse polystyrene standards.

MALDI-TOF Mass spectra were obtained on the Voyager-DETM STR Biospectrometry Workstation using sinapic acid (SA) as the matrix. The high resolution mass spectra were obtained on Waters SYNAPT G2 High Definition Mass Spectrometry System. Analyte molecules were diluted into ESI solvents, methanol, chloroform or acetonitrile/water mixture, for final concentrations of 10 ppm or lower. The solution was injected into the electrospray ionization (ESI) source at a rate of 5 µL/min. Either the ESI+ or ESI- mode was used in reference to the molecular properties. Accurate mass analysis was performed by using the Lock Mass calibration feature with the instrument.

NMR spectra were taken on Inova 400 and Inova 500 spectrometers. CHCl₃ (7.27 ppm), toluene-*d*₈ (2.09 ppm) were used as internal references in ¹H NMR, and CHCl₃ (77.00 ppm) for ¹³C NMR. ¹H NMR data were reported in order: chemical shift, multiplicity (s, singlet; d, doublet; t, triplet; q, quartet; m, multiplet), coupling constants (*J*, Hz), number of protons.

Images on figure 5.4 was taken for HeLa C9 cells after 24 hours of incubation from when the cage was added, held at 37 °C with 5% CO₂ in Dulbecco's Modified Eagle's Medium with 10% fetal bovine serum, penicillin (1U/mL)/streptomycin(1µg/mL), and GlutaMAX.

5.4.2. Synthetic procedures



Compound **61** was synthesized following the reported procedure ⁴¹. ¹H NMR (500 MHz, CDCl₃) δ 9.17 (s, 4H), 8.99 (s, 2H), 1.51 (s, 48H).

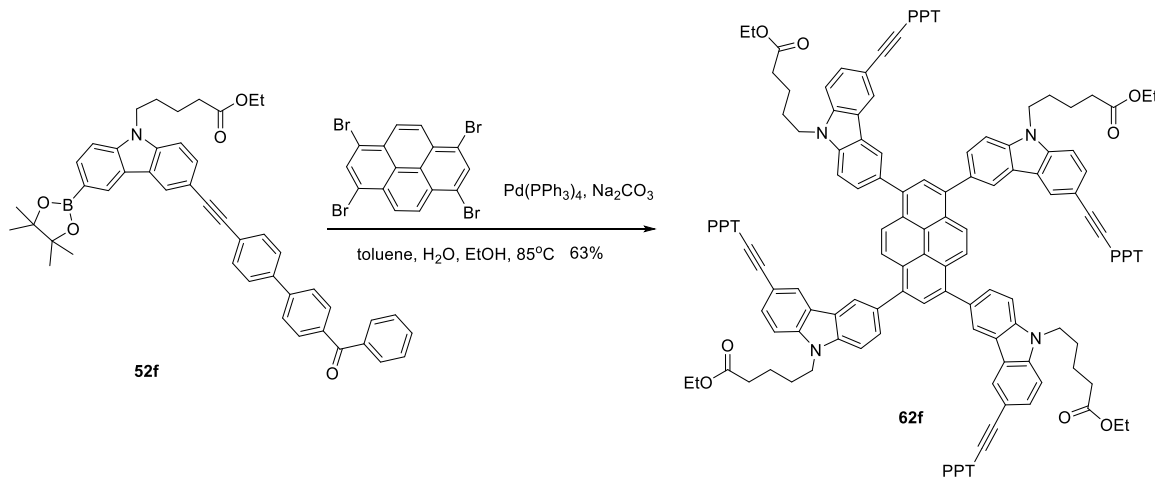
Monomer 62h: Follow the previously described Suzuki coupling procedure. **51h** (150 mg, 0.178 mmol), **61** (29.3 mg, 0.0424 mmol), Pd(PPh₃)₄ (2.4 mg, 0.00212 mmol) and Na₂CO₃ (1 mL, 1M aqueous solution), EtOH (1 mL) and toluene (5 mL) were used. The product was purified by flash column chromatography (eluting with CH₂Cl₂/hexane, 2/1 ~ 3/1) to give pure

monomer **62h** (100 mg, 77%). NMR at room temperature is very broad, mainly due to aggregation. The ¹H NMR was conducted at 59 °C and low concentration. ¹H NMR (400 MHz, CDCl₃) δ 8.50 (d, *J* = 8.5 Hz, 4H), 8.35–8.36 (m, 8H), 8.32 (s, 4H), 8.24 (s, 6H), 7.90 (d, *J* = 9.4 Hz, 4H), 7.85 (d, *J* = 8.4 Hz, 8H), 7.80 (d, *J* = 7.3 Hz, 8H), 7.70 (d, *J* = 8.6 Hz, 4H), 7.56–7.71 (td, 28H), 7.48 (t, *J* = 7.6 Hz, 8H), 4.61 (t, *J* = 6.7 Hz, 8H), 1.99 (q, *J* = 7.1 Hz, 8H), 1.56 (d, *J* = 7.8 Hz, 8H), 1.25 (d, *J* = 18.1 Hz, 96H), 0.85 (t, *J* = 6.4 Hz, 12H). ¹³C NMR showed very broad signal thus a lot of peaks were not resolved. See figure 5.11.

Cage 63h: To a solution of monomer **62h** (100 mg, 0.033 mmol) in CCl₄ (3 mL) and CHCl₃ (4 mL) was added a newly generated catalyst solution (1 mL, generated from the precursor 4.4 mg, 0.0067 mmol and the ligand 2.7 mg, 0.0067 mmol as described previously). The reaction mixture was stirred at 55 °C for 18 h and then another batch of catalyst solution (1 mL, generated from the precursor 4.4 mg, 0.0067 mmol and the ligand 2.7 mg, 0.0067 mmol) and react for another 20 h. The reaction was monitored by GPC. After adding another batch of catalyst (precursor 2.2 mg, and ligand 1.3 mg) and stir for another 20 h, the volatiles removed, the residue was filtered and purified by flash column chromatography (eluting with hexane/CH₂Cl₂, 1/3), yielding cage product (17 mg, 26%). ¹H NMR (500 MHz, CDCl₃) δ 8.32 (d, *J* = 8.5 Hz, 8H), 8.21 (d, *J* = 8.2 Hz, 8H), 8.08 (s, 8H), 8.07 – 8.04 (m, 8H), 8.01 – 7.97 (m, 8H), 7.96 – 7.93 (m, 4H), 7.69 – 7.60 (m, 8H), 7.59 – 7.53 (m, 8H), 4.48 (t, *J* = 6.7 Hz, 16H), 1.84 (d, *J* = 7.7 Hz, 16H), 1.43 (q, *J* = 7.6, 7.0 Hz, 16H), 1.15 (t, *J* = 13.9 Hz, 192H), 0.83 – 0.70 (m, 24H). MALDI-TOF(m/z): [M]⁺ calcd. for C₂₇₂H₃₂₄N₈O₁₆, 3960.48; found, 3961.84.

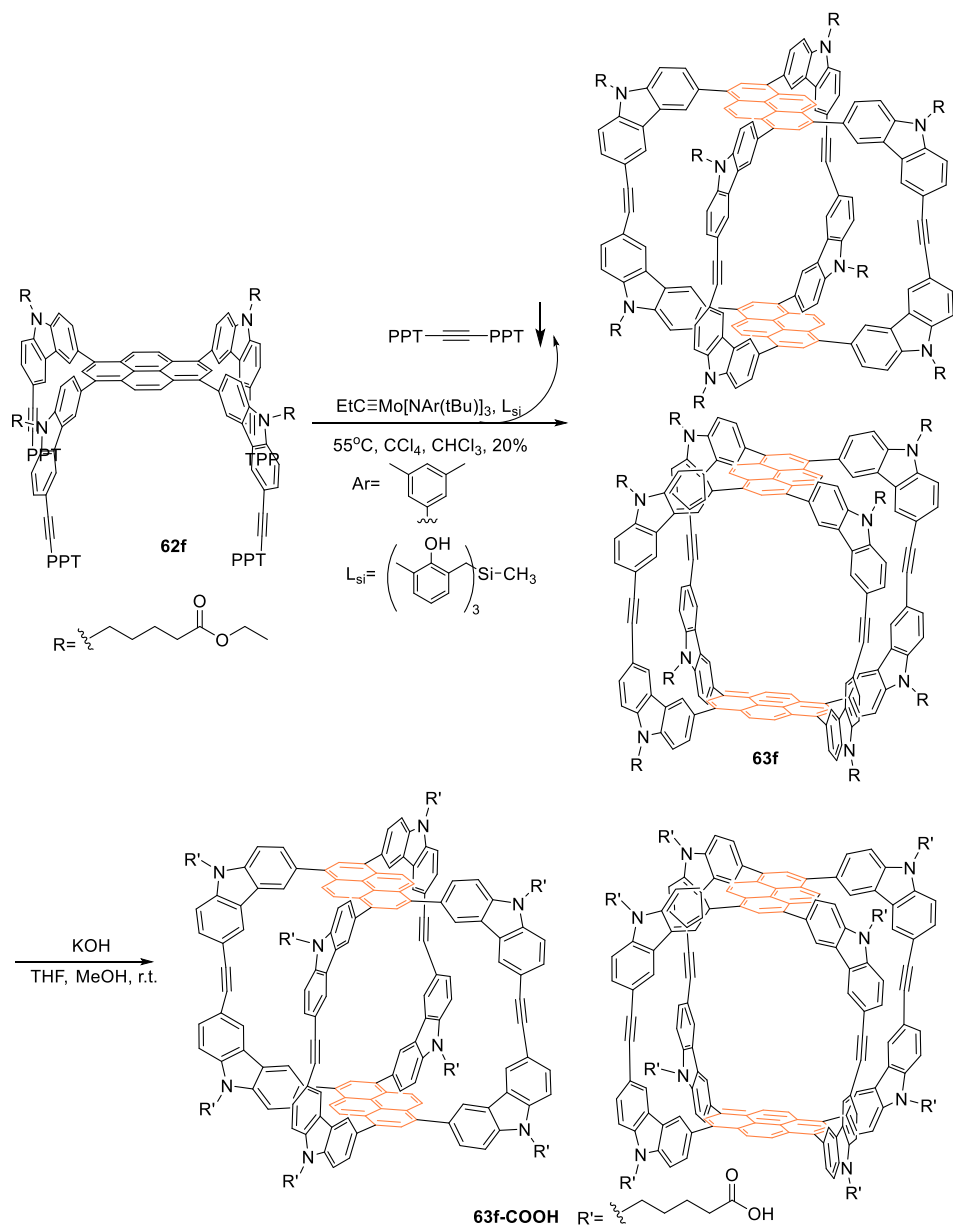
Cage 63-H: To a seal tube, **63h** (2 mg) in THF (1 mL) and NaOH (30 mg) in H₂O (1 mL) were added. The reaction was heated to 75 °C for 6 h and stirred for another 13 h at room temperature. After organic layer was collected by separation, the aqueous phase was extracted with CHCl₃ (10

mL × 2) and the organic layers were combined. After the solvent was removed by reduced pressure, the residue was washed with hexanes to remove soluble compounds. Then the resulting compound passed through a short silica plug. The relatively pure product was collected. ¹H NMR (500 MHz, THF-*d*₈) δ 8.27 (s, 13H), 8.25 (s, 3H), 8.14 (s, 6.5H), 8.06 (s, 0.7H), 8.02 (s, 3.3H), 8.01 (s, 1.5H), 7.70 – 7.64 (m, 8H), 7.58 (d, *J* = 8.2 Hz, 8H), 7.52 – 7.46 (m, 8H), 7.41 (d, *J* = 8.4 Hz, 8H).



Monomer 62f: Follow typical Suzuki coupling condition. **52f** (640 mg, 0.91 mmol), 1,3,6,8-tetrabromo-pyrene (78.8 mg, 0.152 mmol), Pd(PPh₃)₄ (28 mg, 0.024 mmol), Na₂CO₃ (1.5 mL 1 M aqueous solution), EtOH (1.5 mL) and toluene (7 mL) were used. Product was purified by flash chromatography (eluting with hexanes/EtOAc/CHCl₃, 4/1/4~3/2/5) yielding yellow product (240 mg, 63%). ¹H NMR (500 MHz, CHCl₃) δ 8.50 (s, 4H), 8.40 (s, 4H), 8.37 (s, 4H), 8.31 (s, 2H), 7.93 (d, *J* = 8.2 Hz, 4H), 7.87 (d, *J* = 8.1 Hz, 8H), 7.84 – 7.80 (m, 8H), 7.74 – 7.56 (m, 36H), 7.50 (t, *J* = 7.7 Hz, 8H), 7.45 (d, *J* = 8.5 Hz, 4H), 4.44 (t, *J* = 6.9 Hz, 8H), 4.11 (q, *J* = 7.1 Hz, 8H), 2.37 (t, *J* = 7.2 Hz, 8H), 2.03 (dd, *J* = 15.8, 8.1 Hz, 8H), 1.88 – 1.73 (m, 8H), 1.22 (t, *J* = 7.1 Hz, 12H). ¹³C NMR (101 MHz, CHCl₃) δ 196.12, 173.06, 144.21, 140.40, 139.94, 138.81, 137.57, 136.21, 132.61, 132.33, 131.90, 130.68, 129.91, 129.44, 129.29, 128.24, 127.04, 126.62, 126.33, 125.36, 124.22, 123.79, 122.95, 122.67, 113.23, 108.72, 92.26, 87.46, 74.95, 60.36,

33.79, 28.44, 24.80, 22.61, 14.16. MALDI-TOF(m/z): [M]⁺ calcd. for C₁₇₆H₁₃₄N₄O₁₂, 2496.00; found, 2493.34.



Cage 63f: To a solution of monomer **62f** (175 mg, 0.070 mmol) in CCl_4 (14 mL) and CHCl_3 (25 mL) was added a newly generated catalyst solution (2 mL, generated from the precursor 7.0 mg, 0.0105 mmol and the ligand 4.3 mg, 0.0105 mmol as described previously). The reaction mixture was stirred at 55°C for 18 h and then another batch of catalyst solution (1 mL, generated from

the precursor 1.7 mg, 0.0026 mmol and the ligand 1.0 mg, 0.0026 mmol) and react for another 20 h. After removing the volatiles, the residue was filtered and purified by flash column chromatography (eluting with hexane/EtOAc/CHCl₃, 1/1/2), yielding cage product (20 mg, 20%).

¹H NMR (400 MHz, CDCl₃) δ 8.24 – 8.21 (m, 8H), 8.19 (dd, *J* = 4.1, 1.5 Hz, 8H), 8.13 (s, 4H), 8.07 (s, 2H), 8.04 (s, 2H), 8.01 (s, 4H), 7.72–7.67 (m, 8H), 7.59 (dd, *J* = 8.6, 1.5 Hz, 8H), 7.47 (dd, *J* = 8.4, 1.5 Hz, 8H), 7.34 (d, *J* = 8.6 Hz, 8H), 4.36 (d, *J* = 7.8 Hz, 8H), 4.06 (q, *J* = 7.2 Hz, 16H), 2.31 (t, *J* = 7.2 Hz, 16H), 1.95 (p, *J* = 7.2 Hz, 16H), 1.73 (p, *J* = 7.3 Hz, 16H), 1.17 (t, *J* = 7.1 Hz, 24H). ¹³C NMR (101 MHz, CDCl₃) δ 196.10, 173.06, 144.20, 140.40, 139.93, 138.81, 137.57, 136.21, 132.61, 132.33, 131.89, 130.68, 129.90, 129.43, 129.27, 128.24, 127.04, 126.62, 126.33, 125.33, 124.19, 123.79, 122.94, 122.66, 113.23, 108.71, 92.27, 87.46, 60.36, 33.79, 29.67, 28.44, 22.61, 14.16, 14.11, 1.00. MALDI-TOF(m/z): [M]⁺ calcd. for C₁₉₂H₁₆₄N₈O₁₆, 2839.23; found, 2838.90.

Cage 63f-COOH: Cage **63f** (9.0 mg, 0.0032 mmol) and KOH (80 mg, 1.4 mmol) were dissolved in THF (0.3 mL) and MeOH (0.3 mL). After stirring for 41 h, the solvent was removed under reduced pressure. The residue was redissolved in water to give a suspension and the solution was treated with 1M HCl (~ 2 mL) to give pH=1. More precipitates formed. Then the solution was extracted with EtOAc (2 mL × 3). The aqueous phase turned to colorless. The organic layer was concentrated down to give yellow solids. ¹H NMR (500 MHz, THF-*d*8) δ 8.30 (d, *J* = 1.6 Hz, 4H), 8.28 (s, 8H), 8.27 (s, 4H), 8.16 (s, 4H), 8.09 (s, 2H), 8.04 (d, *J* = 1.8 Hz, 4H), 7.76 – 7.73 (m, 4H), 7.73 – 7.67 (m, 12H), 7.61 (d, *J* = 8.6 Hz, 2H), 7.58 – 7.56 (m, 4H), 7.55 (s, 12H), 4.48 (t, *J* = 6.5 Hz, 16H). The crude ¹H NMR is messy on the aliphatic region. The methylene groups were not able to be determined in the NMR. MALDI-TOF(m/z): [M]⁺ calcd. for C₁₇₆H₁₃₂N₈O₁₆, 2612.98; found, 2616.09.

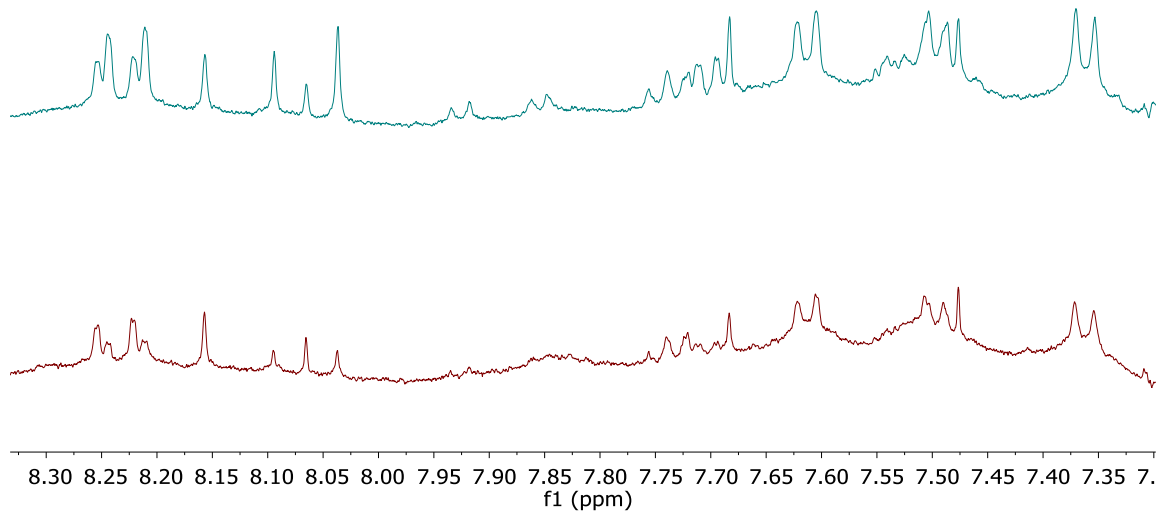
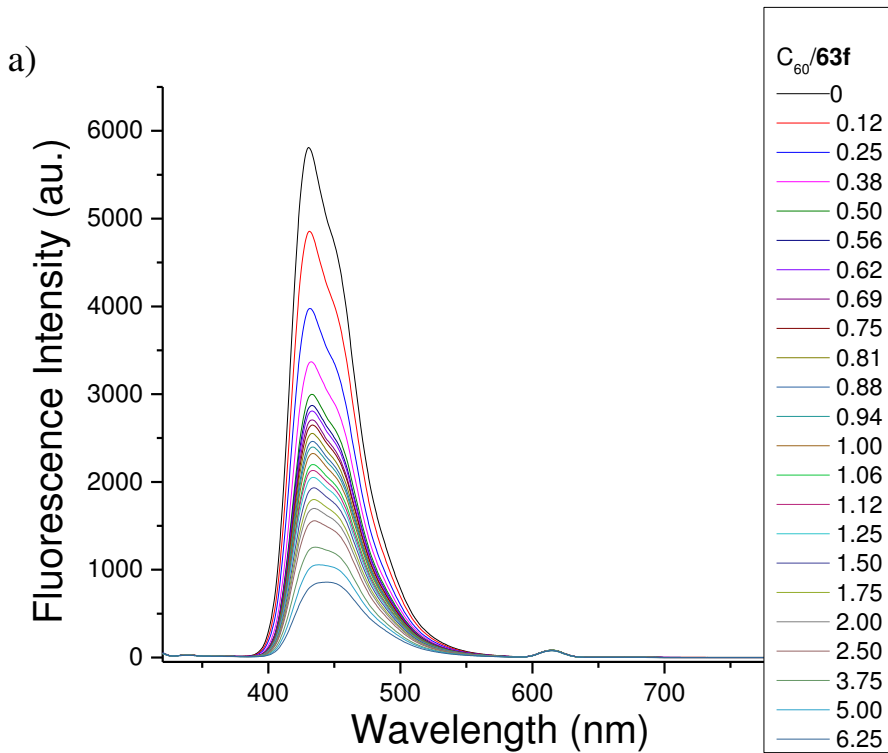
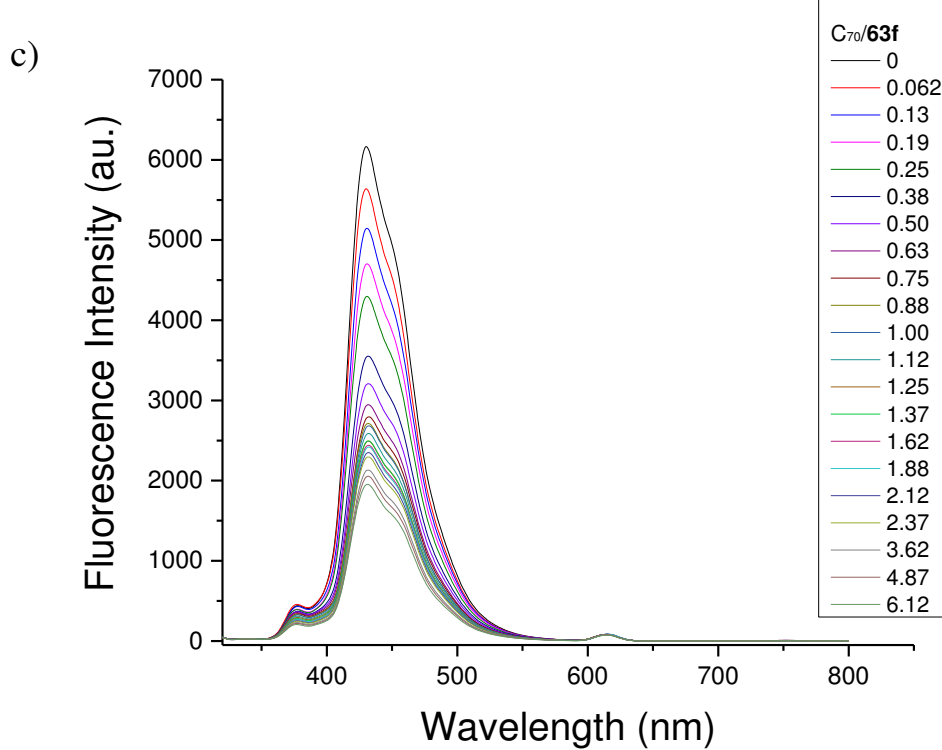
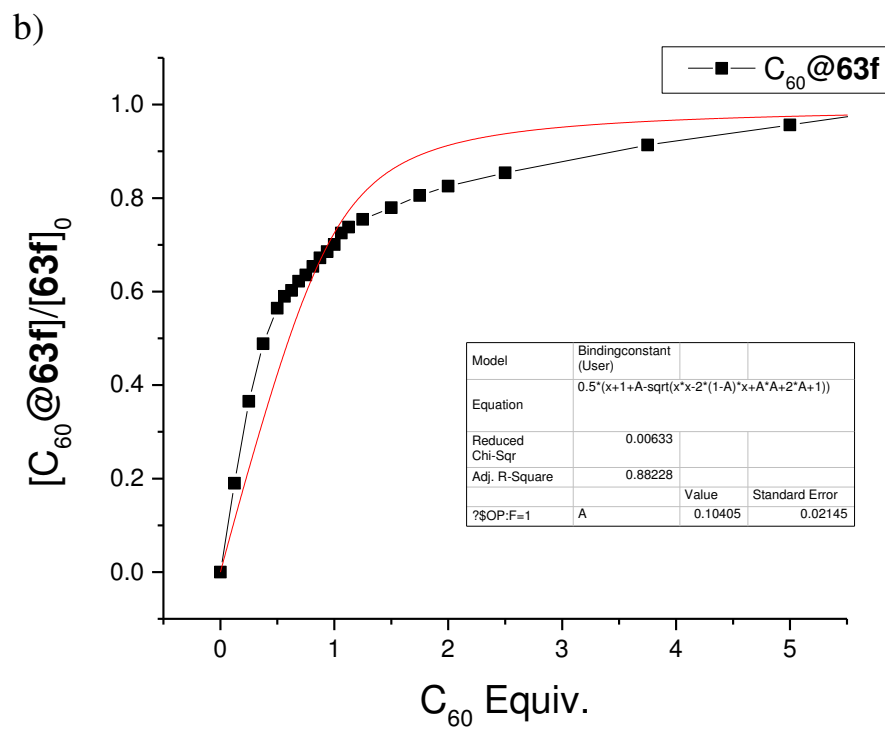


Figure 5.5. The ^1H NMR of the earlier (bottom) and later (top) fractions out of column, showing that the two isomers have little difference in their polarity.

5.4.3. Binding study of cage **63f** and **63h** with fullerenes





d)

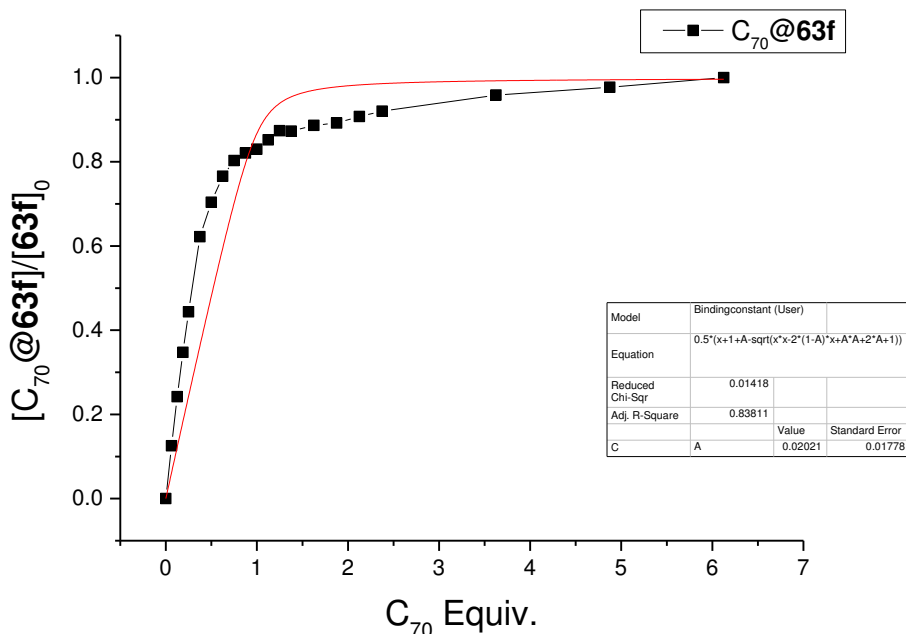


Figure 5.6. The fluorescence titration experiments of cage **63f** with C₆₀ and C₇₀ (exited at 306 nm). The concentration of **63h** in toluene is 3.00×10^{-7} mol/L. Fluorescence titration spectra of cage **63h** with addition of C₆₀ (a) and C₇₀ (c). (b) and (d) are plots of normalized FL at 430.5 nm vs. equivalent of fullerene (C₆₀ and C₇₀) added. The red curves are the fitting curves.

The fluorescence titration experiments were conducted for cage **63f** with fullerenes C₆₀ and C₇₀. The fluorescence of **63f** is very strong and the quenching is very clear. However one problem is that the FL keeps decreasing after 1 e.q. of fullerene addition. The possible reason is that the cage sample may contain some oligomers that can have interactions with fullerenes too. The internal standard normalization using NMR shows about 20% impurities (the concentration of cage is corrected based on the internal standard). The oligomers are difficult to remove. Based on this quenching curve, the fitting is not quantitatively accurate. Nonetheless, the fitting results are shown below:

The binding constant of cage **63f** with C₆₀ is 3.2×10^7 L·mol⁻¹.

The binding constant of cage **63f** with C₇₀ is 1.6×10^8 L·mol⁻¹.

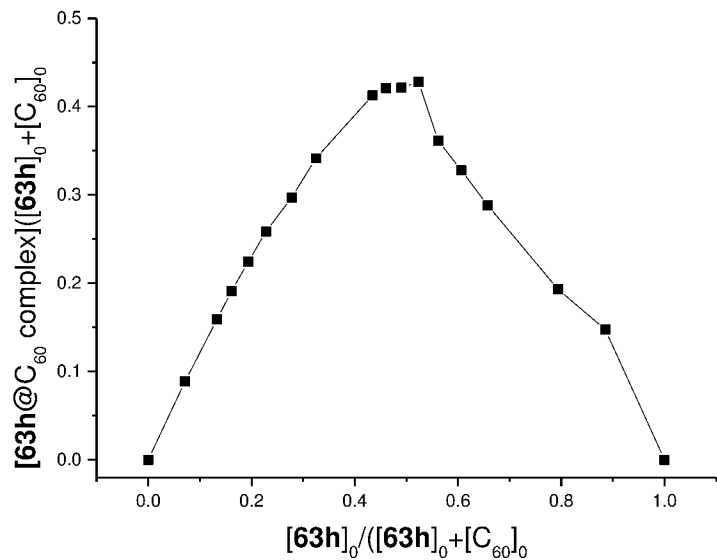


Figure 5.7. Job plot of cage **63h** with addition of C₆₀, indicating that the binding of cage **63h** with C₆₀ is 1:1.

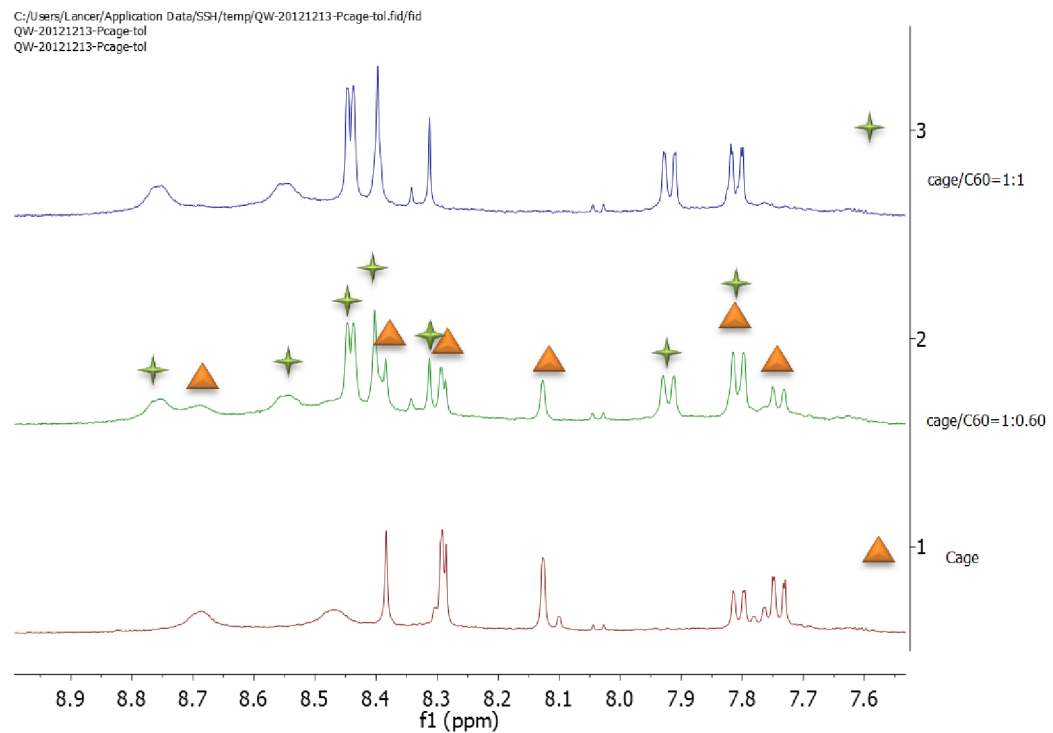


Figure 5.8. ¹H NMR titration of **63h** with C₆₀, 1) **63h**, 2) with 0.6 equiv. C₆₀ addition, 3) with 1.0 equiv. C₆₀ addition.

5.4.4. NMR spectrum of important compounds

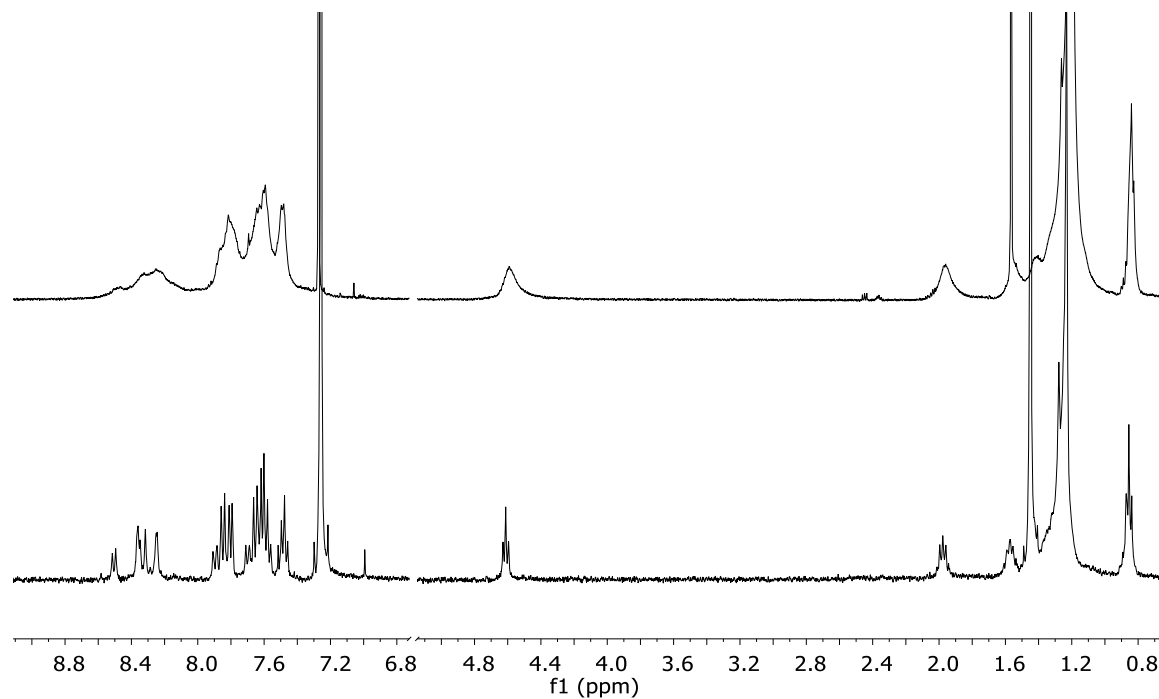


Figure 5.9. The ¹H NMR spectra of monomer **62h** at 20 °C (top) and 58 °C (bottom).

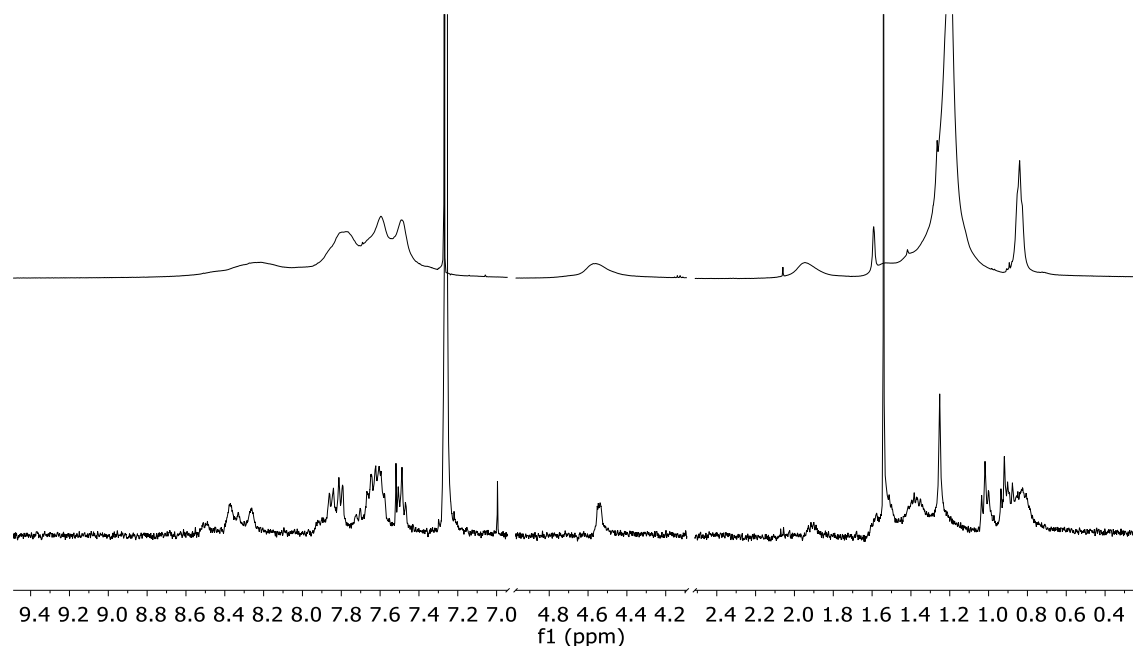


Figure 5.10. The ¹H NMR spectra of **62h** under high concentration (top) and low concentration (bottom).

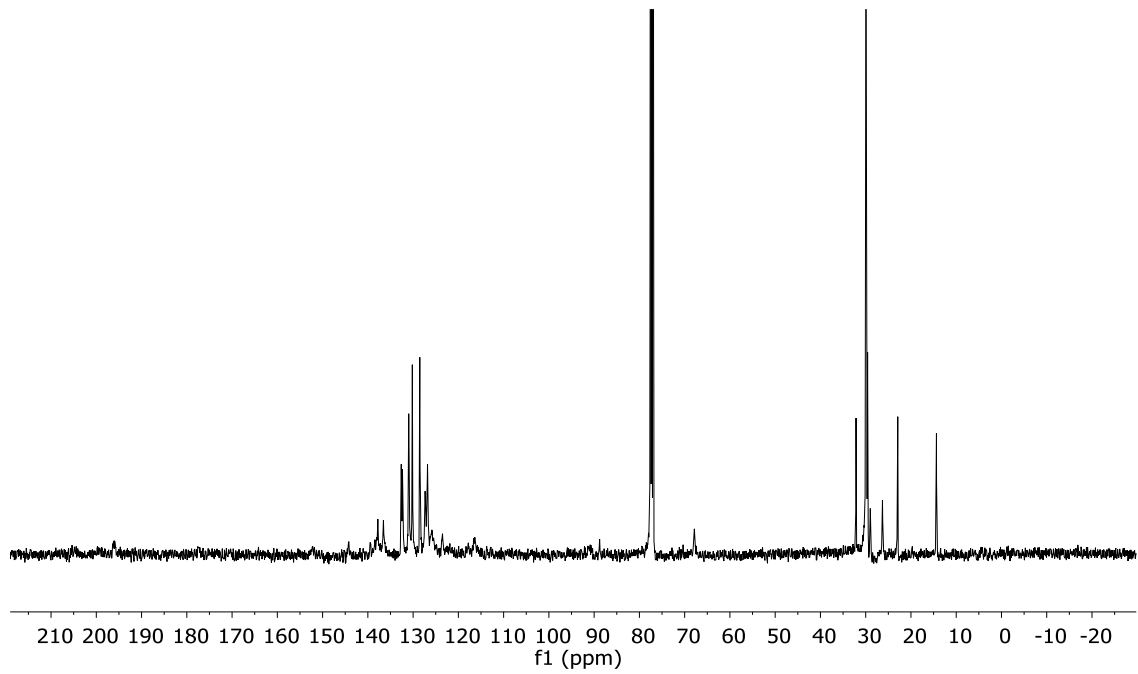


Figure 5.11. The ^{13}C NMR spectrum of monomer **62h**.

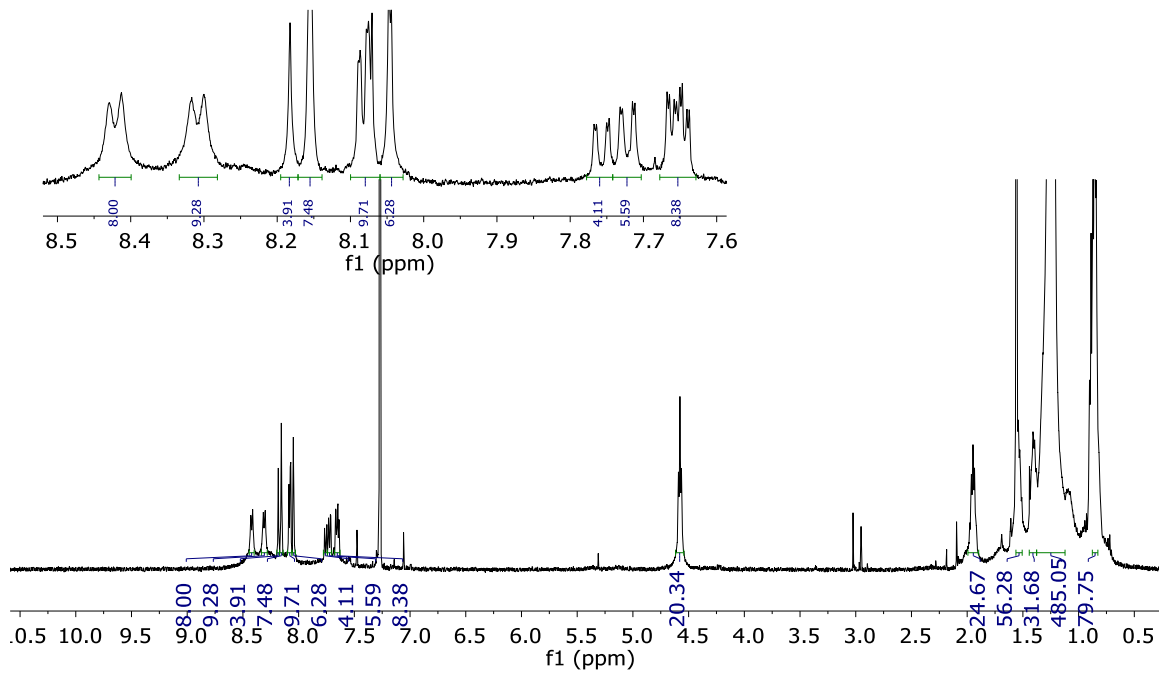


Figure 5.12. The ^1H NMR of the cage **63h** in CDCl_3 (two isomers of the cage with a little different ratio).

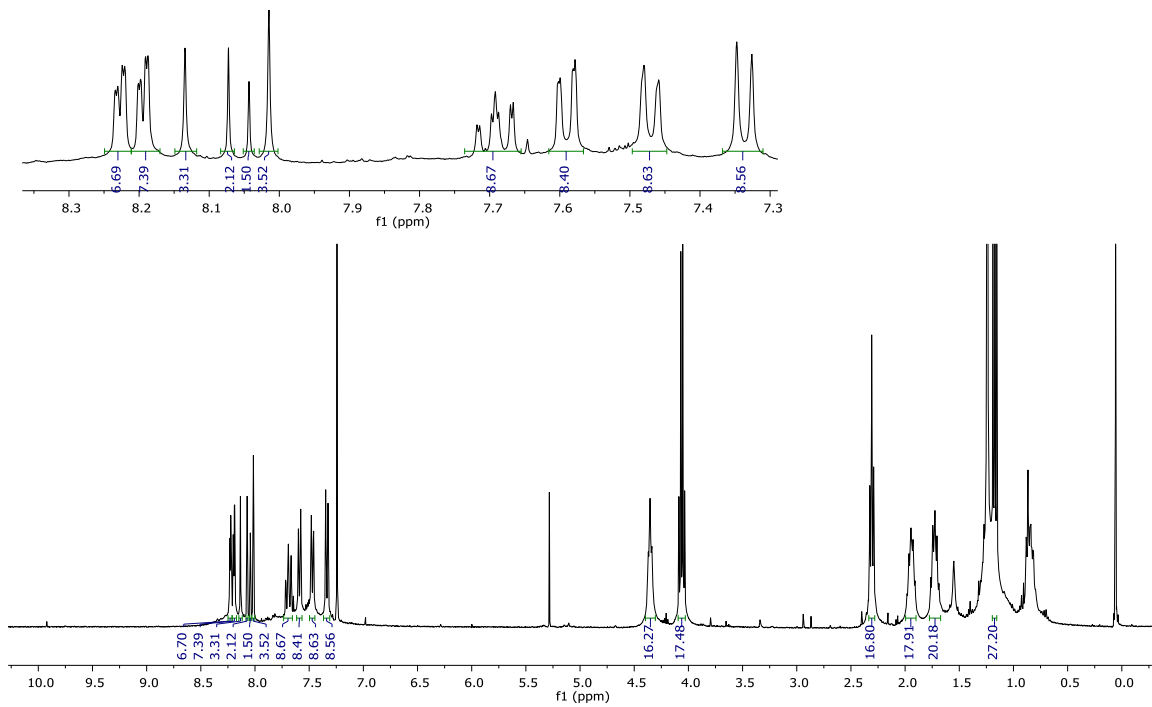


Figure 5.13. The ¹H NMR of the cage **63f** in CDCl_3 .

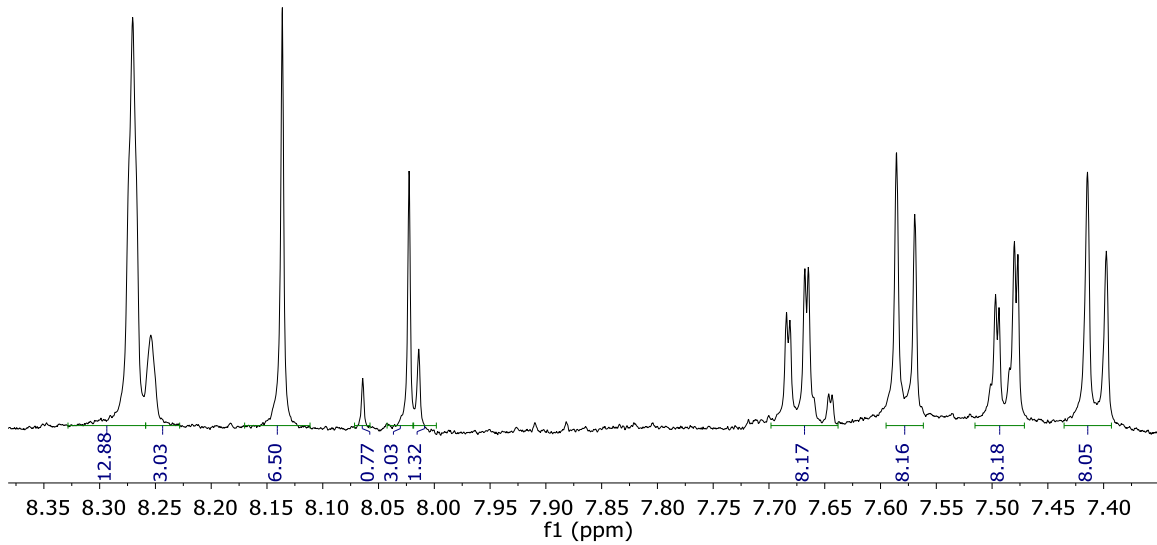


Figure 5.14. The ¹H NMR of the cage **64-H** in $\text{THF}-d_8$.

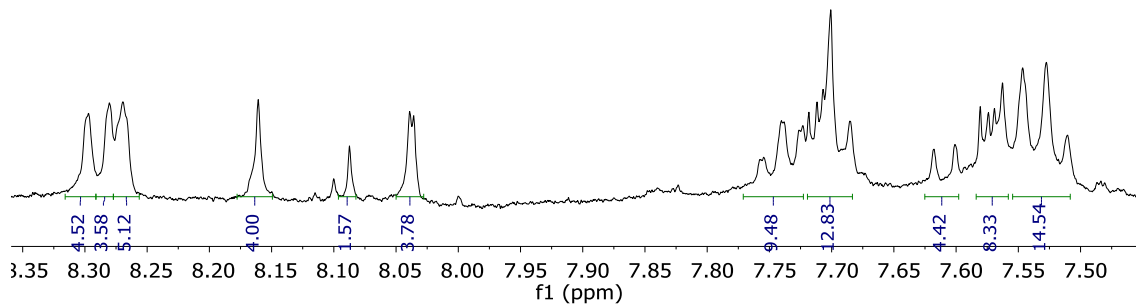


Figure 5.15. The ^1H NMR of the cage **63f**-COOH in $\text{THF}-d_8$.

5.5. References

1. Douglas, T.; Young, M. *Nature* **1998**, *393*, 152-155.
2. Uchida, M.; Klem, M. T.; Allen, M.; Suci, P.; Flenniken, M.; Gillitzer, E.; Varpness, Z.; Liepold, L. O.; Young, M.; Douglas, T. *Adv. Mater.* **2007**, *19*, 1025-1042.
3. Michalet, X.; Pinaud, F. F.; Bentolila, L. A.; Tsay, J. M.; Doose, S.; Li, J. J.; Sundaresan, G.; Wu, A. M.; Gambhir, S. S.; Weiss, S. *Science* **2005**, *307*, 538-544.
4. Medepalli, K.; Alphenaar, B. W.; Keynton, R. S.; Sethu, P. *Nanotechnology* **2013**, *24*.
5. Medintz, I. L.; Uyeda, H. T.; Goldman, E. R.; Mattoussi, H. *Nat. Mater.* **2005**, *4*, 435-446.
6. Gao, X. H.; Cui, Y. Y.; Levenson, R. M.; Chung, L. W. K.; Nie, S. M. *Nat. Biotechnol.* **2004**, *22*, 969-976.
7. Cheng, Y.; Samia, A. C.; Meyers, J. D.; Panagopoulos, I.; Fei, B. W.; Burda, C. *J. Am. Chem. Soc.* **2008**, *130*, 10643-10647.
8. Kataoka, K.; Harada, A.; Nagasaki, Y. *Adv. Drug Delivery Rev.* **2001**, *47*, 113-131.
9. Rösler, A.; Vandermeulen, G. W. M.; Klok, H.-A. *Adv. Drug Delivery Rev.* **2001**, *53*, 95-108.
10. Allen, T. M.; Cullis, P. R. *Science* **2004**, *303*, 1818-1822.
11. Knop, K.; Hoogenboom, R.; Fischer, D.; Schubert, U. S. *Angew. Chem. Int. Ed.* **2010**, *49*, 6288-6308.
12. Semple, S. C.; Akinc, A.; Chen, J. X.; Sandhu, A. P.; Mui, B. L.; Cho, C. K.; Sah, D. W. Y.; Stebbing, D.; Crosley, E. J.; Yaworski, E.; Hafez, I. M.; Dorkin, J. R.; Qin, J.; Lam, K.; Rajeev, K. G.; Wong, K. F.; Jeffs, L. B.; Nechev, L.; Eisenhardt, M. L.; Jayaraman, M.; Kazem, M.;

- Maier, M. A.; Srinivasulu, M.; Weinstein, M. J.; Chen, Q. M.; Alvarez, R.; Barros, S. A.; De, S.; Klimuk, S. K.; Borland, T.; Kosovrasti, V.; Cantley, W. L.; Tam, Y. K.; Manoharan, M.; Ciufolini, M. A.; Tracy, M. A.; de Fougerolles, A.; MacLachlan, I.; Cullis, P. R.; Madden, T. D.; Hope, M. J. *Nat. Biotechnol.* **2010**, *28*, 172-U118.
13. Wissing, S. A.; Kayser, O.; Müller, R. H. *Adv. Drug Delivery Rev.* **2004**, *56*, 1257-1272.
14. Porter, C. J. H.; Trevaskis, N. L.; Charman, W. N. *Nat. Rev. Drug Discovery* **2007**, *6*, 231-248.
15. Zava, O.; Mattsson, J.; Therrien, B.; Dyson, P. J. *Chem. Eur. J.* **2010**, *16*, 1428-1431.
16. He, C.; Lu, K.; Liu, D.; Lin, W. *J. Am. Chem. Soc.* **2014**, *136*, 5181-5184.
17. Therrien, B. *Eur. J. Inorg. Chem.* **2009**, 2445-2453.
18. Schmitt, F.; Freudenreich, J.; Barry, N. P. E.; Juillerat-Jeanneret, L.; Süss-Fink, G.; Therrien, B. *J. Am. Chem. Soc.* **2011**, *134*, 754-757.
19. Therrien, B.; Süss-Fink, G.; Govindaswamy, P.; Renfrew, A. K.; Dyson, P. J. *Angew. Chem. Int. Ed.* **2008**, *120*, 3833-3836.
20. Baban, D. F.; Seymour, L. W. *Adv. Drug Delivery Rev.* **1998**, *34*, 109-119.
21. Tozawa, T.; Jones, J. T. A.; Swamy, S. I.; Jiang, S.; Adams, D. J.; Shakespeare, S.; Clowes, R.; Bradshaw, D.; Hasell, T.; Chong, S. Y.; Tang, C.; Thompson, S.; Parker, J.; Trewin, A.; Bacsa, J.; Slawin, A. M. Z.; Steiner, A.; Cooper, A. I. *Nat. Mater.* **2009**, *8*, 973-978.
22. Tian, J.; Thallapally, P. K.; McGrail, B. P. *CrystEngComm* **2012**, *14*, 1909-1919.
23. Jin, Y.; Voss, B. A.; Jin, A.; Long, H.; Noble, R. D.; Zhang, W. *J. Am. Chem. Soc.* **2011**, *133*, 6650-6658.
24. Cooper, A. I. *Angew. Chem. Int. Ed.* **2011**, *50*, 996-998.
25. Jin, Y. H.; Voss, B. A.; Noble, R. D.; Zhang, W. *Angew. Chem. Int. Ed.* **2010**, *49*, 6348-6351.
26. Francesconi, O.; Ienco, A.; Moneti, G.; Nativi, C.; Roelens, S. *Angew. Chem. Int. Ed.* **2006**, *45*, 6693-6696.
27. Zhang, C. X.; Wang, Q.; Long, H.; Zhang, W. *J. Am. Chem. Soc.* **2011**, *133*, 20995-21001.
28. Zhang, C. X.; Long, H.; Zhang, W. *Chem. Commun.* **2012**, *48*, 6172-6174.
29. Mitra, T.; Jelfs, K. E.; Schmidtmann, M.; Ahmed, A.; Chong, S. Y.; Adams, D. J.; Cooper, A. I. *Nat. Chem.* **2013**, *5*, 276-281.
30. Ferrand, Y.; Crump, M. P.; Davis, A. P. *Science* **2007**, *318*, 619-622.
31. Okamoto, A.; Ichiba, T.; Saito, I. *J. Am. Chem. Soc.* **2004**, *126*, 8364-8365.

32. Wang, L.; Li, W.; Lu, J.; Zhao, Y.-X.; Fan, G.; Zhang, J.-P.; Wang, H. *J. Phys. Chem. C* **2013**, *117*, 26811-26820.
33. Somerharju, P. *Chem. Phys. Lipids* **2002**, *116*, 57-74.
34. Seo, Y. J.; Ryu, J. H.; Kim, B. H. *Org. Lett.* **2005**, *7*, 4931-4933.
35. Yamana, K.; Iwase, R.; Furutani, S.; Tsuchida, H.; Zako, H.; Yamaoka, T.; Murakami, A. *Nucleic Acids Res.* **1999**, *27*, 2387-2392.
36. Tanhuanpaa, K.; Virtanen, J.; Somerharju, P. *Biochim. Biophys. Acta, Mol. Cell. Res.* **2000**, *1497*, 308-320.
37. Sibley, S. P.; Nguyen, Y. T.; Campbell, R. L.; Silber, H. B. *Spectrochim Acta A* **1997**, *53*, 679-684.
38. Bolkskar, R. D.; Benedetto, A. F.; Husebo, L. O.; Price, R. E.; Jackson, E. F.; Wallace, S.; Wilson, L. J.; Alford, J. M. *J. Am. Chem. Soc.* **2003**, *125*, 5471-5478.
39. Ghiassi, K. B.; Olmstead, M. M.; Balch, A. L. *Dalton Trans.* **2014**, *43*, 7346-7358.
40. Zhang, J. Y.; Ye, Y. Q.; Chen, Y.; Pregot, C.; Li, T. H.; Balasubramaniam, S.; Hobart, D. B.; Zhang, Y. F.; Wi, S.; Davis, R. M.; Madsen, L. A.; Morris, J. R.; LaConte, S. M.; Yee, G. T.; Dorn, H. C. *J. Am. Chem. Soc.* **2014**, *136*, 2630-2636.
41. Hammer, B. A. G.; Baumgarten, M.; Mullen, K. *Chem. Commun.* **2014**, *50*, 2034-2036.

Bibliography

- Albrecht, K.; Yamamoto, K. *J. Am. Chem. Soc.* **2009**, *131*, 2244-2251.
- Allen, T. M.; Cullis, P. R. *Science* **2004**, *303*, 1818-1822.
- Anderson, H. L.; Gil-Ramirez, G.; Karlen, S. D.; Shundo, A.; Porfyrakis, K.; Ito, Y.; Briggs, G. A. D.; Morton, J. J. L. *Org. Lett.* **2010**, *12*, 3544-3547.
- Avellaneda, A.; Valente, P.; Burgun, A.; Evans, J. D.; Markwell-Heys, A. W.; Rankine, D.; Nielsen, D. J.; Hill, M. R.; Sumby, C. J.; Doonan, C. *J. Angew. Chem. Int. Ed.* **2013**, *52*, 3746-3749.
- Baban, D. F.; Seymour, L. W. *Adv. Drug Delivery Rev.* **1998**, *34*, 109-119.
- Barin, G.; Forgan, R. S.; Stoddart, J. F. *P Roy Soc. a-Math. Phy.* **2012**, *468*, 2849-2880.
- Bellecôte, M.; Blouin, N.; Boudreault, P.-L. T.; Leclerc, M.; Durocher, G. *J. Phys. Chem. A* **2006**, *110*, 13696-13704.
- Belowich, M. E.; Stoddart, J. F. *Chem. Soc. Rev.* **2012**, *41*, 2003-2024.
- Beves, J. E.; Blight, B. A.; Campbell, C. J.; Leigh, D. A.; McBurney, R. T. *Angew. Chem. Int. Ed.* **2011**, *50*, 9260-9327.
- Bindl, M.; Stade, R.; Heilmann, E. K.; Picot, A.; Goddard, R.; Furstner, A. *J. Am. Chem. Soc.* **2009**, *131*, 9468-9470.
- Bolskar, R. D.; Benedetto, A. F.; Husebo, L. O.; Price, R. E.; Jackson, E. F.; Wallace, S.; Wilson, L. J.; Alford, J. M. *J. Am. Chem. Soc.* **2003**, *125*, 5471-5478.
- Breault, G. A.; Hunter, C. A.; Mayers, P. C. *Tetrahedron* **1999**, *55*, 5265-5293.
- Bunz, U. H. F. *Chem. Rev.* **2000**, *100*, 1605-1644.
- Bunz, U. H. F. *Acc. Chem. Res.* **2001**, *34*, 998-1010.
- Butler, K. V.; Kalin, J.; Brochier, C.; Vistoli, G.; Langley, B.; Kozikowski, A. P. *J. Am. Chem. Soc.* **2010**, *132*, 10842-10846.
- Case, D. A. e. a. *AMBER 11*; University of California, San Francisco.
- Chen, X. Q.; Zhou, G. D.; Peng, X. J.; Yoon, J. *Chem. Soc. Rev.* **2012**, *41*, 4610-4630.
- Cheng, Y.; Samia, A. C.; Meyers, J. D.; Panagopoulos, I.; Fei, B. W.; Burda, C. *J. Am. Chem. Soc.* **2008**, *130*, 10643-10647.
- Cooper, A. I. *Angew. Chem. Int. Ed.* **2011**, *50*, 996-998.

Corbett, P. T.; Leclaire, J.; Vial, L.; West, K. R.; Wietor, J. L.; Sanders, J. K. M.; Otto, S. *Chem. Rev.* **2006**, *106*, 3652-3711.

Cote, A. P.; Benin, A. I.; Ockwig, N. W.; O'Keeffe, M.; Matzger, A. J.; Yaghi, O. M. *Science* **2005**, *310*, 1166-1170.

Dash, A. C.; Dash, B.; Praharaj, S. *J. Chem. Soc. Dalton* **1981**, 2063-2069.

Dietrichbuchecker, C. O.; Sauvage, J. P.; Kintzinger, J. P. *Tetrahedron Lett.* **1983**, *24*, 5095-5098.

Dominique, R.; Goodnow, R. A.; Kowalczyk, A.; Qiao, Q.; Sidduri, A.; Tilley, J. W. In *U.S. Pat. Appl. Publ.*; Google Patents: 2010; Vol. US20100240678 A1.

Douglas, T.; Young, M. *Nature* **1998**, *393*, 152-155.

El-Kaderi, H. M.; Hunt, J. R.; Mendoza-Cortes, J. L.; Cote, A. P.; Taylor, R. E.; O'Keeffe, M.; Yaghi, O. M. *Science* **2007**, *316*, 268-272.

Ferrand, Y.; Crump, M. P.; Davis, A. P. *Science* **2007**, *318*, 619-622.

Forgan, R. S.; Sauvage, J. P.; Stoddart, J. F. *Chem. Rev.* **2011**, *111*, 5434-5464.

Francesconi, O.; Ienco, A.; Moneti, G.; Nativi, C.; Roelens, S. *Angew. Chem. Int. Ed.* **2006**, *45*, 6693-6696.

Frank, M.; Hey, J.; Balcioglu, I.; Chen, Y.-S.; Stalke, D.; Suenobu, T.; Fukuzumi, S.; Frauendorf, H.; Clever, G. H. *Angew. Chem. Int. Ed.* **2013**, *52*, 10102-10106.

Freye, S.; Hey, J.; Torras-Galan, A.; Stalke, D.; Herbst-Irmer, R.; John, M.; Clever, G. H. *Angew. Chem. Int. Ed.* **2012**, *51*, 2191-2194.

Fujita, M.; Fujita, N.; Ogura, K.; Yamaguchi, K. *Nature* **1999**, *400*, 52-55.

Fukuda, M.; Sekiya, R.; Kuroda, R. *Angew. Chem. Int. Ed.* **2008**, *47*, 706-710.

Fürstner, A. *Angew. Chem. Int. Ed.* **2013**, *52*, 2794-2819.

Fürstner, A.; Grela, K. *Angew. Chem. Int. Ed.* **2000**, *39*, 1234-1236.

Fürstner, A.; Radkowski, K.; Grabowski, J.; Wirtz, C.; Mynott, R. *J. Org. Chem.* **2000**, *65*, 8758-8762.

Furukawa, H.; Yaghi, O. M. *J. Am. Chem. Soc.* **2009**, *131*, 8875-8883.

Gao, X. H.; Cui, Y. Y.; Levenson, R. M.; Chung, L. W. K.; Nie, S. M. *Nat. Biotechnol.* **2004**, *22*, 969-976.

Ge, P. H.; Fu, W.; Herrmann, W. A.; Herdtweck, E.; Campana, C.; Adams, R. D.; Bunz, U. H. F. *Angew. Chem. Int. Ed.* **2000**, *39*, 3607-3610.

Ghiassi, K. B.; Olmstead, M. M.; Balch, A. L. *Dalton Trans.* **2014**, *43*, 7346-7358.

Goodson, F. E.; Wallow, T. I.; Novak, B. M. *J. Am. Chem. Soc.* **1997**, *119*, 12441-12453.

Grave, C.; Schluter, A. D. *Eur. J. Org. Chem.* **2002**, 3075-3098.

Gross, D. E.; Discekici, E.; Moore, J. S. *Chem. Commun.* **2012**, *48*, 4426-4428.

Gross, D. E.; Moore, J. S. *Macromolecules* **2011**, *44*, 3685-3687.

Hammer, B. A. G.; Baumgarten, M.; Mullen, K. *Chem. Commun.* **2014**, *50*, 2034-2036.

Han, S. S.; Furukawa, H.; Yaghi, O. M.; Goddard, W. A. *J. Am. Chem. Soc.* **2008**, *130*, 11580-11581.

Hasell, T.; Wu, X. F.; Jones, J. T. A.; Bacsa, J.; Steiner, A.; Mitra, T.; Trewin, A.; Adams, D. J.; Cooper, A. I. *Nat. Chem.* **2010**, *2*, 750-755.

He, C.; Lu, K.; Liu, D.; Lin, W. *J. Am. Chem. Soc.* **2014**, *136*, 5181-5184.

Heinz, T.; Rudkevich, D. M.; Rebek, J. *Nature* **1998**, *394*, 764-766.

Heppekausen, J.; Stade, R.; Goddard, R.; Furstner, A. *J. Am. Chem. Soc.* **2010**, *132*, 11045-11057.

Hosseini, A.; Taylor, S.; Accorsi, G.; Armaroli, N.; Reed, C. A.; Boyd, P. D. W. *J. Am. Chem. Soc.* **2006**, *128*, 15903-15913.

Hu, K. D.; Yang, H. S.; Zhang, W.; Qin, Y. *Chem. Sci.* **2013**, *4*, 3649-3653.

Iyoda, M.; Yamakawa, J.; Rahman, M. *J. Angew. Chem. Int. Ed.* **2011**, *50*, 10522-10553.

Jelinek, R.; Ritenberg, M. *Rsc Adv.* **2013**, *3*, 21192-21201.

Jiang, S.; Jones, J. T. A.; Hasell, T.; Blythe, C. E.; Adams, D. J.; Trewin, A.; Cooper, A. I. *Nat. Commun.* **2011**, *2*.

Jin, Y.; Voss, B. A.; Jin, A.; Long, H.; Noble, R. D.; Zhang, W. *J. Am. Chem. Soc.* **2011**, *133*, 6650-6658.

Jin, Y.; Voss, B. A.; Noble, R. D.; Zhang, W. *Angew. Chem. Int. Ed.* **2010**, *49*, 6348-6351.

Jin, Y.; Wang, Q.; Taynton, P.; Zhang, W. *Acc. Chem. Res.* **2014**.

Jin, Y.; Yu, C.; Denman, R. J.; Zhang, W. *Chem. Soc. Rev.* **2013**, *42*, 6634-6654.

- Jin, Y. H.; Voss, B. A.; Jin, A.; Long, H.; Noble, R. D.; Zhang, W. *J. Am. Chem. Soc.* **2011**, *133*, 6650-6658.
- Jin, Y. H.; Voss, B. A.; Noble, R. D.; Zhang, W. *Angew. Chem. Int. Ed.* **2010**, *49*, 6348-6351.
- Jyothish, K.; Wang, Q.; Zhang, W. *Adv. Synth. Catal.* **2012**, *354*, 2073-2078.
- Jyothish, K.; Zhang, W. *Angew. Chem. Int. Ed.* **2011**, *50*, 3435-3438.
- Jyothish, K.; Zhang, W. *Angew. Chem. Int. Ed. Engl.* **2011**, *50*, 8478-8480.
- Kataoka, K.; Harada, A.; Nagasaki, Y. *Adv. Drug Delivery Rev.* **2001**, *47*, 113-131.
- Kataoka, K.; James, T. D.; Kubo, Y. *J. Am. Chem. Soc.* **2007**, *129*, 15126-15127.
- Kloppenburg, L.; Song, D.; Bunz, U. H. F. *J. Am. Chem. Soc.* **1998**, *120*, 7973-7974.
- Knop, K.; Hoogenboom, R.; Fischer, D.; Schubert, U. S. *Angew. Chem. Int. Ed.* **2010**, *49*, 6288-6308.
- Kondratuk, D. V.; Perdigao, L. M. A.; Sullivan, M. C. O.; Svatek, S.; Smith, G.; Shea, J. N. O.; Beton, P. H.; Anderson, H. L. *Angew. Chem. Int. Ed.* **2012**, *51*, 6696-6699.
- Kotha, S.; Kashinath, D.; Lahiri, K.; Sunoj, Raghavan B. *Eur. J. Org. Chem.* **2004**, *2004*, 4003-4013.
- Krouse, S. A.; Schrock, R. R. *Macromolecules* **1989**, *22*, 2569-2576.
- Krouse, S. A.; Schrock, R. R.; Cohen, R. E. *Macromolecules* **1987**, *20*, 903-904.
- Kuang, X. F.; Wu, X. Y.; Yu, R. M.; Donahue, J. P.; Huang, J. S.; Lu, C. Z. *Nat. Chem.* **2010**, *2*, 461-465.
- Langton, M. J.; Matichak, J. D.; Thompson, A. L.; Anderson, H. L. *Chem. Sci.* **2011**, *2*, 1897-1901.
- Lin, Z. H.; Sun, J. L.; Efremovska, B.; Warmuth, R. *Chem. Eur. J.* **2012**, *18*, 12864-12872.
- Liu, Y.; Niu, F.; Lian, J.; Zeng, P.; Niu, H. *Synthetic Met.* **2010**, *160*, 2055-2060.
- Mastalerz, M. *Angew. Chem. Int. Ed.* **2010**, *49*, 5042-5053.
- Mastalerz, M.; Schneider, M. W.; Oppel, I. M.; Presly, O. *Angew. Chem. Int. Ed.* **2011**, *50*, 1046-1051.
- McCaffrey, R.; Long, H.; Jin, Y.; Sanders, A.; Park, W.; Zhang, W. *J. Am. Chem. Soc.* **2014**, *136*, 1782-1785.

McGowan, K. P.; O'Reilly, M. E.; Ghiviriga, I.; Abboud, K. A.; Veige, A. S. *Chem. Sci.* **2013**, *4*, 1145-1155.

Medepalli, K.; Alphenaar, B. W.; Keynton, R. S.; Sethu, P. *Nanotechnology* **2013**, *24*.

Medintz, I. L.; Uyeda, H. T.; Goldman, E. R.; Mattoussi, H. *Nat. Mater.* **2005**, *4*, 435-446.

Meng, W. J.; Breiner, B.; Rissanen, K.; Thoburn, J. D.; Clegg, J. K.; Nitschke, J. R. *Angew. Chem. Int. Ed.* **2011**, *50*, 3479-3483.

Michalet, X.; Pinaud, F. F.; Bentolila, L. A.; Tsay, J. M.; Doose, S.; Li, J. J.; Sundaresan, G.; Wu, A. M.; Gambhir, S. S.; Weiss, S. *Science* **2005**, *307*, 538-544.

Miljanic, O. S.; Vollhardt, K. P. C.; Whitener, G. D. *Synlett* **2003**, 29-34.

Mitra, T.; Jelfs, K. E.; Schmidtmann, M.; Ahmed, A.; Chong, S. Y.; Adams, D. J.; Cooper, A. I. *Nat. Chem.* **2013**, *5*, 276-281.

Murase, T.; Otsuka, K.; Fujita, M. *J. Am. Chem. Soc.* **2010**, *132*, 7864.

Naddo, T.; Che, Y.; Zhang, W.; Balakrishnan, K.; Yang, X.; Yen, M.; Zhao, J.; Moore, J. S.; Zang, L. *J. Am. Chem. Soc.* **2007**, *129*, 6978-6979.

Nishimura, N.; Kobayashi, K. *Angew. Chem. Int. Ed.* **2008**, *47*, 6255-6258.

Nishimura, N.; Yoza, K.; Kobayashi, K. *J. Am. Chem. Soc.* **2010**, *132*, 777-790.

Nishiyabu, R.; Kubo, Y.; James, T. D.; Fossey, J. S. *Chem. Commun.* **2011**, *47*, 1124-1150.

O'Sullivan, M. C.; Sprafke, J. K.; Kondratuk, D. V.; Rinfray, C.; Claridge, T. D. W.; Saywell, A.; Blunt, M. O.; O'Shea, J. N.; Beton, P. H.; Malfois, M.; Anderson, H. L. *Nature* **2011**, *469*, 72-75.

Okamoto, A.; Ichiba, T.; Saito, I. *J. Am. Chem. Soc.* **2004**, *126*, 8364-8365.

Paley, D. W.; Sedbrook, D. F.; Decatur, J.; Fischer, F. R.; Steigerwald, M. L.; Nuckolls, C. *Angew. Chem. Int. Ed.* **2013**, *52*, 4591-4594.

Pedersen, S. F.; Schrock, R. R.; Churchill, M. R.; Wasserman, H. J. *J. Am. Chem. Soc.* **1982**, *104*, 6808-6809.

Pennella, F.; Banks, R. L.; Bailey, G. C. *Chem. Commun.* **1968**, 1548.

Porter, C. J. H.; Trevaskis, N. L.; Charman, W. N. *Nat. Rev. Drug Discovery* **2007**, *6*, 231-248.

Prachumrak, N.; Pansay, S.; Namuangruk, S.; Kaewin, T.; Jungsuttiwong, S.; Sudyoadsuk, T.; Promarak, V. *Eur. J. Org. Chem.* **2013**, *2013*, 6619-6628.

Prunet, J. *Eur. J. Org. Chem.* **2011**, 3634-3647.

- Rösler, A.; Vandermeulen, G. W. M.; Klok, H.-A. *Adv. Drug Delivery Rev.* **2001**, *53*, 95-108.
- Rowan, S. J.; Cantrill, S. J.; Cousins, G. R. L.; Sanders, J. K. M.; Stoddart, J. F. *Angew. Chem. Int. Ed.* **2002**, *41*, 898-952.
- Rubin, Y.; Parker, T. C.; Khan, S. I.; Holliman, C. L.; McElvany, S. W. *J. Am. Chem. Soc.* **1996**, *118*, 5308-5309.
- Rubin, Y.; Parker, T. C.; Pastor, S. J.; Jalasatgi, S.; Boulle, C.; Wilkins, C. L. *Angew. Chem. Int. Ed.* **1998**, *37*, 1226-1229.
- Rue, N. M.; Sun, J. L.; Warmuth, R. *Isr. J. Chem.* **2011**, *51*, 743-768.
- Sato, S.; Morohara, O.; Fujita, D.; Yamaguchi, Y.; Kato, K.; Fujita, M. *J. Am. Chem. Soc.* **2010**, *132*, 3670-3671.
- Sato, Y.; Yamasaki, R.; Saito, S. *Angew. Chem. Int. Ed.* **2009**, *48*, 504-507.
- Schmitt, F.; Freudenreich, J.; Barry, N. P. E.; Juillerat-Jeanneret, L.; Süss-Fink, G.; Therrien, B. *J. Am. Chem. Soc.* **2011**, *134*, 754-757.
- Schouwey, C.; Scopelliti, R.; Severin, K. *Chem. Eur. J.* **2013**, *19*, 6274-6281.
- Schrock, R. R. *Acc. Chem. Res.* **1986**, *19*, 342-348.
- Schrock, R. R. *Chem. Rev.* **2002**, *102*, 145-179.
- Schrock, R. R.; Czekelius, C. *Adv. Synth. Catal.* **2007**, *349*, 55-77.
- Sedbrook, D. F.; Paley, D. W.; Steigerwald, M. L.; Nuckolls, C.; Fischer, F. R. *Macromolecules* **2012**, *45*, 5040-5044.
- Semple, S. C.; Akinc, A.; Chen, J. X.; Sandhu, A. P.; Mui, B. L.; Cho, C. K.; Sah, D. W. Y.; Stebbing, D.; Crosley, E. J.; Yaworski, E.; Hafez, I. M.; Dorkin, J. R.; Qin, J.; Lam, K.; Rajeev, K. G.; Wong, K. F.; Jeffs, L. B.; Nechev, L.; Eisenhardt, M. L.; Jayaraman, M.; Kazem, M.; Maier, M. A.; Srinivasulu, M.; Weinstein, M. J.; Chen, Q. M.; Alvarez, R.; Barros, S. A.; De, S.; Klimuk, S. K.; Borland, T.; Kosovrasti, V.; Cantley, W. L.; Tam, Y. K.; Manoharan, M.; Ciufolini, M. A.; Tracy, M. A.; de Fougerolles, A.; MacLachlan, I.; Cullis, P. R.; Madden, T. D.; Hope, M. J. *Nat. Biotechnol.* **2010**, *28*, 172-U118.
- Seo, Y. J.; Ryu, J. H.; Kim, B. H. *Org. Lett.* **2005**, *7*, 4931-4933.
- Severin, K. *Dalton Trans.* **2009**, 5254-5264.
- Sibley, S. P.; Nguyen, Y. T.; Campbell, R. L.; Silber, H. B. *Spectrochim. Acta. A* **1997**, *53*, 679-684.
- Sisco, S. W.; Moore, J. S. *J. Am. Chem. Soc.* **2012**, *134*, 9114-9117.

- Sisco, S. W.; Moore, J. S. *Chem. Sci.* **2014**, *5*, 81-85.
- Skowronek, P.; Gawronski, J. *Org. Lett.* **2008**, *10*, 4755-4758.
- Somerharju, P. *Chem. Phys. Lipids* **2002**, *116*, 57-74.
- Sonogashira, K.; Tohda, Y.; Hagiwara, N. *Tetra. Lett.* **1975**, 4467-4470.
- Staab, H. A.; Neunhoefer. *Synthesis-Stuttgart* **1974**, 424-424.
- Sworen, J. C.; Smith, J. A.; Berg, J. M.; Wagener, K. B. *J. Am. Chem. Soc.* **2004**, *126*, 11238-11246.
- Tanhuanpaa, K.; Virtanen, J.; Somerharju, P. *Biochim. Biophys. Acta, Mol. Cell. Res.* **2000**, *1497*, 308-320.
- Therrien, B. *Eur. J. Inorg. Chem.* **2009**, 2445-2453.
- Therrien, B.; Süss-Fink, G.; Govindasamy, P.; Renfrew, A. K.; Dyson, P. J. *Angew. Chem. Int. Ed.* **2008**, *120*, 3833-3836.
- Thomas, S. W.; Joly, G. D.; Swager, T. M. *Chem. Rev.* **2007**, *107*, 1339-1386.
- Tian, J.; Thallapally, P. K.; McGrail, B. P. *CrystEngComm* **2012**, *14*, 1909-1919.
- Tobe, Y.; Nakagawa, N.; Kishi, J. Y.; Sonoda, M.; Naemura, K.; Wakabayashi, T.; Shida, T.; Achiba, Y. *Tetrahedron* **2001**, *57*, 3629-3636.
- Tobe, Y.; Nakagawa, N.; Naemura, K.; Wakabayashi, T.; Shida, T.; Achiba, Y. *J. Am. Chem. Soc.* **1998**, *120*, 4544-4545.
- Tozawa, T.; Jones, J. T.; Swamy, S. I.; Jiang, S.; Adams, D. J.; Shakespeare, S.; Clowes, R.; Bradshaw, D.; Hasell, T.; Chong, S. Y.; Tang, C.; Thompson, S.; Parker, J.; Trewin, A.; Bacsa, J.; Slawin, A. M.; Steiner, A.; Cooper, A. I. *Nat. Mater.* **2009**, *8*, 973-978.
- Tozawa, T.; Jones, J. T. A.; Swamy, S. I.; Jiang, S.; Adams, D. J.; Shakespeare, S.; Clowes, R.; Bradshaw, D.; Hasell, T.; Chong, S. Y.; Tang, C.; Thompson, S.; Parker, J.; Trewin, A.; Bacsa, J.; Slawin, A. M. Z.; Steiner, A.; Cooper, A. I. *Nat. Mater.* **2009**, *8*, 973-978.
- Tranchemontagne, D. J. L.; Ni, Z.; O'Keeffe, M.; Yaghi, O. M. *Angew. Chem. Int. Ed.* **2008**, *47*, 5136-5147.
- Uchida, M.; Klem, M. T.; Allen, M.; Suci, P.; Flenniken, M.; Gillitzer, E.; Varpness, Z.; Liepold, L. O.; Young, M.; Douglas, T. *Adv. Mater.* **2007**, *19*, 1025-1042.
- Wan, S.; Guo, J.; Kim, J.; Ihee, H.; Jiang, D. L. *Angew. Chem. Int. Ed.* **2008**, *47*, 8826-8830.
- Wang, J.; Wolf, R. M.; Caldwell, J. W.; Kollman, P. A.; Case, D. A. *J. Comput. Chem.* **2004**, *25*, 1157-1174.

Wang, L.; Li, W.; Lu, J.; Zhao, Y.-X.; Fan, G.; Zhang, J.-P.; Wang, H. *J. Phys. Chem. C* **2013**, *117*, 26811-26820.

Weiss, K.; Michel, A.; Auth, E. M.; Bunz, U. H. F.; Mangel, T.; Mullen, K. *Angew. Chem. Int. Ed.* **1997**, *36*, 506-509.

Wengrovius, J. H.; Sancho, J.; Schrock, R. R. *J. Am. Chem. Soc.* **1981**, *103*, 3932-3934.

Westcott, A.; Fisher, J.; Harding, L. P.; Rizkallah, P.; Hardie, M. J. *J. Am. Chem. Soc.* **2008**, *130*, 2950-2951.

Wissing, S. A.; Kayser, O.; Müller, R. H. *Adv. Drug Delivery Rev.* **2004**, *56*, 1257-1272.

Wu, X. A.; Tamm, M. *Beilstein J. Org. Chem.* **2011**, *7*, 82-93.

Wu, Z. Y.; Lee, S.; Moore, J. S. *J. Am. Chem. Soc.* **1992**, *114*, 8730-8732.

Xu, J.; Duran, D.; Mao, B. *J. Liq. Chromatogr. R. T.* **2006**, *29*, 2795-2806.

Yamana, K.; Iwase, R.; Furutani, S.; Tsuchida, H.; Zako, H.; Yamaoka, T.; Murakami, A. *Nucleic Acids Res.* **1999**, *27*, 2387-2392.

Yang, H.; Jin, Y.; Du, Y.; Zhang, W. *J. Mat.s Chem. A* **2014**, *2*, 5986-5993.

Yang, H.; Liu, Z.; Zhang, W. *Adv. Synth. Catal.* **2013**, *355*, 885-890.

Yang, H. S.; Liu, Z. N.; Zhang, W. *Adv. Synth. Catal.* **2013**, *355*, 885-890.

Yang, H. W.; Kong, X.; Wei, J. F.; Liu, C. C.; Song, W. J.; Zhang, W.; Wei, W.; He, S. H. *Cell. Physiol. Biochem.* **2012**, *29*, 561-570.

Yoshizawa, M.; Klosterman, J. K.; Fujita, M. *Angew. Chem. Int. Ed.* **2009**, *48*, 3418-3438.

Zava, O.; Mattsson, J.; Therrien, B.; Dyson, P. J. *Chem. Eur. J.* **2010**, *16*, 1428-1431.

Zhang, C.; Chen, C. F. *J. Org. Chem.* **2007**, *72*, 9339-9341.

Zhang, C. X.; Long, H.; Zhang, W. *Chem. Commun.* **2012**, *48*, 6172-6174.

Zhang, C. X.; Wang, Q.; Long, H.; Zhang, W. *J. Am. Chem. Soc.* **2011**, *133*, 20995-21001.

Zhang, G.; Presly, O.; White, F.; Oppel, I. M.; Mastalerz, M. *Angew. Chem. Int. Ed.* **2014**, *53*, 5126-5130.

Zhang, J. Y.; Ye, Y. Q.; Chen, Y.; Pregot, C.; Li, T. H.; Balasubramaniam, S.; Hobart, D. B.; Zhang, Y. F.; Wi, S.; Davis, R. M.; Madsen, L. A.; Morris, J. R.; LaConte, S. M.; Yee, G. T.; Dorn, H. C. *J. Am. Chem. Soc.* **2014**, *136*, 2630-2636.

Zhang, W.; Brombosz, S. M.; Mendoza, J. L.; Moore, J. S. *J. Org. Chem.* **2005**, *70*, 10198-10201.

- Zhang, W.; Jyothish, K.; Yang, H. S.; Wang, Q. *Abstr. Pap. Am. Chem. Soc.* **2013**, 246.
- Zhang, W.; Kraft, S.; Moore, J. S. *J. Am. Chem. Soc.* **2004**, 126, 329-335.
- Zhang, W.; Moore, J. S. *J. Am. Chem. Soc.* **2004**, 126, 12796.
- Zhang, W.; Moore, J. S. *J. Am. Chem. Soc.* **2005**, 127, 11863-11870.
- Zhang, W.; Moore, J. S. *Angew. Chem. Int. Ed.* **2006**, 45, 4416-4439.
- Zhu, C. L.; Liu, L. B.; Yang, Q.; Lv, F. T.; Wang, S. *Chem. Rev.* **2012**, 112, 4687-4735.
- Zhu, Y. L.; Yang, H. S.; Jin, Y. H.; Zhang, W. *Chem. Mater.* **2013**, 25, 3718-3723.

Vita

Qi Wang was born on March, 4th, 1987 in Qingdao, Shandong, China. After her excellent work in junior high school in Pingdu Hangzhou Road Middle School, she was elected into Top Science Class in Pingdu No. 1 High School. After graduation, she then entered Peking University, majoring chemistry in Beijing, China. As an undergraduate student, she joined Professor Dahui Zhao's group as a research assistant, working on the design and synthesis of phenyleneethynylene oligomers and study their folding/unfolding behaviors. Graduated with a B.S. degree in chemistry in June 2009, she then enrolled in the doctoral program in University of Colorado at Boulder. Under the supervision of Professor Wei Zhang, she has been working on the construction of shape-persistent three-dimensional organic molecular cages through alkyne metathesis and their applications in fullerene separations.